UNIVERSITÀ DEGLI STUDI DI NAPOLI
"FEDERICO II"

Dipartimento di Scienze della Terra, dell'Ambiente e delle Risorse

Research Doctorate in
INTERNAL DYNAMICS OF ACTIVE VOLCANOES AND HYDROGEOLOGICAL-ENVIRONMENTAL RISKS
XXVIII CYCLE

PhD Thesis

DISCRIMINATING MAGMA SOURCES AT AEOLIAN ISLANDS, ITALY

Denis Zamboni

Advisors:
Prof. Claudia Cannatelli
Prof. Esteban Gazel

ABSTRACT

This dissertation represents the summary of the work I have done during the 3 years of my PhD project, carried out between the University of Naples "Federico II" (Naples, Italy) and the Virginia Polytechnic Institute and State University (Blacksburg, VA, USA), in the framework of the agreement between the two universities. Supervisors of such agreement are Prof. Benedetto De Vivo (University of Naples "Federico II") and Prof. Robert J. Bodnar (Virginia Polytechnic Institute and State University).

The complex geodynamic evolution of Aeolian Arc in the southern Tyrrhenian Sea resulted in melts with some of the most pronounced along the arc geochemical variation in incompatible trace elements and radiogenic isotopes worldwide, likely reflecting variations in arc magma source components. This study elucidates the effects of subducted components on magma sources along different sections of the Aeolian Arc by evaluating systematics of elements depleted in the upper mantle but enriched in the subducting slab, focusing on a new set of B, Be, As, and Li measurements. Based on our new results, we suggest that both hydrous fluids and silicate melts were involved in element transport from the subducting slab to the mantle wedge. Hydrous fluids strongly influence the chemical composition of lavas in the central arc (Salina) while a melt component from subducted sediments probably plays a key role in metasomatic reactions in the mantle wedge below the peripheral islands (Stromboli). The increasing source metasomatism by the subduction components was confirm by new isotopic data that show the effects of the Ionian subducted sediments on Stromboli rocks, while the olivine high precision chemistry excludes the presence of a pyroxenitic component in the source and point toward partial melts of a normal peridotite source. This research also describes similarities in subducting components between the Aeolian Archipelago, the Phlegrean Fields and other volcanic arcs/arc segments around the world

(e.g., Sunda, Cascades, Mexican Volcanic Belt), suggesting that the presence of melt components in all these locations resulted from an increase in the mantle wedge temperature by inflow of hot asthenospheric material from tears/windows in the slab parallel to the trench and/or from around the edges of the sinking slab.

AKNOWLEDGEMENTS

When I started this PhD I was expecting to be away from my hometown for long time but I wouldn't expect to spend almost the entire 3 years at Virginia Tech. Luckily this wasn't a problem. This was a wonderful opportunity for me and for this reason I'd like to thank prof. De Vivo because in the past he created a great partnership with this university where I had the chance to grow a lot as a scientist and mostly as a person.

Being away wasn't easy, there were a lot of ups and downs, but I met great people, awesome friends that supported me also in the toughest moments (both scientifically and in the everyday life). I for sure couldn't make it through without my love, Susy, that even with an ocean between us, she kept me happy and kept our relationship alive and healthy with all her energy….so, thank you to be so patience with me!!! You are a saint….or not…ehehehehe!!! Finally now we can spend some time together!!!

During these 3 years, another person was fundamental for me, and she was my Italian advisor Claudia Cannatelli, that beside having a baby, moving to Chile, living in the Napolitan chaos, she had always time for me when I needed, giving me precious advices and helping me a lot as a connection between the Italian and American world.

I'd also like to thank Esteban Gazel, my VT advisor, who taught me a lot in these years and helped me make this great project on the Aeolian Islands. You made me a much better scientist.

And at this point I would like to thank everyone, starting with my family that always supported every choice I made (mostly my mum), then moving to the awesome girls in my office, Pilar and Sarah (thanks to be my nurse once) and finishing with my best friends in the States, Jarek-Daniel-Josh (we had great time guys, remember: "Mario Kart is a necessity to recharge the batteries"),

especially Jarek, we shared a lot of….olivine knowledge and you always corrected my poorly written english…see you soon brother!!

For sure I forgot someone, but if you didn't realize until now, I'm really really bad in express my feelings with words….So, I'd like to conclude with a special thanks to my kidney stones that bother me until the very last day…the perfect stone for a geologist, don't you agree??

TABLE OF CONTENTS

Chapter 4.

Conclusion

LIST OF FIGURES

LIST OF TABLES

Chapter 2.

Chapter 3.

Chapter 1.
Introduction

1.1 Summary Of The Recent Western-Central Mediterranean Geodynamic Evolution

The geological evolution of the Western-Central Mediterranean in the last 30-40 Ma is strictly related to the convergence of the African and European continents together with relative movements of other minor plates (e.g., Adria) (e.g., Doglioni et al., 1999; Carminati et al., 2010, 2012). The merging of these two main plates is also responsible for the creation of the Alpine and Apennine chains along with extensional or transitional basins.

These basins (Fig. 1.1) are considered to become younger moving eastward (in order: Alboran, Algerian, Valencia, Ligure-Provencal and Tyrrhenian basin; Carminati et al., 2012 and reference therein) and are constituted by thinned continental lithosphere and new oceanic crust (e.g., Tyrrhenian basin) or by only thinned continental lithosphere (e.g., Alboran basin). In contrast, the Adriatic basin is composed of thick continental lithosphere while the Ionian basin is considered to be a remnant of the Tethyan oceanic crust, both formed during the Mesozoic.

As described in several studies (e.g., Carminati et al., 2010; Billi et al., 2011), the continental collision that occurred during the Eocene along the Alpine-Betic belt, with relative closure of the Ligurian-Piedmontese Ocean (Alpine subduction), was followed by the migration toward southeast of the eastward to southward rollback of the originally west-directed Apennine-Maghrebide subduction zone. This movement caused the opening of the Balearic-Provencal Sea between 35 and 15 Ma (Ligurian-Provencal and Valencia back-arc basins) and originated the separation of the Corsica-Sardinia-Calabria continental block from the southern European margin. This process was also accompanied by widespread calc-alkaline volcanism in Sardinia, Valencian, and Alboran regions.

Around 15 Ma the Tyrrhenian Sea began to open behind the west-dipping Adriatic-Ionian sectors of the African plate together with the counter-clockwise rotation of the Italian peninsula and the Corsica-Sardinia-Calabria block (Carminati et al., 2012 and reference therein). After Corsica and Sardinia arrived to their present positions, the back-arc extension continued in the Tyrrhenian Sea beginning along the southeastern margin of the Corsica-Sardinia block (during Serravallian), and progressively migrating southeastward in the Vavilov (in late Messinian-early

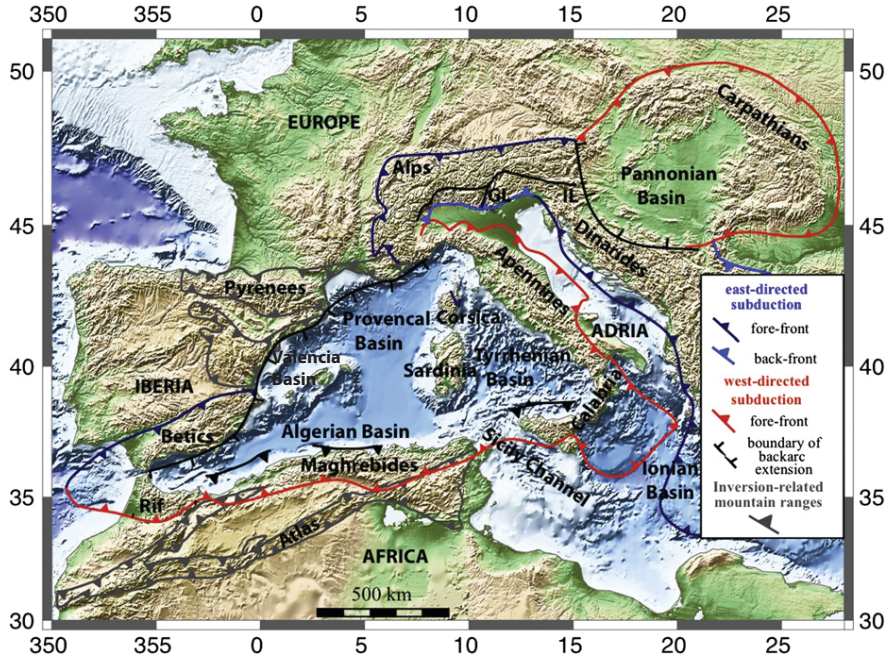

Figure 1.1 Simplify representation of the western-central Mediterranean area from Carminati et al. (2012). GL: Giudicarie Lineament; IL: Insubric Line.

Pliocene) and Marsili (in late Pliocene-early Pleistocene) oceanic basins. These processes forced the Calabria region and the Apennine compression front to reach their actual locations (e.g., Faccenna et al., 2011; Orecchio et al., 2015), as it was also interpreted by the occurrence of a deep focus Wadati-Benioff seismic zone under the southern Tyrrhenian Sea area (e.g., Chiarabba et al., 2008).

The opening of the Tyrrhenian Sea and the counterclockwise rotation of the Italian peninsula caused the longitudinal stretching of the Apennine chain and fragmentation of the subduction zone highlighted by important transverse lithospheric tear faults (e.g., the "41° N parallel line", the Sangineto fault; Rosenbaum et al., 2008 and reference therein). These tectonic lines separated arc sectors characterized by different lithospheric structures, drifting velocity, and block rotation, and by volcanic rocks with different geochemical characteristics (e.g., Lustrino et al., 2011).

1.1.1 *Quick Overview Of The Magmatism*

Various types of magmas characterize the western-central Mediterranean area. As described by several studies (e.g., Lustrino et al., 2011; Peccerillo and Frezzotti, 2015), rocks

characterizing the Provence, Balearic Sea and Sardinia zones are mainly of calc-alkaline compositions with some arc tholeiites from the Oligo-Miocene. On the other hand younger calc-alkaline to shoshonitic and ultrapotassic magma are typical of the Aeolian Arc and central Italy (8 Ma to present) due to the eastward migration of the Apennine subduction system (Ionian rollbacking slab) through the southern Tyrrhenian Sea. These magmas show geochemical signatures typical of arc rocks (high LILE/HFSE, negative Nb, Ta, Ti, etc.) and are referred as "orogenic". These rocks display a large range of radiogenic isotope values from DMM (depleted MORB mantle) to upper continental crust in central Italy.

In contrast, magmas erupted in the back-arc position and along the margin of the African foreland (12 Ma to present) are characterized by little or no arc geochemical signature (low LILE/HFSE, positive spikes of Nb, Ta, etc.). These "anorogenic" rocks, characterized by mafic to felsic composition and tholeiitic to Na-alkaline and nephelinitic affinities, are distributed without a general age scheme from Sardinia to the Sicily Channel (Miocene to present: Pantelleria, Linosa, and several seamounts), including Ustica and several seamounts in the Tyrrhenian basin, and Hyblei and Etna in eastern Sicily (0.5 Ma to present). These rocks are defined by isotopic signatures characteristic of FOZO (focal zone) and EM1 (enriched mantle 1) ocean island basalts (OIB) (Peccerillo and Frezzotti, 2015 and reference therein).

1.2 Italian Volcanism

The Plio-Quaternary igneous activity affecting the Tyrrhenian Sea area is characterized by extremely variable compositions representing almost the entire worldwide volcanic rocks variety. Many studies (e.g., Peccerillo, 2005; Lustrino et al., 2011; Peccerillo and Frezzotti, 2015) identified different compositionally volcanic provinces/districts (Fig. 1.2), based on petrological and geochemical data. The provinces are schematically described as follow (for details see Peccerillo, 2005 and reference therein):

1) The *Tuscany Province* (8.5-0.3 Ma) is characterized by mafic magmas with calc-alkaline to ultrapotassic (lamproites) compositions and by silicic peraluminous magmatism of anatectic origin with intrusive (e.g., Elba) and effusive (e.g., Roccastrada) episodes through southern Tuscany and the Tuscan archipelago. Geochemical and isotopic signatures show closed similarities with upper crust rocks.

2) The *Intra-Apennine Province* (0.6-0.3 Ma) is formed by small monogenic volcanoes (i.e., San Venanzo) and is characterized by mainly pyroclastic rocks. It includes ultrapotassic melilitites (kamafugites) and carbonate-rich pyroclastic material. Incompatible element patterns and radiogenic isotopic values are similar to the Roman Province.
3) The *Roman Province* (0.8-0.006 Ma) consists in large volcanic complexes and stratovolcanoes that spans from Vulsini to Alban Hills. It displays potassic (trachybasalt to trachyte) and ultrapotassic (leucite tephrite to phonolite) volcanism. It is also characterized by high LILE (e.g., K, Rb) and low HFSE (e.g., Nb) contents and by generally high radiogenic Sr but less extreme than Tuscan values.
4) The *Ernici-Roccamonfina Province* (0.7-0.1 Ma) is defined by Ernici monogenetic centers and Roccamonfina stratovolcano that erupted silica undersaturated ultrapotassic Roman-type rocks, and saturated calc-alkaline to potassic rocks similar to the analogous Campania ones. It is considered the transition zone between the Roman and Campania Province.
5) The *Campania Province* (4 Ma to present) represents active volcanoes (e.g., Vesuvius, Phlegrean Fields) mostly made of pyroclastic rocks of shoshonitic-potassic to ultrapotassic compositions. Magmas have lower contents in LILE and Sr isotopes compared to the Roman Province rocks but at the same time are very similar to Stromboli potassic rocks.
6) The *Mount Vulture* (0.7-0.1 Ma) is a stratovolcano east of the southern Apennines. It is composed of silica undersaturated alkaline rocks enriched in both Na and K and late carbonate-rich material. This is a unique volcano, petrologically and geochemically different from any other Italian eruptive center.
7) The *Aeolian Arc Province* (0.27 Ma to present) consists in seven islands characterized by important within-island and along arc variations in elemental and isotopic compositions (for details see paragraph 1.3).
8) The *Sicily Province* (7 Ma to present) includes Etna, Hyblei and Sicily channels volcanoes and seamounts exhibiting incompatible trace elements and Sr-, Nd-, and Pb-isotope signatures representative of FOZO-OIB rocks. Rocks have Na-alkaline to transitional basalts composition (e.g., Etna) with abundant peralkaline trachyte and rhyolite in Pantelleria.
9) The *Sardinia Province* (12-0.1 Ma) is formed by volcanic centers and basaltic plateaux characterized by mafic to silicic sub-alkaline, transitional to Na-alkaline rocks with a mainly unique EM1 radiogenic isotopic signatures.

10) The *Southern Tyrrhenian Sea floor* (12 Ma to present) represents sub-alkaline to transitional MORB rocks from several seamounts and cores in and around the Marsili and Vavilov basin. Rocks include arc-type compositions (shoshonitic to calc-alkaline and arc-tholeiitic), intraplate-type compositions (Na-transitional and alkaline basalt to trachyte), and MORB-type compositions.

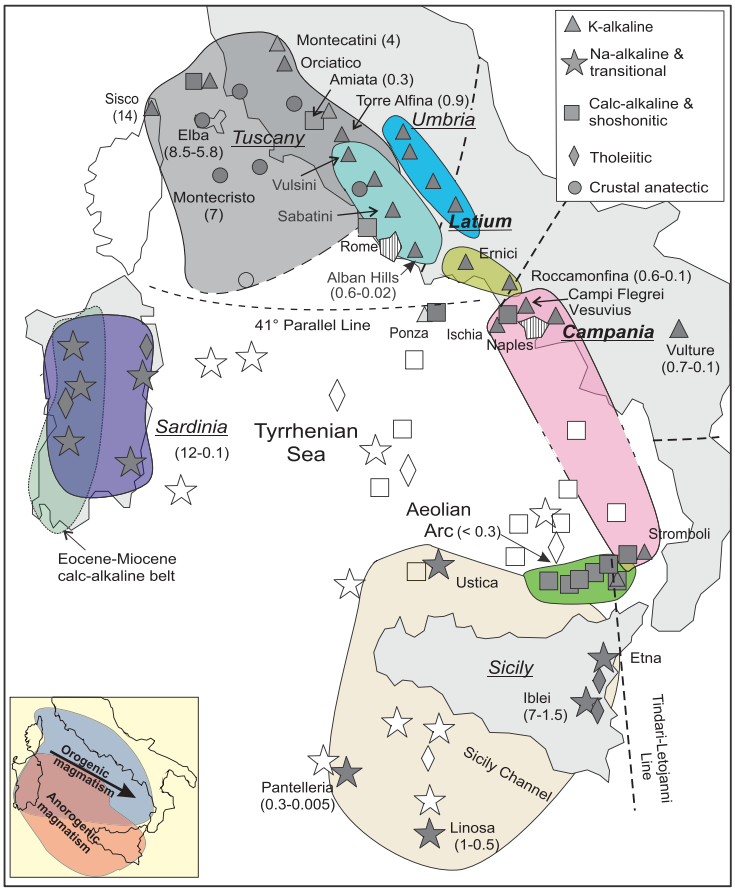

Figure 1.2 Illustration of the different magmatic provinces from Peccerillo and Frezzotti (2015) representing the Plio-Quaternary Italian magmatism. Ages are in Ma between parenthesis. Dashed lines are main tectonic lines.

1.3 The Aeolian Islands

The Aeolian Islands (Fig. 1.3) in the southern Tyrrhenian Sea (Italy) have been a subject of study for centuries, and at present time the archipelago is still an interesting location because of its strong structural, volcanological, and petrological variations.

10) The *Southern Tyrrhenian Sea floor* (12 Ma to present) represents sub-alkaline to transitional MORB rocks from several seamounts and cores in and around the Marsili and Vavilov basin. Rocks include arc-type compositions (shoshonitic to calc-alkaline and arc-tholeiitic), intraplate-type compositions (Na-transitional and alkaline basalt to trachyte), and MORB-type compositions.

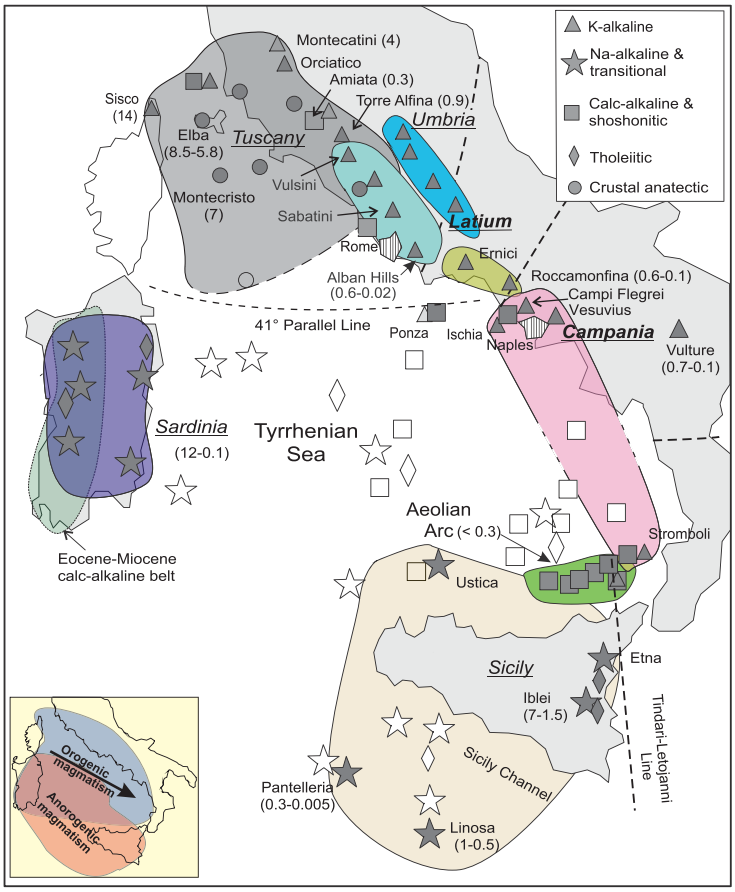

Figure 1.2 Illustration of the different magmatic provinces from Peccerillo and Frezzotti (2015) representing the Plio-Quaternary Italian magmatism. Ages are in Ma between parenthesis. Dashed lines are main tectonic lines.

1.3 The Aeolian Islands

The Aeolian Islands (Fig. 1.3) in the southern Tyrrhenian Sea (Italy) have been a subject of study for centuries, and at present time the archipelago is still an interesting location because of its strong structural, volcanological, and petrological variations.

Many volcanologists, petrologists, and structural geologists have focused on the subaerial Aeolian volcanism, with studies ranging from understanding entire arc evolution through petrology and geochemistry (e.g., Keller, 1974; Barberi et al., 1974; Ellam et al., 1988, 1989; Francalanci et al., 1993, 2007; Tonarini et al., 2001; Schiano et al., 2004; Trua et al., 2004; Peccerillo, 2005; Peccerillo et al., 2013; Peccerillo and Frezzotti, 2015) to understanding its tectonic setting and geodynamics (e.g., Mazzuoli et al., 1995; Gvirtzman and Nur, 1999; De Astis et al., 2003; Trua et al., 2003; Peccerillo, 2005; Panza et al., 2007; Chiarabba et al., 2008; Faccenna et al., 2011; Tumanian et al., 2012; Ventura, 2013) Others concentrated on the geochemical and petrological evolution of a single volcanic system (e.g., Peccerillo and Wu, 1992; Peccerillo et al., 1993, 2004; De Astis et al., 1997, 2000; Gertisser and Keller, 2000; Santo, 2000; Calanchi et al., 2002; Gioncada et al., 2003; Peccerillo et al., 2004; Santo et al., 2004; Tommasini et al., 2007; Santo and Peccerillo, 2008; Davì et al., 2009, 2010; Di Martino et al., 2010, 2011; Doherty et al., 2015; Forni et al., 2015), while different studies tried to understand the plumbing system evolution through thermobarometric investigation using melt inclusion and fluid inclusion (e.g., Gioncada et al., 1998; Frezzotti et al., 2003, 2004; Vaggelli et al., 2003; Zanon et al., 2003; Bonelli et al., 2004; Zanon and Nikogosian, 2004; Peccerillo et al., 2006; Vannucci et al., 2006; Di Martino et al., 2010; Metrich et al., 2009) or based on cell parameters of clinopyroxene phenocrysts (e.g., Nazzareni et al., 2001).

These researches, together with studies focusing on radiogenic age dating (e.g., Gillot and Villari 1980; Beccaluva et al., 1985; Capaldi et al., 1985; Gillot, 1987; Gabbianelli et al., 1990; Crisci et al., 1991; Gillot and Keller, 1993; Santo et al., 1995; De Rosa et al., 2003; Leocat et al., 2009, 2010), xenoliths (e.g., Honnorez and Keller, 1968; Renzulli et al., 2001; Frezzotti el al., 2003, 2004; Zanon and Nikogosian, 2004) and geophysical aspects (e.g., Barberi et al., 1994; Falsaperla et al., 1999; Ventura et al., 1999; Neri et al., 2002; Piromallo and Morelli, 2003; Panza et al., 2004; Billi et

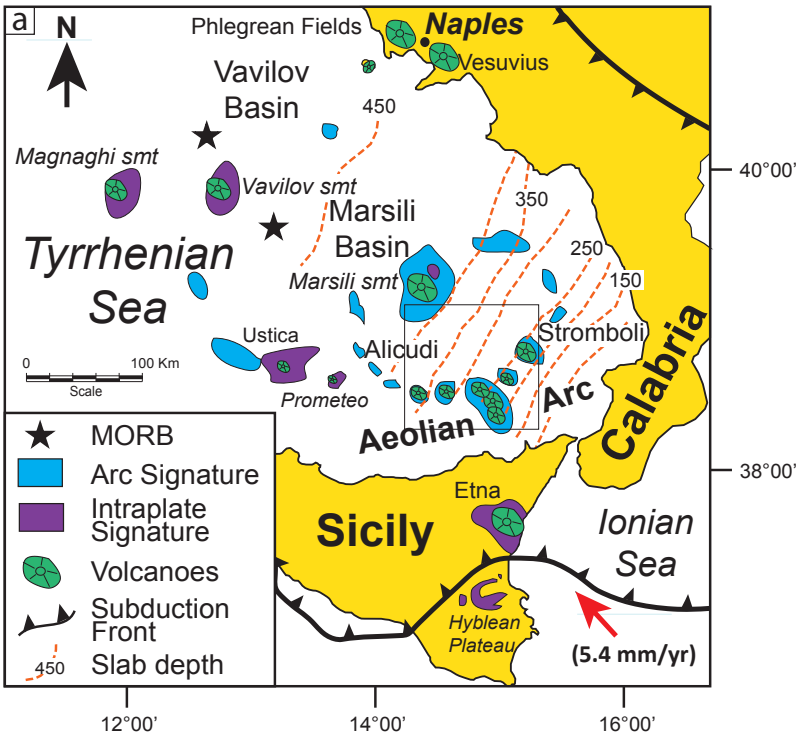

Figure 1.3 Tectonic setting and geochemical signatures of volcanic rocks of the southern Tyrrhenian Sea (Italy). The dominant magma signatures of the main volcanoes are displayed along with the front of the Apennine-Maghrebid fold-and-thrust belt of the central Mediterranean region (after Trua et al., 2007). The depth contours of the Wadati-Benioff zone from Faccenna et al. (2011) are represented with orange dashed lines. The red arrow is a geodetic vector representing the rate of subduction (Faccenna et al., 2011). Abbreviations: smt= seamount

al., 2006; Pontevivo and Panza, 2006), were fundamental chapters in the process for drafting the geological map of every island: *Alicudi* (Villari, 1980a; Manetti et al., 1995a, c; Lucchi et al., 2013d, i); *Filicudi* (Villari, 1980b; Manetti et al., 1988, 1995b, c; Tranne et al., 2002b; Lucchi et al., 2013e, j); *Salina* (Keller, 1980; Gertisser and Keller, 2000; Lucchi et al., 2013a, g); *Lipari* (Crisci et al., 1991; Tranne et al., 2002a; Lucchi et al., 2004, 2010, 2013f; Forni et al., 2013); *Vulcano* (Keller, 1980b; De Astis et al., 2006, 2013a, b); Panarea (Calanchi et al., 1999a, b; Lucchi et al., 2013k, h); and *Stromboli* (Rosi, 1980a, b; Hornig-Kjarsgaard et al., 1993; Keller et al., 1993; Tibaldi and Pasquarè, 2010; Francalanci et al., 2013; Lucchi et al., 2013g).

Understanding the submarine volcanic activity has been also important in developing a comprehensive picture of the arc, with understanding the morphology of submarine portions of

the islands (e.g., Romagnoli et al., 1989, 1993, 2013 and reference therein; Gabbianelli et al., 1990, 1991, 1993; Calanchi et al., 1995; Gamberi et al., 1997, 2006; Bosman et al., 2009; Bortoluzzi et al., 2010; Romagnoli, 2013) and with the seamounts (e.g., Beccaluva et al., 1982, 1985, 1990; Trua et al., 2002, 2004, 2007, 2010, 2011, 2014; Di Roberto et al., 2008; Barca and Trua, 2012; Ventura et al., 2013).

However, despite this important number of studies, there are still some key aspects that need to be understood in order to clarify the complex tectonic and geochemical evolution of this particular region. The present research project provides new geochemical inputs regarding the important within-island and along-arc compositional variations of the Aeolian Islands mafic rocks.

1.3.1 *Geologic and Tectonic Background*

The Aeolian Archipelago is located in the southern Tyrrhenian Sea, north of the Sicilian coast and west of the Calabrian Orogenic Arc (Fig. 1.3). It includes the islands of Alicudi, Filicudi, Salina, Lipari, Vulcano, Panarea, and Stromboli, and several seamounts (e.g., Sisifo, Enarete, Eolo, Lamentini, Alcione and Palinuro) around the Marsili oceanic basin (Fig. 1.4). The islands and seamounts depict a volcanic arc, which has been subdivided into three segments (western, central, and eastern) based on distinct volcanic and structural evidence (De Astis et al., 2003 and references therein; Ventura, 2013). The western segment consists of Alicudi and Filicudi islands and the seamounts to the west, controlled by the WNW–ESE Sisifo-Alicudi Fault System (SA) (Fig. 1b). The volcanism in this segment comprises some of the most primitive lavas of the entire arc with Mg-numbers (molar [MgO/[MgO+FeO]]*100) up to 73 in equilibrium with the mantle (Peccerillo et al., 2004). This segment is currently inactive due to compressional stresses operating west of the NNW–SSE Tindari-Letojanni Fault System (TLF) (Fig. 1.2) that appear to limit magma

ascent (Peccerillo et al., 2004; Ventura, 2013). The central arc segment includes the NNW-aligned Salina, Lipari, and Vulcano islands that are all affected by the TLF (Fig. 1.2), which produces trans-tensional stresses (Ventura, 2013). The eastern arc segment comprises the islands of Panarea and Stromboli (and the seamounts to the north-east) that are strongly influenced by a prevailing NNE–SSW to NE–SW striking fault system responsible for the elongation of dikes and eruptive fissures (Ventura, 2013).

The basement of the Aeolian Arc consists of the Calabrian-Peloritan tectonic terrains (Calabria block; Rottura et al., 1991) related to the European continental plate, whose current position resulted from the opening of the Tyrrhenian Sea during the Miocene-Quaternary. The thickness of the continental crust varies from ≈25 km, under the Calabrian Arc and the western Aeolian Islands, to 10 km, in the Marsili Basin (Piromallo and Morelli, 2003). Deep seismic sounding studies (DSS) define three structural sections in the continental crust. The uppermost

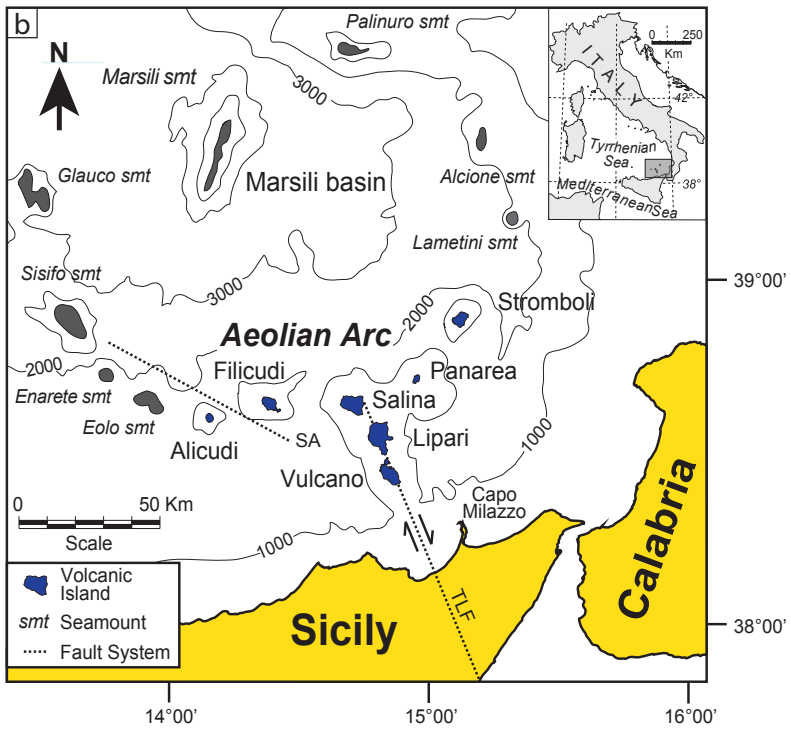

Figure 1.4 Geomorphology and bathymetric features of the Aeolian Arc and surrounding seamounts in the Marsili Basin (modified from Peccerillo et al., 2013). The entire subduction/collision front is represented in the inset map of Italy. Abbreviations: SA= Sisifo-Alicudi Fault System; smt= seamount; TLF= Tindari-Letojanni Fault System.

section consists of 2 km thick layer of unconsolidated sediments and volcanic cover. The middle section consists of 2.5-3 km layer of Calabrian Arc silicic metapelites. The lower section consists of two levels: felsic granulites (5-15 km of depth) and mafic granulites (5-20 km of depth), (Ventura et al., 1999; Peccerillo, 2005).

The lithospheric rifting responsible for the lateral shifting of Calabria block from Sardinia and Corsica blocks to his current position caused the opening of southern Tyrrhenian Sea in late Tortonian. This rifting also leaded to the formation of oceanic domains while the volcanism, due to the subduction of the Ionian lithospheric slab, migrated from W to SE to reach its current position at the Aeolian Islands (Kastens and Mascle, 1990). From Pliocene to Pleistocene new oceanic crust occurred in the Magnaghi-Vavilov back-arc basin and the migration of the subduction front toward SE together with the southern side of Tyrrhenian rifting was controlled by a WNW–ESE striking fault system (Marani and Trua, 2002; Ventura, 2013). From Pleistocene to present, after a change in extensional stress, a NNW–SSE fault system controlled the slab rollback and caused the creation of Marsili back-arc basin followed by the development of the Aeolian Arc (Marani and Trua, 2002; Ventura, 2013). At present time, the occurrence of deep-focus earthquakes beneath the eastern segment of the Aeolian Arc defines the presently active subduction zone (Falsaperla et al., 1999; Panza et al., 2003; 2004). Melting of the mantle wedge above the steep (≈70°) northwest dipping, and rolling-back Ionian slab under the Calabrian Arc is responsible for the Aeolian volcanism (Gvirtzman and Nur, 2001; Chiarabba et al., 2008).

The oldest known volcanic activity in the area was ≈1.3 Ma submarine volcanism at the Sisifo Seamount (Beccaluva et al., 1982), while the Eolo and Enarete seamounts around the Marsili Basin range between 850 – 640 ka in age (Beccaluva et al., 1985). The subaerial volcanic activity began in Salina, Filicudi and Lipari around 250 – 270 ka (Forni et al., 2013; Lucchi et al., 2013a; Lucchi et al., 2013e) and continues at present time in the central–eastern segments of the arc

(Stromboli and Vulcano) above or at the margins of the deep seismicity zone (Panza et al., 2003). The eruptive products show a large variability in composition from east to west. Generally, the initial volcanic activity of the islands was dominated by calc-alkaline (CA) to high K calc-alkaline (HKCA) products that have been emplaced mostly in the western and central sectors of the arc (Alicudi, Filicudi, Salina, Lipari and Panarea). On the other hand, the mature to recent volcanic activity in the eastern and central sectors shows products ranging from shoshonitic to K alkaline composition (De Astis et al., 2003; Peccerillo 2005, Peccerillo et al., 2013; Peccerillo and Frezzotti, 2015). The Marsili seamount has products ranging from CA basalt to basaltic andesite composition with few andesite and arc tholeites on its margin (Trua et al., 2011). The other seamounts show a dominating calc-alkaline mafic to intermediate composition, recording few shoshonites on the Eolo and Enarete seamounts (Trua et al., 2004, Peccerillo 2005).

Geochemical studies on the Marsili Seamount (Trua et al., 2007; 2011) suggest a compositional variation from a dominant arc signature to a younger, sporadic intraplate signature, geochemically similar to the Etna-Hyblean Plateau and related to the African mantle source (Trua et al., 2003). Because of similarities in isotopic and trace element compositions between Alicudi lavas and the intraplate Marsili lavas (Trua et al., 2004; 2011), several authors propose that the western segment of the Aeolian Arc includes some contribution of asthenospheric flow from the northern African mantle into the southern Tyrrhenian mantle wedge around the edges of the subducting Ionian slab (Trua et al., 2003; 2011; Chiarabba et al., 2008). De Astis et al. (2006) also hypothesize that a similar mantle flow from the northeastern side of the slab might be responsible for the alkaline volcanism of Vesuvius and Stromboli. Additionally, Peccerillo (2001) proposes that the eastern segment of the Aeolian Islands might extend to Vesuvius and the Phlegrean Fields, based on compositional affinities (radiogenic isotopes and incompatible element ratios) between the Campanian Province lavas and Stromboli potassic rocks; although U-series disequilibria

suggest the possibility of different metasomatizing components for Stromboli and Vesuvius (Voltaggio et al., 2004; Tommasini et al., 2007; Avanzinelli et al., 2008).

1.4 Scope of the study

This dissertation is addressed to give a contribution in understanding the magma source(s) in the Aeolian archipelago. For this purpose we used high precision olivine chemistry analyses and defined what is the contribution of sediments to the source while understanding the role that subducting components play in the along-arc geochemical signatures variations.

Magmas from the Aeolian Arc display some of the largest along-arc geochemical variations in the world (e.g., Peccerillo, 2005; Peccerillo et al., 2013). Literature data for $^{87}Sr/^{86}Sr$ and $^{143}Nd/^{144}Nd$ isotopes ratios showed a drastic change in these values in less than 90 km along the volcanic front. Current interpretations (Francalanci et al., 2007; Peccerillo et al., 2013) suggest that this signature is controlled by a depleted mantle source at Alicudi with an increasing role for subduction components or crustal contamination from west to east. However, crustal contamination cannot account for the entire geochemical variation along the arc (Ellam and Harmon, 1990; Peccerillo et al., 2004; 2013) because it requires unrealistic extents of assimilation (up to 40% of average Calabrian crust), while at the same time maintaining a primitive basaltic composition in the erupted material (De Astis et al., 2000; Peccerillo, 2005). Therefore, the regional geochemical trends recorded in the mafic lavas in the Aeolian Arc are most likely controlled by the addition of subduction components to the mantle wedge in the form of fluids and/or melts.

We investigated which slab-derived components (i.e., slab fluids or melts derived from the subducting crust and/or sediments) control the extreme along-arc variations in the geochemical

signatures of these magmas using new B, Be, Li, As data from olivine bearing mafic lavas, representative of primitive magmas largely unaffected by crustal contamination (e.g., De Astis et al., 2000; Peccerillo, 2005).

Furthermore, we adopted the minor and trace elements in olivine approach (Sobolev et al., 2007) to characterize the mantle lithologies in order to understand if differences in mantle source compositions might control the along arc variations. We evaluated if a possible influence from a pyroxenitic source at the edges of the arc, in addition to the peridotitic source, could result in the isotopic and geochemical variations described in the literature using high-precision microprobe analyses on olivine crystals from the same samples collected for the B and Be analyses, a technique never applied to the Aeolian Islands mafic magmas.

Chapter 2.
New B - Be and Trace Element Systematics: Discrimination of Subduction Components

2.1 Introduction

The geochemical evolution of the Earth is inherently related to subduction as this process recycles crustal material back into the mantle. The release of slab-derived fluids and melts transports water and other elements in the mantle wedge during progressive subduction, and lowers the solidus, viscosity, and density of the mantle wedge triggering partial melting (e.g. Schmidt and Poli, 1998; Elliott, 2003; Manning, 2004; Hermann et al., 2006; Syracuse et al., 2010; Spandler and Pirard, 2013; Pirard and Hermann, 2014). Element recycling via subduction directly influences the geochemical variability in the deep mantle and contributes to the formation of distinct mantle domains evident in intraplate volcanoes (Zindler and Hart, 1986; Plank and Langmuir, 1993; Rudnick, 1995; Hofmann, 1997; Ryan and Chauvel, 2014).

Compared to intraplate and mid-ocean ridge magmas the typical arc geochemical signature is characterized by the lower abundances of high field strength elements (HFSE) relative to the light rare earth elements (LREE) and the large ion lithophile elements (LILE). This signature depends on the composition and proportion of the different source components (subducting oceanic crust, the overlying sediment, and mantle) and the thermal regime of the subduction system will control the mineral phases stability and the solidus of the subducted material. Variations in these conditions define the stability of key potential mineral phases (e.g, rutile for Ti, Nb and HFSE, garnet for HREE, phengite for LILE, zircon for Zr and Hf, allanite, monazite and apatite for Th, U and REE) resulting in a slab-signal that will manifest differently in every arc

depending on the potential of extracting fluids or melts from the subducting slab (e.g., Hermann, 2002; Hermann et al., 2006; Klimm et al., 2008; Hermann and Rubatto, 2009; Skora and Blundy, 2010; Avanzinelli et al., 2012; Martindale et al., 2013; Skora et al., 2015).

Volcanic arcs are emplaced above subducting oceanic slabs (e.g., van Keken et al., 2011) and in some locations the arc is also accompanied by a back-arc basin spreading center, dominated by extensional stresses and adiabatic decompression melting that can also be influenced by fluids derived from the subducting plate (e.g., Marianas, Izu-Bonin, Tonga-Kermadec, South Sandwich; Elliott et al., 1997; Barry et al., 2006; Turner et al., 2009; Tollstrup et al., 2010). Such a tectonic scenario is also found in the southern Tyrrhenian Sea (Italy), where the Aeolian Volcanic Arc and associated Marsili back-arc basin (Fig. 1.3) resulted from the subduction of the Ionian Plate under the Calabrian Arc (e.g., De Astis et al., 2003; Ventura, 2013; Peccerillo et al., 2013). Current geochemical data for volcanic rocks from the southern Tyrrhenian Sea proximal to the Aeolian Islands highlights the co-existence of mid-ocean ridge basalts (MORB) (i.e., Vavilov basin), intraplate oceanic island basalts (OIB) (i.e., Ustica and Prometeo seamounts) and typical arc geochemical signatures (i.e., Marsili) (Ellam et al., 1989; Beccaluva et al., 1990; Trua et al., 2004; 2011; Peccerillo, 2005) as a result of the tectonic complexity of the region.

Although crustal assimilation can explain localized processes in the genesis of felsic magmas (e.g., record of anatexis process beneath Lipari, Di Martino et al., 2010; 2011), the extreme variations in trace element and isotopic compositions within a single island and along the entire Aeolian volcanic front cannot be explained by crustal interactions (e.g., Peccerillo et al., 2013). Current interpretations for the geochemical variability along this arc include differences in melt sources to regional variations in the degree of partial melting (Ellam et al., 1988; Francalanci et al., 1993; De Astis et al., 2000; Peccerillo, 2005; Peccerillo et al., 2013).

The sediment supply to the central Ionian Sea derives from outflow from the Adriatic Sea and Gulf of Taranto, and turbidity flows of terrigenous sediment from both the African margin and Calabrian Arc (Weldeab et al., 2002). Subducted sediments and altered oceanic crust components play an important role in arc magmatism worldwide (Plank and Langmuir, 1998) and there is a general consensus about the role of subducted components in the genesis of Aeolian magmas (Ellam et al., 1988; Tonarini et al., 2001; Francalanci et al., 2007; Peccerillo et al., 2013). Nonetheless, it is still necessary to discriminate between the effects of subduction-derived fluids and melts, in order to better understand the role that the different subduction-zone contributors play in modifying the mantle wedge and their effects on the volcanic output (e.g., Class et al., 2000; Saginor et al., 2013; Ryan and Chauvel, 2014).

2.2 Materials and methods

During fieldwork, we collected 49 samples on four islands of the Aeolian archipelago: 14 from Alicudi, 6 from Filicudi, 12 from Salina and 17 from Stromboli. We sampled the most mafic magmas, often olivine-bearing basalts, along with olivine-rich tephra, based on studies (e.g., Francalanci et al., 2013; Lucchi et al., 2013a; Lucchi et al., 2013d; Lucchi et al., 2013e) that suggested that the units collected are not only the most mafic but also they do not show any important evidence of crustal contamination. In the fieldwork campaign we did not include the islands of Vulcano and Lipari as the isotopic signature of lavas from these islands clearly points towards a lithospheric component (De Astis et al., 2013; Forni et al., 2013). We revisited outcrops of these well-studied units and collected samples from olivine bearing scoria and lavas with the goal of elucidate the effects of subducted components on the magmas sources and avoid any significant crustal contamination signatures. GPS locations are reported in Table 2A. For additional

geologic background Lucchi et al. (2013c) presents a comprehensive geologic description and history of the Aeolian archipelago and the units selected for this study.

All the samples were processed in the geochemistry laboratory at the Department of Geosciences at Virginia Polytechnic Institute and State University. All rock samples were cut, crushed and sieved. The sieved medium size gravels with abundant and fresh olivines from the best primitive mafic samples, also representative of different potassium (K) trends (high K vs. low K, based on literature reviews for Stromboli), were selected and powdered into 10.5 g aliquots using an alumina mill. These aliquots were then analyzed for major and trace element composition following the procedures described in Mazza et al. (2014). Analyses for Beryllium (Be) and fluid mobile elements, as Boron (B), were also conducted on those same samples.

2.2.1 *Bulk composition*

For major element composition determinations, rock powders were fluxed into homogeneous glass disks with a combination of $Li_2B_4O_7$ $LiBO_2$-LiBr from Spex ® (certified ≪1 ppm blank for all trace elements) and analyzed with X-ray fluorescence (XRF) at Virginia Tech. Additional trace element compositions for samples of Stromboli were collected at Virginia Tech by laser ablation inductively coupled plasma mass spectrometry (LA-ICP-MS) in the same glasses. For the major elements, the relative standard deviation (RSD) for 10 replicates of BHVO-2 was < 1% for all major elements while for AGV-2 was <1% with accuracy better than 2%.

Trace elements were collected from the same fluxed glasses with an Agilent 7500ce ICPMS coupled with a Geolas laser ablation system, with a He flow rate of ≈1 L/m−5 Hz and an energy density on sample ≈7–10 J/cm2. Data were calibrated against USGS standards BHVO-2 and BCR-2, using Ti from XRF as an internal standard and the standard element values reported in Kelley et al.

(2003). The accuracy for 12 replicates of BHVO-2 was better than 5% for all elements except for Sc, Zr, La, Ba (7-9%) and Ga (12%), with precision better than 5% except for Zr (7%). The replicates for BCR-2 display a RSD < 4% for all the elements with the exception of Cu (12%) and Zr (6%), with accuracy better than 6% with the exceptions of Ga, Ba and La (< 10%). Trace elements contents from the island of Alicudi, Filicudi, and Salina were also determined by solution ICP-MS at the USF Center for Geochemical Research at the University of South Florida together with Be and Li contents (also for Stromboli). Sample preparation for ICP-MS follows the analytical method described by Kelley et al. (2003), with sample dissolution by HF-HNO_3 digestion, using distilled acids. Data were calibrated against GSJ (Geological Survey of Japan) standard JB-3 with RSD for 4 replicates <5% for all elements. Errors on the analyses were generally 6% on Be and better than 10% on Li.

2.2.2 *Beryllium and fluid mobile elements*

Boron and arsenic contents were determined by solution ICP-MS at the Center for Geochemical Analysis at the University of South Florida. 0.5 g of each sample was mixed with 2 g of Na_2CO_3 flux (>99.9% purity) in 20 mL Pt crucibles. The covered crucibles were heated in a muffle furnace to 1050 °C (conditions that are not reducing enough to make element compounds that are volatile under fusion conditions, like As hydrides), and then cooled to room temperature. The cooled crucibles were immersed in 80 mL of de-ionized B-free water 180 mL Savillex jars, sealed and placed on a hot plate at 100 °C for 12 hours. Boron and arsenic are separated as part of the water-soluble fraction of the fusion cake (compose of highly water soluble but poorly volatile oxides), along with the heavier alkali metals; other species remain sequestered in the water-insoluble portion. The fusion cakes were extracted from the crucibles with Teflon spatulas, and

rinsed profusely in B-free DI water. The resulting solution was evaporated to ≈20 mL total volume. These solutions were then centrifuged and rinsed for 15 minutes to separate the insolubles, and the supernates were collected in Savillex jars, dried, and re-suspended in 20 mL of B-free water and 5 mL of distilled HNO_3. The acidified solutions were allowed to sit at room temperature for several hours for SiO_2 to precipitate, and were then centrifuged to separate silica, and diluted to 50 g total solution weight using de-ionized B-free water.

Fluid mobile element solutions were analyzed on a Perkin Elmer Elan DRC II Q-ICPMS using a PFA Teflon front end attached to a pure quartz concentric spray chamber. Since the potential for contamination by boron in glass is high, blanks were repeatedly run to ensure that there was no contamination from the sample introduction system. Analytical conditions on the ICP were standard mode for all elements (including As) and tuning was performed by standard routines with special emphasis on low mass elements. Since no chloride matrix was present there was no potential for ArCl interference at mass 75; which was confirmed by our blank analysis. Reproducibility of the As and some of the other volatiles measured in the HF-HNO_3 solution confirm our results from the Na_2CO_3 fusion fluxed method. Errors on analysis were generally 5% on B and better than 10% on As as obtained by replicate analysis of the reference material JB-3. Additionally Rb, Cs, Sr, and Ba were analyzed by this method with good reproducibility on JB-3. Data from the additional elements were compared with analysis by the previous methods with good agreement within the analytical error.

2.3 Results

2.3.1. *Major and trace elements*

A)

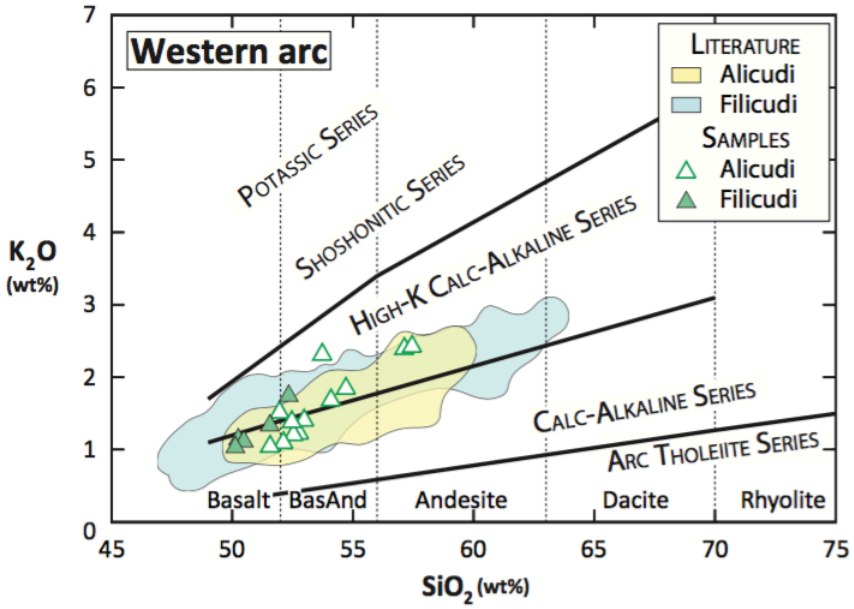
Western arc
Literature
Alicudi
Filicudi
Samples
Alicudi
Filicudi
Potassic Series
Shoshonitic Series
High-K Calc-Alkaline Series
Calc-Alkaline Series
Arc Tholeiite Series
Basalt
BasAnd
Andesite
Dacite
Rhyolite
K2O (wt%)
SiO2 (wt%)

B)

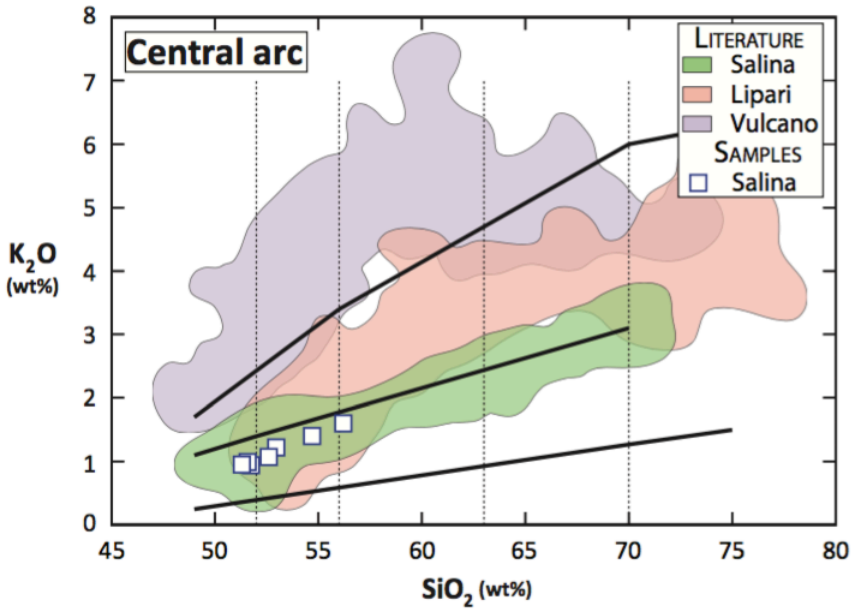
Central arc
Literature
Salina
Lipari
Vulcano
Samples
Salina
K2O (wt%)
SiO2 (wt%)

C)

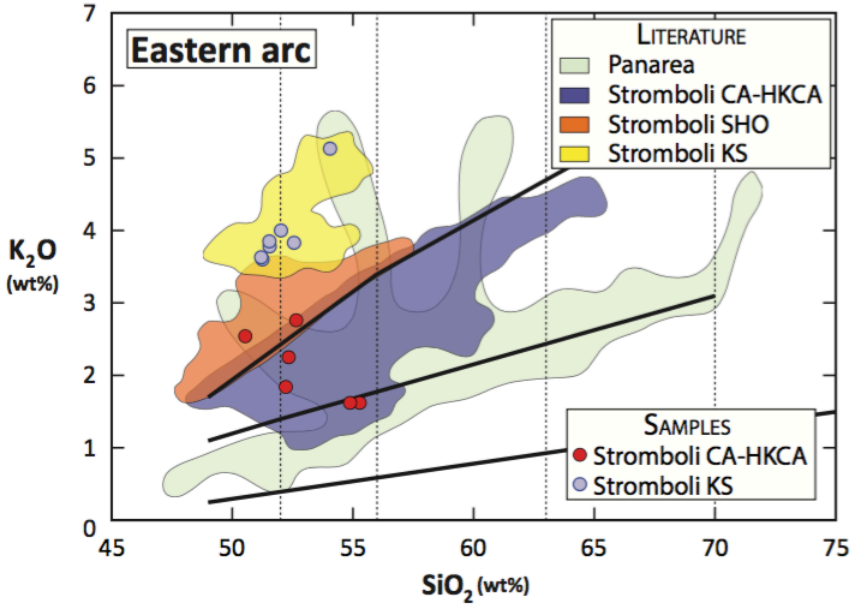
Eastern arc
Literature
Panarea
Stromboli CA-HKCA
Stromboli SHO
Stromboli KS
Samples
Stromboli CA-HKCA
Stromboli KS
K2O (wt%)
SiO2 (wt%)

Figure 2.1 K_2O versus SiO_2 geochemical classification after Peccerillo and Taylor (1976) for the volcanic rocks of the Aeolian Arc showing our new data compared with previous data collected in these islands from the compilation of Lucchi et al. (2013c).

The samples collected range in composition from calc-alkaline to high potassium basalt to andesite. The samples are characterized by porphyritic texture with variable phenocryst content. When plotted in the classic SiO_2 vs K_2O diagram from Peccerillo and Taylor (1976), our new data (Table 2B) have compositions in agreement with previously collected major element data (Fig. 2.1). In the western segment of the Aeolian Arc (Fig. 2.1a), samples from Alicudi vary from basalt to andesite and plot in the calc-alkaline and high potassic calc-alkaline fields. Most of the Filicudi samples are basalts that plot near the boundary between the calc-alkaline and high potassic calc-alkaline series. Samples from Salina in the central arc segment (Fig. 2.1b) are calc-alkaline basalts and basaltic-andesites. In the eastern arc segment, Stromboli displays an important separation between lavas with high potassium contents (K_2O > 3.5 wt%) that belong to the potassic series and other samples that plot in a range between the calc-alkaline and shoshonitic series (Fig. 2.1c), in agreement with the compositional behavior described by Francalanci et al. (2013). Major element trends are consistent with observed mineral phases in the samples that evidence the cotectic crystallization of olivine and clinopyroxene typical of wet arc magmas, characterized by an overall decreasing CaO and MgO and increasing Al_2O_3 during fractionation (e.g., Zimmer et al., 2010).

Fluids and melts derived from subducting sediments and oceanic lithosphere are known to be responsible for the chemical and rheological modification of the mantle wedge in subduction systems (e.g., Ryan and Langmuir, 1993; Elliott et al., 1997; Johnson and Plank, 1999; Kelemen et al., 2003; Eiler et al., 2005; Kimura et al., 2008; Gazel et al., 2009; Hermann and Rubatto, 2009; Saginor et al., 2013; Martin et al., 2014; Gazel et al., 2015). Although at higher P-T conditions the distinction between fluids and melts may not be possible if the system reaches a supercritical fluid phase (Manning, 2004; Kessel et al., 2005; Pirard and Hermann, 2014). Kawamoto et al. (2012)

demonstrated that a supercritical fluid derived from the slab could separate to form fluid and melt components in most subduction zones. Therefore we can use trace elements that are compatible in either hydrous fluids or melts to discriminate between these two subduction components. For

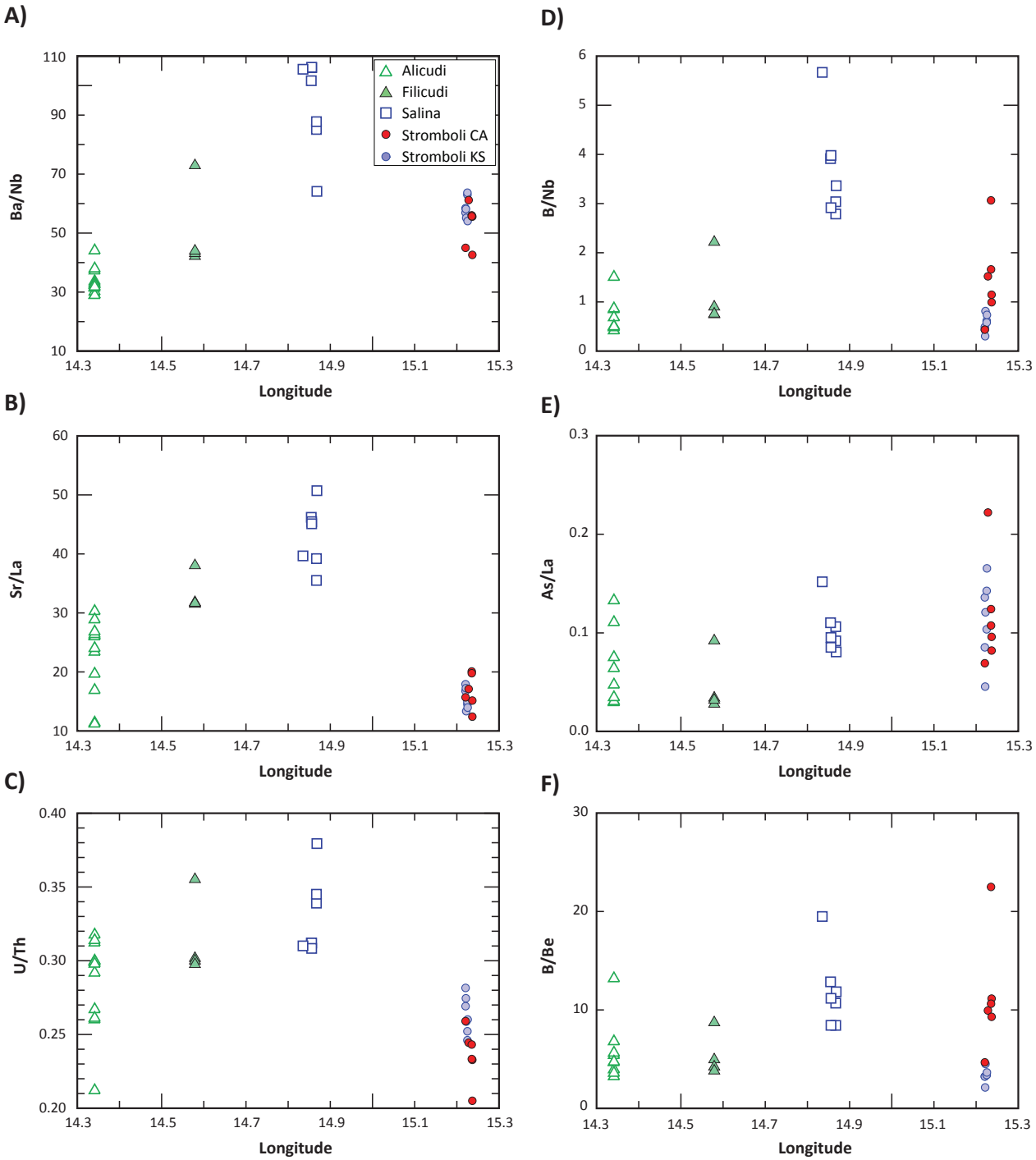

Figure 2.2 Regional along-arc variations of elements mobilized by hydrous fluids (e.g., Ba, Sr, U, B, As) over elements soluble in melts (e.g., Nb, Th, Be) for the Aeolian samples of this study. Note how the central segment of the arc has higher fluid/melt ratios while the peripheral arc segments are controlled by melt soluble elements.

instance, the high field strength elements (HFSE, e.g., Nb, Ta, Zr, Th) and middle to heavy rare earth elements (REE) preferentially partition into melts. The alkali metals (e.g., K, Rb), the alkaline earth metals (e.g., Ba, Sr) and U are soluble-lithophile elements because hydrous fluids preferentially mobilize these elements. Similarly, light REE (e.g., La) are mobilized more easily by hydrous fluid than the rest of the REE (Brenan et al., 1995; Johnson and Plank, 1999; Elliott, 2003; Turner et al., 2003).

Once elemental behaviors are understood, then element ratios can be used to minimize the effect of partial melting and fractionation processes on the determination of geochemical signatures. For example, commonly used ratios of elements mobilized by subduction related fluids to those mobilized only in melts (e.g., Ba/Nb, U/Th, Sr/La) are highest in the central segment of the Aeolian Arc (Salina), while for the external islands (particularly Stromboli) these ratios are low, consistent with the increased contribution of silicate melt components (Fig. 2.2). These along-arc variations suggest that fluids play a major role in element transport into the mantle wedge beneath the central region of the arc (Salina), while under Stromboli and, to a lesser extent under Alicudi, a silicate melt is the dominant contributing component. Based on isotopic evidence Tonarini et al. (2001) also suggested the important role of a hydrous fluid component in the magma genesis in the central sector of the Aeolian arc.

2.3.2 *Boron and Beryllium*

We further explored the trace element systematics by the use of additional fluid mobile elements (e.g., B, As, Li), and Be a melt-soluble element, as geochemical indicators of subduction components (Fig. 2.3) (Leeman, 1996; Ryan et al., 1996a) with the goal to better discriminate

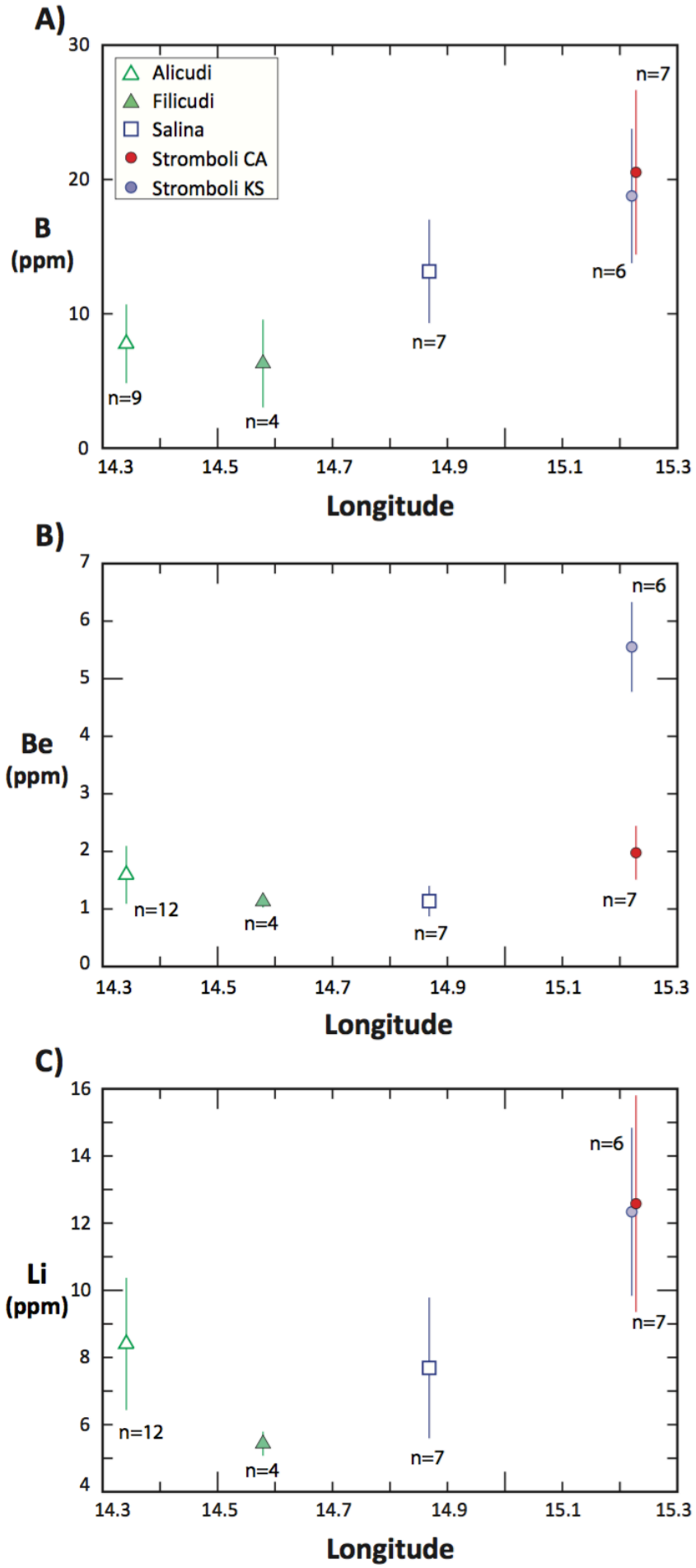
A)
Alicudi
Filicudi
Salina
Stromboli CA
Stromboli KS
B (ppm)
n=9
n=4
n=7
n=6
n=7
Longitude
B)
Be (ppm)
n=12
n=4
n=7
n=7
n=6
Longitude
C)
Li (ppm)
n=12
n=4
n=7
n=6
n=7
Longitude

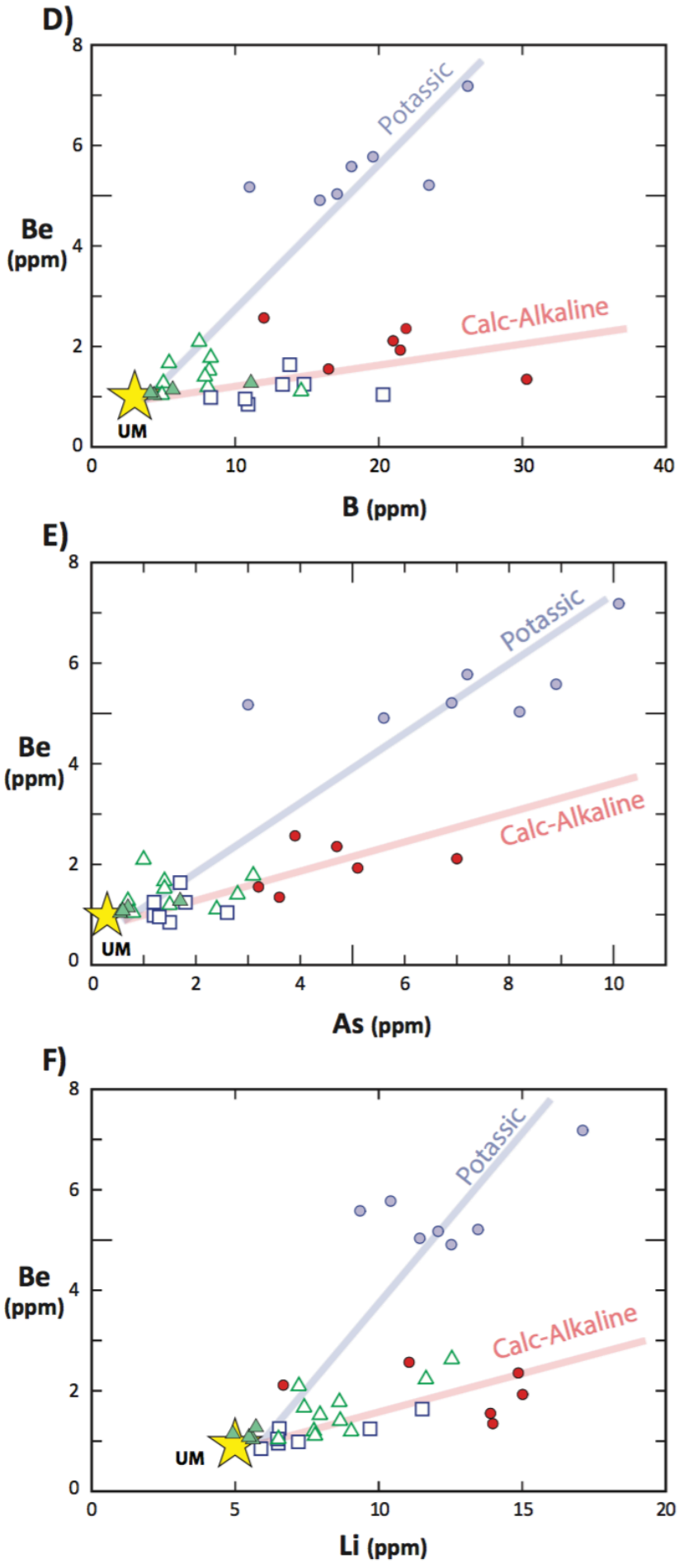
D)
Be (ppm)
B (ppm)
Potassic
Calc-Alkaline
UM
E)
Be (ppm)
As (ppm)
Potassic
Calc-Alkaline
UM
F)
Be (ppm)
Li (ppm)
Potassic
Calc-Alkaline
UM

Figure 2.3 Regional along-arc variations of B (a), Be (b) and Li (c) for the Aeolian volcanic rocks collected in this study. Note the two trends between the calc-alkaline and potassic units in (d), (e) and (f) with respect to the average B, Be, Li and As contents in the upper mantle derived melts (UM). Upper mantle melts consist of MORB values from Gale et al. (2013) and White and Klein, (2014), and OIB values from Ryan et al. (1996b) and Krienitz et al. (2012). No significant studies qualitatively measure As in MORB or intraplate magmas, thus we assume that the composition of these melts will plot at the convergence of the two trends as evident in the other elements. n= number of samples.

between slab derived fluid and melt signatures in the Aeolian Arc. While B and As mobilize in slab fluids starting very early in the subduction process, Li is largely retained on the slab until temperatures increase, and it is also retained in the mantle wedge much better than B or As, because it can substitute for Mg (Bebout et al., 1999; Bebout, 2007; Savov et al., 2005; 2007). Boron and Be are most likely going to be hosted by phengitic white micas in the subducting slab, but due to B high mobility in fluids while Be is going to be strongly retained in phengite and only mobilized by melts (e.g., Bebout et al., 1999), then their relative concentration in resulting arc magmas are powerful indicators of the role of fluids vs melt components in subduction zones. Arsenic behaves in slab metasediments very much like B, so we can infer that its phengite-fluid partitioning behavior is similar to B. Additionally, neither B or Be are going to be impacted by accessory phases like tourmaline and beryl as these phases are only stable under extreme high silica concentrations (London and Evensen, 2002; Marschall et al., 2009). Arsenic concentrations can be strongly controlled by segregating sulfide phases, but the oxidized nature of volcanic arc melts generally suppresses sulfide during fractional crystallization (Hattori et al., 2002).

Our new B, Be, Li, and As data are reported in Table 2D and average values are plotted in Figure 2.3a, b, c to highlight the regional variations of these elements along the volcanic front. The Aeolian Arc shows varying B abundances, increasing from west to east, with Alicudi and Filicudi characterized by the lowest average B contents (≈7 ppm) and Stromboli showing the highest (19.6 ppm). Samples from Salina and Filicudi have the lowest average Be concentrations (1.1 ppm), while Alicudi and Stromboli samples have the highest (1.6 and 3.9 ppm, respectively). The

maximum Be contents in the range 4.9-7.2 ppm are found in the potassic rocks of Stromboli and are ≈5 times greater than any other island in the Aeolian Arc. Lithium and arsenic (not shown) contents vary similarly to B, increasing from west to east along the arc with the highest values in Stromboli. When fluid mobile elements (B, As and Li) are plotted against Be, there is a clear bimodal behavior with distinct trends for the calc-alkaline rocks and the potassic samples of Stromboli (Fig. 2.3d, e, f).

Boron is particularly useful as it is strongly enriched in marine sediments and altered oceanic crust, and is extremely depleted in the upper mantle (Leeman and Sisson, 1996; Bebout et al., 1999; Plank, 2014; Ryan and Chauvel, 2014). The general increase in B contents toward the eastern segment of the Aeolian Arc (Fig. 2.3a) is best explained by hydrous fluid inputs derived from the dehydrating subducting slab and sediments, as also evident by other trace element systematics (Fig. 2.2a-c). Boron enrichment can be evaluated also in details with B/Nb and B/Be ratios (Fig. 2.2d, f), because these ratios reflect the extent of influence of fluid-related process more than varying extents of partial melting and fractional crystallization. B/Nb and B/Be increase from west to east reaching a peak in Salina and then drop in Stromboli. This “chevron pattern” indicates that the degree of enrichment of boron is higher in Salina and lower at the peripheral islands regardless of the element concentration that can be controlled by degree of melting of fractional crystallization. A very similar trend is also observed for the other fluid mobile elements (e.g., Li/Nb) along the volcanic front; nevertheless, As (e.g., As/La, Fig. 2.2e) shows an overall increase from east to west.

Typically B and other fluid-mobile elements (e.g. As, Sb) are also highly enriched in serpentinite, which is a very important component in a shallow mantle wedge due to its strong enrichment in water and its consequently important role in triggering melt in sub-arc mantle depths due to processes of dehydration (Scambelluri and Tonarini, 2012). Although the extent of

mobilization of these elements via low-temperature hydrous fluid can be considerable (as much as 70% of the slab budget for B and >15% for As; Savov et al., 2005; 2007), a serpentinite component appears not to be involved in the genesis of the Aeolian Arc magmas. This consideration can be deduced by the B isotopic data presented by Tonarini et al. (2001), in which the value of $\delta^{11}B$ are too low (-6.1 to +2.3‰) to be derived from a serpentinite source, in contrast to the high B isotopic values (up to +18‰) that would be characteristic of a serpentinite-derived fluid (e.g., Benton et al., 2001), and the generally elevated $\delta^{11}B$ signatures of B-enriched arcs such as South Sandwich (Tonarini et al., 2011), the Izu-Bonin-Mariana (Ishikawa and Nakamura, 1994; Ishikawa and Tera, 1999; Straub and Layne, 2002) and the Kuril-Kamchatka (Ishikawa and Tera, 1997; Ishikawa et al., 2001). The global compilation of volcanic arc B and $\delta^{11}B$ data in Ryan and Chauvel (2014) demonstrates a dichotomy in subduction systems, correlated to their overall thermal structures, in which most show evidence for the involvement of a high B, high $\delta^{11}B$ component, consistent with serpentinite-derived fluids, with a few "hot" systems (e.g. Cascades, Mexico) in which this component appears to play no role, due perhaps to the release of B early enough during subduction that it is not carried to mantle depths (see additional discussion in Section 2.4).

Beryllium is typically concentrated in marine sediments, and is very depleted in the upper mantle, mimicking the terrestrial distribution pattern of boron (Morris et al., 1990; Ryan, 2002; Plank, 2014; Ryan and Chauvel, 2014). Although Be is also a light element, it is very different from boron in terms of behavior, in that it is immobile in hydrous fluids but highly mobile in silicate melts derived from a subducting slab (Brenan et al., 1998; Ryan, 2002). Although, the beryllium contents in calc-alkaline lavas from across the Aeolian Arc are largely similar (Fig. 2.3b), it is strongly enriched in the potassic samples from Stromboli (Fig. 2.3b), as are other incompatible trace elements. This behavior can be explained by partial melting of a source that is broadly enriched in incompatible trace elements, including Be. Thus, we suggest that this source is

consistent with subducted sediments transported into the mantle wedge by the Ionian slab. The role of silicate melts in Stromboli is also evident when Be contents of different islands are plotted against B in respect to Upper Mantle (UP) values (Fig. 2.3d). Due to the different compositional trends displayed in Figure 2.3d, we suggest two different sources for the calc-alkaline and potassic rocks of Stromboli (in agreement with other geochemical tracers used by Tommasini et al., 2007 and Francalanci et al., 2013): 1) a fluid component derived from the oceanic slab for the calc-alkaline magmas and 2) a sediment melt component for the potassic rocks. The potassic lavas of Stromboli show high Th/Ce and low $^{143}Nd/^{144}Nd$ as compared to the other islands of the Aeolian Arc (Francalanci et al., 2007), a clear signature of the influence of a sediment melt component (Elliott et al., 1997; Hawkesworth et al., 1997; Johnson and Plank, 1999; Class et al., 2000).

Similarities in the trends of other fluid mobile elements (e.g., As and Li) relative to B vs. Be (Fig. 2.3e, f) provide additional evidence for a clear separation between the two magmatic end-members in this arc. Figure 2.2d shows that values in B/Nb, with a peak found at Salina, are similar to the values reported by Ryan et al. (1996b), in which the partition coefficients of B and Nb are very similar (DB≈DNb). Also, the fact that the Li/Nb and K/La both show patterns similar to those of the B/Nb and B/La suggests that the slab component being sampled in this area is enriched in alkali elements. Furthermore, the Be/Nd ratio for Alicudi, Filicudi and Salina rocks varies slightly from the global arc ratio (≈0.05, Ryan and Langmuir, 1988), while Stromboli basalts are characterized by higher ratios relative to typical arc magmas.

In order to explain the higher values for Be and Nb in the potassic lavas from Stromboli (Table 2C, 2D), the sediment-melt component must be dominant in the genesis of these lavas. Experimental work suggested that silica-undersaturated alkaline arc lavas could be produced via the reaction of sediment-derived siliceous melt with peridotite in the mantle wedge (Avanzinelli et al., 2008; Mallik and Dasgupta, 2013). More recently, an experimental study by Mallik et al. (2015)

demonstrated that ultrapotassic magmas (resembling the ones from Stromboli) could be generated by mantle reaction with hydrous sediment-derived melts. Mallik et al. indicated that during reactions between hydrous sediment-derived partial melts of rhyolitic composition and peridotite, the stabilization of orthopyroxene and phlogopite reduces the silica content of the melt and buffers the composition toward higher K_2O contents, yielding compositions resembling the ultrapotassic lavas from the Sunda Arc and from the Roman Magmatic Province.

2.4 Contrasting the Aeolian Arc with other global volcanic arc examples

Understanding how these new data fit into global systematics of volcanic arcs is the key for the interpretation of the geodynamic complexity of the Aeolian Arc. We have compared our new B, Be, and trace element data with samples from the Phlegrean Fields, along with other well studied volcanic arcs and arc segments in the world by assembling a dataset via the GEOROC database (*http://georoc.mpch-mainz. gwdg.de/georoc/*) accessed in February 2015.

Boron enrichments in Aeolian Arc lavas are consistently low, with B/Be ratios ranging between ≈2 and 15 in most samples (Fig. 2.2f). This makes the Aeolian Arc comparable to the Cascades and the Mexican Volcanic Belt arcs as "low boron" subduction systems, a trait that is also evident in its B-isotopic systematics (e.g., Tonarini et al., 2001). These similarities are clear in Figure 2.4a, a plot of Th/Nb vs. La/Nb, in which mixing between potential end-members will form linear arrays. This plot allows us to distinguish between melt components (high Th/Nb and low La/Nb) and fluid components (low Th/Nb and high La/Nb) as slab-derived metasomatizing agents in the different arcs. In this diagram the Stromboli data overlap with data for the Sunda Arc, the Phlegrean Fields, and partially with the Cascades data along a trend controlled by a melt-dominated component, clearly separating from the other Aeolian Islands, which display increasing

La/Nb, from west to east. Alicudi, Filicudi, and Salina overlap the data field for the Aleutian Arc, and part of the Marianas and the Mexican Volcanic Belt, indicating a transitional nature between the melt and fluid trends. Meanwhile, the fluid component dominates in the Izu-Bonin, Marianas and Tonga Arcs. Comparable behaviors can also be inferred from a plot of Th/Nb vs. Ba/Nb (Fig. 2.4b).

Figure 2.4c plots B/Nb vs. Th/Nd to further discriminate between fluid and melt components. B/Nb is a tracer of slab fluid released by dehydration of sediment and altered oceanic crust (Ishikawa and Tera, 1997) while Th/Nd is a tracer of sediment melt in arc magmas (Class et al., 2000). The curved line represents a mixing between a potential fluid-controlled end-member (represented by Izu Bonin samples), and a melt-dominated end-member (represented by the Sunda Arc, Phlegrean Fields, and Stromboli). The fact that the arc samples included in this comparison plot between these end-members suggests that in all arcs worldwide slab-derived fluids and melts are responsible in different proportions for the subduction-related elemental enrichments seen in arc lavas. The dominant component will depend on the thermal structure of the arc, as is evident in arc B/La vs. Ba/La systematics (Fig. 2.4d; see Ryan and Chauvel, 2014). The Aeolian suite forms a trend at low B/La consistent with the mixing of a "hot" slab-derived B source and the upper mantle (Ryan and Chauvel, 2014). The fluid-mobile element systematics of Aeolian lavas are thus different from those volcanic arcs such as Izu-Bonin, Marianas and Central America (Honduras-Nicaragua) as there is no evidence for the involvement of a "cool" slab-derived B source, suggested to involve contributions from subduction-related serpentinite (e.g., Straub and Layne, 2002; Savov et al., 2005; 2007; Hattori and Guillot, 2007; Tonarini et al., 2007; Ryan and Chauvel, 2014). While the "cool" fluid-mobile element component is not evident in Aeolian lavas, the fact that they nonetheless show boron enrichment indicates that a slab-derived fluid component is involved.

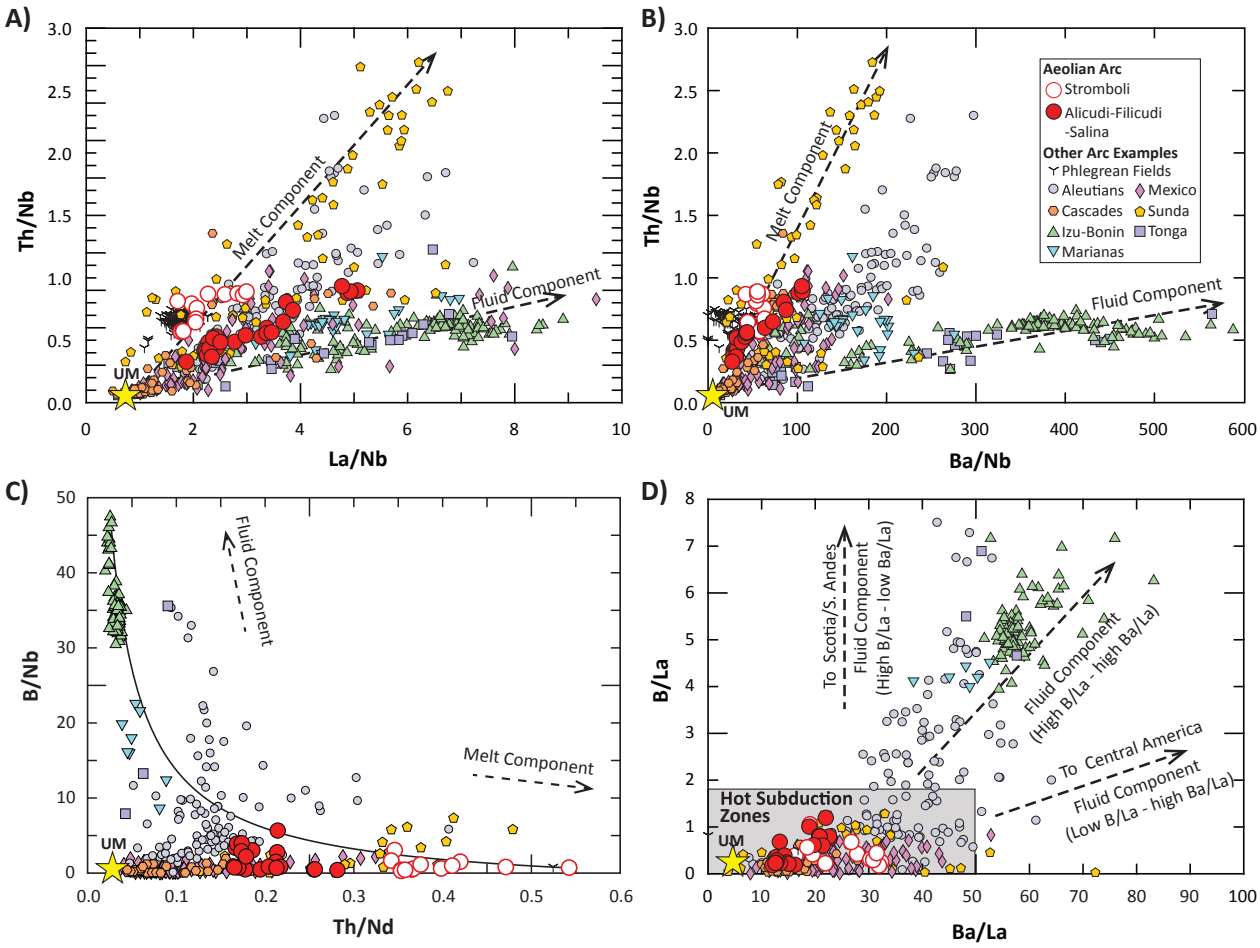

Figure 2.4 Element ratios discriminating between slab-derived fluid components vs. melt components. Different elements ratios (Th/Nb, La/Nb, Ba/Nb, B/Nb, and Th/Nd) are used to discriminate between sediment melts and slab-fluid components for volcanic arcs/arc segments (a, b, c). In (c) the curve represents a binary mixing between a fluid (Izu-Bonin) and melt (Stromboli, Phlegrean Fields and Sunda) end-member. In (d) low values of B/La and Ba/La define the "hot subduction zones" where fluid mobile elements get removed early during subduction processes as described by Ryan and Chauvel (2014). Global data for the Phlegrean Fields, Aleutians, Izu-Bonin, Tonga, Sunda, Marianas, Mexican Volcanic Belt, and Cascades are from the GEOROC geochemical database (*http://georoc.mpch-mainz.gwdg.de/georoc/*). Upper Mantle (UM) derived melts are from the same reference sources as in Fig. 3.

2.5 Geodynamic implications

Global thermal models for subduction systems from Syracuse et al. (2010) describe different pressure-temperature (P-T) paths of subducting slabs using kinematically defined slabs based on physical parameters (e.g., slab geometries, ages, convergence velocities). This portrays the subduction of the Ionian slab beneath Calabria as one of the coldest subduction zones on

Earth (Fig. 2.5) but this observation is not consistent with the observed geochemical signatures, which suggest a substantial sediment melt component, as the slab P-T path will not even cross the water saturated sediment solidus (Fig. 2.5). Nevertheless, Syracuse et al. (2010) results come from a two-dimensional model that does not consider the 3D complications of lateral or trench-parallel asthenospheric mantle flow, due to slab rollback or slab windows, (Buttles and Olson, 1998; Stegman et al., 2006; Schellart, 2008), a process that may exist in many subduction systems, like Sunda Arc (Richards et al., 2007; Whittaker et al., 2007; Kundu and Gahalaut, 2011), the northern segment of the Cascades (Mullen and Weis, 2015), and the heterogeneous mantle under the Mexican Volcanic Belt and Southern Central America (Ferrari, 2004; Gazel et al., 2011; Ferrari et al., 2012).

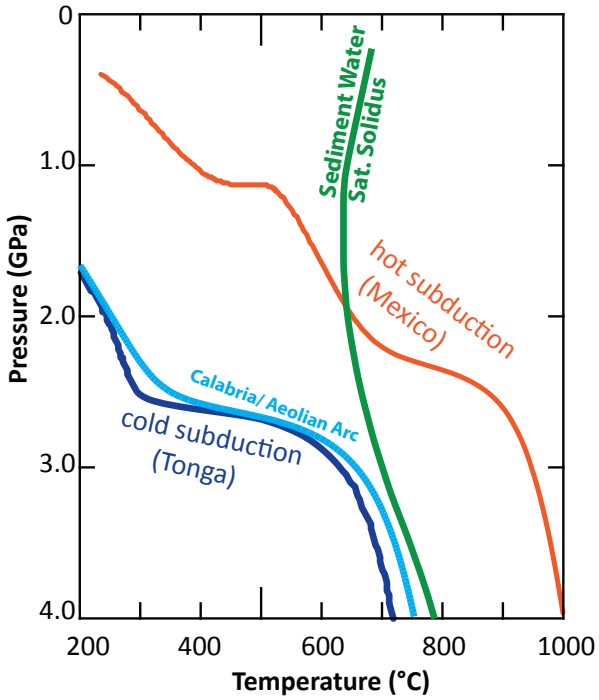

Figure 2.5 Pressure-temperature diagram for the Aeolian Arc (Calabria) subducting slab from Syracuse et al. (2010) compared to a cold subduction zone end-member (Tonga) and a hot subducting zone end-member (Mexico). Note that according to the numerical models the Ionian slab does not intersect the water saturated-sediment solidus (from Mann and Schmidt, 2015). Thus, in order to have sediment melt signatures we need another process that will either increase the temperature of the slab or cause the separation of sediment diapirs that will cross the solidus before the slab gets dehydrated.

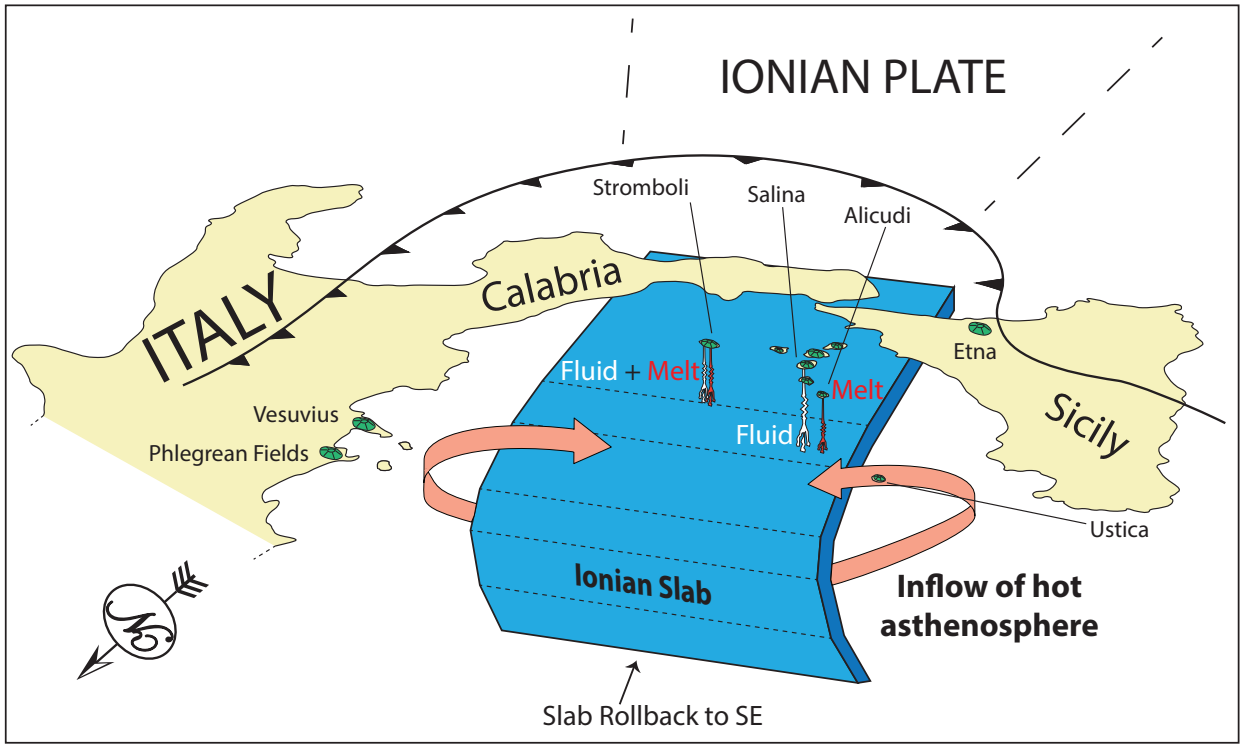

Figure 2.6 Schematic model representing the Ionian slab subduction system below the Aeolian Arc modified from Trua et al. (2007). Orange arrows indicate the asthenospheric mantle inflow over the edges of the Ionian Plate rollbacking towards the SE. The predominant melt components are represented in red under Stromboli and Alicudi. The predominant fluid component is represented in white under Stromboli and Salina.

Seismic studies and numerical models in the southern Tyrrhenian area (Chiarabba et al., 2008; Baccheschi et al., 2008; 2011; Faccenna et al., 2011; Neri et al., 2012) suggest the presence of African-related asthenospheric flow around the edges of the narrow Ionian Plate due to a slab tear caused by the rollback motion of the Ionian slab (Gvirtzman and Nur, 1999; Gutscher et al., 2016), which heavily affected the mantle wedge of the Aeolian Arc (e.g., Faccenna et al., 2011). Also, recent work by Chen et al. (2015) based on dynamic laboratory models of progressive subduction in three-dimensional space, highlights the possibility of a toroidal asthenosphere return flow induced by the slab rollback of the Ionian Plate. Our new data confirm a sediment melt component at the edges of the arc, possibly connected to hot asthenosphere flow at the edges of the slab that may be responsible for the melt signature (Fig. 2.6). Alternatively, buoyant diapirs of slab material can potentially detach from the subducting slab and enter a regime of elevated

temperatures in the mantle wedge that will cause devolatilization and melting of such rocks and the deliver of the different slab component signatures (Hacker et al., 2011; Marschall and Schumacher, 2012). Nevertheless this model still does not explain the systematic variations in the different arc segments of the Aeolian arc (one section of the arc is controlled by hydrous fluids and another is controlled by both slab melts and fluids components), which does not exclude the presence of hot asthenosphere flow at the edge of the subducting slab and/or parallel to the trench.

Table 2A *GPS locations and lithology of the samples*

Sample	Island	Latitude (°N)	Longitude (°E)	Formation*	Lithology
SL-13-01	Salina	38.54760	14.86819	CALDARA	Basaltic andesite
SL-13-02	Salina	38.55119	14.86712	VALLONE DEI ZAPPINI	Basaltic andesite
SL-13-03	Salina	38.55119	14.86712	VALLONE DEI ZAPPINI	Basaltic andesite
SL-13-05	Salina	38.57301	14.85487	VALLONE DELLA FONTANA	Basalt
SL-13-07	Salina	38.57330	14.85583	VALLONE DELLA FONTANA	Basalt
SL-13-08	Salina	38.57330	14.85583	VALLONE DELLA FONTANA	Basalt
SL-13-09	Salina	38.56810	14.83519	SERRO FAVAROLO	Basalt
AL-13-01	Alicudi	38.54174	14.34124	SCOGLIO GALERA I	Basaltic andesite
AL-13-02	Alicudi	38.54174	14.34124	SCOGLIO GALERA I	Basalt
AL-13-03	Alicudi	38.54174	14.34124	SCOGLIO GALERA I	Basalt
AL-13-04	Alicudi	38.54174	14.34124	SCOGLIO GALERA I	Basaltic andesite
AL-13-05	Alicudi	38.54174	14.34124	SCOGLIO GALERA I	Basalt
AL-13-06	Alicudi	38.54174	14.34124	SCOGLIO GALERA I	Andesite
AL-13-07	Alicudi	38.54174	14.34124	SCOGLIO GALERA I	Basalt
AL-13-08	Alicudi	38.54174	14.34124	SCOGLIO GALERA I	Basalt
AL-13-09	Alicudi	38.54174	14.34124	SCOGLIO GALERA I	Basaltic andesite
AL-13-12	Alicudi	38.54174	14.34124	SCOGLIO GALERA I	Andesite
AL-13-13	Alicudi	38.54174	14.34124	SCOGLIO GALERA I	Basaltic andesite
AL-13-14	Alicudi	38.54174	14.34124	PUNTA DI MALAPASSO	Basalt
FL-13-02	Filicudi	38.55825	14.57902	MONTEGUARDIA	Basalt
FL-13-03A	Filicudi	38.55825	14.57902	MONTEGUARDIA	Basalt
FL-13-03B	Filicudi	38.55825	14.57902	MONTEGUARDIA	Basalt
FL-13-05	Filicudi	38.55825	14.57902	MONTEGUARDIA	Basalt
FIL 24	Filicudi	38.58224	14.52708	SCOGLIO DI MONTENASSARI	Basalt
ST-13-01	Stromboli	38.81190	15.22066	PUNTA LA BRONZO	Basalt
ST-13-02	Stromboli	38.81190	15.22066	PUNTA LA BRONZO	Basalt
ST-13-03	Stromboli	38.81190	15.22066	L'OMO	Basalt
ST-13-04	Stromboli	38.81181	15.22144	SERRO ADORNO	Basalt
ST-13-05	Stromboli	38.81146	15.22223	FILO DEL FUOCO	Basaltic andesite
ST-13-06	Stromboli	38.81054	15.22503	PISCITA	Basalt
ST-13-07	Stromboli	38.81054	15.22503	GINOSTRA	Basalt
ST-13-08	Stromboli	38.81038	15.22556	VALLONAZZO	Basaltic andesite
ST-13-09	Stromboli	38.81037	15.22799	SAN BARTOLO	Basalt
ST-13-11	Stromboli	38.79622	15.23671	CAVONI (Member A)	Basaltic andesite
ST-13-13	Stromboli	38.79611	15.23668	CAVONI	Basaltic andesite
ST-13-16	Stromboli	38.79284	15.23529	L'OMO	Basaltic andesite
ST-13-17	Stromboli	38.79293	15.23538	L'OMO	Basaltic andesite

**Geologic formations from Lucchi et al. (2013b, g, i, j)*

Table 2B

XRF (Virginia Tech)

Standard	**BHVO-2 (N=10)**				**AGV-2 (N=10)**			
Analyte	**Avg (wt%)**	**STD 1σ**	**RSD**	**Accepted Value***	**Avg (wt%)**	**STD 1σ**	**RSD**	**Accepted Value***
SiO_2	49.66	0.11	0.21	49.90	60.22	0.36	0.60	59.30
TiO_2	2.71	0.01	0.26	2.73	1.06	0.00	0.28	1.05
Al_2O_3	13.57	0.04	0.31	13.50	17.00	0.07	0.41	16.91
Fe_2O_3	12.12	0.04	0.35	12.30	6.75	0.02	0.30	6.69
MnO	0.16	0.00	0.43	0.17	0.10	0.00	0.89	0.10
MgO	7.37	0.01	0.19	7.23	1.81	0.02	1.10	1.79
CaO	11.29	0.04	0.31	11.40	5.24	0.01	0.19	5.20
Na_2O	2.06	0.01	0.69	2.22	4.27	0.04	0.94	4.19
K_2O	0.51	0.01	1.40	0.52	2.89	0.01	0.24	2.88
P_2O_5	0.259	0.002	0.82	0.27	0.47	0.01	1.06	0.48
Total	99.693			100.24	99.81			98.59

LA-ICP-MS (Virginia Tech)

Standard	**BHVO-2 (N=12)**				**BCR-2 (N=12)**			
Analyte	**Avg (ppm)**	**STD 1σ**	**RSD**	**Accepted Value***	**Avg (ppm)**	**STD 1σ**	**RSD**	**Accepted Value***
P_2O_5 (wt%)	0.25	0.00	0.78	0.27	0.31	0.00	0.84	0.35
Sc	33.28	0.48	1.45	30.80	36.87	0.26	0.72	34.54
TiO_2 (wt%)	2.62	0.00	0.00	2.62	2.29	0.00	0.00	2.29
V	285.41	2.55	0.89	289.00	394.89	5.18	1.31	388.90
Cr	287.18	2.38	0.83	289.80	-	-	-	13.79
FeO (wt%)	10.94	0.03	0.26	11.07	12.96	0.06	0.44	12.42
Co	42.75	0.21	0.49	43.00	38.05	0.16	0.42	39.30
Ni	110.94	0.93	0.84	111.00	-	-	-	10.36
Cu	129.28	1.09	0.84	133.00	28.84	3.55	12.32	28.53
Zn	100.58	3.49	3.47	99.00	143.94	2.01	1.39	152.09
Ga	18.62	0.18	0.98	21.20	35.95	0.17	0.48	33.10
Rb	9.91	0.26	2.65	9.80	50.44	1.48	2.93	52.50
Sr	405.19	1.31	0.32	391.00	361.53	3.13	0.86	348.10
Y	26.09	0.34	1.32	26.40	38.60	0.30	0.78	38.40
Zr	168.19	12.51	7.44	184.00	197.25	11.70	5.93	208.90
Nb	18.92	0.37	1.96	19.50	13.93	0.25	1.80	14.00
Cs	0.14	-	-	0.10	1.19	0.03	2.29	1.19
Ba	140.53	0.88	0.63	129.07	736.36	1.75	0.24	670.00
La	15.80	0.32	2.01	14.79	27.44	0.92	3.34	25.50
Ce	37.00	0.04	0.10	37.26	55.44	0.39	0.70	55.10
Pr	5.58	0.04	0.70	5.40	7.51	0.14	1.87	7.10
Nd	25.40	0.19	0.75	24.25	31.30	0.64	2.06	30.00
Sm	6.07	0.01	0.20	6.00	7.04	0.09	1.27	6.90
Eu	2.01	0.01	0.63	1.96	2.05	0.01	0.58	2.10
Gd	6.28	0.14	2.25	6.35	7.38	0.07	1.01	7.50
Tb	0.96	0.01	0.74	0.96	1.17	0.00	0.15	1.16
Dy	5.37	0.06	1.12	5.39	7.01	0.04	0.57	6.99

Ho	0.98	0.02	2.46	1.00		1.41	0.02	1.22	1.40
Er	2.44	0.07	3.02	2.49		3.86	0.05	1.28	3.87
Tm	0.31	0.01	2.60	0.33		0.53	0.01	0.96	0.51
Yb	2.01	0.04	1.89	2.04		3.69	0.03	0.75	3.71
Lu	0.29	0.01	2.08	0.30		0.58	0.00	0.80	0.58
Hf	4.21	0.06	1.42	4.46		5.08	0.19	3.76	5.43
Ta	1.16	0.01	0.64	1.20		0.85	0.02	1.86	0.89
Pb	1.63	0.08	4.60	1.61		11.25	0.09	0.77	11.10
Th	1.21	0.01	0.56	1.18		6.26	0.19	2.96	6.29
U	0.42	0.01	1.28	0.42		1.75	0.02	0.96	1.77

Solution-ICP-MS (University of South Florida)

Standard	**JB-3 (N=4)**			
Analyte	**Avg (ppm)**	**STD 1σ**	**RSD**	**Accepted Value****
B	16.43	1.44	8.76	18.00
As	1.96	0.12	6.08	1.84
Rb	14.12	0.30	2.10	15.10
Sr	404.80	8.78	2.17	403.00
In	-	-	-	-
Sb	0.43	0.05	12.43	0.12
Cs	0.95	0.03	2.87	0.94
Ba	276.63	9.42	3.40	245.00
Pb	4.31	0.30	7.03	5.58

Standard	**JB-3 (N=4)**			
Analyte	**Avg (ppm)**	**STD 1σ**	**RSD**	**Accepted Value****
Li	7.87	0.16	2.00	7.21
Be	0.85	0.03	3.35	0.81
Sc	33.75	0.40	1.20	33.80
Ti	8736.95	46.88	0.54	8600.00
V	415.93	3.97	0.95	372.00
Cr	68.65	1.89	2.76	58.10
Co	35.21	0.72	2.05	34.30
Ni	35.59	0.72	2.03	36.20
Cu	-	-	-	194.00
Zn	95.79	2.14	2.24	100.00
Ga	19.17	0.20	1.04	19.80
As	1.55	0.03	1.74	1.84
Rb	14.71	0.60	4.05	15.10
Sr	417.48	4.27	1.02	403.00
Y	27.11	0.31	1.15	26.90
Zr	96.93	1.18	1.22	97.80
Nb	2.39	0.06	2.67	2.47
In	-	-	-	-
Cs	0.90	0.01	0.63	0.94
Ba	246.85	0.65	0.26	245.00

La	8.59	0.05	0.55	8.81
Ce	23.59	1.09	4.64	21.50
Pr	3.37	0.02	0.46	3.11
Nd	17.15	0.81	4.71	15.60
Eu	1.35	0.01	0.95	1.32
Sm	4.34	0.02	0.52	4.27
Eu	1.34	0.01	0.45	1.32
Gd	4.53	0.03	0.55	4.67
Tb	0.74	0.01	1.20	0.73
Dy	4.48	0.05	1.03	4.54
Ho	0.91	0.01	1.24	0.80
Er	2.49	0.01	0.55	2.49
Yb	2.55	0.03	1.03	2.55
Lu	0.39	0.01	2.02	0.39
Hf	2.65	0.04	1.40	2.67
Hf	2.67	0.04	1.56	2.67
Ta	0.18	0.01	3.55	0.15
Pb	5.52	0.09	1.60	5.58
Th	1.31	0.02	1.75	1.27
U	0.50	0.01	1.39	0.48

**Standards accepted value from Wilson (1997a, b; 1998) and Kelley et. (2003)*

***Standards accepted value from Imai et al. (1995)*

Table 2C. *Major element, wt% (XRF) and trace element, ppm (LA ICP-MS) data for rocks from the Aeolian volcanoes*

Sample	SL-13-01	SL-13-02	SL-13-03	SL-13-05	SL-13-07	SL-13-08	SL-13-09	AL-13-01	AL-13-02	AL-13-03	AL-13-04	AL-13-05	AL-13-06	AL-13-07
Island	Salina	Salina	Salina	Salina	Salina	Salina	Salina	Alicudi	Alicudi	Alicudi	Alicudi	Alicudi	Alicudi	Alicudi
SiO_2	52.96	56.20	54.69	51.74	51.58	51.30	52.60	54.09	52.77	52.54	52.98	51.96	57.13	52.12
TiO_2	0.72	0.71	0.69	0.63	0.63	0.63	0.61	0.71	0.75	0.75	0.73	0.74	0.71	0.69
Al_2O_3	18.51	17.49	17.69	16.95	17.19	17.05	16.91	17.29	16.54	16.58	16.49	17.48	17.34	15.68
FeO	8.84	7.93	8.28	8.75	8.70	8.68	8.50	6.60	7.55	7.49	7.82	7.52	6.14	7.98
Fe_2O_3	9.82	8.81	9.20	9.72	9.67	9.65	9.45	7.33	8.39	8.32	8.69	8.36	6.82	8.87
MnO	0.17	0.18	0.18	0.17	0.17	0.17	0.16	0.13	0.15	0.15	0.15	0.15	0.14	0.16
MgO	4.15	3.77	4.29	7.47	7.10	7.13	6.82	5.54	7.29	7.24	6.65	6.19	3.81	8.27
CaO	9.75	7.96	8.83	11.27	11.08	11.15	11.06	9.59	10.72	10.71	11.29	10.91	6.69	11.26
Na_2O	2.49	2.88	2.72	2.03	1.84	1.99	1.86	2.87	2.41	2.40	2.09	2.43	3.51	2.26
K_2O	1.22	1.60	1.40	0.94	0.99	0.95	1.07	1.68	1.22	1.20	1.40	1.51	2.39	1.09
P_2O_5	0.195	0.216	0.199	0.139	0.137	0.145	0.139	0.318	0.247	0.250	0.268	0.407	0.428	0.248
Total	99.98	99.82	99.89	101.06	100.38	100.16	100.68	99.55	100.49	100.14	100.74	100.14	98.97	100.65
Sc	30.08	29.00	30.11	39.45	36.67	36.95	40.98	27.01	32.64	30.71	35.84	36.17	31.61	36.69
V	335.94	241.23	267.33	275.26	269.92	272.86	317.03	224.24	217.49	198.72	246.05	228.72	165.69	220.53
Cr	2.69	14.17	12.08	151.25	121.41	128.50	106.59	181.81	326.67	297.32	156.52	119.58	42.27	376.87
Co	27.85	22.53	24.70	35.68	33.37	33.88	31.89	25.03	32.42	30.60	31.35	30.35	18.86	36.77
Ni	13.43	9.92	12.04	54.95	46.28	47.94	31.80	44.86	83.15	77.63	46.36	53.36	18.98	91.47
Cu	123.64	64.81	89.14	123.81	126.05	126.73	124.75	49.49	104.67	93.06	95.18	96.11	57.41	92.88
Zn	72.81	76.68	74.43	81.11	79.12	82.55	58.49	49.59	59.29	67.40	56.80	73.69	92.17	65.04
Ga	18.23	21.07	19.62	19.60	19.13	19.90	18.08	21.47	16.79	15.90	15.99	27.67	35.57	16.21
Rb	33.31	37.43	35.20	23.40	23.14	23.12	23.82	41.00	35.54	33.47	40.82	39.10	72.46	27.72
Sr	753.82	656.71	663.81	628.19	619.99	634.24	679.25	691.12	593.07	563.61	613.44	800.02	709.24	628.15
Y	20.37	23.50	21.28	16.23	16.23	16.67	15.26	20.30	21.30	19.99	20.00	25.22	23.95	20.14
Zr	62.60	77.17	68.23	43.09	43.71	45.10	50.80	96.97	90.47	84.89	80.43	106.88	157.23	79.13
Nb	4.40	4.95	4.38	2.78	2.69	2.85	3.58	12.93	10.25	9.70	10.27	17.05	25.56	9.55
Cs	0.77	1.01	0.90	0.62	0.59	0.59	0.72	0.29	0.71	0.62	0.75	0.81	1.65	0.51
Ba	282.22	421.36	384.26	283.01	285.21	302.29	377.97	481.67	297.43	292.07	297.16	573.25	828.37	300.13
La	14.86	18.49	16.93	13.60	13.63	14.06	17.12	29.56	22.67	21.68	23.26	47.36	62.35	23.42
Ce	30.27	37.19	34.14	25.47	25.57	26.29	31.54	54.99	42.64	41.32	44.48	73.69	97.75	44.00
Pr	3.90	4.60	4.29	3.35	3.37	3.54	4.08	5.99	5.08	4.87	5.30	8.70	10.85	5.14
Nd	15.72	18.57	17.40	14.48	13.86	14.56	15.53	22.07	18.96	18.29	20.00	32.37	36.36	19.14
Sm	3.65	4.29	4.02	3.16	3.11	3.16	3.52	4.25	3.95	3.78	4.21	5.84	5.87	3.92
Eu	1.12	1.30	1.24	0.92	0.96	0.98	1.22	1.30	1.20	1.15	1.27	1.56	1.56	1.17
Gd	3.65	4.28	4.00	3.30	3.06	3.07	3.27	4.24	4.06	3.89	4.27	5.28	5.34	3.97
Tb	0.55	0.63	0.59	0.46	0.48	0.49	0.46	0.58	0.59	0.57	0.60	0.80	0.73	0.57
Dy	3.23	3.69	3.47	2.86	2.87	3.03	2.93	3.18	3.40	3.24	3.33	4.38	4.14	3.25
Ho	0.66	0.77	0.71	0.56	0.59	0.63	0.52	0.65	0.70	0.67	0.66	0.89	0.81	0.67
Er	1.85	2.16	1.99	1.67	1.62	1.62	1.44	1.84	1.95	1.87	1.82	2.54	2.39	1.86
Tm	-	-	-	0.25	0.25	0.26	-	-	-	-	-	0.33	0.34	-
Yb	1.97	2.32	2.12	1.57	1.78	1.72	1.49	1.91	2.07	1.96	1.86	2.41	2.51	1.94
Lu	0.31	0.37	0.33	0.27	0.27	0.26	0.23	0.30	0.32	0.30	0.29	0.39	0.41	0.30
Hf	1.62	1.99	1.78	1.36	1.24	1.27	1.30	2.24	2.15	2.02	1.88	2.68	3.57	1.88
Ta	0.26	0.28	0.24	0.14	0.14	0.13	0.18	0.61	0.55	0.49	0.48	0.73	1.12	0.49
Pb	5.63	6.84	6.07	4.63	4.49	4.32	5.84	4.09	4.54	4.00	4.09	4.59	8.85	4.36
Th	2.62	3.97	3.23	2.44	2.41	2.52	3.33	6.21	4.23	3.88	3.89	8.26	13.44	4.16
U	0.99	1.35	1.12	0.76	0.75	0.78	1.03	1.94	1.26	1.16	1.24	1.75	3.50	1.21

Sample	AL-13-08	AL-13-09	AL-13-12	AL-13-13	AL-13-14	FL-13-02	FL-13-03a	FL-13-03b	FL-13-05	FIL 24	ST-13-01	ST-13-02	ST-13-04	ST-13-05
Island	Alicudi	Alicudi	Alicudi	Alicudi	Alicudi	Filicudi	Filicudi	Filicudi	Filicudi	Filicudi	Stromboli	Stromboli	Stromboli	Stromboli
SiO_2	52.47	53.73	57.45	54.71	51.57	50.25	50.48	50.13	51.56	52.34	51.55	51.25	51.20	52.56
TiO_2	0.80	0.72	0.71	0.83	0.82	0.82	0.78	0.76	0.76	0.85	0.94	0.94	0.92	0.93
Al_2O_3	17.20	17.03	17.36	18.04	17.39	16.62	16.56	15.73	17.76	17.76	18.89	17.78	17.95	18.47
FeO	8.08	7.08	6.12	6.93	8.39	9.77	9.25	9.18	8.67	7.27	7.01	7.23	7.19	6.88
Fe_2O_3	8.98	7.87	6.80	7.70	9.32	10.86	10.28	10.20	9.63	8.08	7.79	8.03	7.99	7.65
MnO	0.16	0.14	0.14	0.13	0.16	0.19	0.18	0.18	0.17	0.13	0.13	0.14	0.14	0.13
MgO	6.49	5.93	3.71	4.62	6.13	6.95	6.99	7.70	5.15	5.61	4.10	4.61	4.66	4.03
CaO	10.50	9.60	6.57	8.50	11.33	12.22	12.56	12.79	11.34	11.16	9.53	9.71	9.95	8.48
Na_2O	2.19	2.28	3.37	3.07	2.24	1.98	2.04	1.68	2.35	2.28	2.59	2.64	2.50	2.71
K_2O	1.38	2.31	2.42	1.84	1.04	1.14	1.11	1.03	1.33	1.74	3.78	3.60	3.63	3.83
P_2O_5	0.278	0.353	0.455	0.348	0.296	0.263	0.252	0.235	0.207	0.353	0.673	0.678	0.670	0.581
Total	100.44	99.97	98.99	99.79	100.30	101.29	101.23	100.43	100.26	100.30	99.98	99.38	99.61	99.37
Sc	32.75	35.86	33.23	33.48	33.32	39.99	40.54	44.71	33.65	37.52	29.81	31.86	32.10	30.94
V	280.22	233.83	169.11	218.52	282.65	347.39	329.99	336.06	336.58	248.07	222.50	235.39	236.29	220.35
Cr	152.56	128.58	38.93	75.46	124.49	86.65	144.13	147.60	30.19	130.01	38.90	54.20	58.11	19.21
Co	31.83	27.71	18.86	23.97	30.22	36.10	33.69	35.44	29.42	26.73	24.39	26.37	25.63	22.91
Ni	45.99	42.00	20.92	36.79	37.52	29.57	35.57	37.31	20.23	32.41	28.64	28.38	31.55	21.57
Cu	96.17	98.92	48.69	53.57	107.51	118.36	93.70	93.33	129.86	87.34	114.04	120.35	91.21	54.30
Zn	63.95	84.92	85.02	76.04	57.78	66.46	62.02	61.66	66.12	69.81	75.47	81.64	78.61	66.64
Ga	17.33	25.16	36.30	30.41	16.25	16.03	15.58	14.79	18.58	23.78	72.96	73.52	72.08	58.14
Rb	38.79	70.15	74.39	47.70	26.85	31.78	30.06	28.22	31.30	46.47	130.02	143.62	138.35	147.54
Sr	638.33	785.84	695.55	810.14	668.14	647.89	628.37	596.52	702.21	677.50	1172.27	1099.45	1136.02	761.78
Y	22.46	22.91	23.11	23.63	19.85	21.19	20.10	19.60	19.07	23.34	27.84	28.75	29.72	30.06
Zr	82.23	101.06	156.30	114.87	71.90	61.22	59.90	57.00	62.90	85.12	195.05	194.89	198.84	213.63
Nb	9.15	10.97	26.11	16.40	9.84	6.29	5.86	5.43	5.01	14.61	36.93	36.32	36.23	28.90
Cs	0.81	1.33	1.62	0.52	0.52	0.54	0.51	0.49	0.79	0.53	7.03	7.69	7.00	7.21
Ba	302.21	483.04	848.99	621.96	312.56	264.90	252.70	238.75	365.32	404.89	2101.59	2122.48	2107.10	1593.53
La	21.08	32.73	62.09	41.22	23.14	20.57	19.77	18.84	18.46	27.40	65.43	65.60	65.88	57.07
Ce	41.16	57.60	98.17	68.94	44.49	41.11	39.42	37.61	36.65	47.22	126.99	130.39	127.86	107.46
Pr	4.96	7.03	10.67	8.22	5.21	5.11	4.87	4.69	4.60	6.26	15.35	15.73	15.55	13.21
Nd	19.19	27.55	35.79	30.87	20.13	20.06	19.08	18.39	18.07	25.49	57.02	57.95	58.33	48.41
Sm	4.17	5.60	5.46	5.08	4.11	4.42	4.26	4.15	4.09	5.16	10.27	10.71	10.61	9.37
Eu	1.25	1.58	1.56	1.52	1.26	1.29	1.25	1.23	1.22	1.36	2.87	2.75	2.84	2.22
Gd	4.28	5.09	4.99	4.76	4.15	4.37	4.21	4.12	3.96	4.74	8.39	8.66	8.97	8.10
Tb	0.63	0.76	0.70	0.68	0.59	0.63	0.61	0.60	0.57	0.73	1.08	1.15	1.17	1.07
Dy	3.58	4.11	3.80	4.05	3.33	3.50	3.37	3.35	3.20	4.30	5.39	5.70	5.93	5.72
Ho	0.73	0.83	0.82	0.84	0.68	0.69	0.67	0.66	0.65	0.84	0.99	1.00	1.06	1.05
Er	2.04	2.22	2.32	2.35	1.87	1.98	1.87	1.82	1.81	2.27	2.41	2.58	2.56	2.73
Tm	-	0.30	0.32	0.33	-	-	-	-	-	0.33	0.33	0.37	0.36	0.39
Yb	2.09	2.07	2.38	2.39	1.87	1.98	1.87	1.83	1.87	2.09	2.27	2.32	2.38	2.72
Lu	0.32	0.33	0.37	0.39	0.29	0.30	0.29	0.28	0.28	0.33	0.34	0.39	0.38	0.42
Hf	2.02	2.45	3.35	2.82	1.74	1.59	1.50	1.45	1.67	2.22	4.47	4.53	4.50	4.98
Ta	0.48	0.54	1.11	0.76	0.46	0.30	0.29	0.26	0.28	0.74	2.06	1.95	2.03	1.45
Pb	4.74	8.04	8.46	6.03	3.18	3.71	3.54	3.40	5.31	3.49	31.96	32.87	29.12	19.85
Th	3.92	5.86	13.38	7.91	3.58	3.30	3.24	3.04	3.23	4.74	20.82	20.73	20.61	22.81
U	1.17	1.84	3.57	2.06	1.07	0.99	0.97	0.91	1.15	1.39	5.86	5.58	5.66	5.90

Sample	ST-13-06	ST-13-07	ST-13-08	ST-13-09	ST-13-11	ST-13-13	ST-13-16	ST-13-17	ST-13-03
Island	Stromboli	Stromboli	Stromboli	Stromboli	Stromboli	Stromboli	Stromboli	Stromboli	Stromboli
SiO_2	52.02	51.54	54.05	52.22	52.65	52.34	55.28	54.88	50.54
TiO_2	0.96	0.96	0.90	0.80	1.03	0.89	0.71	0.70	1.00
Al_2O_3	18.12	18.00	19.45	17.59	18.60	18.63	16.04	15.94	19.46
FeO	7.05	7.19	6.07	7.20	7.28	7.32	7.48	7.43	7.21
Fe_2O_3	7.84	7.99	6.75	8.00	8.09	8.13	8.31	8.26	8.01
MnO	0.13	0.14	0.12	0.14	0.15	0.16	0.16	0.16	0.14
MgO	4.56	4.39	2.43	6.94	4.35	4.56	6.25	6.31	4.43
CaO	9.05	9.11	6.95	10.76	8.66	9.86	9.59	9.62	10.64
Na_2O	2.54	2.68	3.04	2.24	3.11	2.92	2.33	2.26	2.66
K_2O	4.00	3.85	5.13	1.84	2.76	2.25	1.62	1.62	2.54
P_2O_5	0.641	0.731	0.536	0.287	0.407	0.385	0.200	0.197	0.661
Total	99.86	99.39	99.36	100.82	99.81	100.12	100.49	99.94	100.08
Sc	29.90	30.49	28.25	35.24	30.92	30.85	34.07	35.30	30.36
V	229.00	235.17	180.51	238.14	234.85	235.40	229.83	230.45	247.97
Cr	73.24	41.07	14.04	169.99	39.25	6.50	147.73	160.89	39.17
Co	23.49	24.39	16.60	29.79	23.00	24.19	28.17	28.99	24.62
Ni	29.67	24.87	13.93	60.74	29.39	18.13	42.05	44.38	27.70
Cu	85.45	92.29	57.35	95.20	63.01	73.08	66.93	68.04	78.74
Zn	67.47	70.30	66.35	67.99	73.38	82.33	78.48	80.18	73.01
Ga	61.83	73.41	69.89	35.15	40.34	43.25	26.46	27.28	48.26
Rb	147.67	155.39	219.62	66.14	89.82	70.58	50.00	50.14	85.70
Sr	834.32	1037.75	852.05	539.26	710.69	804.81	582.27	588.77	884.38
Y	30.78	32.71	29.83	23.36	36.04	30.58	20.96	22.34	28.19
Zr	204.97	211.15	258.85	114.13	208.31	153.74	108.50	113.33	173.78
Nb	27.71	33.74	35.61	13.81	22.05	18.75	9.89	9.93	27.51
Cs	3.37	8.88	10.02	4.35	3.75	3.92	2.08	2.10	2.40
Ba	1745.02	2148.63	1925.80	844.96	939.53	1042.43	553.68	553.11	1238.02
La	57.48	69.48	61.04	31.51	57.23	53.13	28.99	29.77	56.34
Ce	107.82	128.80	112.48	58.74	98.36	94.43	54.66	53.94	110.95
Pr	13.55	16.12	13.96	7.39	12.15	11.64	6.61	6.71	13.24
Nd	52.45	61.45	53.12	28.52	46.38	43.50	24.48	25.70	49.88
Sm	9.93	11.66	9.81	5.88	8.41	8.12	4.95	4.86	9.27
Eu	2.41	2.78	2.27	1.44	2.05	2.06	1.22	1.28	2.40
Gd	8.45	9.49	8.00	5.41	7.74	6.99	4.49	4.65	7.37
Tb	1.12	1.24	1.10	0.74	1.12	1.00	0.66	0.68	1.01
Dy	5.86	6.27	5.40	4.02	6.37	5.54	3.61	3.91	5.36
Ho	1.09	1.12	1.04	0.82	1.27	1.04	0.75	0.78	0.99
Er	2.74	2.98	2.77	2.29	3.40	2.89	2.07	2.14	2.58
Tm	0.39	0.39	0.39	0.32	0.48	0.41	0.29	0.30	0.37
Yb	2.60	2.63	2.79	2.18	3.24	2.93	1.98	2.15	2.60
Lu	0.41	0.41	0.41	0.37	0.52	0.44	0.32	0.34	0.38
Hf	4.98	4.88	5.81	2.90	5.10	3.73	2.82	2.92	3.99
Ta	1.48	1.93	1.96	0.68	1.17	0.90	0.52	0.51	1.36
Pb	24.68	31.36	28.94	14.18	15.71	15.31	9.46	9.31	17.33
Th	20.89	22.54	28.82	11.97	19.05	16.32	8.47	8.79	17.61
U	5.27	5.55	7.50	2.93	3.91	3.80	2.06	2.05	4.56

Table 2D. *FME, Be and Li data (ppm) for rocks from the Aeolian volcanoes*

Sample	Island	B	Be	Li	As	Sb
SL-13-01	**Salina**	14,80	1,25	6,54	1,20	0,50
SL-13-02	**Salina**	13,80	1,64	11,52	1,70	0,40
SL-13-03	**Salina**	13,30	1,24	9,70	1,80	0,40
SL-13-05	**Salina**	10,90	0,85	5,90	1,50	0,50
SL-13-07	**Salina**	10,70	0,96	6,50	1,30	0,60
SL-13-08	**Salina**	8,30	0,98	7,20	1,20	0,40
SL-13-09	**Salina**	20,30	1,04	6,48	2,60	0,40
AL-13-01	**Alicudi**	5,40	1,67	7,40	1,40	0,40
AL-13-02	**Alicudi**	-	1,20	7,74	-	-
AL-13-03	**Alicudi**	14,60	1,11	7,78	2,40	0,50
AL-13-04	**Alicudi**	5,00	1,27	5,69	0,70	0,40
AL-13-05	**Alicudi**	8,20	1,52	7,96	1,40	0,40
AL-13-06	**Alicudi**	-	2,23	11,65	-	-
AL-13-07	**Alicudi**	8,10	1,19	9,04	1,50	0,30
AL-13-08	**Alicudi**	7,90	1,40	8,66	2,80	0,50
AL-13-09	**Alicudi**	7,50	2,09	7,22	1,00	0,30
AL-13-12	**Alicudi**	-	2,63	12,55	-	-
AL-13-13	**Alicudi**	8,30	1,78	8,63	3,10	0,20
AL-13-14	**Alicudi**	4,90	1,04	6,51	0,80	0,50
FL-13-02	**Filicudi**	5,65	1,14	4,92	0,70	0,35
FL-13-03A	**Filicudi**	4,35	1,03	5,62	0,55	0,25
FL-13-03B	**Filicudi**	4,10	1,08	5,48	0,60	0,40
FL-13-05	**Filicudi**	11,10	1,27	5,72	1,70	0,40
ST-13-01	**Stromboli**	18,10	5,58	9,35	8,90	0,60
ST-13-02	**Stromboli**	15,90	4,91	12,53	5,60	0,40
ST-13-04	**Stromboli**	11,00	5,17	12,07	3,00	0,40
ST-13-05	**Stromboli**	23,50	5,21	13,46	6,90	0,40
ST-13-06	**Stromboli**	17,10	5,03	11,43	8,20	0,50
ST-13-07	**Stromboli**	19,60	5,78	10,42	7,20	0,40
ST-13-08	**Stromboli**	26,20	7,18	17,11	10,10	0,80
ST-13-09	**Stromboli**	21,00	2,11	6,67	7,00	0,50
ST-13-11	**Stromboli**	21,90	2,36	14,86	4,70	0,70
ST-13-13	**Stromboli**	21,50	1,93	15,01	5,10	1,00
ST-13-16	**Stromboli**	30,30	1,35	13,98	3,60	0,40
ST-13-17	**Stromboli**	16,50	1,55	13,90	3,20	0,60
ST-13-03	**Stromboli**	12,00	2,57	11,06	3,90	0,30

Chapter 3.
New Insights Into The Aeolian Source Compositions

3.1 Introduction

The physical and chemical evolution of the Earth depends on the recycling of elements and crust in subduction zones at convergent plate margins. The downgoing slab undergoes metamorphic processes that induce the addition of volatiles and fluids (aqueous fluids, hydrous melts, or supercritical liquids) back into the mantle (Grove et al., 2012). The release of hydrous slab components lowers the solidus and triggers melting within the mantle wedge causing the formation of magmas beneath active arc volcanoes and back-arc basin spreading centers (Schmidt and Poli, 1998; Manning, 2004; Syracuse et al., 2010; Spandler and Pirard, 2013). The Aeolian Islands and the associate Marsili back-arc basin in the southern Tyrrhenian Sea (Italy) represent a typical volcanic arc – back-arc basin scenario (Fig. 1.3).

The subduction of the oceanic lithosphere introduces heterogeneities into the mantle that will influence subsequent melting dynamics. In the mantle wedge, peridotitic mantle rocks, subducted oceanic crust and the overlying sediments contribute to the generation of arc magmas. The source composition of the Aeolian Islands magmas was investigated by several geochemical studies (e.g., Francalanci et al., 2007; Peccerillo et al., 2013). These researches suggest that the important geochemical variations characterizing the mafic rocks along the arc reflect differences in the mantle wedge source. These studies describe the well-known negative correlation between $^{87}Sr/^{86}Sr$ and $^{143}Nd/^{144}Nd$ isotopes ratios from west to east as the result of an increasing metasomatism by subduction components (fluid and melt from the slab) together with local crustal contamination processes (e.g., anatexis process in Lipari, Di Martino et al., 2010; 2011). In

support of this interpretation, in my recent study (Chapter 2.) I used B, Be, As and Li measurements to infer that fluids from the subducted lithosphere affect the entire archipelago but especially Salina (central sector), while a slab melt component (sediments) plays an important role in the metasomatism of the peripheral islands, particularly at Stromboli.

These previous studies described how the interaction between crust and mantle end-members induced a source contamination. An approach to determine the mantle end-member (the source lithology) that melted to produce arc basalts is to examine olivines, the main constituent of a peridotite. Olivine is the most abundant mineral in the upper mantle and the first silicate mineral to crystallize from almost all primary mantle-derived melts in equilibrium with their source. This mineral phase is made of a continuous solid-solution between two end-members, forsterite (Mg_2SiO_4; Fo100) and fayalite (Fe_2SiO_4; Fa100 or Fo0), and the magnesian end-member is expressed by the Mg-numbers (molar [MgO/[MgO+FeO]]*100) because it is the only major compositional factor that varies significantly during olivine fractionation (Herzberg, 2011).

A lot of information is carried by minor and trace elements contents (e.g., Ni, Mn, Ca, Cr, Ti; 10 to several thousand ppm) and their investigation is useful to infer the lithology of the mantle source (Sobolev et al., 2007; De Hoog et al., 2010). During the last decade several studies used an approach based on these elements and used olivine as a lithology discriminant between a depleted (NMORB-peridotite) and a recycled (OIB-pyroxenite) source (Sobolev et al., 2005; 2007; Gurenko et al., 2009; 2013; Herzberg, 2011; Barker et al., 2014; Herzberg at al., 2014; Søager et al., 2015).

This discrimination is based on the observation that magmas crystallized from a pyroxenitic lithology (an olivine poor and pyroxene rich mantle source) are characterized by high Ni, low Ca, low Mn highly forsteritic olivines compared to a peridotitic one (Sobolev et al., 2005; 2007).

Furthermore, other studies on Zn, Co and other first row transition elements (FRTE) contents in pyroxenite (Le Roux et al., 2011; Davis et al., 2013) revealed how these elements are enriched similarly to Ni in melt from olivine-free sources. However is important to consider that the partition coefficient of Ni (D_{Ni}) in olivine depends on pressure and temperature conditions (P-T), along with melt and mineral compositions. Changes in these factors might cause high-Ni olivines to crystallize from "normal" mantle peridotite partial melts without the involvement of an olivine-free source (Putirka et al., 2011; Matzen et al., 2013). The petrological experiment results of Matzen et al. (2013) relates the Ni budget to the inverse correlation between temperature and the partitioning of Ni between olivine and melt. Deep peridotitic mantle source will produce Ni rich partial melts (high T, low D_{Ni}) that will crystallize high Ni olivine at low T (high D_{Ni}). Also, recent experimental studies by Mallik and Dasgupta (2012; 2013; 2014) described elevated Fe/Mn in melts made from mixtures of eclogite melt and peridotite in equilibrium with residues characterized by lower olivine modal abundance than in peridotite, but not necessarily olivine free.

Few studies on subduction related setting rocks (Straub et al., 2008, Foley et al., 2013; Prelević et al., 2013) reported olivines with high Ni content and associated this characteristic to an olivine free source. We think it is imperative to distinguish between possible different source lithology at the Aeolian Islands, in order to better characterize the fundamental inputs for the magma genesis of this area.

3.2 Materials and methods

3.2.1 *Sr-, Nd-, Pb-, and Hf-isotope analyses*

From the processed rocks I selected the most mafic samples (generally MgO>6 wt%) with B and Be contents that can also be correlated to the olivine chemistry. From these powders and the Ionian sediment samples, Nd, Hf, Pb, and Sr were isolated using standard ion exchange chromatography techniques described in Chauvel et al. (2011). Prior to dissolution in Savillex beakers, the volcanic rock powders were leached for two hours using ultrapure 6M HCl in order to remove potential surficial alteration products. In contrast, the sediment samples were not leached and they were dissolved in Parr bombs instead of Savillex beakers to insure proper dissolution of all mineral phases. Blanks obtained using the same chemical treatment were 13 pg for Nd, 9 pg for Hf, 18 pg for Pb, and 5 pg for Sr, values that are completely negligible relative to the amounts of elements present in the samples.

Nd, Hf, and Pb isotopic compositions were analyzed on a high-resolution multicollector ICP-MS (Nu plasma 500 HR) at Ecole Nationale Supérieure of Lyon (France). Mass fractionation bias corrections for Nd and Hf isotopic measurements were corrected using $^{146}Nd/^{144}Nd = 0.7219$ and $^{179}Hf/^{177}Hf = 0.7325$. The average $^{143}Nd/^{144}Nd$ acquired for the Nd Ames–Rennes standard was 0.511976 ± 19 and 0.511971 ± 11 (2σ, n = 12 & 10 on two different days) while the average $^{176}Hf/^{177}Hf$ obtained for the Hf Ames–Grenoble standard was 0.282181 ± 11 and 0.282168 ± 12 (2σ, n = 17 & 10 on two different days). Both standards were run every 2 or 3 samples, and all isotopic ratios were normalized to reference values of 0.511961 for $^{143}Nd/^{144}Nd$ (Chauvel and Blichert-Toft, 2001), and 0.282160 for $^{176}Hf/^{177}Hf$ (Chauvel et al., 2011). The Pb isotopic data were corrected for mass fractionation bias using the Thallium addition technique (White et al., 2000) and the instrumental drift was corrected using the standard bracketing method, with run of NBS 981 standard every 2 or 3 samples and values recommended by Jochum et al. (2011). The Pb isotopic ratios, $^{208}Pb/^{204}Pb$, $^{207}Pb/^{204}Pb$ and $^{206}Pb/^{204}Pb$, for NBS 981 standard averaged 36.70 ± 0.01, 15.494 ± 0.005, and 16.938 ± 0.005 (2σ, n = 24), respectively. The Sr isotopic compositions

were measured on a Thermo Scientific Triton mass spectrometer TIMS at Pôle Spectrométrie Océan (PSO, Brest, France). The average $^{87}Sr/^{86}Sr$ obtained for the NBS 987 standard was 0.710281 ± 15 (2σ, n = 19). The standard was run every 2 or 3 samples and the measured $^{87}Sr/^{86}Sr$ ratios were normalized to the recommended standard value of 0.710250 to correct any potential drift.

3.2.2 *High precision olivine chemistry*

For the olivine chemistry analyses I prepared epoxy disks with handpicked olivine phenocrysts from olivine-bearing scoria and lavas representative of the most mafic units on Alicudi, Filicudi, Salina and Stromboli. The olivine crystals selection was based on MgO bulk contents. The phenocrysts were picked under stereoscopic microscope from basalts and basaltic andesite with MgO>6 wt% from the sampled islands. For Stromboli we collected olivine from both the calc-alkaline and the potassic lavas. We analyzed olivine from potassic lava with MgO>4 wt% because these rocks have MgO bulk content lower than 5 wt%. The polished disks with the olivine were later carbon coated with a 20 nm film using a Q150TE high-vacuum carbon coater. Then I performed high precision major (Si, Fe, Mg), minor and trace (Ni, Mn, Ca, Al, Cr, Co, Ti, Zn, P and Na) element analyses on the olivine phenocrysts using a new JEOL JXA-8230 EPMA at the Institute des Sciences de la Terre (ISTerre), University Grenoble-Alpes, France.

Samples were analyzed at 25 kV accelerating voltage and 900 nA of primary beam current following the new analytical protocol described in Batanova et al. (2015). Major elements were analyzed by ED spectrometer with element count times of 500s for Si, Fe, and Mg. Minor and trace elements were analyzed by WD spectrometer. Element counts were as follow: 160 s for Na, 180 s for Al, 160 s for Co, 180 s for Zn, 180 s for Ca, 160 s for P, 180 s for Ti, 90 s for Cr, 160 s for Mn, and 80 s for Ni. The calibration was made on Olivine USNM111312-44 for Si, Fe, and Mg; Albite for Na;

pure Al_2O_3 for Al; pure CoO for Co; ZnS for Zn; Wollastonite for Ca; Apatite Durango for P; pure TiO_2 for Ti; pure Cr_2O_3 for Cr; Rhodonite for Mn; pure NiO for Ni. The obtained results (total of 513 analyses) have precision better than 10 ppm (2 standard errors). For further details about the method see Batanova et al. (2015). The San Carlos olivine standard (USNM111312-44, Jarosewich et al., 1980) was analyzed as an unknown 3 times every 30 measurements in order to monitor potential instrumental drift and to estimate accuracy and precision.

3.3 Results

3.3.1 *Isotopic variations along the arc*

The Italian magmatism with all its important variations in geochemical, petrological and isotopic compositions, represents the product of heterogenous sources. The Aeolian Islands-Calabrian subduction zone was the subject of different studies in the last decade (e.g. Peccerillo et al., 2013; Peccerillo and Frezzotti, 2015) that described how the upper crust materials contaminate the mantle wedge. The variations trend in Sr-, Nd-, and Pb-isotopes characterizing this particular area, lead these scientists to define a source contaminated mainly by fluids and melts from the slab with secondary magma contamination.

Our new isotopic data for Alicudi, Filicudi, Salina, Stromboli, and the Ionian sediments (Zamboni et al., in preparation) are plotted in Fig. 3.1, along with previously published data for the entire Aeolian archipelago, Vesuvius and Calabro-Peloritano basement compositions. In Figure 3.1c our samples perfectly fit with the continuos trend from Sicily toward Vesuvius already described for the Southern Tyrrhenian Sea area (e.g. Peccerillo and Frezzotti, 2015). The new Sr and Nd isotopic compositions of Alicudi (0.703555-0.704058 and 0.512805-0.512863, respectively)

are close to upper mantle MORB-like source values, which varies toward a more radiogenic source in Sr (0.705418-0.707280), and lower Nd (0.512489-0.512554), under Stromboli. Here the potassic rocks have a more radiogenic signature than the calc-alkaline ones attesting the strong presence of the Ionian subducted sediment in the source. Our new Filicudi (0.704289-0.704295; 0.512728-0.512731) and Salina data (0.704143-0.704383; 0.512788-0.512814) have comparable $^{87}Sr/^{86}Sr$, $^{143}Nd/^{144}Nd$ values to Alicudi. The same observations can be inferred by the good correlation between $^{176}Hf/^{177}Hf$ and $^{143}Nd/^{144}Nd$ (Fig. 3.1d).

Contrary to Sr and Nd isotopic values, in the Pb isotopic series (Fig 3.1a and 3.1b) samples from Salina are the most radiogenic (highest values for $^{206}Pb/^{204}Pb$=19.8286, $^{207}Pb/^{204}Pb$=15.6883, $^{208}Pb/^{204}Pb$=39.6036) and alike to the HIMU signature characteristics of Etna rocks. Our data also

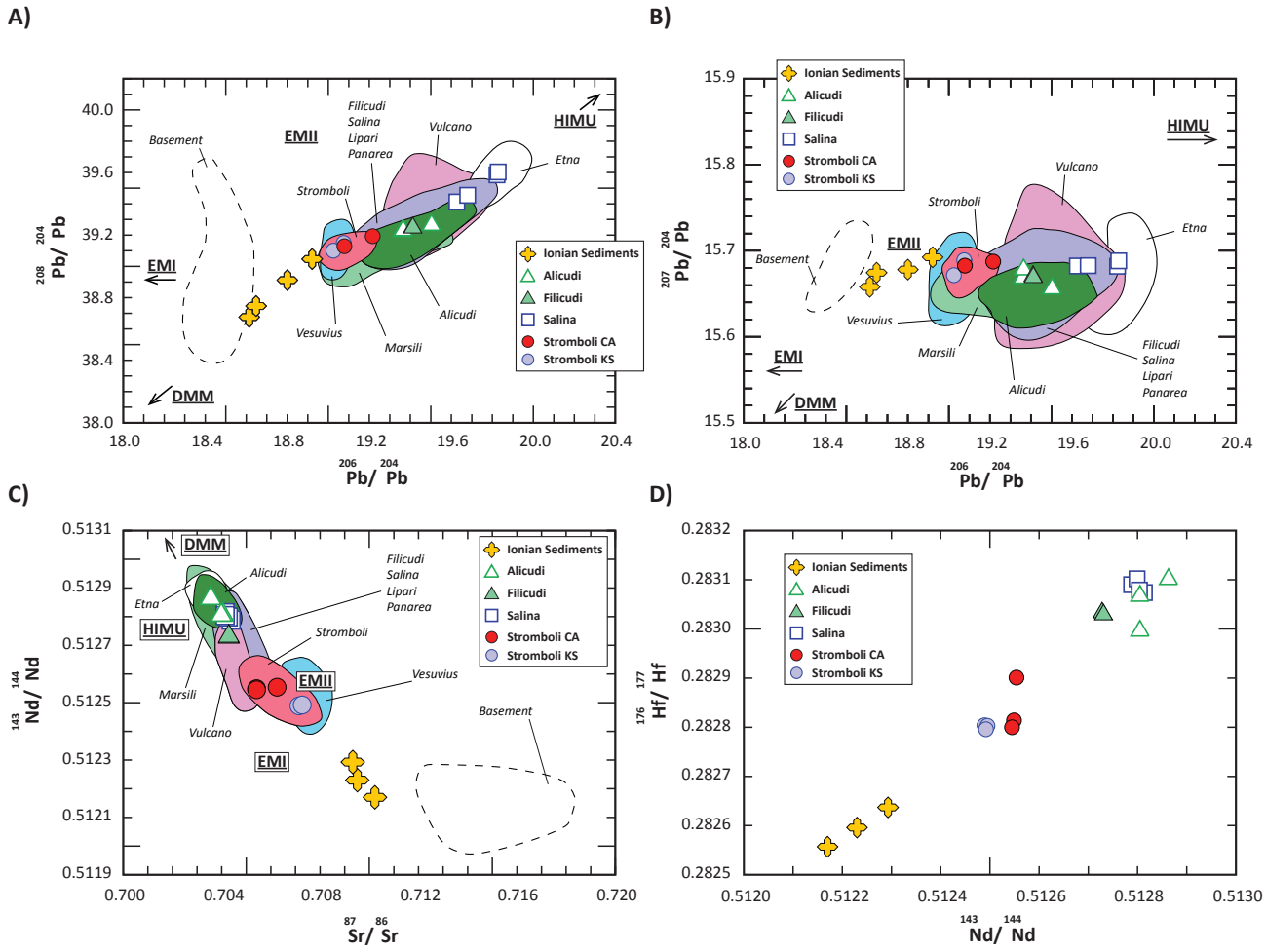

Figure 3.1 Isotopic diagrams showing how the new data for Alicudi, Filicudi, Salina, Stromboli and the Ionian sediment compare to other samples from the Aeolian Arc, Marsili seamount, Etna, Vesuvius and Calabro-Peloritano basement. (a) $^{208}Pb/^{204}Pb$ vs. $^{206}Pb/^{204}Pb$, (b) $^{207}Pb/^{204}Pb$ vs. $^{206}Pb/^{204}Pb$, (c) $^{143}Nd/^{144}Nd$ vs. $^{87}Sr/^{86}Sr$ and (d) $^{176}Hf/^{177}Hf$ vs. $^{143}Nd/^{144}Nd$. Data compiled from: Alicudi, *Peccerillo and Wu* (1992); *Peccerillo et al.* (1993; 2004). Filicudi, *Francalanci and Santo* (1993); *Santo* (2000); *Santo et al.* (2004). Salina, *Ellam* (1986); *Ellam et al.* (1988; 1989); *Ellam and Harmon* (1990); *Gertisser and Keller* (2000); *Peccerillo* (2005); *Lucchi et al.* (2013c). Stromboli, *Ellam et al.* (1989); *Francalanci et al.* (1989; 1993; 1999; 2004; 2008; 2012; 2013); *De Astis et al.* (2000); *Landi et al.* (2006; 2009); *Tommasini et al.* (2007); *Corazzato et al.* (2008); *Petrone et al.* (2009).

shows how the low Pb signatures characteristic of Stromboli are dictated by the input of the subducted sediments in agreement with Sr and Nd isotopes. Furthermore, our new Stromboli values for $^{208}Pb/^{204}Pb$=39.1007-39.1931, $^{207}Pb/^{204}Pb$=15.6716-15.6890, and $^{206}Pb/^{204}Pb$=19.0248-19.2166 resemble closely the isotopic values of Vesuvius as already described by Peccerillo (2001).

These isotope arrays supposedly represent a linear mixing between the subducted sediment and a mantle endmember (Etna). To explain this trend several studies (e.g., Ellam et al., 1988; Peccerillo et al., 2013; Peccerillo and Frezzotti, 2015) hypothesized the source contamination by an OIB type component, possibly provided by asthenospheric mantle inflow around the edges of the slab, while others (e.g., Francalanci et al., 2007) suggested a MORB type pre-metasomatic source later modified by slab fluids and melts. We can argue that intraplate and depleted components seems to be present in a source heavily metasomatized by slab fluid and melts (e.g., B – Be data) all complicated by possible asthenospheric flows. The southern Tyrrhenian Sea area may be one of the most beautiful combinations of intraplate setting and subduction zone.

3.3.2 *Ni, Ca, and Mn contents in the Aeolian olivines*

Our new high precision olivine major, minor and trace elements composition for the olivines bearing rocks of Alicudi, Filicudi, Salina and Stromboli are reported in Table 3A.1 and 3A.2. We conducted 133 high precision olivine analyses for Alicudi, 92 for Filicudi, 183 for Salina, and 105 for Stromboli. The peripheral islands are characterized by higher forsteritic content (high Mg-number) than the central sector of the arc (Fig. 3.2). As a matter of fact the Mg-number in Alicudi is the highest with 92.21 while Stromboli reaches value of 90.77. It is noteworthy the low and constant forsterite for the olivine representing the potassic rock series (67.87 – 75.88). In contrast of the olivine from the external islands, the forsteritic content of the olivine phenocryst from Filicudi reaches a maximum value of 86.84, while the majority of Salina olivine are characterized by Mg-number around 80 (87.55 as the highest).

For several tectonic environments, highly forsteritic olivines suggested to be derived from mantle peridotite are characterized by a small range in Ni, 2800-3100 ppm (Herzberg et al., 2013).

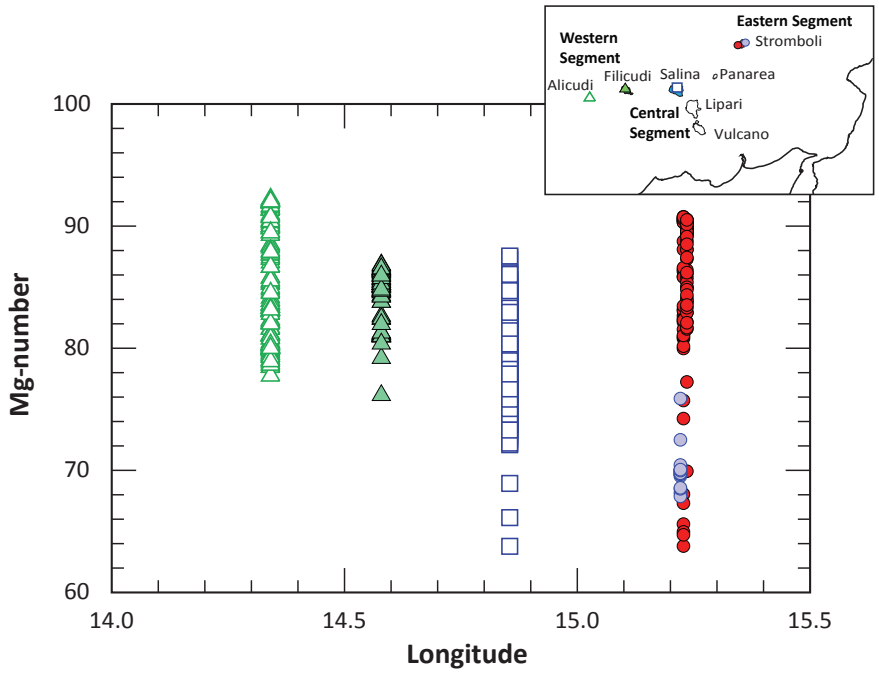

Figure 3.2 Representation of Mg-number variation for olivines from the most mafic rocks of the Aeolian Islands. The island of Alicudi is characterized by the highest Mg-number of 92.21. A Mg-number is defined as 100*MgO/(MgO+FeO). Alicudi, Filicudi, Salina, and Stromboli are color-coded.

Figure 3.3a shows how Ni concentrations of the most primitive olivine (Mg-number >87) are approaching these values. The external islands are characterized by higher Ni contents respect to the central sector. Olivines from Alicudi have the highest Ni values in the arc (maximum of 3243 ppm) while Stromboli follows with 2604 ppm. In contrast, Filicudi and Salina are characterized by lower Ni contents (1046 and 2232 ppm, respectively) also due to lower forsteritic contents. These islands, all together or singularly, show a general positive trend that goes from higher to lower Ni contents and Mg-number that reflects a typical olivine fractional crystallization trend. Similar observations can also be made from the negative correlation between Mn and Mg-number (not shown).

These Ni values in primitive olivine seem to resemble the typical content of olivines crystallized from melts of normal MORB-like peridotite (Herzberg 2011; Herzberg et al., 2013) and reveal no sign of a possible presence of pyroxenite or refertilized peridotite into the source (e.g.,

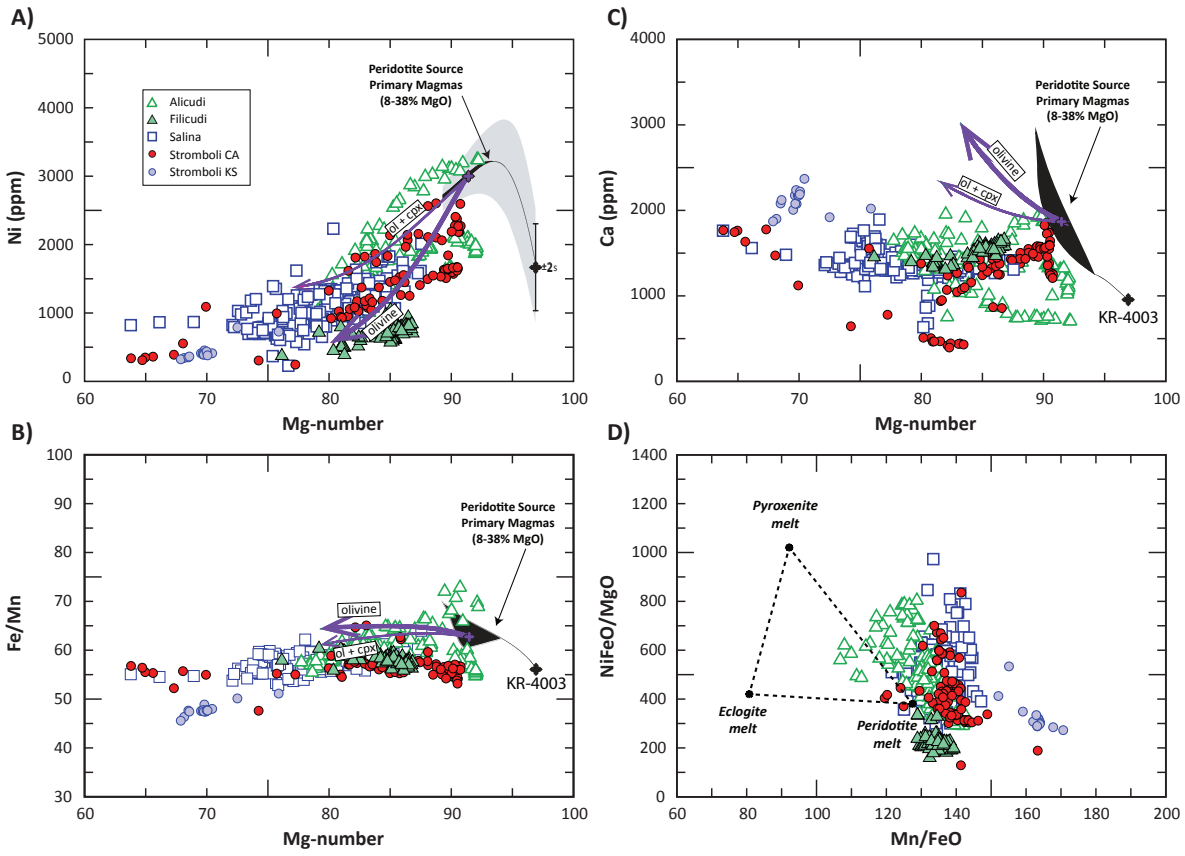

Figure 3.3 Plots of Mg-numbers vs. Ni (a), Ca (b), Fe/Mn (c), and Ni*FeO/MgO vs Mn/FeO ratios for new high precision olivines data from Alicudi, Filicudi, Salina and Stromboli magmas. Black forms define computed compositions of olivine that crystallize from all primary melts derived from a fertile peridotite modeled by Herzberg (2011). Purple lines intend to represent the general trajectory of olivine and olivine+clinopyroxene (ol+cpx) fractionation (from Herzberg, 2011). The grey field in Mg-number vs. Ni (a) represents ±1σ uncertainty for Ni (Herzberg et al., 2013). The endmembers at the triangle vertexes in panel d (modified after Barker et al., 2014) are the best fit values for peridotite and pyroxenite melts end-member of Sobolev et al. (2005; 2007) and the eclogite melt from Pertermann and Hirschmann (2002).

no high Ni olivine) even when compared to other volcanic olivines (Fig. 3.4 and Fig. 3.5).Low values in Fe/Mn (Fig. 3.3b) for olivine with Mg-number >87, generally between 50 and 65, might support this hypothesis while Ca budgets (<2000 ppm) are too low. Only few olivine data points from Alicudi seem to behave differently (higher Fe/Mn and Ca values). Nonetheless, the plot of all Aeolian data next to the peridotitic melt end-member in Fig. 3.3d, representing Ni*FeO/MgO and Mn/FeO ratios, point towards a main peridotitic component.

3.3.3 *The role of olivine in the Aeolian magma sources*

Heterogeneous mantle sources are caused by the introduction of upper crust material into the mantle source by subduction processes. Generally in the mantle wedge, three different end-members, peridotitic mantle rocks, subducted oceanic crust and the overlying sediments, are considered to contribute to the generation of arc magmas. In the last few years various geochemical studies (e.g. Francalanci et al., 2007; Peccerillo et al., 2013; Peccerillo and Frezzotti, 2015) suggested that slab derived fluids (e.g. hydrous fluid, sediment melt) flux the mantle wedge under the Aeolian Islands and modified its original composition with the consequence of creating the observed trace elements and isotopic heterogeneities along the archipelago.

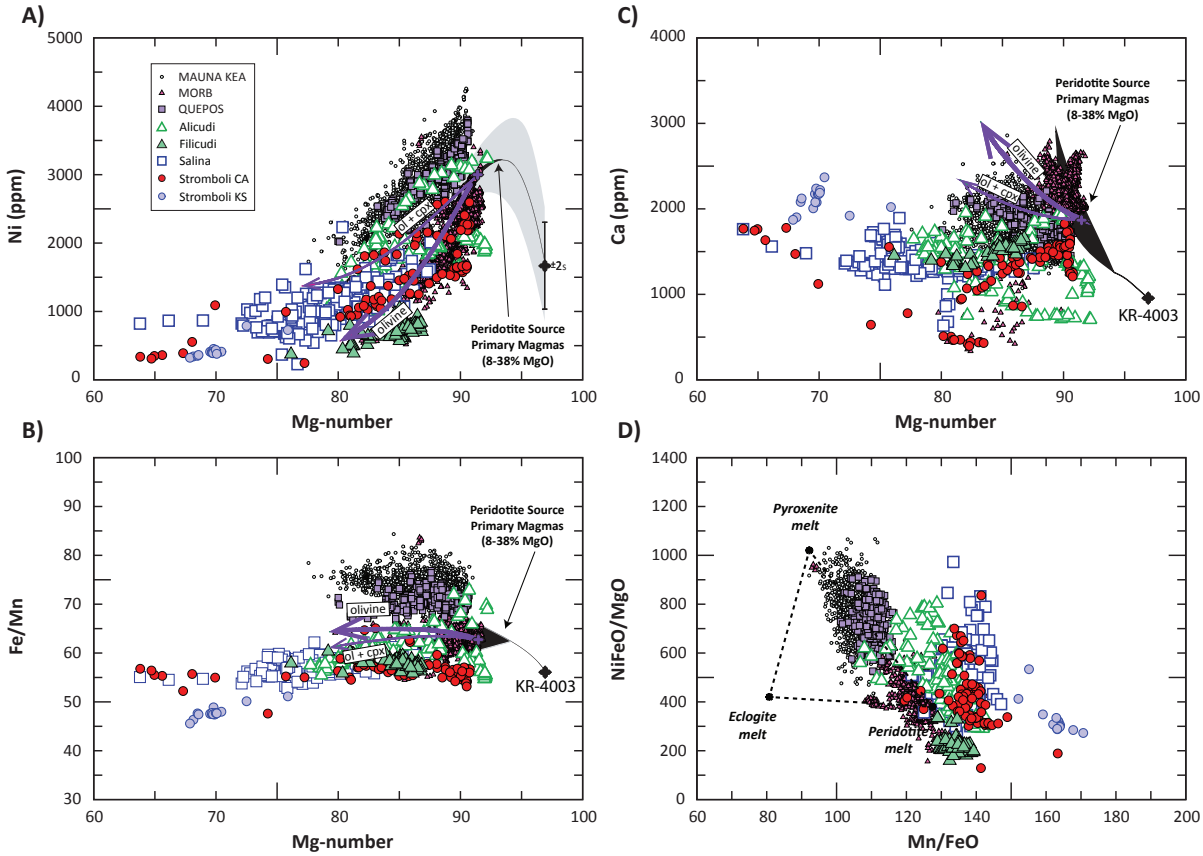

Figure 3.4 Mg-numbers versus Ni (a), Ca (b), Fe/Mn (c), and Ni*FeO/MgO vs Mn/FeO ratios for the Aeolian Islands olivines (Fig. 3) compare to peridotite source derived olivines (MORB, Sobolev et al., 2007) and pyroxenite source derived olivines (Mauna Kea, Sobolev et al., 2007; Quepos, Trela et al., 2015).

My research described in Chapter 2 supported this hypothesis using new results for fluid mobile elements (e.g. B, As) and Be data. This study reported how hydrous fluid strongly characterized the lavas in the central arc (Salina) and how the mantle wedge of the peripheral islands, particular Stromboli, is metasomatized by a melt component. This study also noticed similarities with other hot subduction zones (e.g. Sunda, Cascades) and explained the presence of the melt component with increases of the mantle wedge temperature by inflow of hot asthenospheric mantle.

We can use olivines from the most primitive erupted magmas to distinguish which source lithology melted to produce the arc basalts, a peridotite or a pyroxenite source, analyzing the

minor and trace elements budgets (Sobolev et al., 2005; 2007; Herzberg, 2011) as their contents are not affected by the metasomatic process typical of subduction settings.

The study by Sobolev et al. (2007) described how highly forsteritic olivines (Fo >90) crystallized from a melt of pyroxenite, are characterized by high Ni, low Ca and Mn contents and high Fe/Mn ratio in comparison to peridotite source-derived melts. These contents resulted from the interaction of silica rich melts (derived from the slab or from pyroxenitic/eclogitic lithologies in intraplate setting) with peridotites that caused the formation of an olivine-free pyroxenite. Melts from this hybrid pyroxenitic source will be Ni-rich melts compared to peridotite-derived melts because there is no residual olivines and Ni is more incompatible in the pyroxenite, differently than Ca and Mn (higher bulk partition coefficient).

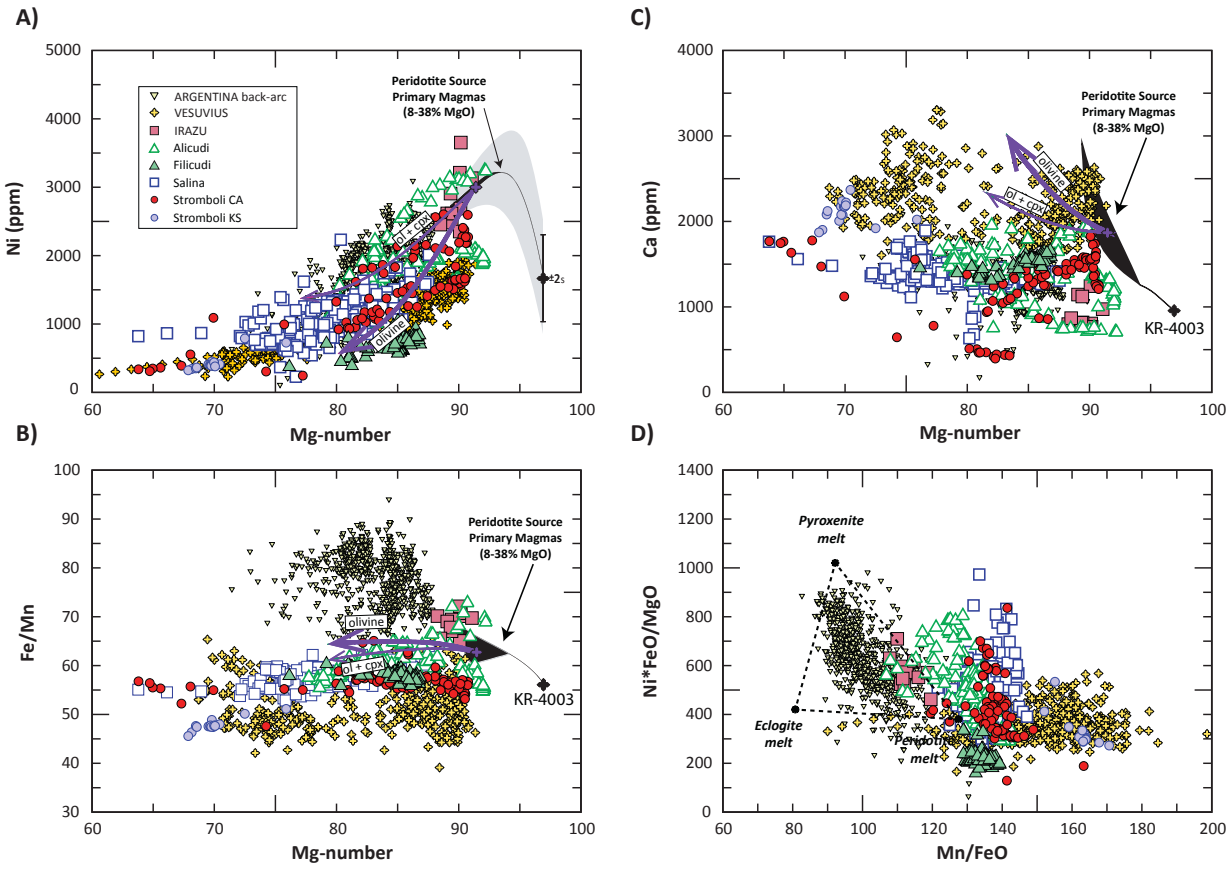

Figure 3.5 Figure 5. Plots of Mg-numbers versus Ni (a), Ca (b), Fe/Mn (c), and Ni*FeO/MgO vs Mn/FeO ratios for subduction related olivines. The panels display olivines from Aeolian Islands (Fig. 2), Irazu (Ruprecht and Plank, 2013), Vesuvius (Redi, 2014, PhD thesis), and Argentina Back-arc (Søager et al., 2015). Irazu olivines represent averages of the most forsteritic points (Mg-number >88) of each sample traverse core to rim.

In order to discriminate between peridotite source and pyroxenite source we evaluated our new trace element budgets. In Figure 3.3 we represented our data with the modeled peridotitic source for anhydrous magma (e.g., intraplate magma) and a general olivine fractionation path together with olivine+clinopyroxene (ol+cpx) cotectic fractionation trend described in Herzberg (2011). In general the Aeolian olivines plot for Ni (Fig. 3.3a) likely match the olivine liquid line of descent trend from a peridotitic source. Worth to note is the possibility to distinguish two separate trends in Alicudi for primitive olivines (Mg-number >87). A lower Ni trend is consistent with the rest of the arc olivines, and a higher Ni trend is closed to the ol+cpx path due to the fact that the cotectic crystallization of olivine and clinopyroxene will cause a shallower liquid line of descent trajectory. Similar observations (peridotite source, differences in Alicudi olivines) can also be inferred from Fe/Mn values (Fig. 3.3b).

In contrast, Ca budgets (Fig. 3.3c) seem to be too low to be derived from a peridotitic source, in fact generally there are no olivines resembling the olivine and ol+cpx fractionation paths. This might be resulted from a different source, where olivines crystallized from parental magmas low in Ca like a pyroxenite source (Herzberg, 2006; 2011) or it may be related to the presence of water in the peridotite source. Water heavily affected the partitioning of Ca between olivine and melt as suggested by Feig et al. (2006), resulting in Ca depletions in olivines of arc magmas and causing olivine fractionation path to become very flat. The represented olivine fractionation trajectories and the corresponding peridotitic source (Herzberg, 2011) were modeled for anhydrous magmas, without considering H_2O in the source, as it should be for a subduction zone setting. Typically, many volcanic arcs are characterized by a maximum content of 4% H_2O (measured in melt inclusions, Plank et al., 2013).

The Aeolian Islands olivines seem to be consistent with parental magmas from peridotitic source also when our data plot closed to the peridotite melt end-member of Fig. 3.3d. Vertexes of

this schematic triangle (modified from Barker et al., 2014) represents the most likely compositions of the pyroxenite-peridotite melts end-member of Sobolev et al. (2005; 2007) and the eclogite melt from Pertermann and Hirschmann (2002).

In order to support the hypothesis of a peridotite source for the Aeolian Islands we compared our high precision olivine data with olivine compositions from different volcanic settings in the world known to have a pyroxenite, peridotite or a mixing of the two, source. In Figure 3.4 the Aeolian data is plotted with intraplate olivines from Mauna Kea and Quepos, together with MORB olivines. The Aeolian olivines generally overlap partially the MORB olivines that are consistent with peridotite source melting (Sobolev et al., 2007; Herzberg, 2011), while they always plot far away from the intraplate olivines. Only very few high-Ni trend samples from Alicudi overlap the intraplate olivines (Fig. 3.4a). This can be seen also in Fig. 3.4c where few high forsteritic samples of Alicudi, due to their higher Fe/Mn ratio, overlap with intraplate olivines but the fractionation trajectories seems to be different. In contrast, low Ca contents and relative schematic olivine liquid line of descent are not consistent with either a pyroxenite or peridotite source. However, the difference between the Aeolian olivine compositions and these plots (high Ni and low Mn and Ca for the intraplate olivines) is due to the origin of these olivines that were interpreted as crystallized from pyroxenite-derived primary magmas (Sobolev et al., 2007; Trela et al., 2015). Quepos olivines data were correlated to fractional crystallization coupled with magma recharge and mixing from a pyroxenite source (Trela et al., 2015), while Hawaiian olivines point toward an olivine free mantle source (Sobolev et al., 2007; Herzberg, 2011).

We also plot our new data with olivines from subduction setting related volcanoes in Fig. 3.5. We can notice how Irazu and Argentinian back-arc olivines overlap the higher Ni Alicudi data while Vesuvius is consistent with Stromboli and other Aeolian olivine phenocrysts (Fig. 3.5a). In Figure 3.5b, Ca budgets of Irazu and Argentinian olivine are low and very alike our data due to the

fact that Ca is controlled by H_2O. In contrast, Vesuvius is characterized by higher Ca contents (>2000 ppm) that may be related to the important metasomatism of carbonated sediment and assimilation of carbonated crust that typically affect magmas from this area (Dallai et al., 2011; Jolis et al., 2013). Carbonate-rich melts with very low silica activities would react with orthopyroxene to produce olivine as observed in experiments from Neumann et al. (2002). The Argentinian olivine phenocrysts from Søager et al. (2015) seem to be analogous to our data, but these olivine phenocrysts are characterized by high Fe/Mn ratios that exceeds the modeled bound of 70 for observed olivines of a peridotite source provenance (Herzberg, 2011), pointing toward a pyroxenitic origin. Therefore, these back-arc olivines were interpreted as the results of mixing in the mantle wedge between a pyroxene rich mantle and a peridotitic metasomatized mantle (Søager et al., 2015). Also, Irazu olivine plot alike a small range of olivines from Alicudi with slightly higher Fe/Mn values, similar to Ni in Fig. 3.5a. In the study of Ruprecht and Plank, 2013 these olivine from Irazu were analyzed in traverse core-rim, and the authors described them as zoned and some with forsteritic core (Mg-number 90) that could reach value of 4000 ppm in Ni, likely due to a pyroxenitic component in the source (in Fig. 3.5 we represent average of the most forsteritic points, Mg-number >88).

In Figure 3.4d and 3.5d the schematic triangle indicates the best-fit values of pyroxenite, peridotite, and eclogite melts composition. These diagrams display how the data with an inferred pyroxenitic component (e.g. Mauna Kea, Quepos) plot close to the pyroxenite melt endmember and on the global array (pyroxenite-peridotite melt) from Sobolev et al. (2005; 2007). In contrast, the majority of the Aeolian olivine points are concentrated around the peridotite end-member, like the MORB olivines. Only the island of Alicudi displays some olivine phenocrysts that plot more toward the pyroxenite end-member, and approximately parallel to the global array. Our data also seem to not have any influence from an eclogite melts, differently than for the Argentinian

olivines. Moreover, our data plot completely outside the modeled triangle (together with Vesuvius olivines) and this is probably due to the fact that this model was optimized for intraplate magmas without considering all the possible variables and complications of a subduction setting region.

Table 3A.1 *Olivine analyses, wt% (EPMA)*
Olivine cores, wt% (n=287)

Island	Sample	Olivine	Na_2O	Al_2O_3	CoO	ZnO	P_2O_5	CaO	TiO_2	NiO	MnO	Cr_2O_3	MgO	FeO	SiO_2	Total
Alicudi	AL-13-02	Al2_ol1	0.0041	0.0303	0.0176	0.0118	0.0062	0.0989	0.0030	0.4129	0.1108	0.1132	50.52	7.70	40.95	99.98
Alicudi	AL-13-02	Al2_ol2	0.0035	0.0179	0.0241	0.0167	0.0038	0.2044	0.0031	0.1405	0.3225	0.0112	42.39	18.65	39.25	101.04
Alicudi	AL-13-02	Al2_ol3	0.0024	0.0208	0.0243	0.0170	0.0054	0.2305	0.0047	0.1392	0.3276	0.0121	42.00	18.74	39.02	100.54
Alicudi	AL-13-02	Al2_ol4	0.0046	0.0208	0.0237	0.0173	0.0071	0.2198	0.0049	0.1493	0.3254	0.0162	42.31	18.89	39.38	101.36
Alicudi	AL-13-02	Al2_ol5	0.0032	0.0217	0.0239	0.0174	0.0040	0.2137	0.0045	0.1323	0.3229	0.0175	42.23	18.82	39.17	100.99
Alicudi	AL-13-02	Al2_ol6	0.0047	0.0193	0.0242	0.0174	0.0050	0.2115	0.0035	0.1229	0.3280	0.0183	42.17	18.87	39.24	101.03
Alicudi	AL-13-02	Al2_ol7	0.0047	0.0204	0.0220	0.0179	0.0505	0.2267	0.0022	0.1597	0.2849	0.0218	43.97	17.11	39.81	101.69
Alicudi	AL-13-02	Al2_ol8	0.0055	0.0194	0.0247	0.0177	0.0032	0.2186	0.0022	0.1363	0.3250	0.0148	42.20	18.88	39.30	101.14
Alicudi	AL-13-02	Al2_ol9	0.0032	0.0247	0.0216	0.0182	0.0117	0.2424	0.0031	0.1699	0.2843	0.0248	43.54	17.01	39.49	100.83
Alicudi	AL-13-02	Al2_ol10	0.0068	0.0235	0.0232	0.0172	0.0359	0.2039	0.0053	0.1446	0.3147	0.0198	42.27	18.26	39.39	100.72
Alicudi	AL-13-02	Al2_ol11	0.0030	0.0229	0.0249	0.0176	0.0032	0.1982	0.0030	0.1307	0.3411	0.0214	41.59	19.63	39.14	101.13
Alicudi	AL-13-02	Al2_ol12	0.0048	0.0216	0.0246	0.0178	0.0052	0.2009	0.0031	0.1362	0.3321	0.0127	41.69	19.42	39.31	101.18
Alicudi	AL-13-02	Al2_ol13	0.0043	0.0432	0.0226	0.0192	0.0106	0.1548	0.0086	0.2164	0.2806	0.0345	44.03	16.86	39.78	101.47
Alicudi	AL-13-02	Al2_ol14	0.0014	0.0249	0.0240	0.0166	0.0060	0.1994	0.0046	0.1433	0.3112	0.0166	42.99	18.20	39.66	101.60
Alicudi	AL-13-02	Al2_ol15	0.0025	0.0278	0.0226	0.0169	0.0023	0.1948	0.0023	0.1959	0.2777	0.0258	43.64	17.00	39.68	101.09
Alicudi	AL-13-02	Al2_ol16	0.0020	0.0193	0.0229	0.0158	0.0047	0.2086	0.0027	0.1305	0.3265	0.0129	42.25	18.88	39.39	101.26
Alicudi	AL-13-02	Al2_ol17	0.0014	0.0227	0.0231	0.0171	0.0056	0.2219	0.0030	0.1452	0.3019	0.0181	42.91	17.86	39.37	100.89
Alicudi	AL-13-02	Al2_ol18	0.0022	0.0215	0.0244	0.0160	0.0050	0.2085	0.0025	0.1404	0.3334	0.0183	42.34	19.02	39.59	101.72
Alicudi	AL-13-02	Al2_ol19	0.0033	0.0200	0.0237	0.0174	0.0061	0.2145	0.0050	0.1194	0.3354	0.0118	42.27	19.14	39.49	101.65
Alicudi	AL-13-02	Al2_ol20	0.0031	0.0184	0.0241	0.0159	0.0034	0.2114	0.0046	0.1258	0.3316	0.0114	42.39	19.02	39.49	101.64
Alicudi	AL-13-02	Al2_ol21	0.0016	0.0228	0.0249	0.0174	0.0218	0.2237	0.0057	0.1280	0.3288	0.0151	42.32	18.80	39.44	101.35
Alicudi	AL-13-02	Al2_ol22	0.0028	0.0211	0.0249	0.0159	0.0188	0.2114	0.0079	0.1219	0.3270	0.0115	42.33	18.84	39.29	101.22
Alicudi	AL-13-02	Al2_ol23	0.0020	0.0243	0.0248	0.0162	0.0225	0.2269	0.0055	0.1089	0.3515	0.0095	41.36	19.69	39.03	100.88
Alicudi	AL-13-02	Al2_ol24	0.0004	0.0187	0.0243	0.0163	0.0059	0.2133	0.0051	0.1195	0.3290	0.0115	42.26	18.83	39.28	101.11
Alicudi	AL-13-02	Al2_ol25	0.0017	0.0262	0.0239	0.0176	0.0986	0.2118	0.0076	0.1166	0.3333	0.0126	42.00	19.18	39.36	101.39
Alicudi	AL-13-02	Al2_ol26	0.0014	0.0208	0.0238	0.0158	0.0059	0.2198	0.0028	0.1591	0.3234	0.0269	42.21	18.88	39.28	101.17
Alicudi	AL-13-02	Al2_ol27	0.0014	0.0357	0.0192	0.0121	0.0048	0.0996	0.0027	0.3958	0.1486	0.0667	49.40	9.98	40.95	101.12
Alicudi	AL-13-02	Al2_ol28	0.0036	0.0222	0.0238	0.0162	0.0126	0.2060	0.0052	0.1280	0.3282	0.0417	42.42	18.83	39.42	101.47
Alicudi	AL-13-02	Al2_ol29	0.0046	0.0301	0.0222	0.0173	0.0031	0.1052	0.0052	0.2432	0.2733	0.0385	43.81	16.99	39.79	101.34

Alicudi	AL-13-02	Al2_ol30	0.0026	0.0355	0.0193	0.0136	0.0032	0.1044	0.0028	0.3848	0.1726	0.0668	48.31	11.24	40.68	101.03
Alicudi	AL-13-02	Al2_ol31	0.0014	0.0306	0.0203	0.0145	0.0082	0.1943	0.0025	0.2115	0.2586	0.0388	44.85	15.37	39.94	100.94
Alicudi	AL-13-02	Al2_ol32	0.0027	0.0251	0.0199	0.0133	0.0086	0.1945	0.0032	0.2474	0.1877	0.0341	48.66	11.56	41.08	102.05
Alicudi	AL-13-02	Al2_ol33	0.0018	0.0315	0.0180	0.0111	0.0032	0.1022	0.0018	0.3965	0.1439	0.0644	49.42	9.76	40.64	100.60
Alicudi	AL-13-02	Al2_ol34	0.0029	0.0197	0.0202	0.0171	0.0056	0.2287	0.0033	0.2479	0.2292	0.0291	45.71	14.80	40.12	101.44
Alicudi	AL-13-02	Al2_ol35	0.0039	0.0298	0.0217	0.0133	0.0018	0.1588	0.0026	0.2435	0.2538	0.0398	44.90	15.40	39.87	100.94
Alicudi	AL-13-02	Al2_ol36	0.0024	0.0220	0.0251	0.0157	0.0033	0.2255	0.0065	0.1247	0.3230	0.0116	42.49	18.52	39.54	101.30
Alicudi	AL-13-02	Al2_ol37	0.0042	0.0207	0.0248	0.0164	0.0085	0.2340	0.0033	0.1497	0.3282	0.0233	42.18	18.83	39.50	101.32
Alicudi	AL-13-02	Al2_ol38	0.0019	0.0305	0.0185	0.0132	0.0075	0.1771	0.0047	0.2571	0.1433	0.0444	50.55	8.57	41.27	101.09
Alicudi	AL-13-02	Al2_ol39	0.0031	0.0341	0.0209	0.0155	0.0041	0.1304	0.0029	0.2606	0.2183	0.0430	46.12	14.03	40.28	101.17
Alicudi	AL-13-02	Al2_ol40	0.0040	0.0332	0.0185	0.0147	0.0033	0.1039	0.0024	0.3540	0.1801	0.0628	47.81	11.92	40.50	101.01
Alicudi	AL-13-02	Al2_ol41	0.0041	0.0211	0.0232	0.0173	0.0031	0.2324	0.0025	0.1445	0.3021	0.0178	42.85	17.89	39.26	100.77
Alicudi	AL-13-02	Al2_ol42	0.0019	0.0189	0.0209	0.0177	0.0121	0.2309	0.0032	0.1871	0.2535	0.0329	44.45	15.90	39.47	100.60
Alicudi	AL-13-02	Al2_ol43	0.0000	0.0361	0.0180	0.0087	0.0063	0.1566	0.0058	0.2449	0.1446	0.0405	50.93	7.88	41.20	100.66
Alicudi	AL-13-02	Al2_ol44	0.0002	0.0209	0.0195	0.0192	0.0040	0.2404	0.0028	0.1823	0.2759	0.0256	43.79	16.87	39.60	101.06
Alicudi	AL-13-02	Al2_ol45	0.0020	0.0235	0.0214	0.0187	0.0014	0.2066	0.0033	0.1826	0.2970	0.0300	43.56	17.46	39.70	101.50
Alicudi	AL-13-02	Al2_ol46	0.0034	0.0177	0.0255	0.0176	0.0050	0.2390	0.0027	0.1108	0.3534	0.0164	41.30	20.22	39.11	101.43
Alicudi	AL-13-02	Al2_ol47	0.0034	0.0333	0.0230	0.0178	0.0026	0.1967	0.0046	0.1980	0.3178	0.0375	42.34	18.56	39.24	100.98
Alicudi	AL-13-03	Al3_ol1	0.0017	0.0215	0.0242	0.0183	0.0221	0.2134	0.0081	0.1400	0.3267	0.0130	41.89	18.53	38.86	100.07
Alicudi	AL-13-03	Al3_ol2	0.0026	0.0340	0.0242	0.0162	0.0040	0.1808	0.0032	0.1734	0.3188	0.0214	42.08	18.39	38.60	99.86
Alicudi	AL-13-03	Al3_ol3	0.0007	0.0193	0.0238	0.0165	0.0068	0.2106	0.0025	0.1248	0.3521	0.0212	40.84	19.98	38.75	100.34
Alicudi	AL-13-03	Al3_ol4	0.0034	0.0210	0.0211	0.0169	0.0047	0.2672	0.0036	0.1877	0.2601	0.0237	44.51	15.54	39.60	100.46
Alicudi	AL-13-03	Al3_ol5	0.0035	0.0216	0.0245	0.0212	0.0093	0.2302	0.0071	0.1112	0.3614	0.0083	40.58	20.72	38.73	100.83
Alicudi	AL-13-03	Al3_ol6	0.0037	0.0215	0.0228	0.0161	0.0018	0.1965	0.0033	0.1559	0.3042	0.0138	42.75	17.84	39.34	100.67
Alicudi	AL-13-03	Al3_ol7	0.0053	0.0219	0.0230	0.0163	0.0014	0.1833	0.0045	0.1782	0.2966	0.0198	43.12	17.36	39.50	100.74
Alicudi	AL-13-03	Al3_ol8	0.0008	0.0223	0.0249	0.0173	0.0054	0.2155	0.0041	0.1207	0.3496	0.0149	41.12	19.79	39.06	100.74
Alicudi	AL-13-03	Al3_ol9	0.0017	0.0229	0.0245	0.0155	0.0126	0.2423	0.0080	0.1143	0.3350	0.0105	41.61	19.17	39.12	100.68
Alicudi	AL-13-03	Al3_ol10	0.0046	0.0154	0.0257	0.0153	0.0033	0.2153	0.0042	0.1178	0.3342	0.0128	41.75	19.19	39.14	100.83
Alicudi	AL-13-03	Al3_ol11	0.0005	0.0227	0.0234	0.0151	0.0136	0.2219	0.0040	0.1419	0.3144	0.0206	42.20	18.33	39.30	100.61
Alicudi	AL-13-03	Al3_ol12	0.0020	0.0180	0.0246	0.0165	0.0215	0.2089	0.0092	0.1146	0.3385	0.0110	41.70	19.28	39.24	100.98
Alicudi	AL-13-03	Al3_ol13	0.0038	0.0205	0.0231	0.0156	0.0038	0.2134	0.0030	0.1463	0.2986	0.0237	42.74	17.72	39.35	100.56
Alicudi	AL-13-03	Al3_ol14	0.0035	0.0182	0.0254	0.0156	0.0128	0.2094	0.0057	0.1106	0.3446	0.0099	41.24	19.46	38.98	100.44

Alicudi	AL-13-03	Al3_ol15	0.0059	0.0208	0.0258	0.0151	0.0192	0.2053	0.0097	0.1173	0.3579	0.0123	40.79	19.77	38.72	100.07
Alicudi	AL-13-03	Al3_ol16	0.0023	0.0210	0.0246	0.0169	0.0138	0.2026	0.0045	0.1179	0.3278	0.0083	41.28	19.21	38.90	100.13
Alicudi	AL-13-03	Al3_ol17	0.0039	0.0332	0.0224	0.0152	0.0009	0.1582	0.0029	0.2134	0.2646	0.0372	43.55	16.12	39.22	99.64
Alicudi	AL-13-03	Al3_ol18	0.0009	0.0217	0.0243	0.0130	0.0026	0.1980	0.0056	0.1280	0.2707	0.0065	44.26	15.82	39.53	100.28
Alicudi	AL-13-03	Al3_ol19	0.0031	0.0183	0.0210	0.0148	0.0035	0.2507	0.0021	0.1795	0.2389	0.0223	45.28	14.30	39.84	100.17
Alicudi	AL-13-03	Al3_ol20	0.0036	0.0213	0.0239	0.0160	0.0068	0.2065	0.0043	0.1440	0.3115	0.0163	42.11	18.37	39.10	100.34
Alicudi	AL-13-03	Al3_ol21	0.0022	0.0179	0.0247	0.0155	0.0028	0.2170	0.0050	0.1118	0.3406	0.0111	41.18	19.60	38.85	100.39
Alicudi	AL-13-03	Al3_ol22	0.0028	0.0308	0.0234	0.0170	0.0024	0.1504	0.0026	0.2181	0.2881	0.0365	42.52	17.70	39.09	100.09
Alicudi	AL-13-03	Al3_ol23	0.0047	0.0232	0.0239	0.0139	0.1126	0.2135	0.0077	0.1259	0.3209	0.0127	42.07	18.51	38.89	100.32
Alicudi	AL-13-03	Al3_ol24	0.0025	0.0204	0.0245	0.0128	0.0046	0.1961	0.0030	0.1224	0.3078	0.0115	42.54	18.03	39.37	100.64
Alicudi	AL-13-03	Al3_ol25	0.0029	0.0231	0.0227	0.0158	0.0029	0.2732	0.0037	0.1661	0.2872	0.0188	43.44	16.99	39.52	100.77
Alicudi	AL-13-03	Al3_ol26	0.0026	0.0173	0.0242	0.0159	0.0048	0.2000	0.0043	0.1593	0.3156	0.0185	42.12	18.45	39.21	100.54
Alicudi	AL-13-03	Al3_ol27	0.0021	0.0163	0.0245	0.0176	0.0036	0.2160	0.0018	0.1320	0.3191	0.0177	42.06	18.74	39.19	100.74
Filicudi	FL-13-03B	fl03b_ol1	0.0024	0.0159	0.0228	0.0125	0.0098	0.2189	0.0045	0.1239	0.2478	0.0057	44.70	14.45	39.05	98.86
Filicudi	FL-13-03B	fl03b_ol2	0.0003	0.0181	0.0255	0.0125	0.0040	0.1865	0.0052	0.1009	0.2958	0.0011	42.36	17.76	38.73	99.50
Filicudi	FL-13-03B	fl03b_ol3	0.0002	0.0167	0.0220	0.0113	0.0050	0.2269	0.0041	0.1192	0.2257	0.0085	46.68	13.00	39.93	100.25
Filicudi	FL-13-03B	fl03b_ol4	0.0002	0.0220	0.0269	0.0145	0.0069	0.1952	0.0078	0.0908	0.3227	0.0019	41.38	19.39	38.75	100.21
Filicudi	FL-13-03B	fl03b_ol5	0.0012	0.0184	0.0236	0.0109	0.0018	0.2159	0.0037	0.1051	0.2407	0.0048	45.47	14.22	39.69	100.01
Filicudi	FL-13-03B	fl03b_ol6	0.0009	0.0186	0.0225	0.0109	0.0058	0.2178	0.0057	0.0970	0.2371	0.0073	45.81	13.69	39.65	99.78
Filicudi	FL-13-03B	fl03b_ol7	0.0000	0.0185	0.0227	0.0110	0.0030	0.2115	0.0049	0.0892	0.2471	0.0036	45.69	14.43	39.91	100.64
Filicudi	FL-13-03B	fl03b_ol8	0.0001	0.0175	0.0243	0.0108	0.0164	0.2181	0.0055	0.0917	0.2449	0.0074	45.77	14.32	39.94	100.67
Filicudi	FL-13-03B	fl03b_ol9	0.0008	0.0162	0.0242	0.0124	0.0046	0.2147	0.0041	0.0903	0.2509	0.0044	45.37	14.62	39.72	100.33
Filicudi	FL-13-03B	fl03b_ol10	0.0012	0.0159	0.0222	0.0110	0.0052	0.2209	0.0031	0.1023	0.2381	0.0046	45.81	14.10	39.85	100.39
Filicudi	FL-13-03B	fl03b_ol11	0.0000	0.0203	0.0242	0.0106	0.0060	0.2223	0.0044	0.0918	0.2368	0.0076	45.99	13.65	39.78	100.04
Filicudi	FL-13-03B	fl03b_ol12	0.0026	0.0179	0.0220	0.0100	0.0026	0.2217	0.0043	0.1020	0.2333	0.0077	46.12	13.51	39.83	100.08
Filicudi	FL-13-03B	fl03b_ol13	0.0030	0.0247	0.0269	0.0171	0.0209	0.2022	0.0072	0.0493	0.3023	0.0014	43.03	17.68	39.25	100.62
Filicudi	FL-13-03B	fl03b_ol14	0.0019	0.0205	0.0237	0.0111	0.0024	0.2197	0.0046	0.0897	0.2488	0.0050	45.49	14.52	39.84	100.47
Filicudi	FL-13-03B	fl03b_ol15	0.0020	0.0164	0.0228	0.0104	0.0045	0.2216	0.0038	0.1018	0.2308	0.0088	46.24	13.45	39.96	100.27
Filicudi	FL-13-03B	fl03b_ol16	0.0012	0.0247	0.0274	0.0115	0.0198	0.2050	0.0084	0.0653	0.2843	0.0021	43.69	16.65	39.39	100.38
Filicudi	FL-13-03B	fl03b_ol17	0.0013	0.0170	0.0225	0.0122	0.0049	0.2162	0.0031	0.1007	0.2396	0.0096	46.05	14.00	40.05	100.72
Filicudi	FL-13-03B	fl03b_ol18	0.0005	0.0154	0.0241	0.0108	0.0105	0.2258	0.0030	0.0884	0.2487	0.0044	45.53	14.57	39.89	100.61

Filicudi	FL-13-03B	fl03b_ol19	0.0023	0.0162	0.0224	0.0110	0.0088	0.2255	0.0037	0.1023	0.2308	0.0091	46.41	13.17	39.85	100.06
Filicudi	FL-13-03B	fl03b_ol20	0.0018	0.0161	0.0228	0.0120	0.0137	0.2165	0.0053	0.0914	0.2447	0.0101	45.49	14.30	39.67	100.10
Filicudi	FL-13-03B	fl03b_ol21	0.0009	0.0203	0.0222	0.0105	0.0072	0.2188	0.0065	0.1030	0.2364	0.0079	45.96	13.72	39.88	100.19
Filicudi	FL-13-03B	fl03b_ol22	0.0015	0.0159	0.0223	0.0100	0.0022	0.2275	0.0038	0.1031	0.2258	0.0110	46.64	13.00	39.98	100.24
Filicudi	FL-13-03B	fl03b_ol23	0.0015	0.0161	0.0219	0.0099	0.0175	0.2247	0.0040	0.0968	0.2298	0.0095	46.38	13.45	40.02	100.49
Filicudi	FL-13-03B	fl03b_ol24	0.0000	0.0139	0.0229	0.0104	0.0060	0.2199	0.0033	0.1043	0.2265	0.0095	46.57	12.79	39.90	99.87
Filicudi	FL-13-03B	fl03b_ol25	0.0004	0.0197	0.0239	0.0120	0.0048	0.2142	0.0062	0.0831	0.2564	0.0033	44.93	14.89	39.54	99.99
Filicudi	FL-13-03B	fl03b_ol26	0.0013	0.0166	0.0218	0.0111	0.0072	0.2305	0.0042	0.1050	0.2281	0.0092	46.40	13.13	39.90	100.07
Filicudi	FL-13-03B	fl03b_ol27	0.0009	0.0177	0.0227	0.0122	0.0047	0.2158	0.0037	0.0921	0.2448	0.0059	45.60	14.31	39.81	100.33
Filicudi	FL-13-03B	fl03b_ol28	0.0011	0.0183	0.0246	0.0106	0.0055	0.2201	0.0041	0.0820	0.2521	0.0023	45.18	14.66	39.60	100.06
Filicudi	FL-13-03B	fl03b_ol29	0.0000	0.0226	0.0241	0.0119	0.0137	0.2114	0.0068	0.0824	0.2571	0.0040	45.18	15.10	39.76	100.67
Filicudi	FL-13-03B	fl03b_ol30	0.0014	0.0216	0.0223	0.0104	0.0139	0.2213	0.0063	0.0895	0.2227	0.0091	47.28	12.78	40.49	101.17
Filicudi	FL-13-03B	fl03b_ol31	0.0028	0.0152	0.0228	0.0106	0.0075	0.2242	0.0035	0.1037	0.2304	0.0091	46.36	13.18	39.89	100.06
Filicudi	FL-13-03B	fl03b_ol32	0.0001	0.0176	0.0242	0.0100	0.0019	0.2155	0.0039	0.0863	0.2535	0.0036	45.13	14.52	39.49	99.76
Filicudi	FL-13-03B	fl03b_ol33	0.0000	0.0232	0.0230	0.0103	0.0037	0.2186	0.0075	0.0945	0.2316	0.0076	46.33	13.17	39.91	100.03
Filicudi	FL-13-03B	fl03b_ol34	0.0000	0.0206	0.0250	0.0122	0.0108	0.2016	0.0058	0.0804	0.2645	0.0028	44.66	15.41	39.59	100.28
Filicudi	FL-13-03B	fl03b_ol35	0.0000	0.0186	0.0232	0.0106	0.0062	0.2162	0.0046	0.0922	0.2427	0.0069	45.99	13.82	39.95	100.38
Filicudi	FL-13-03B	fl03b_ol36	0.0013	0.0189	0.0266	0.0114	0.0041	0.1904	0.0039	0.0754	0.2860	0.0019	43.91	16.52	39.51	100.56
Filicudi	FL-13-03B	fl03b_ol37	0.0025	0.0168	0.0232	0.0117	0.0219	0.2163	0.0037	0.0725	0.2494	0.0052	46.13	14.48	40.28	101.51
Filicudi	FL-13-03B	fl03b_ol38	0.0014	0.0186	0.0228	0.0106	0.0028	0.2168	0.0051	0.1036	0.2272	0.0102	46.43	13.02	39.84	99.91
Filicudi	FL-13-03B	fl03b_ol39	0.0009	0.0162	0.0243	0.0133	0.0042	0.1907	0.0057	0.0804	0.2753	0.0028	43.89	16.43	39.38	100.32
Filicudi	FL-13-03B	fl03b_ol40	0.0018	0.0152	0.0235	0.0115	0.0100	0.2164	0.0041	0.1026	0.2371	0.0091	45.92	13.88	39.89	100.32
Filicudi	FL-13-03B	fl03b_ol41	0.0005	0.0214	0.0242	0.0117	0.0047	0.2112	0.0069	0.0831	0.2552	0.0033	45.38	14.78	39.84	100.63
Filicudi	FL-13-03B	fl03b_ol42	0.0020	0.0228	0.0262	0.0136	0.0096	0.2056	0.0084	0.0569	0.3322	0.0010	42.42	18.48	39.16	100.73
Filicudi	FL-13-03B	fl03b_ol43	0.0006	0.0223	0.0289	0.0151	0.0212	0.2033	0.0098	0.0475	0.3812	0.0002	39.36	21.98	38.42	100.49
Filicudi	FL-13-03B	fl03b_ol44	0.0010	0.0225	0.0239	0.0106	0.0121	0.2129	0.0072	0.0938	0.2296	0.0075	46.30	13.11	39.86	99.89
Filicudi	FL-13-03B	fl03b_ol45	0.0016	0.0198	0.0244	0.0125	0.0056	0.2079	0.0045	0.0878	0.2576	0.0035	44.87	15.48	39.82	100.80
Filicudi	FL-13-03B	fl03b_ol46	0.0029	0.0148	0.0222	0.0110	0.0117	0.2279	0.0039	0.0974	0.2262	0.0092	47.15	12.85	40.42	101.05
Filicudi	FL-13-03B	fl03b_ol47	0.0001	0.0200	0.0231	0.0105	0.0050	0.2115	0.0054	0.0843	0.2619	0.0033	45.08	14.96	39.60	100.26
Filicudi	FL-13-03B	fl03b_ol48	0.0020	0.0231	0.0247	0.0109	0.0049	0.2022	0.0088	0.0798	0.2587	0.0019	45.00	15.04	39.60	100.25
Filicudi	FL-13-03B	fl03b_ol49	0.0000	0.0199	0.0253	0.0113	0.0026	0.1876	0.0048	0.0820	0.2806	0.0031	43.59	16.56	39.19	99.96
Filicudi	FL-13-03B	fl03b_ol50	0.0000	0.0173	0.0234	0.0104	0.0051	0.2132	0.0039	0.0825	0.2544	0.0036	45.34	14.62	39.83	100.40

Filicudi	FL-13-03B	fl03b_ol51	0.0026	0.0155	0.0224	0.0102	0.0045	0.2321	0.0035	0.1066	0.2261	0.0089	46.66	12.67	40.03	100.00
Filicudi	FL-13-03B	fl03b_ol52	0.0000	0.0149	0.0224	0.0100	0.0065	0.2257	0.0037	0.1023	0.2308	0.0078	46.56	12.99	39.97	100.14
Filicudi	FL-13-03B	fl03b_ol53	0.0004	0.0199	0.0238	0.0104	0.0213	0.2110	0.0049	0.1331	0.2510	0.0051	46.05	14.45	40.33	101.50
Filicudi	FL-13-03B	fl03b_ol54	0.0000	0.0227	0.0272	0.0104	0.0206	0.1832	0.0043	0.0840	0.2982	0.0036	43.87	17.22	39.71	101.45
Filicudi	FL-13-03B	fl03b_ol55	0.0000	0.0205	0.0235	0.0098	0.0041	0.2055	0.0051	0.0878	0.2405	0.0065	46.45	13.38	40.12	100.56
Filicudi	FL-13-03B	fl03b_ol56	0.0018	0.0195	0.0227	0.0080	0.0037	0.2171	0.0055	0.1006	0.2392	0.0079	46.17	13.75	39.97	100.51
Filicudi	FL-13-03B	fl03b_ol57	0.0003	0.0175	0.0230	0.0105	0.0051	0.2198	0.0034	0.0946	0.2414	0.0047	45.71	14.06	39.77	100.16
Filicudi	FL-13-03B	fl03b_ol58	0.0013	0.0189	0.0220	0.0093	0.0517	0.2150	0.0051	0.0982	0.2365	0.0060	46.13	13.53	39.85	100.18
Filicudi	FL-13-03B	fl03b_ol59	0.0014	0.0205	0.0233	0.0087	0.0051	0.2149	0.0029	0.0993	0.2379	0.0075	45.89	13.63	39.93	100.07
Filicudi	FL-13-03B	fl03b_ol60	0.0022	0.0140	0.0227	0.0100	0.0094	0.2284	0.0033	0.1035	0.2281	0.0103	46.58	12.93	39.96	100.10
Filicudi	FL-13-03B	fl03b_ol61	0.0011	0.0159	0.0242	0.0107	0.0068	0.2172	0.0036	0.0894	0.2538	0.0041	45.58	14.59	39.79	100.58
Filicudi	FL-13-03B	fl03b_ol62	0.0010	0.0259	0.0235	0.0103	0.0123	0.2153	0.0122	0.0935	0.2369	0.0040	46.13	13.46	39.94	100.17
Salina	SL-13-05	sl5_ol1	0.0031	0.0159	0.0236	0.0210	0.0084	0.1927	0.0036	0.1167	0.2732	0.0121	43.49	16.93	39.27	100.35
Salina	SL-13-05	sl5_ol2	0.0033	0.0235	0.0272	0.0188	0.0096	0.2077	0.0040	0.1023	0.3338	0.0056	41.65	19.10	39.10	100.59
Salina	SL-13-05	sl5_ol3	0.0000	0.0204	0.0216	0.0158	0.0203	0.1807	0.0042	0.1363	0.2412	0.0157	45.87	13.99	39.93	100.44
Salina	SL-13-05	sl5_ol4	0.0024	0.0207	0.0206	0.0184	0.0072	0.1772	0.0030	0.2212	0.2173	0.0301	46.21	13.39	39.94	100.26
Salina	SL-13-05	sl5_ol5	0.0012	0.0169	0.0214	0.0155	0.0057	0.1884	0.0023	0.1672	0.2230	0.0271	46.38	13.27	39.99	100.31
Salina	SL-13-05	sl5_ol6	0.0012	0.0189	0.0248	0.0225	0.0032	0.1808	0.0034	0.1403	0.3284	0.0202	41.81	18.78	39.07	100.41
Salina	SL-13-05	sl5_ol7	0.0014	0.0215	0.0207	0.0154	0.0026	0.1849	0.0042	0.1360	0.2452	0.0145	45.46	14.24	39.73	100.08
Salina	SL-13-05	sl5_ol8	0.0046	0.0184	0.0213	0.0189	0.0045	0.1829	0.0022	0.2561	0.1884	0.0318	47.36	12.01	40.18	100.27
Salina	SL-13-05	sl5_ol9	0.0056	0.0216	0.0262	0.0226	0.0038	0.2648	0.0035	0.0881	0.3804	0.0048	38.99	21.26	38.64	99.71
Salina	SL-13-05	sl5_ol10	0.0047	0.0195	0.0260	0.0247	0.0077	0.1939	0.0031	0.0955	0.4148	0.0087	37.54	22.82	38.44	99.59
Salina	SL-13-05	sl5_ol11	0.0047	0.0180	0.0220	0.0217	0.0048	0.1694	0.0025	0.2079	0.2807	0.0231	43.32	16.71	39.47	100.26
Salina	SL-13-05	sl5_ol12	0.0040	0.0191	0.0273	0.0239	0.0188	0.1969	0.0058	0.0794	0.3920	0.0036	38.84	22.20	38.27	100.08
Salina	SL-13-05	sl5_ol13	0.0040	0.0195	0.0230	0.0243	0.0047	0.1781	0.0021	0.1619	0.3052	0.0220	42.19	18.23	39.04	100.19
Salina	SL-13-05	sl5_ol14	0.0037	0.0251	0.0207	0.0186	0.0037	0.1984	0.0033	0.2054	0.2159	0.0334	46.03	13.30	39.74	99.79
Salina	SL-13-05	sl5_ol15	0.0018	0.0214	0.0225	0.0203	0.0146	0.1806	0.0038	0.1335	0.2692	0.0128	44.14	15.89	39.35	100.07
Salina	SL-13-05	sl5_ol16	0.0028	0.0227	0.0258	0.0237	0.0054	0.2128	0.0092	0.0892	0.3552	0.0058	40.62	20.03	38.42	99.82
Salina	SL-13-05	sl5_ol17	0.0017	0.0192	0.0235	0.0208	0.0048	0.1782	0.0043	0.1213	0.2983	0.0116	42.97	17.39	39.14	100.18
Salina	SL-13-05	sl5_ol18	0.0062	0.0214	0.0271	0.0232	0.0382	0.1940	0.0064	0.0849	0.3634	0.0036	39.64	21.38	38.29	100.08
Salina	SL-13-05	sl5_ol19	0.0048	0.0199	0.0247	0.0219	0.0085	0.1828	0.0028	0.1362	0.2903	0.0183	42.83	17.20	39.08	99.81

Salina	SL-13-05	sl5_ol20	0.0085	0.0185	0.0276	0.0270	0.0075	0.1949	0.0034	0.1011	0.4472	0.0096	35.84	24.56	37.85	99.10
Salina	SL-13-05	sl5_ol21	0.0015	0.0146	0.0230	0.0243	0.0027	0.1906	0.0022	0.1540	0.3223	0.0175	41.66	18.74	38.82	99.98
Salina	SL-13-05	sl5_ol22	0.0049	0.0180	0.0219	0.0181	0.0067	0.1929	0.0025	0.1592	0.2564	0.0250	44.47	15.42	39.46	100.05
Salina	SL-13-05	sl5_ol23	0.0029	0.0215	0.0277	0.0239	0.0136	0.1982	0.0047	0.0771	0.3859	0.0035	39.03	21.98	38.21	99.97
Salina	SL-13-05	sl5_ol24	0.0037	0.0215	0.0238	0.0198	0.0029	0.1929	0.0033	0.1293	0.3449	0.0235	41.29	19.28	38.76	100.09
Salina	SL-13-05	sl5_ol25	0.0030	0.0170	0.0200	0.0222	0.0044	0.1817	0.0031	0.1909	0.2988	0.0316	43.47	16.73	39.46	100.43
Salina	SL-13-05	sl5_ol26	0.0005	0.0184	0.0250	0.0232	0.0055	0.1979	0.0036	0.1025	0.3378	0.0084	41.16	19.53	38.77	100.18
Salina	SL-13-05	sl5_ol27	0.0026	0.0169	0.0216	0.0182	0.0033	0.1851	0.0029	0.1566	0.2442	0.0224	45.15	14.53	39.62	99.98
Salina	SL-13-05	sl5_ol28	0.0038	0.0183	0.0230	0.0218	0.0030	0.1779	0.0027	0.1455	0.3120	0.0186	42.00	18.11	39.02	99.86
Salina	SL-13-05	sl5_ol29	0.0056	0.0187	0.0257	0.0225	0.0071	0.2069	0.0028	0.1179	0.3852	0.0191	38.26	22.67	38.20	99.94
Salina	SL-13-05	sl5_ol30	0.0031	0.0238	0.0214	0.0215	0.0036	0.1852	0.0036	0.1830	0.2632	0.0235	44.07	15.77	39.64	100.21
Salina	SL-13-05	sl5_ol31	0.0043	0.0153	0.0242	0.0230	0.0051	0.1818	0.0024	0.1624	0.3393	0.0202	40.94	19.16	38.65	99.52
Salina	SL-13-05	sl5_ol32	0.0054	0.0142	0.0261	0.0211	0.0026	0.2031	0.0029	0.1355	0.3469	0.0152	40.14	20.65	38.39	99.95
Salina	SL-13-05	sl5_ol33	0.0035	0.0204	0.0221	0.0225	0.0078	0.1879	0.0033	0.1603	0.2652	0.0188	43.99	16.12	39.52	100.34
Salina	SL-13-05	sl5_ol34	0.0029	0.0164	0.0239	0.0247	0.0029	0.1836	0.0021	0.1518	0.3791	0.0219	40.34	20.36	38.45	99.96
Salina	SL-13-05	sl5_ol35	0.0052	0.0167	0.0240	0.0229	0.0057	0.1826	0.0029	0.1082	0.3721	0.0073	40.11	20.54	38.66	100.06
Salina	SL-13-05	sl5_ol36	0.0008	0.0155	0.0230	0.0247	0.0079	0.1860	0.0017	0.1257	0.3459	0.0219	41.15	19.53	38.74	100.17
Salina	SL-13-05	sl5_ol37	0.0044	0.0166	0.0270	0.0201	0.0035	0.2165	0.0030	0.1198	0.3727	0.0157	38.94	21.62	38.35	99.71
Salina	SL-13-05	sl5_ol38	0.0009	0.0181	0.0233	0.0232	0.0050	0.1746	0.0025	0.1574	0.3680	0.0197	40.68	20.13	38.86	100.47
Salina	SL-13-05	sl5_ol39	0.0023	0.0156	0.0225	0.0247	0.0022	0.1826	0.0022	0.1730	0.3028	0.0262	42.93	17.45	38.99	100.12
Salina	SL-13-05	sl5_ol40	0.0014	0.0177	0.0266	0.0269	0.0049	0.2022	0.0046	0.0977	0.4480	0.0114	37.27	24.20	37.90	100.21
Salina	SL-13-05	sl5_ol41	0.0011	0.0179	0.0247	0.0264	0.0066	0.1819	0.0030	0.1276	0.3702	0.0135	40.49	20.67	38.62	100.55
Salina	SL-13-05	sl5_ol42	0.0017	0.0221	0.0265	0.0260	0.0043	0.1941	0.0054	0.0869	0.3949	0.0044	39.45	22.41	38.70	101.33
Salina	SL-13-05	sl5_ol43	0.0037	0.0193	0.0244	0.0262	0.0087	0.1840	0.0027	0.1530	0.4004	0.0244	39.81	21.59	38.50	100.74
Salina	SL-13-05	sl5_ol44	0.0037	0.0264	0.0259	0.0250	0.0333	0.1965	0.0067	0.0953	0.3627	0.0062	40.88	20.68	38.96	101.30
Salina	SL-13-05	sl5_ol45	0.0035	0.0209	0.0244	0.0255	0.0356	0.1827	0.0037	0.2842	0.3235	0.0135	43.09	18.78	40.00	102.79
Salina	SL-13-08	sl8_ol1	0.0029	0.0178	0.0277	0.0246	0.0009	0.2372	0.0008	0.1045	0.3802	0.0023	39.15	21.82	38.21	99.98
Salina	SL-13-08	sl8_ol2	0.0040	0.0215	0.0243	0.0209	0.0113	0.1884	0.0052	0.1136	0.3199	0.0089	41.95	18.22	38.81	99.70
Salina	SL-13-08	sl8_ol3	0.0034	0.0183	0.0221	0.0232	0.0055	0.1918	0.0024	0.1333	0.3353	0.0105	41.40	18.81	38.99	99.94
Salina	SL-13-08	sl8_ol4	0.0016	0.0239	0.0202	0.0207	0.0050	0.1863	0.0040	0.1872	0.2618	0.0290	44.90	15.11	39.66	100.41
Salina	SL-13-08	sl8_ol5	0.0057	0.0294	0.0254	0.0232	0.0656	0.2056	0.0083	0.1018	0.3396	0.0076	41.78	18.91	39.03	100.52
Salina	SL-13-08	sl8_ol6	0.0052	0.0198	0.0245	0.0257	0.0081	0.2027	0.0032	0.0928	0.3968	0.0070	38.56	21.82	38.55	99.71

Salina	SL-13-08	sl8_ol7	0.0026	0.0244	0.0209	0.0213	0.0150	0.2040	0.0039	0.1622	0.2751	0.0196	43.80	16.26	39.43	100.24
Salina	SL-13-08	sl8_ol8	0.0052	0.0270	0.0254	0.0234	0.0323	0.1988	0.0064	0.1138	0.3558	0.0041	39.85	20.29	38.77	99.70
Salina	SL-13-08	sl8_ol9	0.0013	0.0196	0.0241	0.0235	0.0072	0.1915	0.0050	0.1033	0.3430	0.0064	40.96	19.59	38.68	99.96
Salina	SL-13-08	sl8_ol10	0.0050	0.0187	0.0264	0.0230	0.0095	0.2313	0.0044	0.1063	0.3900	0.0027	38.72	21.97	38.38	99.89
Salina	SL-13-08	sl8_ol11	0.0102	0.0183	0.0246	0.0209	0.0060	0.2334	0.0033	0.1118	0.3815	0.0071	39.11	21.71	38.42	100.06
Salina	SL-13-08	sl8_ol12	0.0057	0.0209	0.0249	0.0197	0.0120	0.2075	0.0031	0.2062	0.3540	0.0117	39.82	20.81	38.36	99.85
Salina	SL-13-08	sl8_ol13	0.0041	0.0181	0.0223	0.0208	0.0082	0.1835	0.0031	0.1247	0.2994	0.0122	42.98	17.58	39.32	100.58
Salina	SL-13-08	sl8_ol14	0.0012	0.0205	0.0276	0.0157	0.0141	0.1557	0.0061	0.0470	0.3846	0.0014	38.63	22.48	38.38	100.16
Salina	SL-13-08	sl8_ol15	0.0057	0.0179	0.0231	0.0223	0.0064	0.1895	0.0026	0.1215	0.3220	0.0076	42.58	18.16	39.24	100.70
Salina	SL-13-08	sl8_ol16	0.0006	0.0189	0.0212	0.0183	0.0112	0.1735	0.0036	0.1395	0.2709	0.0163	44.55	15.53	39.67	100.42
Salina	SL-13-08	sl8_ol17	0.0033	0.0189	0.0212	0.0234	0.0082	0.1900	0.0029	0.1824	0.3021	0.0377	43.11	17.38	39.53	100.82
Salina	SL-13-08	sl8_ol18	0.0023	0.0195	0.0222	0.0232	0.0063	0.1797	0.0042	0.1692	0.3134	0.0111	42.80	18.00	39.46	101.01
Salina	SL-13-08	sl8_ol19	0.0000	0.0176	0.0220	0.0201	0.0052	0.1780	0.0030	0.1425	0.2750	0.0161	44.47	16.25	39.96	101.36
Salina	SL-13-08	sl8_ol20	0.0016	0.0198	0.0212	0.0170	0.0075	0.1878	0.0027	0.1766	0.2564	0.0226	45.17	15.26	39.87	101.02
Salina	SL-13-08	sl8_ol21	0.0023	0.0192	0.0246	0.0209	0.0085	0.1866	0.0046	0.1123	0.3083	0.0087	43.26	17.99	39.75	101.70
Salina	SL-13-08	sl8_ol22	0.0030	0.0179	0.0238	0.0208	0.0103	0.1878	0.0039	0.1164	0.3346	0.0068	41.76	19.23	39.45	101.16
Salina	SL-13-08	sl8_ol23	0.0046	0.0216	0.0244	0.0195	0.0348	0.2237	0.0075	0.0828	0.3450	0.0043	41.83	19.32	39.24	101.16
Salina	SL-13-08	sl8_ol24	0.0010	0.0183	0.0206	0.0183	0.0043	0.1968	0.0023	0.1716	0.2426	0.0198	45.69	14.80	40.17	101.36
Salina	SL-13-08	sl8_ol25	0.0020	0.0195	0.0224	0.0213	0.0047	0.1904	0.0032	0.1366	0.3218	0.0175	42.63	18.22	39.36	100.95
Salina	SL-13-08	sl8_ol26	0.0063	0.0181	0.0242	0.0233	0.0047	0.1768	0.0027	0.1134	0.3479	0.0090	41.51	19.26	39.22	100.72
Salina	SL-13-08	sl8_ol27	0.0020	0.0188	0.0228	0.0190	0.0038	0.1885	0.0029	0.1362	0.3034	0.0174	42.98	17.21	39.17	100.07
Salina	SL-13-08	sl8_ol28	0.0068	0.0169	0.0246	0.0194	0.0048	0.2106	0.0031	0.1048	0.3510	0.0077	40.45	20.47	38.61	100.27
Salina	SL-13-08	sl8_ol29	0.0045	0.0188	0.0256	0.0219	0.0038	0.2172	0.0033	0.1268	0.3809	0.0078	39.42	21.56	38.55	100.34
Salina	SL-13-08	sl8_ol30	0.0038	0.0218	0.0257	0.0208	0.0809	0.1703	0.0071	0.0691	0.3536	0.0003	40.45	20.37	38.48	100.05
Salina	SL-13-08	sl8_ol31	0.0033	0.0214	0.0243	0.0260	0.0095	0.1813	0.0042	0.1037	0.3928	0.0051	39.63	21.01	38.56	99.96
Salina	SL-13-08	sl8_ol32	0.0028	0.0167	0.0218	0.0187	0.0071	0.1884	0.0027	0.1483	0.2698	0.0232	44.08	15.94	39.51	100.23
Salina	SL-13-08	sl8_ol33	0.0034	0.0205	0.0256	0.0201	0.0359	0.1834	0.0083	0.0733	0.3626	0.0026	40.05	20.94	38.58	100.30
Salina	SL-13-08	sl8_ol34	0.0022	0.0208	0.0222	0.0183	0.0076	0.1823	0.0031	0.1600	0.2787	0.0157	43.93	16.25	39.64	100.53
Salina	SL-13-08	sl8_ol35	0.0031	0.0184	0.0218	0.0185	0.0028	0.1991	0.0028	0.1509	0.2810	0.0189	43.74	16.56	39.71	100.73
Salina	SL-13-08	sl8_ol36	0.0023	0.0144	0.0227	0.0204	0.0117	0.1569	0.0035	0.1088	0.2832	0.0116	43.99	16.58	39.79	101.00
Salina	SL-13-08	sl8_ol37	0.0061	0.0206	0.0207	0.0192	0.0100	0.1834	0.0029	0.1908	0.2919	0.0184	44.30	16.24	39.88	101.17
Salina	SL-13-08	sl8_ol38	0.0000	0.0191	0.0180	0.0208	0.0046	0.1879	0.0026	0.1620	0.3084	0.0128	42.47	18.11	39.30	100.62

Salina	SL-13-08	sl8_ol39	0.0054	0.0243	0.0233	0.0194	0.0073	0.1989	0.0062	0.1276	0.3315	0.0071	40.97	20.53	39.12	101.37
Salina	SL-13-08	sl8_ol40	0.0094	0.0179	0.0235	0.0253	0.0063	0.2051	0.0029	0.1159	0.4034	0.0151	38.83	21.70	38.93	100.28
Salina	SL-13-08	sl8_ol41	0.0132	0.0165	0.0237	0.0248	0.0108	0.1818	0.0030	0.1310	0.3899	0.0172	37.67	20.98	38.75	98.20
Salina	SL-13-08	sl8_ol42	0.0127	0.0238	0.0247	0.0252	0.0161	0.1866	0.0048	0.0904	0.4171	0.0033	36.61	23.22	38.79	99.42
Salina	SL-13-08	sl8_ol43	0.0073	0.0439	0.0214	0.0220	0.0073	0.1807	0.0045	0.1605	0.3266	0.0200	41.11	18.14	39.48	99.52
Salina	SL-13-08	sl8_ol44	0.0066	0.0169	0.0249	0.0275	0.0108	0.1886	0.0034	0.0912	0.4195	0.0039	38.82	22.27	38.36	100.25
Salina	SL-13-08	sl8_ol45	0.0068	0.0185	0.0246	0.0291	0.0098	0.2016	0.0033	0.0876	0.4206	0.0051	39.00	22.15	38.45	100.40
Salina	SL-13-08	sl8_ol46	0.0074	0.0190	0.0250	0.0226	0.0049	0.1830	0.0033	0.1060	0.3480	0.0094	41.12	19.60	39.14	100.59
Salina	SL-13-08	sl8_ol47	0.0073	0.0243	0.0270	0.0254	0.0054	0.2470	0.0068	0.1017	0.4098	0.0018	38.59	22.56	38.28	100.29
Stromboli CA	ST-13-09	st9_ol1	0.0023	0.0211	0.0179	0.0112	0.0042	0.2042	0.0036	0.2897	0.1643	0.0340	48.78	9.34	40.44	99.31
Stromboli CA	ST-13-09	st9_ol2	0.0028	0.0132	0.0259	0.0180	0.0152	0.0707	0.0058	0.1303	0.2998	0.0008	42.33	17.94	39.01	99.87
Stromboli CA	ST-13-09	st9_ol3	0.0012	0.0235	0.0190	0.0087	0.0240	0.1736	0.0047	0.2890	0.1642	0.0438	49.30	9.15	40.84	100.04
Stromboli CA	ST-13-09	st9_ol4	0.0013	0.0079	0.0254	0.0154	0.0091	0.062	0.0038	0.1370	0.2810	0.0012	44.21	15.95	39.41	100.11
Stromboli CA	ST-13-09	st9_ol5	0.0007	0.0093	0.0265	0.0122	0.0162	0.0613	0.0044	0.1414	0.2471	0.0025	44.03	16.01	39.54	100.11
Stromboli CA	ST-13-09	st9_ol6	0.0206	0.0185	0.0243	0.0208	0.0219	0.2286	0.0088	0.0460	0.5226	0.0006	30.81	28.80	37.09	97.61
Stromboli CA	ST-13-09	st9_ol7	0.0002	0.0083	0.0254	0.0169	0.0121	0.0603	0.0047	0.1332	0.2792	0.0020	44.73	15.80	39.83	100.91
Stromboli CA	ST-13-09	st9_ol8	0.0000	0.0082	0.0269	0.0159	0.0091	0.0588	0.0048	0.1373	0.2619	0.0003	43.58	16.87	39.42	100.39
Stromboli CA	ST-13-09	st9_ol9	0.0043	0.0117	0.0218	0.0099	0.0098	0.1200	0.0047	0.1592	0.2315	0.0147	47.02	12.98	40.52	101.11
Stromboli CA	ST-13-09	st9_ol10	0.0000	0.0089	0.0239	0.0184	0.0194	0.0621	0.0059	0.1305	0.2918	0.0028	44.01	16.76	39.76	101.09
Stromboli CA	ST-13-09	st9_ol11	0.0007	0.0091	0.0235	0.0202	0.0113	0.0651	0.0036	0.1198	0.3290	0.0019	42.92	18.03	39.51	101.05
Stromboli CA	ST-13-09	st9_ol12	0.0007	0.0114	0.0268	0.0165	0.0050	0.0656	0.0034	0.1213	0.3014	0.0015	43.43	17.52	39.67	101.17
Stromboli CA	ST-13-09	st9_ol13	0.0009	0.0095	0.0248	0.0151	0.0082	0.0554	0.0005	0.1494	0.2947	0.0006	43.90	16.84	39.73	101.02
Stromboli CA	ST-13-09	st9_ol14	0.0108	0.0194	0.0244	0.0233	0.0096	0.2060	0.0039	0.0706	0.4968	0.0023	32.93	27.57	38.07	99.43
Stromboli CA	ST-13-09	st9_ol15	0.0000	0.0076	0.0269	0.0172	0.0116	0.0715	0.0051	0.1172	0.3182	0.0005	42.31	18.66	39.50	101.04
Stromboli CA	ST-13-09	st9_ol17	0.0008	0.0077	0.0245	0.0203	0.0212	0.0654	0.0048	0.1184	0.3297	0.0008	42.96	17.90	39.43	100.89
Stromboli CA	ST-13-09	st9_ol18	0.0124	0.0173	0.0264	0.0250	0.0117	0.2487	0.0077	0.0497	0.5458	0.0002	32.80	28.39	37.74	99.88
Stromboli CA	ST-13-09	st9_ol19	0.0037	0.0243	0.0183	0.0073	0.0157	0.1691	0.0049	0.3304	0.1616	0.0418	49.58	9.02	41.28	100.65
Stromboli CA	ST-13-09	st9_ol20	0.0048	0.0180	0.0257	0.0182	0.0230	0.0902	0.0082	0.0389	0.4913	0.0006	37.68	23.30	38.80	100.50
Stromboli CA	ST-13-09	st9_ol21	0.0225	0.0284	0.0253	0.0206	0.0275	0.2467	0.0172	0.0444	0.5327	0.0000	30.63	29.45	37.29	98.34
Stromboli CA	ST-13-09	st9_ol22	0.0178	0.0258	0.0265	0.0227	0.0508	0.2442	0.0213	0.0395	0.5307	0.0004	30.69	29.83	36.77	98.26
Stromboli CA	ST-13-17	st17_ol1	0.0021	0.0119	0.0232	0.0143	0.0002	0.0000	0.0000	0.1501	0.2647	0.0082	45.08	14.90	39.65	100.09

Stromboli CA	ST-13-17	st17_ol2	0.0017	0.0110	0.0180	0.0119	0.0023	0.2048	0.0023	0.2625	0.1916	0.0262	48.83	10.51	40.46	100.53
Stromboli CA	ST-13-17	st17_ol3	0.0007	0.0097	0.0169	0.0110	0.0110	0.2161	0.0026	0.2345	0.1766	0.0331	49.03	9.99	40.67	100.40
Stromboli CA	ST-13-17	st17_ol4	0.0074	0.0094	0.0171	0.0091	0.0046	0.2173	0.0014	0.2787	0.1758	0.0316	49.08	9.68	40.45	99.96
Stromboli CA	ST-13-17	st17_ol5	0.0008	0.0121	0.0268	0.0147	0.0057	0.1314	0.0037	0.2058	0.3056	0.0037	43.14	17.36	39.15	100.36
Stromboli CA	ST-13-17	st17_ol6	0.0024	0.0103	0.0186	0.0091	0.0017	0.2038	0.0020	0.1921	0.1874	0.0253	48.75	10.12	40.47	99.99
Stromboli CA	ST-13-17	st17_ol7	0.0027	0.0135	0.0182	0.0084	0.0057	0.2168	0.0023	0.2062	0.1733	0.0327	49.41	9.29	40.72	100.10
Stromboli CA	ST-13-17	st17_ol8	0.0011	0.0153	0.0256	0.0144	0.0039	0.1463	0.0053	0.1494	0.2825	0.0061	43.85	16.10	39.27	99.87
Stromboli CA	ST-13-17	st17_ol9	0.0034	0.0107	0.0175	0.0107	0.0044	0.2188	0.0017	0.2116	0.1694	0.0334	48.71	9.49	40.26	99.15
Stromboli CA	ST-13-17	st17_ol10	0.0003	0.0127	0.0236	0.0130	0.0067	0.1508	0.0040	0.1545	0.2798	0.0076	44.25	15.79	39.45	100.14
Stromboli CA	ST-13-17	st17_ol11	0.0017	0.0131	0.0250	0.0137	0.0170	0.1329	0.0047	0.1347	0.3042	0.0059	43.29	17.29	39.42	100.66
Stromboli CA	ST-13-17	st17_ol12	0.0014	0.0114	0.0252	0.0146	0.0115	0.1497	0.0036	0.1377	0.2952	0.0052	43.56	16.94	39.45	100.61
Stromboli CA	ST-13-17	st17_ol13	0.0000	0.0121	0.0250	0.0157	0.0093	0.1536	0.0037	0.1477	0.2764	0.0063	44.76	15.72	39.55	100.68
Stromboli CA	ST-13-17	st17_ol14	0.0008	0.0141	0.0189	0.0100	0.0028	0.2089	0.0020	0.1950	0.1893	0.0252	48.71	10.57	40.63	100.58
Stromboli CA	ST-13-17	st17_ol15	0.0009	0.0105	0.0208	0.0129	0.0048	0.2024	0.0017	0.1845	0.2372	0.0243	46.35	13.24	40.01	100.29
Stromboli CA	ST-13-17	st17_ol16	0.0033	0.0130	0.0188	0.0103	0.0053	0.2225	0.0027	0.2122	0.1742	0.0393	49.35	9.22	40.62	99.89
Stromboli CA	ST-13-17	st17_ol17	0.0004	0.0152	0.0276	0.0170	0.0322	0.1091	0.0085	0.0312	0.3857	0.0000	40.23	21.14	38.71	100.71
Stromboli CA	ST-13-17	st17_ol18	0.0023	0.0121	0.0302	0.0287	0.0047	0.1570	0.0036	0.1388	0.4941	0.0030	35.30	27.06	37.61	100.84
Stromboli CA	ST-13-17	st17_ol19	0.0020	0.0134	0.0194	0.0112	0.0137	0.2005	0.0032	0.1903	0.2008	0.0239	47.81	11.55	40.35	100.39
Stromboli CA	ST-13-17	st17_ol20	0.0015	0.0096	0.0203	0.0116	0.0044	0.1979	0.0019	0.1792	0.2114	0.0218	47.25	12.11	40.38	100.41
Stromboli CA	ST-13-17	st17_ol21	0.0018	0.0102	0.0186	0.0107	0.0056	0.2005	0.0028	0.1970	0.2015	0.0278	47.70	11.03	40.09	99.49
Stromboli KS	ST-13-04	st04_ol1	0.0036	0.0167	0.0261	0.0223	0.0274	0.2686	0.0048	0.1005	0.4984	0.0021	36.8178	24.8895	37.9329	100.61
Stromboli KS	ST-13-04	st04_ol2	0.0037	0.0163	0.0257	0.0209	0.0475	0.2827	0.0056	0.0926	0.4361	0.0037	39.2017	22.2158	38.6308	100.98
Stromboli KS	ST-13-04	st04_ol3	0.0070	0.0162	0.0291	0.0222	0.0389	0.2807	0.0089	0.0523	0.5770	0.0001	34.9794	27.3400	37.7765	101.13
Stromboli KS	ST-13-04	st04_ol4	0.0072	0.0189	0.0287	0.0218	0.0294	0.2904	0.0080	0.0576	0.5620	0.0004	35.4880	27.3641	37.8813	101.76
Stromboli KS	ST-13-04	st04_ol5	0.0052	0.0154	0.0295	0.0222	0.0247	0.3043	0.0070	0.0520	0.5760	0.0001	35.1348	27.2724	37.9188	101.36
Stromboli KS	ST-13-04	st04_ol6	0.0093	0.0211	0.0287	0.0218	0.0892	0.2659	0.0202	0.0435	0.6141	0.0003	34.0475	28.3562	37.8319	101.35
Stromboli KS	ST-13-04	st04_ol7	0.0084	0.0255	0.0300	0.0214	0.0332	0.3084	0.0205	0.0515	0.5682	0.0001	35.2789	26.9688	37.8107	101.13
Stromboli KS	ST-13-04	st04_ol8	0.0077	0.0178	0.0283	0.0219	0.0352	0.2908	0.0090	0.0500	0.5754	0.0001	35.3100	27.3712	38.0188	101.74
Stromboli KS	ST-13-04	st04_ol9	0.0075	0.0164	0.0290	0.0214	0.0329	0.3039	0.0054	0.0505	0.5729	0.0000	35.2450	27.0544	37.9304	101.27
Stromboli KS	ST-13-04	st04_ol10	0.0059	0.0181	0.0288	0.0228	0.0507	0.3130	0.0195	0.0496	0.5737	0.0001	35.1025	27.1195	38.1576	101.46
Stromboli KS	ST-13-04	st04_ol11	0.0093	0.0232	0.0270	0.0241	0.1027	0.2619	0.0216	0.0411	0.6330	0.0003	34.0528	28.7359	37.3491	101.28

Stromboli KS	ST-13-04	st04_ol11	0.0093	0.0232	0.0270	0.0241	0.1027	0.2619	0.0216	0.0411	0.6330	0.0003	34.0528	28.7359	37.3491	101.28
Stromboli KS	ST-13-04	st04_ol12	0.0070	0.0158	0.0295	0.0215	0.0332	0.3106	0.0081	0.0500	0.5658	0.0001	35.3688	26.9156	37.8981	101.22
Stromboli KS	ST-13-04	st04_ol13	0.0072	0.0265	0.0288	0.0218	0.0339	0.3314	0.0183	0.0524	0.5573	0.0004	35.6224	26.6443	38.1000	101.44
Stromboli KS	ST-13-04	st04_ol14	0.0089	0.0182	0.0285	0.0227	0.0382	0.3042	0.0058	0.0557	0.5722	0.0001	35.5788	27.2017	38.1008	101.94
Stromboli KS	ST-13-04	st04_ol15	0.0120	0.0176	0.0289	0.0242	0.0565	0.2911	0.0156	0.0447	0.5943	0.0002	34.3928	28.2056	37.6822	101.37
Stromboli KS	ST-13-04	st04_ol16	0.0071	0.0144	0.0284	0.0238	0.0378	0.2968	0.0112	0.0463	0.5933	0.0001	34.3169	28.0382	37.5443	100.96
Stromboli KS	ST-13-04	st04_ol17	0.0051	0.0158	0.0271	0.0235	0.0409	0.3061	0.0102	0.0484	0.5663	0.0006	35.2916	26.8817	38.1246	101.34

Olivine points around spinels, wt% (n=202)

Island	Sample	Olivine	Na_2O	Al_2O_3	CoO	ZnO	P_2O_5	CaO	TiO_2	NiO	MnO	Cr_2O_3	MgO	FeO	SiO_2	Total
Alicudi	AL-13-02	Al2-ol16-sp1-1	0.0041	0.0333	0.0208	0.0175	0.0025	0.1437	0.0028	0.2897	0.2501	0.0539	45.18	15.19	40.04	101.23
Alicudi	AL-13-02	Al2-ol16-sp1-2	0.0013	0.0266	0.0222	0.0153	0.0030	0.1517	0.0022	0.2612	0.2629	0.0443	44.76	15.74	39.93	101.23
Alicudi	AL-13-02	Al2-ol16-sp1-3	0.0031	0.0355	0.0211	0.0157	0.0033	0.1208	0.0024	0.3376	0.2216	0.0650	46.67	13.79	40.53	101.82
Alicudi	AL-13-02	Al2-ol16-sp1-4	0.0018	0.0343	0.0188	0.0147	0.0028	0.1108	0.0025	0.3617	0.1974	0.0670	47.48	12.63	40.72	101.64
Alicudi	AL-13-02	Al2-ol16-sp1-5	0.0017	0.0357	0.0199	0.0168	0.0022	0.1271	0.0018	0.3236	0.2295	0.0611	46.19	14.25	40.37	101.63
Alicudi	AL-13-02	Al2-ol17-sp1-1	0.0020	0.0328	0.0214	0.0181	0.0028	0.1929	0.0035	0.2095	0.2693	0.0501	45.32	15.89	40.54	102.56
Alicudi	AL-13-02	Al2-ol17-sp1-2	0.0021	0.0272	0.0213	0.0160	0.0026	0.1927	0.0027	0.2036	0.2742	0.0638	45.16	16.14	40.47	102.58
Alicudi	AL-13-02	Al2-ol17-sp1-3	0.0025	0.0297	0.0217	0.0165	0.0032	0.1937	0.0036	0.2006	0.2785	0.0858	44.89	16.37	40.32	102.42
Alicudi	AL-13-02	Al2-ol17-sp1-4	0.0051	0.0296	0.0223	0.0170	0.0023	0.1938	0.0030	0.2021	0.2774	0.0569	44.65	16.29	40.12	101.86
Alicudi	AL-13-02	Al2-ol17-sp1-5	0.0041	0.0297	0.0205	0.0171	0.0023	0.1915	0.0031	0.2080	0.2705	0.0598	44.66	15.96	40.00	101.43
Alicudi	AL-13-02	Al2-ol18-sp1-1	0.0000	0.0335	0.0217	0.0155	0.0060	0.1997	0.0039	0.2036	0.2464	0.0458	43.71	15.37	38.71	98.56
Alicudi	AL-13-02	Al2-ol18-sp1-2	0.0022	0.0322	0.0191	0.0146	0.0068	0.1960	0.0028	0.2255	0.2195	0.0508	45.74	14.04	39.70	100.24
Alicudi	AL-13-02	Al2-ol18-sp1-3	0.0010	0.0314	0.0200	0.0145	0.0076	0.1957	0.0030	0.2332	0.2115	0.0625	45.97	13.58	39.79	100.12
Alicudi	AL-13-02	Al2-ol18-sp1-4	0.0015	0.0344	0.0208	0.0146	0.0062	0.1946	0.0035	0.2240	0.2227	0.0824	45.01	14.36	39.29	99.46
Alicudi	AL-13-02	Al2-ol18-sp1-5	0.0026	0.0327	0.0212	0.0166	0.0072	0.1974	0.0032	0.2020	0.2540	0.0525	44.00	15.99	39.19	99.96
Alicudi	AL-13-02	Al2-ol18-sp2-1	0.0019	0.0363	0.0184	0.0083	0.0076	0.1826	0.0060	0.2656	0.1500	0.0679	50.30	8.44	40.94	100.42
Alicudi	AL-13-02	Al2-ol18-sp2-2	0.0021	0.0359	0.0184	0.0110	0.0092	0.1875	0.0068	0.2710	0.1535	0.0599	50.01	8.99	40.95	100.71
Alicudi	AL-13-02	Al2-ol18-sp2-3	0.0041	0.0367	0.0181	0.0119	0.0079	0.1903	0.0044	0.2683	0.1617	0.0563	49.72	9.65	40.92	101.05
Alicudi	AL-13-02	Al2-ol18-sp2-4	0.0043	0.0319	0.0181	0.0090	0.0097	0.1855	0.0043	0.2693	0.1621	0.0551	49.82	9.42	41.04	101.02
Alicudi	AL-13-02	Al2-ol18-sp2-5	0.0026	0.0329	0.0190	0.0077	0.0086	0.1818	0.0050	0.2663	0.1506	0.0533	50.46	8.54	41.19	100.92
Alicudi	AL-13-02	Al2-ol19-sp1-1	0.0016	0.0325	0.0207	0.0177	0.0424	0.2000	0.0028	0.2558	0.2539	0.0700	43.28	15.74	38.66	98.58

Alicudi	AL-13-02	Al2-ol19-sp1-2	0.0036	0.0302	0.0202	0.0171	0.0540	0.1982	0.0026	0.2505	0.2604	0.0500	44.05	15.93	39.37	100.24
Alicudi	AL-13-02	Al2-ol19-sp1-3	0.0025	0.0288	0.0204	0.0168	0.0243	0.1984	0.0031	0.2645	0.2541	0.0520	44.30	15.74	39.54	100.44
Alicudi	AL-13-02	Al2-ol19-sp1-4	0.0026	0.0280	0.0206	0.0160	0.0039	0.2013	0.0027	0.2640	0.2580	0.0415	43.86	15.92	39.21	99.83
Alicudi	AL-13-02	Al2-ol19-sp1-5	0.0010	0.0283	0.0210	0.0167	0.0167	0.2025	0.0033	0.2611	0.2597	0.0397	44.00	15.97	39.48	100.31
Alicudi	AL-13-02	Al2-ol20-sp1-1	0.0028	0.0260	0.0194	0.0149	0.0105	0.2434	0.0034	0.2323	0.2024	0.0567	47.25	12.25	40.02	100.33
Alicudi	AL-13-02	Al2-ol20-sp1-2	0.0036	0.0278	0.0199	0.0147	0.0056	0.2302	0.0029	0.2337	0.1981	0.0464	48.06	12.31	40.92	102.07
Alicudi	AL-13-02	Al2-ol20-sp1-3	0.0015	0.0296	0.0190	0.0138	0.0113	0.2553	0.0037	0.2464	0.1867	0.0507	48.53	11.38	40.75	101.47
Alicudi	AL-13-02	Al2-ol20-sp1-4	0.0043	0.0226	0.0191	0.0129	0.0048	0.2589	0.0039	0.2401	0.1957	0.0473	47.23	11.88	40.28	100.19
Alicudi	AL-13-02	Al2-ol20-sp1-5	0.0039	0.0245	0.0183	0.0145	0.0044	0.2635	0.0028	0.2455	0.1885	0.0441	48.40	11.37	40.42	101.00
Alicudi	AL-13-03	Al3-ol21-sp1-1	0.0039	0.0203	0.0193	0.0081	0.0060	0.2619	0.0031	0.2108	0.1798	0.0446	49.14	9.82	40.66	100.38
Alicudi	AL-13-03	Al3-ol21-sp1-2	0.0054	0.0205	0.0192	0.0083	0.0087	0.2611	0.0032	0.2105	0.1790	0.0567	49.19	9.74	40.75	100.45
Alicudi	AL-13-03	Al3-ol21-sp1-3	0.0042	0.0218	0.0187	0.0092	0.0050	0.2695	0.0033	0.2094	0.1822	0.0579	48.99	9.90	40.63	100.30
Alicudi	AL-13-03	Al3-ol21-sp1-4	0.0037	0.0197	0.0193	0.0115	0.0048	0.2684	0.0030	0.2073	0.1841	0.0493	48.82	10.20	40.67	100.46
Alicudi	AL-13-03	Al3-ol21-sp1-5	0.0045	0.0204	0.0194	0.0098	0.0071	0.2686	0.0032	0.2101	0.1799	0.0559	49.13	9.91	40.76	100.57
Filicudi	FL-13-03B	fl03b-ol30-sp1-1	0.0008	0.0250	0.0274	0.0124	0.0093	0.1874	0.0153	0.0631	0.2992	0.0018	42.36	17.77	38.78	99.55
Filicudi	FL-13-03B	fl03b-ol30-sp1-2	0.0008	0.0242	0.0281	0.0108	0.0185	0.1908	0.0143	0.0646	0.2977	0.0010	42.39	17.70	38.83	99.57
Filicudi	FL-13-03B	fl03b-ol30-sp1-3	0.0006	0.0250	0.0276	0.0117	0.0173	0.1923	0.0123	0.0656	0.2980	0.0004	42.75	17.69	39.09	100.18
Filicudi	FL-13-03B	fl03b-ol30-sp1-4	0.0011	0.0250	0.0279	0.0108	0.0352	0.1915	0.0140	0.0648	0.2979	0.0005	42.56	17.69	38.92	99.84
Filicudi	FL-13-03B	fl03b-ol30-sp1-5	0.0050	0.0277	0.0279	0.0118	0.0446	0.1905	0.0149	0.0639	0.2985	0.0000	42.48	17.73	38.94	99.84
Filicudi	FL-13-03B	fl03b-ol30-sp2-1	0.0026	0.0235	0.0278	0.0116	0.0155	0.1936	0.0195	0.0625	0.2984	0.0008	42.43	17.80	38.82	99.72
Filicudi	FL-13-03B	fl03b-ol30-sp2-2	0.0032	0.0253	0.0288	0.0121	0.0164	0.1895	0.0167	0.0626	0.3012	0.0015	42.64	17.84	39.02	100.16
Filicudi	FL-13-03B	fl03b-ol30-sp2-3	0.0000	0.0237	0.0281	0.0110	0.0149	0.1896	0.0142	0.0628	0.2997	0.0000	42.90	17.81	39.20	100.54
Filicudi	FL-13-03B	fl03b-ol30-sp2-4	0.0009	0.0240	0.0289	0.0110	0.0291	0.1944	0.0205	0.0632	0.2989	0.0009	42.33	17.76	38.69	99.45
Filicudi	FL-13-03B	fl03b-ol30-sp2-5	0.0011	0.0247	0.0276	0.0110	0.0170	0.1908	0.0148	0.0646	0.2969	0.0008	42.39	17.71	38.72	99.47
Filicudi	FL-13-03B	fl03b-ol30-sp3-1	0.0014	0.0262	0.0285	0.0110	0.0195	0.1935	0.0342	0.0638	0.2979	0.0021	42.74	17.84	39.16	100.41
Filicudi	FL-13-03B	fl03b-ol30-sp3-2	0.0009	0.0245	0.0286	0.0120	0.0128	0.1919	0.0153	0.0643	0.2981	0.0008	42.91	17.76	39.21	100.52
Filicudi	FL-13-03B	fl03b-ol30-sp3-3	0.0016	0.0249	0.0277	0.0118	0.0096	0.1943	0.0135	0.0629	0.2980	0.0013	43.16	17.74	39.41	100.95
Filicudi	FL-13-03B	fl03b-ol30-sp3-4	0.0004	0.0262	0.0283	0.0114	0.0131	0.1962	0.0208	0.0634	0.2982	0.0018	42.68	17.68	38.96	99.97
Filicudi	FL-13-03B	fl03b-ol30-sp3-5	0.0028	0.0261	0.0282	0.0115	0.0145	0.1935	0.0267	0.0639	0.2995	0.0010	42.39	17.71	38.72	99.49
Filicudi	FL-13-03B	fl03b-ol31-sp1-1	0.0022	0.0233	0.0232	0.0102	0.0134	0.2210	0.0119	0.1030	0.2260	0.0134	47.34	13.10	40.64	101.73
Filicudi	FL-13-03B	fl03b-ol31-sp1-2	0.0023	0.0250	0.0228	0.0097	0.0180	0.2223	0.0089	0.1014	0.2299	0.0131	46.62	13.08	40.02	100.37

Filicudi	FL-13-03B	fl03b-ol31-sp1-3	0.0010	0.0220	0.0224	0.0099	0.0196	0.2221	0.0104	0.1024	0.2299	0.0156	46.62	13.05	39.96	100.27
Filicudi	FL-13-03B	fl03b-ol31-sp1-4	0.0016	0.0232	0.0224	0.0090	0.0227	0.2228	0.0113	0.1023	0.2285	0.0131	46.27	13.02	39.70	99.64
Filicudi	FL-13-03B	fl03b-ol31-sp1-5	0.0029	0.0264	0.0219	0.0107	0.0182	0.2255	0.0149	0.1045	0.2281	0.0132	45.60	13.05	39.14	98.46
Filicudi	FL-13-03B	fl03b-ol32-sp1-1	0.0040	0.0274	0.0246	0.0104	0.0219	0.2166	0.0113	0.0772	0.2454	0.0041	46.15	14.03	40.35	101.17
Filicudi	FL-13-03B	fl03b-ol32-sp1-2	0.0021	0.0261	0.0250	0.0098	0.0189	0.2134	0.0111	0.0792	0.2482	0.0028	46.29	14.09	40.42	101.44
Filicudi	FL-13-03B	fl03b-ol32-sp1-3	0.0030	0.0266	0.0241	0.0096	0.0199	0.2189	0.0106	0.0790	0.2507	0.0038	45.61	14.03	39.92	100.21
Filicudi	FL-13-03B	fl03b-ol32-sp1-4	0.0017	0.0262	0.0237	0.0088	0.0199	0.2130	0.0126	0.0779	0.2524	0.0030	45.23	14.14	39.52	99.53
Filicudi	FL-13-03B	fl03b-ol32-sp1-5	0.0031	0.0271	0.0248	0.0094	0.0188	0.2113	0.0129	0.0745	0.2490	0.0043	45.45	14.06	39.74	99.88
Filicudi	FL-13-03B	fl03b-ol32-sp2-1	0.0019	0.0263	0.0244	0.0108	0.0171	0.2153	0.0128	0.0787	0.2495	0.0030	45.64	14.07	39.81	100.16
Filicudi	FL-13-03B	fl03b-ol32-sp2-2	0.0000	0.0263	0.0252	0.0109	0.0249	0.2199	0.0122	0.0824	0.2477	0.0055	45.57	14.02	39.81	100.06
Filicudi	FL-13-03B	fl03b-ol32-sp2-3	0.0009	0.0249	0.0240	0.0111	0.0133	0.2245	0.0116	0.0818	0.2487	0.0041	45.43	14.01	39.73	99.82
Filicudi	FL-13-03B	fl03b-ol32-sp2-4	0.0021	0.0244	0.0236	0.0085	0.0059	0.2197	0.0131	0.0811	0.2509	0.0050	45.57	14.09	39.87	100.16
Filicudi	FL-13-03B	fl03b-ol32-sp2-5	0.0019	0.0257	0.0243	0.0097	0.0195	0.2188	0.0139	0.0781	0.2525	0.0046	45.26	14.11	39.59	99.61
Salina	SL-13-05	sl5-ol3-sp1-1	0.0020	0.0184	0.0189	0.0161	0.0027	0.1978	0.0028	0.2032	0.2247	0.0410	45.66	13.07	39.35	98.81
Salina	SL-13-05	sl5-ol3-sp1-2	0.0009	0.0184	0.0194	0.0150	0.0036	0.1982	0.0029	0.2055	0.2037	0.0640	47.13	12.01	40.13	99.99
Salina	SL-13-05	sl5-ol3-sp1-3	0.0014	0.0185	0.0195	0.0147	0.0027	0.1978	0.0029	0.2014	0.2035	0.0429	46.92	12.20	40.08	99.91
Salina	SL-13-05	sl5-ol3-sp1-4	0.0027	0.0199	0.0198	0.0176	0.0034	0.1932	0.0029	0.1970	0.2295	0.0479	45.22	13.55	39.30	98.81
Salina	SL-13-05	sl5-ol4-sp1-1	0.0028	0.0191	0.0235	0.0246	0.0079	0.1896	0.0032	0.1278	0.3637	0.0129	40.83	20.31	39.05	100.97
Salina	SL-13-05	sl5-ol4-sp1-2	0.0009	0.0192	0.0210	0.0185	0.0027	0.1833	0.0025	0.1769	0.2558	0.0335	44.68	15.46	39.73	100.58
Salina	SL-13-05	sl5-ol4-sp1-3	0.0030	0.0202	0.0201	0.0188	0.0042	0.1840	0.0027	0.1917	0.2457	0.0342	45.47	14.61	40.02	100.82
Salina	SL-13-05	sl5-ol4-sp1-4	0.0025	0.0188	0.0220	0.0224	0.0025	0.1926	0.0028	0.1587	0.3133	0.0321	42.84	17.91	39.50	101.02
Salina	SL-13-05	sl5-ol5-sp1-1	0.0014	0.0234	0.0229	0.0170	0.0016	0.1860	0.0026	0.1511	0.2997	0.0229	42.92	17.54	39.34	100.53
Salina	SL-13-05	sl5-ol5-sp1-2	0.0037	0.0196	0.0234	0.0182	0.0037	0.1827	0.0021	0.1641	0.2926	0.0240	43.21	17.20	39.43	100.57
Salina	SL-13-05	sl5-ol5-sp1-3	0.0029	0.0209	0.0237	0.0183	0.0030	0.1858	0.0031	0.1562	0.2997	0.0217	43.04	17.42	39.60	100.80
Salina	SL-13-05	sl5-ol5-sp1-4	0.0017	0.0224	0.0232	0.0186	0.0020	0.1880	0.0028	0.1488	0.3030	0.0225	42.86	17.59	39.50	100.69
Salina	SL-13-05	sl5-ol6-sp1-1	0.0030	0.0221	0.0222	0.0221	0.0054	0.1824	0.0025	0.1631	0.3230	0.0400	42.49	18.66	39.73	101.67
Salina	SL-13-05	sl5-ol6-sp1-2	0.0027	0.0214	0.0223	0.0218	0.0064	0.1829	0.0027	0.1729	0.2982	0.0409	43.18	17.59	39.57	101.12
Salina	SL-13-05	sl5-ol6-sp1-3	0.0035	0.0192	0.0214	0.0206	0.0053	0.1828	0.0026	0.1825	0.2677	0.0314	44.38	16.10	39.69	100.91
Salina	SL-13-05	sl5-ol6-sp1-4	0.0015	0.0195	0.0224	0.0218	0.0045	0.1834	0.0029	0.1774	0.2859	0.0419	43.86	17.02	39.76	101.40
Salina	SL-13-05	sl5-ol7-sp1-1	0.0089	0.0220	0.0224	0.0235	0.0042	0.1823	0.0033	0.1597	0.3529	0.0260	39.67	20.02	38.83	99.33
Salina	SL-13-05	sl5-ol7-sp1-2	0.0072	0.0229	0.0225	0.0237	0.0063	0.1846	0.0027	0.1590	0.3520	0.0223	39.64	19.96	38.82	99.22

Salina	SL-13-05	sl5-ol7-sp1-3	0.0064	0.0217	0.0214	0.0242	0.0033	0.1878	0.0030	0.1485	0.3628	0.0271	39.94	20.28	39.09	100.12
Salina	SL-13-05	sl5-ol7-sp1-4	0.0043	0.0210	0.0217	0.0248	0.0028	0.1836	0.0026	0.1526	0.3553	0.0268	40.39	20.08	39.28	100.54
Salina	SL-13-05	sl5-ol8-sp1-1	0.0086	0.0252	0.0265	0.0191	0.0051	0.2358	0.0034	0.1107	0.3801	0.0191	37.70	22.19	38.68	99.40
Salina	SL-13-05	sl5-ol8-sp1-2	0.0102	0.0230	0.0271	0.0186	0.0047	0.2215	0.0033	0.1084	0.3801	0.0144	37.60	22.30	38.84	99.55
Salina	SL-13-05	sl5-ol8-sp1-3	0.0101	0.0274	0.0259	0.0181	0.0036	0.2290	0.0040	0.1111	0.3788	0.0167	37.87	22.18	39.03	99.91
Salina	SL-13-05	sl5-ol8-sp1-4	0.0062	0.0275	0.0265	0.0202	0.0079	0.2273	0.0042	0.1064	0.3739	0.0159	38.89	21.89	38.93	100.52
Salina	SL-13-05	sl5-ol8-sp2-1	0.0090	0.0263	0.0267	0.0188	0.0033	0.2142	0.0021	0.1018	0.3749	0.0133	38.41	22.03	38.84	100.07
Salina	SL-13-05	sl5-ol8-sp2-2	0.0110	0.0305	0.0257	0.0183	0.0036	0.2169	0.0019	0.1024	0.3783	0.0202	38.29	22.02	38.80	99.92
Salina	SL-13-05	sl5-ol8-sp2-3	0.0116	0.0281	0.0260	0.0184	0.0055	0.2298	0.0029	0.1060	0.3821	0.0171	37.94	22.33	38.86	99.96
Salina	SL-13-05	sl5-ol9-sp1-1	0.0058	0.0205	0.0233	0.0227	0.0070	0.1813	0.0023	0.1601	0.3414	0.0458	38.75	20.20	38.14	97.90
Salina	SL-13-05	sl5-ol9-sp1-2	0.0063	0.0200	0.0234	0.0218	0.0088	0.1777	0.0023	0.1602	0.3356	0.0717	39.86	20.00	38.42	99.10
Salina	SL-13-05	sl5-ol9-sp1-3	0.0051	0.0229	0.0238	0.0245	0.0062	0.1776	0.0024	0.1612	0.3336	0.0606	40.79	19.85	38.96	100.42
Salina	SL-13-05	sl5-ol9-sp1-4	0.0029	0.0202	0.0233	0.0232	0.0043	0.1791	0.0021	0.1623	0.3332	0.0445	40.55	19.79	38.76	99.89
Salina	SL-13-05	sl5-ol10-sp1-1	0.0028	0.0185	0.0216	0.0228	0.0065	0.1744	0.0023	0.1438	0.3104	0.0275	41.94	18.01	39.14	99.81
Salina	SL-13-05	sl5-ol10-sp1-2	0.0054	0.0178	0.0215	0.0217	0.0044	0.1715	0.0022	0.1473	0.2970	0.0408	42.95	17.42	39.46	100.56
Salina	SL-13-05	sl5-ol10-sp1-3	0.0049	0.0212	0.0212	0.0208	0.0047	0.1788	0.0025	0.1491	0.2907	0.0436	42.99	17.19	39.75	100.66
Salina	SL-13-05	sl5-ol10-sp1-4	0.0049	0.0185	0.0215	0.0209	0.0061	0.1802	0.0019	0.1444	0.2989	0.0277	42.72	17.50	39.65	100.60
Salina	SL-13-05	sl5-ol11-sp1-1	0.0039	0.0218	0.0259	0.0257	0.0062	0.1750	0.0025	0.0881	0.4174	0.0122	37.28	22.94	38.48	99.48
Salina	SL-13-05	sl5-ol11-sp1-2	0.0032	0.0207	0.0253	0.0262	0.0065	0.1697	0.0026	0.0893	0.4030	0.0145	38.19	22.32	38.53	99.80
Salina	SL-13-05	sl5-ol11-sp1-3	0.0055	0.0208	0.0246	0.0265	0.0048	0.1723	0.0025	0.0905	0.4117	0.0247	37.74	22.70	38.80	100.02
Salina	SL-13-05	sl5-ol11-sp1-4	0.0101	0.0251	0.0249	0.0260	0.0083	0.1792	0.0034	0.0883	0.4240	0.0113	36.34	23.46	38.43	99.03
Salina	SL-13-05	sl5-ol12-sp1-1	0.0062	0.0200	0.0241	0.0241	0.0050	0.1932	0.0026	0.1311	0.4254	0.0259	35.35	23.83	38.52	98.56
Salina	SL-13-05	sl5-ol12-sp1-2	0.0104	0.0240	0.0251	0.0259	0.0037	0.1875	0.0028	0.1247	0.4303	0.0221	35.96	23.95	38.43	99.19
Salina	SL-13-05	sl5-ol12-sp1-3	0.0122	0.0260	0.0253	0.0244	0.0060	0.1926	0.0030	0.1283	0.4144	0.0448	35.96	23.43	38.58	98.85
Salina	SL-13-05	sl5-ol12-sp1-4	0.0124	0.0233	0.0240	0.0243	0.0066	0.1912	0.0032	0.1379	0.4049	0.0306	36.50	23.09	38.63	99.07
Salina	SL-13-05	sl5-ol12-sp2-1	0.0171	0.0273	0.0252	0.0254	0.0045	0.2072	0.0032	0.1105	0.4797	0.0143	32.54	26.15	37.64	97.24
Salina	SL-13-05	sl5-ol12-sp2-4	0.0039	0.0257	0.0270	0.0264	0.0020	0.1904	0.0031	0.1049	0.4641	0.0148	36.04	24.86	37.93	99.69
Salina	SL-13-05	sl5-ol13-sp1-1	0.0053	0.0190	0.0224	0.0212	0.0055	0.1899	0.0027	0.1717	0.3128	0.0277	41.70	18.36	39.26	100.11
Salina	SL-13-05	sl5-ol13-sp1-2	0.0055	0.0200	0.0231	0.0217	0.0032	0.1888	0.0028	0.1709	0.3234	0.0266	40.91	18.99	39.47	100.16
Salina	SL-13-05	sl5-ol13-sp1-3	0.0086	0.0184	0.0230	0.0222	0.0014	0.1892	0.0031	0.1696	0.3289	0.0290	41.02	19.16	39.57	100.55
Salina	SL-13-05	sl5-ol13-sp1-4	0.0054	0.0205	0.0220	0.0227	0.0030	0.1912	0.0023	0.1681	0.3231	0.0270	41.22	18.79	39.44	100.23
Salina	SL-13-05	sl5-ol14-sp1-1	0.0115	0.0278	0.0279	0.0189	0.0046	0.2357	0.0027	0.0990	0.3800	0.0236	37.89	22.43	39.16	100.30

Salina	SL-13-05	sl5-ol14-sp1-2	0.0105	0.0245	0.0275	0.0188	0.0033	0.2354	0.0025	0.0991	0.3827	0.0251	37.06	22.50	38.48	98.87
Salina	SL-13-05	sl5-ol14-sp1-3	0.0065	0.0237	0.0275	0.0200	0.0076	0.2319	0.0028	0.1045	0.3724	0.0220	38.18	21.99	38.78	99.77
Salina	SL-13-05	sl5-ol14-sp1-4	0.0097	0.0294	0.0265	0.0188	0.0081	0.2365	0.0031	0.1090	0.3745	0.0252	37.85	22.32	39.39	100.41
Salina	SL-13-05	sl5-ol14-sp2-1	0.0105	0.0365	0.0270	0.0184	0.0082	0.2355	0.0063	0.0992	0.3795	0.0255	36.53	22.55	38.17	98.09
Salina	SL-13-05	sl5-ol14-sp2-2	0.0120	0.0330	0.0267	0.0190	0.0045	0.2415	0.0056	0.1008	0.3821	0.0259	36.77	22.53	38.52	98.67
Salina	SL-13-05	sl5-ol14-sp2-3	0.0097	0.0262	0.0267	0.0196	0.0038	0.2352	0.0044	0.1016	0.3827	0.0327	37.11	22.53	38.67	99.15
Salina	SL-13-05	sl5-ol14-sp2-4	0.0111	0.0329	0.0269	0.0187	0.0037	0.2366	0.0049	0.1000	0.3855	0.0279	36.74	22.73	38.60	98.91
Salina	SL-13-05	sl5-ol15-sp1-1	0.0049	0.0182	0.0238	0.0269	0.0074	0.1824	0.0027	0.1722	0.3994	0.0772	38.88	22.31	39.60	101.70
Salina	SL-13-05	sl5-ol15-sp1-2	0.0108	0.0209	0.0238	0.0268	0.0046	0.1900	0.0029	0.1502	0.4268	0.1031	36.81	23.53	39.13	100.43
Salina	SL-13-05	sl5-ol15-sp1-3	0.0090	0.0242	0.0242	0.0250	0.0103	0.1882	0.0050	0.1531	0.4203	0.1369	37.12	23.22	39.16	100.49
Salina	SL-13-05	sl5-ol15-sp1-4	0.0076	0.0209	0.0234	0.0247	0.0098	0.1838	0.0024	0.1772	0.3977	0.0911	38.36	22.29	39.34	100.93
Salina	SL-13-08	sl8-ol22-sp1-1	0.0025	0.0200	0.0257	0.0235	0.0032	0.2229	0.0043	0.0914	0.3809	0.0337	39.94	21.67	38.82	101.24
Salina	SL-13-08	sl8-ol22-sp1-2	0.0035	0.0201	0.0255	0.0215	0.0037	0.2245	0.0027	0.0935	0.3819	0.0538	39.37	21.77	38.78	100.76
Salina	SL-13-08	sl8-ol22-sp1-3	0.0034	0.0201	0.0249	0.0226	0.0037	0.2234	0.0034	0.0979	0.3824	0.0565	39.34	21.80	38.73	100.72
Salina	SL-13-08	sl8-ol22-sp1-4	0.0059	0.0188	0.0257	0.0218	0.0076	0.2110	0.0051	0.0901	0.3850	0.0214	39.92	21.86	38.95	101.52
Salina	SL-13-08	sl8-ol22-sp1-5	0.0053	0.0227	0.0259	0.0215	0.0047	0.2227	0.0045	0.0964	0.3870	0.0260	39.28	21.85	38.72	100.67
Salina	SL-13-08	sl8-ol22-sp2-1	0.0064	0.0198	0.0260	0.0231	0.0026	0.2284	0.0032	0.0903	0.3930	0.0479	39.07	22.04	38.37	100.32
Salina	SL-13-08	sl8-ol22-sp2-2	0.0061	0.0185	0.0259	0.0225	0.0078	0.2315	0.0027	0.0902	0.3921	0.0439	38.87	22.13	38.39	100.22
Salina	SL-13-08	sl8-ol22-sp2-3	0.0061	0.0191	0.0262	0.0221	0.0041	0.2256	0.0033	0.0862	0.3906	0.0528	38.43	22.13	38.02	99.42
Salina	SL-13-08	sl8-ol22-sp2-4	0.0065	0.0201	0.0257	0.0223	0.0067	0.2214	0.0046	0.0857	0.3917	0.0411	38.70	22.21	38.44	100.18
Salina	SL-13-08	sl8-ol22-sp2-5	0.0051	0.0185	0.0260	0.0224	0.0058	0.2203	0.0037	0.0871	0.3884	0.0433	39.02	22.11	38.51	100.46
Salina	SL-13-08	sl8-ol23-sp1-1	0.0025	0.0193	0.0247	0.0237	0.0033	0.1400	0.0026	0.1661	0.3202	0.1291	42.00	18.16	38.82	99.81
Salina	SL-13-08	sl8-ol23-sp1-2	0.0021	0.0191	0.0243	0.0218	0.0030	0.0950	0.0021	0.1675	0.3181	0.0544	42.03	18.11	38.80	99.65
Salina	SL-13-08	sl8-ol23-sp1-3	0.0017	0.0201	0.0227	0.0222	0.0028	0.1237	0.0027	0.1694	0.3084	0.0545	41.92	17.93	38.90	99.48
Salina	SL-13-08	sl8-ol23-sp1-4	0.0022	0.0174	0.0236	0.0217	0.0068	0.1690	0.0023	0.1681	0.3052	0.0359	42.33	17.87	39.05	100.00
Salina	SL-13-08	sl8-ol23-sp1-5	0.0039	0.0195	0.0236	0.0219	0.0061	0.1885	0.0031	0.1649	0.3108	0.0339	42.08	18.03	39.06	99.95
Salina	SL-13-08	sl8-ol23-sp2-1	0.0042	0.0178	0.0232	0.0229	0.0036	0.1662	0.0032	0.1627	0.3187	0.1619	42.23	18.16	39.09	100.36
Salina	SL-13-08	sl8-ol23-sp2-2	0.0000	0.0198	0.0234	0.0224	0.0037	0.1925	0.0026	0.1626	0.3160	0.0488	42.11	18.07	39.15	100.12
Salina	SL-13-08	sl8-ol23-sp2-3	0.0042	0.0199	0.0237	0.0225	0.0061	0.2022	0.0027	0.1596	0.3221	0.0380	42.02	18.41	39.45	100.68
Salina	SL-13-08	sl8-ol23-sp2-4	0.0038	0.0216	0.0237	0.0227	0.0038	0.0887	0.0029	0.1570	0.3346	0.0227	42.47	18.73	39.65	101.53
Salina	SL-13-08	sl8-ol23-sp2-5	0.0021	0.0193	0.0234	0.0228	0.0033	0.1207	0.0029	0.1619	0.3211	0.0962	41.88	18.24	38.83	99.71
Salina	SL-13-08	sl8-ol24-sp1-1	0.0014	0.0176	0.0217	0.0192	0.0070	0.1800	0.0025	0.1527	0.2571	0.0258	44.70	15.32	39.51	100.21

Salina	SL-13-08	sl8-ol24-sp1-2	0.0044	0.0170	0.0207	0.0189	0.0076	0.1811	0.0025	0.1510	0.2604	0.0231	44.76	15.34	39.57	100.36
Salina	SL-13-08	sl8-ol24-sp1-3	0.0019	0.0165	0.0225	0.0185	0.0084	0.1794	0.0024	0.1498	0.2606	0.0219	44.77	15.37	39.62	100.45
Salina	SL-13-08	sl8-ol24-sp1-4	0.0028	0.0170	0.0218	0.0187	0.0067	0.1796	0.0024	0.1516	0.2584	0.0232	44.69	15.38	39.58	100.33
Salina	SL-13-08	sl8-ol24-sp1-5	0.0032	0.0212	0.0213	0.0198	0.0088	0.1813	0.0027	0.1517	0.2575	0.0348	44.34	15.33	39.26	99.63
Salina	SL-13-08	sl8-ol25-sp1-1	0.0033	0.0173	0.0206	0.0199	0.0065	0.1927	0.0025	0.2232	0.2616	0.0524	44.69	14.90	39.55	99.94
Salina	SL-13-08	sl8-ol25-sp1-2	0.0009	0.0194	0.0205	0.0197	0.0070	0.1865	0.0031	0.2218	0.2677	0.0591	44.37	15.21	39.50	99.88
Salina	SL-13-08	sl8-ol25-sp1-3	0.0035	0.0186	0.0200	0.0200	0.0044	0.1869	0.0026	0.2270	0.2596	0.0782	44.65	14.77	39.34	99.58
Salina	SL-13-08	sl8-ol25-sp1-4	0.0022	0.0200	0.0204	0.0204	0.0063	0.1919	0.0028	0.2322	0.2500	0.0597	45.07	14.41	39.61	99.90
Salina	SL-13-08	sl8-ol25-sp1-5	0.0010	0.0186	0.0200	0.0197	0.0062	0.1890	0.0026	0.2325	0.2480	0.0587	45.33	14.34	39.76	100.22
Stromboli CA	ST-13-09	st9_ol1-sp1-1	0.0013	0.0237	0.0182	0.0092	0.0271	0.1769	0.0055	0.2782	0.1634	0.0591	50.10	9.19	41.40	101.46
Stromboli CA	ST-13-09	st9_ol1-sp1-2	0.0031	0.0235	0.0184	0.0072	0.0301	0.1769	0.0052	0.2780	0.1640	0.0517	49.93	9.26	41.38	101.33
Stromboli CA	ST-13-09	st9_ol1-sp1-3	0.0047	0.0244	0.0183	0.0068	0.0176	0.1780	0.0057	0.2948	0.1641	0.0645	49.29	9.25	41.43	100.74
Stromboli CA	ST-13-09	st9_ol1-sp1-4	0.0046	0.0204	0.0177	0.0076	0.0134	0.1751	0.0045	0.2892	0.1612	0.0457	50.20	9.10	41.66	101.70
Stromboli CA	ST-13-09	st9_ol1-sp2-1	0.0084	0.0259	0.0228	0.0193	0.0212	0.2175	0.0076	0.1266	0.3902	0.0493	37.54	21.46	37.96	97.84
Stromboli CA	ST-13-09	st9_ol1-sp2-2	0.0062	0.0213	0.0210	0.0161	0.0154	0.1928	0.0057	0.1688	0.3230	0.0433	40.59	18.11	39.00	98.52
Stromboli CA	ST-13-09	st9_ol1-sp2-3	0.0034	0.0205	0.0182	0.0160	0.0139	0.1747	0.0050	0.2631	0.2295	0.0540	45.93	12.86	40.13	99.71
Stromboli CA	ST-13-09	st9_ol1-sp2-4	0.0022	0.0253	0.0193	0.0144	0.0167	0.1755	0.0054	0.2504	0.2261	0.0544	45.85	13.01	39.92	99.57
Stromboli CA	ST-13-09	st9_ol1-sp3-1	0.0059	0.0209	0.0178	0.0081	0.0101	0.1935	0.0049	0.3026	0.1642	0.0967	48.84	9.19	40.97	99.83
Stromboli CA	ST-13-09	st9_ol1-sp3-2	0.0160	0.0254	0.0169	0.0076	0.0102	0.2167	0.0051	0.3315	0.1785	0.1026	44.99	10.16	41.47	97.53
Stromboli CA	ST-13-09	st9_ol1-sp3-3	0.0110	0.0346	0.0180	0.0098	0.0078	0.1927	0.0054	0.3263	0.1845	0.0573	45.46	10.96	40.68	97.95
Stromboli CA	ST-13-09	st9_ol1-sp3-4	0.0046	0.0219	0.0167	0.0082	0.0046	0.1901	0.0045	0.3063	0.1647	0.0764	48.86	9.32	41.15	100.13
Stromboli CA	ST-13-09	st9_ol2-sp1-1	0.0022	0.0176	0.0238	0.0081	0.0094	0.1215	0.0044	0.1607	0.2212	0.0060	46.74	13.71	41.25	102.28
Stromboli CA	ST-13-09	st9_ol2-sp1-2	0.0080	0.0190	0.0213	0.0118	0.0159	0.1880	0.0035	0.1747	0.2763	0.0169	43.02	16.09	40.32	100.17
Stromboli CA	ST-13-09	st9_ol2-sp1-3	0.0083	0.0210	0.0211	0.0088	0.0155	0.2001	0.0031	0.1927	0.2143	0.0207	45.46	13.38	41.15	100.70
Stromboli CA	ST-13-17	st17-ol26-sp1-1	0.0020	0.0136	0.0216	0.0143	0.0058	0.1856	0.0022	0.1939	0.2437	0.0289	45.33	13.41	39.20	98.66
Stromboli CA	ST-13-17	st17-ol26-sp1-2	0.0009	0.0122	0.0222	0.0131	0.0203	0.1737	0.0038	0.1852	0.2574	0.0310	45.03	14.18	39.29	99.23
Stromboli CA	ST-13-17	st17-ol26-sp1-3	0.0012	0.0104	0.0236	0.0133	0.0378	0.1619	0.0044	0.1750	0.2698	0.0216	44.65	15.07	39.33	99.77
Stromboli CA	ST-13-17	st17-ol26-sp1-4	0.0011	0.0121	0.0217	0.0134	0.0040	0.1884	0.0019	0.1979	0.2377	0.0334	45.65	13.13	39.23	98.72
Stromboli CA	ST-13-17	st17-ol26-sp1-5	0.0017	0.0118	0.0217	0.0122	0.0043	0.1797	0.0034	0.1881	0.2500	0.0304	45.38	13.83	39.43	99.34
Stromboli CA	ST-13-17	st17-ol27-sp1-1	0.0022	0.0126	0.0209	0.0136	0.0028	0.1876	0.0019	0.2719	0.2458	0.0439	44.98	14.16	39.22	99.17
Stromboli CA	ST-13-17	st17-ol27-sp1-2	0.0013	0.0113	0.0193	0.0127	0.0031	0.2000	0.0020	0.2746	0.2103	0.0459	46.75	12.12	39.77	99.41

Stromboli CA	ST-13-17	st17-ol27-sp1-3	0.0000	0.0109	0.0181	0.0109	0.0043	0.2105	0.0019	0.2676	0.1906	0.0685	47.70	10.76	39.91	99.15
Stromboli CA	ST-13-17	st17-ol27-sp1-4	0.0015	0.0093	0.0174	0.0123	0.0045	0.2104	0.0014	0.2686	0.2000	0.0553	47.13	11.34	39.69	98.94
Stromboli CA	ST-13-17	st17-ol27-sp1-5	0.0015	0.0105	0.0192	0.0141	0.0043	0.1925	0.0021	0.2728	0.2238	0.0623	45.81	12.84	39.29	98.75
Stromboli CA	ST-13-17	st17-ol28-sp1-1	0.0002	0.0128	0.0240	0.0162	0.0031	0.1773	0.0024	0.2321	0.2775	0.0670	43.18	15.85	38.67	98.52
Stromboli CA	ST-13-17	st17-ol28-sp1-2	0.0015	0.0130	0.0240	0.0162	0.0072	0.1899	0.0027	0.2373	0.2649	0.0895	43.82	15.12	38.75	98.54
Stromboli CA	ST-13-17	st17-ol28-sp1-3	0.0021	0.0131	0.0226	0.0133	0.0040	0.1995	0.0024	0.2332	0.2523	0.0648	44.98	14.38	39.61	99.78
Stromboli CA	ST-13-17	st17-ol28-sp1-4	0.0009	0.0123	0.0249	0.0140	0.0036	0.1863	0.0028	0.2219	0.2672	0.0932	44.66	15.32	39.84	100.64
Stromboli CA	ST-13-17	st17-ol28-sp1-5	0.0014	0.0136	0.0234	0.0160	0.0054	0.1731	0.0027	0.2303	0.2842	0.0666	42.56	16.47	38.57	98.41
Stromboli CA	ST-13-17	st17-ol29-sp1-1	0.0003	0.0120	0.0165	0.0094	0.0037	0.2589	0.0024	0.2001	0.1751	0.0566	48.99	9.52	40.53	99.77
Stromboli CA	ST-13-17	st17-ol29-sp1-2	0.0004	0.0117	0.0181	0.0083	0.0030	0.2441	0.0030	0.2104	0.1707	0.0692	49.07	9.28	40.46	99.54
Stromboli CA	ST-13-17	st17-ol29-sp1-3	0.0024	0.0116	0.0174	0.0091	0.0013	0.2432	0.0021	0.2129	0.1716	0.0550	49.31	9.28	40.63	99.94
Stromboli CA	ST-13-17	st17-ol29-sp1-4	0.0010	0.0133	0.0174	0.0102	0.0024	0.2416	0.0021	0.2097	0.1731	0.0387	49.25	9.46	40.65	100.06
Stromboli CA	ST-13-17	st17-ol29-sp1-5	0.0034	0.0120	0.0175	0.0103	0.0027	0.2555	0.0029	0.2032	0.1744	0.0430	49.03	9.62	40.51	99.89
Stromboli CA	ST-13-17	st17-ol29-sp2-1	0.0023	0.0120	0.0181	0.0080	0.0034	0.2233	0.0021	0.2112	0.1697	0.0491	48.80	9.20	40.21	98.91
Stromboli CA	ST-13-17	st17-ol29-sp2-2	0.0002	0.0132	0.0172	0.0092	0.0016	0.2228	0.0018	0.2107	0.1696	0.0364	48.93	9.17	40.34	99.12
Stromboli CA	ST-13-17	st17-ol29-sp2-3	0.0065	0.0116	0.0179	0.0078	0.0030	0.2299	0.0025	0.2096	0.1695	0.0393	49.07	9.14	40.44	99.35
Stromboli CA	ST-13-17	st17-ol29-sp2-4	0.0002	0.0134	0.0170	0.0091	0.0026	0.2233	0.0024	0.2113	0.1699	0.0373	49.08	9.21	40.44	99.42
Stromboli CA	ST-13-17	st17-ol29-sp2-5	0.0013	0.0131	0.0180	0.0084	0.0025	0.2226	0.0027	0.2119	0.1692	0.0386	49.04	9.21	40.46	99.39
Stromboli CA	ST-13-17	st17-ol29-sp3-1	0.0002	0.0119	0.0169	0.0088	0.0023	0.2202	0.0024	0.2092	0.1781	0.1282	48.06	9.86	40.01	98.72
Stromboli CA	ST-13-17	st17-ol29-sp3-2	0.0010	0.0130	0.0176	0.0103	0.0014	0.2193	0.0033	0.2079	0.1802	0.1646	48.00	10.16	40.02	98.99
Stromboli CA	ST-13-17	st17-ol29-sp3-3	0.0003	0.0124	0.0178	0.0093	0.0041	0.2212	0.0025	0.2069	0.1815	0.1318	48.12	10.09	40.14	99.13
Stromboli CA	ST-13-17	st17-ol29-sp3-4	0.0022	0.0115	0.0177	0.0107	0.0041	0.2206	0.0022	0.2082	0.1776	0.0834	48.21	9.87	40.13	98.94
Stromboli CA	ST-13-17	st17-ol29-sp3-5	0.0024	0.0132	0.0168	0.0087	0.0029	0.2201	0.0025	0.2092	0.1772	0.0828	48.39	9.82	40.18	99.12
Stromboli CA	ST-13-17	st17-ol29-sp3-6	0.0019	0.0128	0.0177	0.0097	0.0034	0.2201	0.0027	0.2099	0.1761	0.0822	48.19	9.86	40.28	99.06

Olivine transect core-rim, wt% (n=24)

Island	Sample	Olivine	Na_2O	Al_2O_3	CoO	ZnO	P_2O_5	CaO	TiO_2	NiO	MnO	Cr_2O_3	MgO	FeO	SiO_2	Total
Alicudi	AL-13-02	Al2_ol1-6 core	0.0034	0.0290	0.0181	0.0092	0.0052	0.0984	0.0025	0.4118	0.1120	0.0721	51.04	7.68	41.25	100.74
Alicudi	AL-13-02	Al2_ol1-5	0.0019	0.0313	0.0176	0.0123	0.0036	0.1011	0.0028	0.4063	0.1357	0.0713	50.18	8.91	41.16	101.03
Alicudi	AL-13-02	Al2_ol1-4	0.0034	0.0328	0.0178	0.0123	0.0020	0.1054	0.0029	0.3994	0.1646	0.0689	49.10	10.52	40.95	101.39
Alicudi	AL-13-02	Al2_ol1-3	0.0034	0.0313	0.0189	0.0153	0.0043	0.1263	0.0018	0.3654	0.2114	0.0614	47.64	13.08	40.99	102.55

Alicudi	AL-13-02	Al2_ol38-1 rim	0.0020	0.0302	0.0194	0.0130	0.0074	0.1859	0.0039	0.2414	0.2154	0.0435	46.07	12.64	39.65	99.13
Alicudi	AL-13-02	Al2_ol38-2	0.0022	0.0307	0.0178	0.0119	0.0074	0.1850	0.0041	0.2495	0.1965	0.0450	47.80	11.64	40.61	100.80
Alicudi	AL-13-02	Al2_ol38-3	0.0022	0.0413	0.0175	0.0102	0.0065	0.1876	0.0100	0.2588	0.1588	0.0463	49.73	9.29	41.09	100.85
Alicudi	AL-13-02	Al2_ol38-4	0.0028	0.0306	0.0179	0.0075	0.0058	0.1604	0.0052	0.2510	0.1430	0.0405	50.95	8.01	41.44	101.07
Alicudi	AL-13-02	Al2_ol38-5 core	0.0024	0.0315	0.0175	0.0092	0.0065	0.1714	0.0060	0.2551	0.1439	0.0428	50.77	8.37	41.41	101.24
Alicudi	AL-13-02	Al2_ol43-5 core	0.0014	0.0308	0.0176	0.0087	0.0066	0.1531	0.0048	0.2420	0.1439	0.0378	51.33	7.88	41.53	101.39
Alicudi	AL-13-02	Al2_ol43-4	0.0021	0.0259	0.0176	0.0086	0.0063	0.1685	0.0051	0.2482	0.1424	0.0392	51.36	7.86	41.61	101.49
Alicudi	AL-13-02	Al2_ol43-3	0.0028	0.0201	0.0175	0.0098	0.0051	0.1851	0.0040	0.2596	0.1481	0.0471	51.01	8.28	41.49	101.48
Alicudi	AL-13-02	Al2_ol43-2	0.0019	0.0214	0.0176	0.0102	0.0069	0.1904	0.0034	0.2652	0.1591	0.0505	50.45	9.18	41.51	101.86
Alicudi	AL-13-02	Al2_ol43-1 rim	0.0022	0.0230	0.0176	0.0112	0.0060	0.1923	0.0026	0.2657	0.1656	0.0507	50.34	9.63	41.66	102.37
Alicudi	AL-13-02	Al2-ol16-sp1-1 bis (rim)	0.0022	0.0324	0.0212	0.0146	0.0045	0.1448	0.0022	0.2831	0.2694	0.0542	44.89	16.21	40.31	102.23
Alicudi	AL-13-02	Al2-ol16-sp1-2 bis	0.0038	0.0325	0.0187	0.0132	0.0027	0.1037	0.0022	0.3807	0.1794	0.0767	48.20	11.86	40.85	101.72
Alicudi	AL-13-02	Al2-ol16-sp1-3 bis	0.0008	0.0333	0.0178	0.0119	0.0037	0.1061	0.0026	0.3931	0.1342	0.0710	49.81	9.45	41.11	101.14
Alicudi	AL-13-02	Al2-ol16-sp1-4 bis (core)	0.0081	0.1895	0.0174	0.0110	0.0040	0.1397	0.0028	0.3911	0.1241	0.2640	49.41	9.00	41.06	100.62
Alicudi	AL-13-02	Al2-ol16-sp1-5 bis	0.0012	0.0325	0.0192	0.0108	0.0018	0.1053	0.0021	0.3761	0.1439	0.0646	49.15	10.32	40.98	101.21
Alicudi	AL-13-02	Al2-ol18-sp1-1 bis (rim)	0.0032	0.0282	0.0182	0.0086	0.0130	0.1454	0.0042	0.2376	0.1459	0.0366	51.18	7.96	41.49	101.27
Alicudi	AL-13-02	Al2-ol18-sp1-2 bis	0.0037	0.0281	0.0176	0.0059	0.0173	0.1425	0.0053	0.2385	0.1438	0.0338	50.85	7.92	41.11	100.51
Alicudi	AL-13-02	Al2-ol18-sp1-3 bis	0.0018	0.0284	0.0173	0.0065	0.0147	0.1491	0.0051	0.2417	0.1421	0.0354	51.00	7.89	41.23	100.77
Alicudi	AL-13-02	Al2-ol18-sp1-4 bis	0.0011	0.0295	0.0187	0.0074	0.0132	0.1650	0.0044	0.2529	0.1430	0.0416	50.88	7.94	41.15	100.65
Alicudi	AL-13-02	Al2-ol18-sp1-5 bis (core)	0.0033	0.0342	0.0177	0.0065	0.0118	0.1648	0.0053	0.2522	0.1422	0.0435	51.12	7.92	41.40	101.12

Table 3A.2 *Olivine analyses, ppm (EPMA)*
Olivine cores (ppm)

Island	Sample	Olivine	Fo	Ca	Ni	Mn	Fe	Fe/Mn	Mn/FeO	FeO/MnO	Ni*FeO/MgO	NiO*FeO/MgO
Alicudi	AL-13-02	Al2_ol1	92.12	706.93	3243.34	858.34	59861.82	69.74	111.499	69.47	494.199	0.063
Alicudi	AL-13-02	Al2_ol2	80.21	1461.04	1103.42	2497.98	144992.76	58.04	133.968	57.82	485.376	0.062
Alicudi	AL-13-02	Al2_ol3	79.98	1647.61	1093.20	2537.89	145719.49	57.42	135.430	57.20	487.779	0.062
Alicudi	AL-13-02	Al2_ol4	79.97	1571.12	1173.15	2520.83	146870.36	58.26	133.465	58.04	523.741	0.067
Alicudi	AL-13-02	Al2_ol5	80.00	1527.52	1039.52	2501.42	146337.85	58.50	132.920	58.28	463.206	0.059
Alicudi	AL-13-02	Al2_ol6	79.93	1511.79	965.21	2540.56	146764.36	57.77	134.607	57.54	432.026	0.055
Alicudi	AL-13-02	Al2_ol7	82.08	1620.44	1254.83	2206.59	133012.40	60.28	129.000	60.05	488.186	0.062
Alicudi	AL-13-02	Al2_ol8	79.94	1562.54	1070.54	2517.35	146797.14	58.31	133.348	58.09	478.908	0.061
Alicudi	AL-13-02	Al2_ol9	82.03	1732.67	1334.89	2202.10	132233.07	60.05	129.496	59.82	521.396	0.066
Alicudi	AL-13-02	Al2_ol10	80.49	1457.47	1135.55	2437.94	141992.17	58.24	133.511	58.02	490.494	0.062
Alicudi	AL-13-02	Al2_ol11	79.06	1416.73	1026.40	2641.80	152676.50	57.79	134.551	57.57	484.527	0.062
Alicudi	AL-13-02	Al2_ol12	79.28	1436.03	1069.98	2572.43	151018.95	58.71	132.456	58.48	498.481	0.063
Alicudi	AL-13-02	Al2_ol13	82.31	1106.50	1700.03	2173.58	131136.03	60.33	128.888	60.10	651.169	0.083
Alicudi	AL-13-02	Al2_ol14	80.80	1425.30	1125.50	2410.25	141560.53	58.73	132.397	58.51	476.630	0.061
Alicudi	AL-13-02	Al2_ol15	82.07	1392.42	1538.74	2151.12	132184.98	61.45	126.544	61.21	599.319	0.076
Alicudi	AL-13-02	Al2_ol16	79.95	1491.07	1025.09	2529.14	146819.89	58.05	133.951	57.83	458.135	0.058
Alicudi	AL-13-02	Al2_ol17	81.07	1586.13	1140.73	2338.72	138899.99	59.39	130.928	59.16	474.899	0.060
Alicudi	AL-13-02	Al2_ol18	79.87	1490.35	1102.79	2582.46	147892.64	57.27	135.783	57.05	495.385	0.063
Alicudi	AL-13-02	Al2_ol19	79.74	1533.24	938.17	2598.19	148830.48	57.28	135.749	57.06	424.837	0.054
Alicudi	AL-13-02	Al2_ol20	79.89	1511.08	988.10	2568.62	147873.95	57.57	135.073	57.35	443.303	0.056
Alicudi	AL-13-02	Al2_ol21	80.04	1599.00	1005.58	2546.86	146228.29	57.42	135.436	57.19	446.853	0.057
Alicudi	AL-13-02	Al2_ol22	80.02	1511.08	957.33	2532.91	146488.69	57.83	134.454	57.61	426.027	0.054
Alicudi	AL-13-02	Al2_ol23	78.92	1621.87	855.23	2722.82	153115.65	56.23	138.280	56.02	407.143	0.052
Alicudi	AL-13-02	Al2_ol24	80.00	1524.66	938.42	2548.75	146435.72	57.45	135.344	57.23	418.152	0.053
Alicudi	AL-13-02	Al2_ol25	79.60	1513.94	916.30	2581.66	149141.50	57.77	134.605	57.55	418.469	0.053
Alicudi	AL-13-02	Al2_ol26	79.94	1571.12	1249.78	2505.22	146811.50	58.60	132.692	58.38	559.029	0.071
Alicudi	AL-13-02	Al2_ol27	89.82	711.94	3109.58	1150.71	77608.51	67.44	115.297	67.18	628.290	0.080

Alicudi	AL-13-02	Al2_ol28	80.06	1472.48	1005.16	2542.15	146408.53	57.59	135.019	57.37	446.093	0.057
Alicudi	AL-13-02	Al2_ol29	82.13	751.97	1910.62	2117.24	132150.74	62.42	124.583	62.17	741.149	0.094
Alicudi	AL-13-02	Al2_ol30	88.46	746.25	3022.94	1336.81	87387.89	65.37	118.954	65.12	703.251	0.090
Alicudi	AL-13-02	Al2_ol31	83.87	1388.85	1661.28	2003.35	119553.87	59.68	130.302	59.45	569.511	0.072
Alicudi	AL-13-02	Al2_ol32	88.24	1390.28	1943.42	1454.13	89908.44	61.83	125.766	61.59	461.735	0.059
Alicudi	AL-13-02	Al2_ol33	90.02	730.52	3114.55	1114.28	75927.77	68.14	114.118	67.88	615.374	0.078
Alicudi	AL-13-02	Al2_ol34	84.63	1634.74	1947.59	1775.43	115072.90	64.81	119.974	64.56	630.465	0.080
Alicudi	AL-13-02	Al2_ol35	83.86	1135.10	1912.83	1966.18	119738.26	60.90	127.688	60.66	656.035	0.084
Alicudi	AL-13-02	Al2_ol36	80.35	1611.87	979.45	2501.59	144000.23	57.56	135.087	57.34	426.856	0.054
Alicudi	AL-13-02	Al2_ol37	79.97	1672.62	1176.03	2542.34	146443.02	57.60	134.997	57.38	525.129	0.067
Alicudi	AL-13-02	Al2_ol38	91.31	1265.90	2019.66	1109.97	66644.97	60.04	129.510	59.81	342.421	0.044
Alicudi	AL-13-02	Al2_ol39	85.42	932.09	2047.51	1690.82	109119.59	64.54	120.491	64.29	622.948	0.079
Alicudi	AL-13-02	Al2_ol40	87.73	742.67	2780.90	1395.40	92713.97	66.44	117.034	66.19	693.502	0.088
Alicudi	AL-13-02	Al2_ol41	81.03	1661.19	1135.25	2339.84	139095.22	59.45	130.807	59.22	473.871	0.060
Alicudi	AL-13-02	Al2_ol42	83.28	1650.46	1469.88	1963.89	123673.97	62.97	123.480	62.73	525.953	0.067
Alicudi	AL-13-02	Al2_ol43	92.01	1119.37	1923.48	1120.37	61262.34	54.68	142.209	54.47	297.563	0.038
Alicudi	AL-13-02	Al2_ol44	82.23	1718.37	1431.98	2136.85	131196.79	61.40	126.651	61.16	551.696	0.070
Alicudi	AL-13-02	Al2_ol45	81.64	1476.77	1434.44	2300.36	135734.31	59.01	131.785	58.78	574.855	0.073
Alicudi	AL-13-02	Al2_ol46	78.45	1708.36	870.70	2737.56	157241.75	57.44	135.380	57.22	426.299	0.054
Alicudi	AL-13-02	Al2_ol47	80.26	1406.00	1555.13	2461.64	144336.01	58.63	132.620	58.41	681.810	0.087
Alicudi	AL-13-03	Al3_ol1	80.11	1525.38	1099.99	2530.56	144124.86	56.95	136.533	56.73	486.693	0.062
Alicudi	AL-13-03	Al3_ol2	80.31	1292.35	1361.78	2469.67	143036.20	57.92	134.261	57.69	595.239	0.076
Alicudi	AL-13-03	Al3_ol3	78.47	1505.36	980.35	2727.07	155338.33	56.96	136.514	56.74	479.567	0.061
Alicudi	AL-13-03	Al3_ol4	83.62	1909.94	1474.56	2014.69	120863.84	59.99	129.620	59.76	514.867	0.066
Alicudi	AL-13-03	Al3_ol5	77.74	1645.46	873.36	2799.26	161104.90	57.55	135.112	57.33	445.871	0.057
Alicudi	AL-13-03	Al3_ol6	81.03	1404.57	1224.84	2356.67	138714.56	58.86	132.110	58.63	511.087	0.065
Alicudi	AL-13-03	Al3_ol7	81.57	1310.22	1399.85	2297.56	135023.27	58.77	132.317	58.54	563.683	0.072
Alicudi	AL-13-03	Al3_ol8	78.74	1540.39	948.27	2707.72	153856.25	56.82	136.851	56.60	456.274	0.058
Alicudi	AL-13-03	Al3_ol9	79.46	1731.95	897.66	2594.74	149049.38	57.44	135.370	57.22	413.524	0.053
Alicudi	AL-13-03	Al3_ol10	79.50	1538.96	925.35	2588.58	149198.48	57.64	134.914	57.41	425.213	0.054
Alicudi	AL-13-03	Al3_ol11	80.40	1586.13	1114.39	2435.05	142559.23	58.54	132.822	58.32	484.119	0.062
Alicudi	AL-13-03	Al3_ol12	79.40	1493.21	900.06	2622.26	149949.42	57.18	135.984	56.96	416.256	0.053

Alicudi	AL-13-03	Al3_ol13	81.13	1525.38	1149.22	2312.76	137773.07	59.57	130.535	59.34	476.347	0.061
Alicudi	AL-13-03	Al3_ol14	79.06	1496.78	868.45	2669.19	151351.49	56.70	137.136	56.48	409.919	0.052
Alicudi	AL-13-03	Al3_ol15	78.63	1467.48	921.45	2772.20	153695.84	55.44	140.256	55.23	446.487	0.057
Alicudi	AL-13-03	Al3_ol16	79.29	1448.18	926.20	2539.11	149386.74	58.83	132.169	58.61	431.079	0.055
Alicudi	AL-13-03	Al3_ol17	82.80	1130.81	1676.04	2049.44	125350.20	61.16	127.136	60.93	620.412	0.079
Alicudi	AL-13-03	Al3_ol18	83.30	1415.30	1005.32	2097.07	122983.92	58.65	132.594	58.42	359.279	0.046
Alicudi	AL-13-03	Al3_ol19	84.95	1791.99	1410.31	1850.68	111168.23	60.07	129.452	59.84	445.279	0.057
Alicudi	AL-13-03	Al3_ol20	80.34	1476.05	1131.11	2413.05	142824.56	59.19	131.378	58.96	493.303	0.063
Alicudi	AL-13-03	Al3_ol21	78.92	1551.11	878.00	2638.52	152433.50	57.77	134.598	57.55	417.910	0.053
Alicudi	AL-13-03	Al3_ol22	81.06	1075.05	1713.31	2231.46	137653.68	61.69	126.055	61.45	713.360	0.091
Alicudi	AL-13-03	Al3_ol23	80.20	1526.09	988.76	2485.79	143936.71	57.90	134.293	57.68	435.092	0.055
Alicudi	AL-13-03	Al3_ol24	80.79	1401.72	961.88	2384.46	140174.38	58.79	132.276	58.56	407.634	0.052
Alicudi	AL-13-03	Al3_ol25	82.00	1952.82	1304.41	2224.63	132150.54	59.40	130.902	59.17	510.354	0.065
Alicudi	AL-13-03	Al3_ol26	80.27	1429.59	1251.42	2444.66	143478.66	58.69	132.492	58.46	548.222	0.070
Alicudi	AL-13-03	Al3_ol27	80.00	1543.96	1037.06	2472.03	145733.06	58.95	131.903	58.72	462.146	0.059
Filicudi	FL-13-03B	fl03b_ol1	84.65	1564.94	973.12	1919.44	112349.23	58.53	132.851	58.31	314.547	0.040
Filicudi	FL-13-03B	fl03b_ol2	80.96	1333.20	792.40	2291.25	138066.61	60.26	129.045	60.02	332.121	0.042
Filicudi	FL-13-03B	fl03b_ol3	86.48	1621.54	936.05	1748.26	101114.33	57.84	134.447	57.61	260.734	0.033
Filicudi	FL-13-03B	fl03b_ol4	79.18	1395.62	713.49	2499.61	150797.71	60.33	128.895	60.09	334.372	0.043
Filicudi	FL-13-03B	fl03b_ol5	85.07	1543.50	825.58	1864.45	110601.02	59.32	131.084	59.09	258.260	0.033
Filicudi	FL-13-03B	fl03b_ol6	85.64	1556.76	761.66	1836.56	106461.28	57.97	134.144	57.74	227.639	0.029
Filicudi	FL-13-03B	fl03b_ol7	84.95	1512.04	700.90	1914.02	112198.37	58.62	132.654	58.39	221.361	0.028
Filicudi	FL-13-03B	fl03b_ol8	85.07	1558.93	720.64	1896.98	111329.85	58.69	132.498	58.46	225.397	0.029
Filicudi	FL-13-03B	fl03b_ol9	84.69	1534.98	709.61	1943.45	113696.38	58.50	132.919	58.28	228.704	0.029
Filicudi	FL-13-03B	fl03b_ol10	85.27	1578.97	803.55	1844.31	109674.16	59.47	130.764	59.24	247.414	0.031
Filicudi	FL-13-03B	fl03b_ol11	85.73	1589.35	721.47	1834.24	106104.93	57.85	134.425	57.62	214.051	0.027
Filicudi	FL-13-03B	fl03b_ol12	85.89	1584.70	801.21	1807.13	105037.67	58.12	133.783	57.90	234.683	0.030
Filicudi	FL-13-03B	fl03b_ol13	81.26	1445.00	387.59	2341.60	137505.12	58.72	132.420	58.50	159.295	0.020
Filicudi	FL-13-03B	fl03b_ol14	84.81	1570.42	704.93	1927.19	112890.13	58.58	132.748	58.35	224.962	0.029
Filicudi	FL-13-03B	fl03b_ol15	85.97	1583.65	799.67	1787.76	104612.51	58.52	132.888	58.29	232.676	0.030
Filicudi	FL-13-03B	fl03b_ol16	82.38	1465.46	513.12	2202.17	129489.92	58.80	132.243	58.57	195.598	0.025

Filicudi	FL-13-03B	fl03b_ol17	85.43	1545.10	791.01	1855.93	108859.36	58.66	132.573	58.43	240.473	0.031
Filicudi	FL-13-03B	fl03b_ol18	84.78	1614.00	694.71	1926.41	113274.69	58.80	132.244	58.57	222.285	0.028
Filicudi	FL-13-03B	fl03b_ol19	86.27	1612.22	803.67	1787.76	102373.61	57.26	135.794	57.04	227.972	0.029
Filicudi	FL-13-03B	fl03b_ol20	85.00	1547.88	717.66	1895.43	111231.95	58.68	132.507	58.46	225.662	0.029
Filicudi	FL-13-03B	fl03b_ol21	85.65	1563.95	809.26	1831.14	106691.92	58.27	133.459	58.04	241.601	0.031
Filicudi	FL-13-03B	fl03b_ol22	86.48	1625.82	810.06	1749.03	101054.35	57.78	134.587	57.55	225.713	0.029
Filicudi	FL-13-03B	fl03b_ol23	86.00	1606.15	760.33	1780.02	104621.49	58.78	132.301	58.55	220.556	0.028
Filicudi	FL-13-03B	fl03b_ol24	86.65	1572.15	819.56	1754.45	99426.72	56.67	137.214	56.45	225.024	0.029
Filicudi	FL-13-03B	fl03b_ol25	84.32	1530.99	652.97	1986.06	115798.75	58.31	133.367	58.08	216.410	0.028
Filicudi	FL-13-03B	fl03b_ol26	86.30	1647.31	825.11	1766.85	102129.15	57.80	134.527	57.58	233.541	0.030
Filicudi	FL-13-03B	fl03b_ol27	85.03	1542.41	723.27	1896.20	111245.64	58.67	132.544	58.44	226.903	0.029
Filicudi	FL-13-03B	fl03b_ol28	84.60	1573.55	644.32	1952.75	114022.43	58.39	133.173	58.16	209.118	0.027
Filicudi	FL-13-03B	fl03b_ol29	84.21	1510.86	647.49	1991.48	117398.92	58.95	131.908	58.72	216.354	0.028
Filicudi	FL-13-03B	fl03b_ol30	86.84	1582.14	702.77	1725.02	99350.98	57.59	135.015	57.37	189.894	0.024
Filicudi	FL-13-03B	fl03b_ol31	86.25	1602.56	814.91	1784.66	102469.53	57.42	135.432	57.19	231.632	0.029
Filicudi	FL-13-03B	fl03b_ol32	84.71	1540.55	678.32	1963.59	112896.54	57.49	135.248	57.27	218.202	0.028
Filicudi	FL-13-03B	fl03b_ol33	86.25	1562.40	742.29	1793.96	102392.09	57.08	136.240	56.86	210.985	0.027
Filicudi	FL-13-03B	fl03b_ol34	83.78	1440.83	631.75	2048.80	119822.47	58.48	132.960	58.26	217.984	0.028
Filicudi	FL-13-03B	fl03b_ol35	85.57	1545.17	724.15	1879.94	107466.12	57.16	136.029	56.94	217.612	0.028
Filicudi	FL-13-03B	fl03b_ol36	82.57	1361.11	592.28	2215.34	128443.04	57.98	134.118	57.75	222.788	0.028
Filicudi	FL-13-03B	fl03b_ol37	85.02	1545.85	569.39	1931.84	112609.70	58.29	133.399	58.07	178.768	0.023
Filicudi	FL-13-03B	fl03b_ol38	86.40	1549.79	814.22	1759.88	101261.55	57.54	135.144	57.32	228.377	0.029
Filicudi	FL-13-03B	fl03b_ol39	82.64	1363.46	631.80	2132.46	127758.68	59.91	129.792	59.68	236.489	0.030
Filicudi	FL-13-03B	fl03b_ol40	85.50	1546.89	806.35	1836.56	107949.05	58.78	132.296	58.55	243.771	0.031
Filicudi	FL-13-03B	fl03b_ol41	84.55	1509.88	653.14	1976.76	114962.16	58.16	133.708	57.93	212.796	0.027
Filicudi	FL-13-03B	fl03b_ol42	80.36	1469.27	447.02	2573.20	143681.02	55.84	139.262	55.62	194.719	0.025
Filicudi	FL-13-03B	fl03b_ol43	76.14	1453.07	372.79	2952.75	170947.76	57.89	134.314	57.67	208.215	0.027
Filicudi	FL-13-03B	fl03b_ol44	86.30	1521.68	736.89	1778.47	101909.06	57.30	135.704	57.08	208.589	0.027
Filicudi	FL-13-03B	fl03b_ol45	83.78	1486.07	689.52	1995.35	120374.30	60.33	128.898	60.09	237.884	0.030
Filicudi	FL-13-03B	fl03b_ol46	86.74	1628.79	765.35	1752.13	99910.61	57.02	136.368	56.80	208.565	0.027
Filicudi	FL-13-03B	fl03b_ol47	84.31	1511.79	662.10	2028.29	116304.82	57.34	135.610	57.12	219.684	0.028
Filicudi	FL-13-03B	fl03b_ol48	84.21	1445.32	627.23	2004.24	116946.35	58.35	133.267	58.12	209.647	0.027

Filicudi	FL-13-03B	fl03b_ol49	82.43	1340.96	643.77	2173.38	128783.83	59.26	131.230	59.03	244.590	0.031
Filicudi	FL-13-03B	fl03b_ol50	84.68	1523.95	648.45	1970.94	113707.62	57.69	134.785	57.47	209.142	0.027
Filicudi	FL-13-03B	fl03b_ol51	86.78	1659.04	837.36	1751.34	98530.33	56.26	138.216	56.04	227.373	0.029
Filicudi	FL-13-03B	fl03b_ol52	86.47	1613.30	803.27	1788.04	100983.67	56.48	137.685	56.26	224.031	0.029
Filicudi	FL-13-03B	fl03b_ol53	85.03	1508.22	1045.88	1943.96	112370.14	57.80	134.523	57.58	328.224	0.042
Filicudi	FL-13-03B	fl03b_ol54	81.96	1309.51	660.03	2309.49	133866.25	57.96	134.154	57.74	258.979	0.033
Filicudi	FL-13-03B	fl03b_ol55	86.09	1468.91	689.99	1863.11	104045.10	55.84	139.244	55.63	198.749	0.025
Filicudi	FL-13-03B	fl03b_ol56	85.68	1551.82	790.28	1853.08	106905.13	57.69	134.789	57.47	235.335	0.030
Filicudi	FL-13-03B	fl03b_ol57	85.28	1571.12	742.78	1869.53	109360.03	58.50	132.933	58.27	228.545	0.029
Filicudi	FL-13-03B	fl03b_ol58	85.87	1536.81	771.15	1832.22	105202.95	57.42	135.428	57.20	226.152	0.029
Filicudi	FL-13-03B	fl03b_ol59	85.72	1536.10	779.75	1842.44	105953.34	57.51	135.219	57.28	231.512	0.029
Filicudi	FL-13-03B	fl03b_ol60	86.52	1632.59	812.85	1766.93	100567.65	56.92	136.622	56.70	225.711	0.029
Filicudi	FL-13-03B	fl03b_ol61	84.78	1552.54	702.18	1965.77	113429.24	57.70	134.762	57.48	224.713	0.029
Filicudi	FL-13-03B	fl03b_ol62	85.93	1538.96	734.56	1835.22	104663.30	57.03	136.349	56.81	214.315	0.027
Salina	SL-13-05	sl5_ol1	82.08	1377.41	916.91	2116.56	131622.83	62.19	125.043	61.95	356.883	0.045
Salina	SL-13-05	sl5_ol2	79.54	1484.63	803.76	2585.96	148527.24	57.44	135.386	57.21	368.584	0.047
Salina	SL-13-05	sl5_ol3	85.39	1291.64	1070.35	1868.55	108797.59	58.23	133.550	58.00	326.483	0.042
Salina	SL-13-05	sl5_ol4	86.02	1266.62	1738.00	1682.83	104119.67	61.87	125.680	61.63	503.635	0.064
Salina	SL-13-05	sl5_ol5	86.17	1346.68	1313.16	1727.46	103186.83	59.73	130.180	59.50	375.702	0.048
Salina	SL-13-05	sl5_ol6	79.87	1292.35	1101.93	2543.74	146036.27	57.41	135.447	57.19	494.917	0.063
Salina	SL-13-05	sl5_ol7	85.05	1321.66	1068.68	1899.54	110731.89	58.29	133.394	58.07	334.759	0.043
Salina	SL-13-05	sl5_ol8	87.55	1307.36	2011.56	1459.13	93362.21	63.99	121.529	63.74	509.923	0.065
Salina	SL-13-05	sl5_ol9	76.57	1892.78	692.13	2946.58	165342.25	56.11	138.578	55.90	377.433	0.048
Salina	SL-13-05	sl5_ol10	74.57	1385.99	749.86	3213.19	177411.52	55.21	140.836	55.00	455.782	0.058
Salina	SL-13-05	sl5_ol11	82.21	1210.86	1633.36	2174.31	129962.31	59.77	130.096	59.54	630.136	0.080
Salina	SL-13-05	sl5_ol12	75.72	1407.43	624.07	3036.28	172592.70	56.84	136.797	56.62	356.622	0.045
Salina	SL-13-05	sl5_ol13	80.49	1273.05	1271.84	2363.71	141722.89	59.96	129.692	59.73	549.462	0.070
Salina	SL-13-05	sl5_ol14	86.05	1418.16	1613.49	1672.30	103416.02	61.84	125.743	61.60	466.192	0.059
Salina	SL-13-05	sl5_ol15	83.19	1290.92	1048.75	2085.05	123598.82	59.28	131.178	59.05	377.617	0.048
Salina	SL-13-05	sl5_ol16	78.34	1521.09	700.74	2751.09	155721.37	56.60	137.377	56.38	345.428	0.044
Salina	SL-13-05	sl5_ol17	81.50	1273.77	953.01	2310.45	135196.69	58.52	132.889	58.29	385.579	0.049

Salina	SL-13-05	sl5_ol18	76.77	1386.70	666.70	2814.79	166231.51	59.06	131.672	58.83	359.528	0.046
Salina	SL-13-05	sl5_ol19	81.61	1306.65	1070.02	2249.02	133719.49	59.46	130.785	59.23	429.648	0.055
Salina	SL-13-05	sl5_ol20	72.23	1393.14	794.00	3464.07	191012.78	55.14	141.021	54.93	544.184	0.069
Salina	SL-13-05	sl5_ol21	79.85	1362.40	1209.96	2496.40	145697.82	58.36	133.236	58.14	544.144	0.069
Salina	SL-13-05	sl5_ol22	83.72	1378.84	1250.27	1986.00	119871.70	60.36	128.832	60.12	433.427	0.055
Salina	SL-13-05	sl5_ol23	75.99	1416.73	605.75	2989.38	170880.88	57.16	136.034	56.94	341.060	0.043
Salina	SL-13-05	sl5_ol24	79.25	1378.84	1015.36	2671.32	149894.19	56.11	138.580	55.90	474.003	0.060
Salina	SL-13-05	sl5_ol25	82.25	1298.78	1499.29	2314.11	130055.59	56.20	138.361	55.98	576.880	0.073
Salina	SL-13-05	sl5_ol26	78.98	1414.58	804.98	2616.95	151862.83	58.03	133.999	57.81	381.972	0.049
Salina	SL-13-05	sl5_ol27	84.71	1323.09	1230.38	1891.28	113000.72	59.75	130.147	59.52	395.967	0.050
Salina	SL-13-05	sl5_ol28	80.52	1271.62	1142.59	2417.07	140844.84	58.27	133.447	58.05	492.747	0.063
Salina	SL-13-05	sl5_ol29	75.06	1478.91	925.92	2983.61	176256.18	59.07	131.631	58.85	548.500	0.070
Salina	SL-13-05	sl5_ol30	83.28	1323.80	1437.47	2038.76	122659.93	60.16	129.248	59.93	514.576	0.066
Salina	SL-13-05	sl5_ol31	79.21	1299.50	1275.36	2628.05	148977.58	56.69	137.174	56.47	596.786	0.076
Salina	SL-13-05	sl5_ol32	77.60	1451.75	1064.23	2686.92	160606.62	59.77	130.092	59.54	547.601	0.070
Salina	SL-13-05	sl5_ol33	82.94	1343.10	1259.50	2054.06	125383.02	61.04	127.390	60.81	461.628	0.059
Salina	SL-13-05	sl5_ol34	77.93	1312.37	1192.27	2936.15	158347.31	53.93	144.187	53.72	601.832	0.077
Salina	SL-13-05	sl5_ol35	77.68	1305.22	849.91	2882.36	159753.28	55.42	140.300	55.21	435.317	0.055
Salina	SL-13-05	sl5_ol36	78.97	1329.52	987.46	2679.07	151872.70	56.69	137.171	56.47	468.697	0.060
Salina	SL-13-05	sl5_ol37	76.25	1547.53	940.80	2886.68	168121.83	58.24	133.516	58.01	522.338	0.066
Salina	SL-13-05	sl5_ol38	78.27	1248.03	1236.45	2850.88	156569.27	54.92	141.590	54.71	611.931	0.078
Salina	SL-13-05	sl5_ol39	81.43	1305.22	1358.97	2345.37	135660.84	57.84	134.436	57.62	552.281	0.070
Salina	SL-13-05	sl5_ol40	73.30	1445.32	767.62	3470.55	188161.39	54.22	143.426	54.01	498.406	0.063
Salina	SL-13-05	sl5_ol41	77.74	1300.21	1002.39	2867.93	160721.79	56.04	138.756	55.82	511.644	0.065
Salina	SL-13-05	sl5_ol42	75.83	1387.42	683.00	3059.18	174277.08	56.97	136.497	56.75	388.010	0.049
Salina	SL-13-05	sl5_ol43	76.67	1315.23	1201.55	3101.68	167873.92	54.12	143.672	53.91	651.608	0.083
Salina	SL-13-05	sl5_ol44	77.89	1404.57	748.59	2809.80	160846.25	57.24	135.839	57.02	378.813	0.048
Salina	SL-13-05	sl5_ol45	80.35	1305.93	2232.28	2506.13	146051.02	58.28	133.432	58.05	972.940	0.124
Salina	SL-13-08	sl8_ol1	76.18	1695.50	820.57	2945.19	169672.66	57.61	134.977	57.39	457.310	0.058
Salina	SL-13-08	sl8_ol2	80.41	1346.68	892.37	2477.70	141706.31	57.19	135.962	56.97	387.625	0.049
Salina	SL-13-08	sl8_ol3	79.69	1370.98	1047.12	2597.52	146262.64	56.31	138.097	56.09	475.790	0.061
Salina	SL-13-08	sl8_ol4	84.12	1331.67	1470.47	2028.07	117469.55	57.92	134.251	57.70	494.701	0.063

Salina	SL-13-08	sl8_ol5	79.75	1469.62	799.50	2630.75	147040.83	55.89	139.124	55.68	361.894	0.046
Salina	SL-13-08	sl8_ol6	75.91	1448.89	729.07	3073.73	169642.91	55.19	140.893	54.98	412.493	0.053
Salina	SL-13-08	sl8_ol7	82.76	1458.18	1273.90	2130.56	126454.19	59.35	131.015	59.12	472.995	0.060
Salina	SL-13-08	sl8_ol8	77.78	1421.02	893.87	2755.73	157762.02	57.25	135.829	57.03	455.096	0.058
Salina	SL-13-08	sl8_ol9	78.84	1368.83	811.25	2657.02	152363.88	57.34	135.604	57.12	388.058	0.049
Salina	SL-13-08	sl8_ol10	75.86	1653.32	834.97	3020.92	170829.25	56.55	137.510	56.33	473.716	0.060
Salina	SL-13-08	sl8_ol11	76.25	1668.33	878.42	2954.83	168804.84	57.13	136.115	56.91	487.561	0.062
Salina	SL-13-08	sl8_ol12	77.33	1483.20	1619.61	2742.27	161807.76	59.01	131.786	58.78	846.380	0.108
Salina	SL-13-08	sl8_ol13	81.34	1311.65	979.55	2319.34	136699.62	58.94	131.934	58.71	400.661	0.051
Salina	SL-13-08	sl8_ol14	75.39	1112.94	369.42	2979.36	174792.20	58.67	132.544	58.44	214.967	0.027
Salina	SL-13-08	sl8_ol15	80.69	1354.54	954.39	2494.07	141229.74	56.63	137.322	56.41	407.095	0.052
Salina	SL-13-08	sl8_ol16	83.64	1240.17	1095.76	2098.35	120774.33	57.56	135.102	57.33	382.055	0.049
Salina	SL-13-08	sl8_ol17	81.55	1358.11	1432.93	2340.00	135157.94	57.76	134.627	57.54	577.676	0.074
Salina	SL-13-08	sl8_ol18	80.91	1284.49	1328.79	2427.37	139994.36	57.67	134.829	57.45	558.979	0.071
Salina	SL-13-08	sl8_ol19	82.99	1272.34	1119.62	2129.79	126362.20	59.33	131.062	59.10	409.130	0.052
Salina	SL-13-08	sl8_ol20	84.07	1342.39	1387.36	1985.70	118657.02	59.76	130.131	59.52	468.628	0.060
Salina	SL-13-08	sl8_ol21	81.08	1333.81	882.05	2387.93	139919.70	58.59	132.710	58.37	366.878	0.047
Salina	SL-13-08	sl8_ol22	79.47	1342.39	914.48	2591.45	149519.62	57.70	134.773	57.47	421.094	0.054
Salina	SL-13-08	sl8_ol23	79.42	1599.00	650.75	2672.62	150246.78	56.22	138.322	56.00	300.616	0.038
Salina	SL-13-08	sl8_ol24	84.62	1406.72	1348.17	1879.26	115068.66	61.23	126.995	60.99	436.605	0.056
Salina	SL-13-08	sl8_ol25	80.66	1360.97	1073.38	2492.79	141654.21	56.83	136.841	56.61	458.651	0.058
Salina	SL-13-08	sl8_ol26	79.35	1263.76	890.98	2694.79	149783.42	55.58	139.901	55.37	413.414	0.053
Salina	SL-13-08	sl8_ol27	81.66	1347.39	1069.55	2350.34	133802.16	56.93	136.593	56.71	428.187	0.055
Salina	SL-13-08	sl8_ol28	77.89	1505.36	823.14	2719.18	159149.14	58.53	132.860	58.30	416.457	0.053
Salina	SL-13-08	sl8_ol29	76.52	1552.54	996.19	2950.07	167624.91	56.82	136.852	56.60	544.708	0.069
Salina	SL-13-08	sl8_ol30	77.97	1217.30	542.76	2738.91	158395.81	57.83	134.460	57.61	273.326	0.035
Salina	SL-13-08	sl8_ol31	77.08	1295.93	814.58	3042.32	163341.72	53.69	144.833	53.48	431.802	0.055
Salina	SL-13-08	sl8_ol32	83.14	1346.68	1164.65	2089.64	123921.48	59.30	131.124	59.07	421.020	0.054
Salina	SL-13-08	sl8_ol33	77.32	1310.94	576.04	2808.65	162840.57	57.98	134.120	57.75	301.191	0.038
Salina	SL-13-08	sl8_ol34	82.81	1303.07	1257.23	2158.43	126381.75	58.55	132.805	58.33	465.168	0.059
Salina	SL-13-08	sl8_ol35	82.48	1423.16	1185.39	2176.46	128771.62	59.17	131.429	58.94	448.750	0.057
Salina	SL-13-08	sl8_ol36	82.55	1121.52	854.31	2193.71	128899.97	58.76	132.338	58.53	321.927	0.041

Salina	SL-13-08	sl8_ol37	82.94	1310.94	1498.49	2260.87	126246.12	55.84	139.257	55.62	549.233	0.070
Salina	SL-13-08	sl8_ol38	80.69	1343.10	1272.52	2388.87	140839.89	58.96	131.894	58.73	542.660	0.069
Salina	SL-13-08	sl8_ol39	78.05	1421.73	1002.26	2567.58	159647.19	62.18	125.061	61.94	502.306	0.064
Salina	SL-13-08	sl8_ol40	76.13	1466.05	910.62	3124.60	168718.86	54.00	144.009	53.79	508.834	0.065
Salina	SL-13-08	sl8_ol41	76.20	1299.50	1029.25	3020.21	163117.71	54.01	143.978	53.80	573.154	0.073
Salina	SL-13-08	sl8_ol42	73.76	1333.81	709.92	3230.95	180521.75	55.87	139.174	55.66	450.197	0.057
Salina	SL-13-08	sl8_ol43	80.15	1291.64	1261.00	2529.79	141077.14	55.77	139.440	55.55	556.538	0.071
Salina	SL-13-08	sl8_ol44	75.66	1348.11	716.44	3249.58	173139.59	53.28	145.945	53.07	410.877	0.052
Salina	SL-13-08	sl8_ol45	75.84	1441.03	688.01	3258.30	172228.58	52.86	147.111	52.65	390.748	0.050
Salina	SL-13-08	sl8_ol46	78.90	1308.08	832.77	2695.86	152417.37	56.54	137.538	56.32	396.993	0.051
Salina	SL-13-08	sl8_ol47	75.30	1765.55	798.81	3174.30	175432.80	55.27	140.701	55.05	467.029	0.059
Stromboli CA	ST-13-09	st9_ol1	90.30	1459.61	2275.86	1272.33	72600.96	57.06	136.275	56.84	435.605	0.055
Stromboli CA	ST-13-09	st9_ol2	80.79	505.36	1023.63	2322.39	139497.52	60.07	129.458	59.83	433.823	0.055
Stromboli CA	ST-13-09	st9_ol3	90.57	1240.89	2270.37	1271.62	71133.34	55.94	139.009	55.72	421.257	0.054
Stromboli CA	ST-13-09	st9_ol4	83.17	443.17	1075.87	2176.63	123997.37	56.97	136.500	56.75	388.030	0.049
Stromboli CA	ST-13-09	st9_ol5	83.05	438.17	1110.69	1913.78	124520.69	65.07	119.511	64.81	403.960	0.051
Stromboli CA	ST-13-09	st9_ol6	65.60	1634.02	361.53	4047.68	223952.32	55.33	140.543	55.11	337.955	0.043
Stromboli CA	ST-13-09	st9_ol7	83.46	431.02	1046.63	2162.78	122889.01	56.82	136.854	56.60	369.762	0.047
Stromboli CA	ST-13-09	st9_ol8	82.15	420.30	1078.29	2028.63	131207.24	64.68	120.228	64.43	417.499	0.053
Stromboli CA	ST-13-09	st9_ol9	86.59	857.76	1250.76	1793.05	100931.47	56.29	138.142	56.07	345.235	0.044
Stromboli CA	ST-13-09	st9_ol10	82.40	443.89	1025.31	2260.49	130321.07	57.65	134.880	57.43	390.444	0.050
Stromboli CA	ST-13-09	st9_ol11	80.93	465.33	941.46	2548.49	140212.88	55.02	141.337	54.80	395.482	0.050
Stromboli CA	ST-13-09	st9_ol12	81.54	468.91	952.54	2334.75	136252.57	58.36	133.246	58.13	384.303	0.049
Stromboli CA	ST-13-09	st9_ol13	82.29	396.00	1173.28	2282.54	130944.35	57.37	135.547	57.15	450.056	0.057
Stromboli CA	ST-13-09	st9_ol14	68.05	1472.48	554.61	3848.04	214356.96	55.71	139.592	55.49	464.215	0.059
Stromboli CA	ST-13-09	st9_ol15	80.17	511.08	920.93	2464.50	145070.75	58.86	132.101	58.64	406.113	0.052
Stromboli CA	ST-13-09	st9_ol17	81.05	467.48	930.45	2553.68	139216.35	54.52	142.638	54.30	387.744	0.049
Stromboli CA	ST-13-09	st9_ol18	67.31	1777.70	390.07	4227.90	220795.94	52.22	148.899	52.02	337.632	0.043
Stromboli CA	ST-13-09	st9_ol19	90.74	1208.72	2595.19	1251.94	70125.19	56.01	138.825	55.80	472.081	0.060
Stromboli CA	ST-13-09	st9_ol20	74.24	644.75	305.41	3805.87	181187.98	47.61	163.337	47.42	188.866	0.024
Stromboli CA	ST-13-09	st9_ol21	64.96	1763.40	348.93	4126.00	229028.60	55.51	140.087	55.29	335.496	0.043

Stromboli CA	ST-13-09	st9_ol22	64.72	1745.53	310.17	4110.51	231926.60	56.42	137.817	56.20	301.418	0.038
Stromboli CA	ST-13-17	st17_ol1	84.36	0.00	1178.72	2050.35	115830.68	56.49	137.646	56.27	389.507	0.050
Stromboli CA	ST-13-17	st17_ol2	89.23	1463.65	2062.41	1484.12	81699.36	55.05	141.257	54.84	443.795	0.056
Stromboli CA	ST-13-17	st17_ol3	89.74	1544.62	1842.31	1367.93	77700.50	56.80	136.899	56.58	375.448	0.048
Stromboli CA	ST-13-17	st17_ol4	90.03	1552.91	2189.50	1361.74	75300.35	55.30	140.622	55.08	431.985	0.055
Stromboli CA	ST-13-17	st17_ol5	81.58	939.16	1616.71	2367.16	135003.24	57.03	136.346	56.81	650.638	0.083
Stromboli CA	ST-13-17	st17_ol6	89.57	1456.59	1509.42	1451.59	78695.44	54.21	143.434	54.00	313.369	0.040
Stromboli CA	ST-13-17	st17_ol7	90.46	1549.71	1619.92	1342.37	72230.97	53.81	144.513	53.60	304.508	0.039
Stromboli CA	ST-13-17	st17_ol8	82.92	1045.61	1173.33	2188.23	125225.92	57.23	135.880	57.01	430.904	0.055
Stromboli CA	ST-13-17	st17_ol9	90.14	1564.11	1662.58	1312.16	73819.93	56.26	138.221	56.04	323.993	0.041
Stromboli CA	ST-13-17	st17_ol10	83.32	1078.18	1213.61	2167.31	122787.97	56.65	137.254	56.44	433.054	0.055
Stromboli CA	ST-13-17	st17_ol11	81.69	950.11	1058.18	2356.31	134461.38	57.06	136.268	56.84	422.641	0.054
Stromboli CA	ST-13-17	st17_ol12	82.09	1069.80	1081.87	2286.60	131742.94	57.62	134.965	57.39	420.743	0.054
Stromboli CA	ST-13-17	st17_ol13	83.54	1098.28	1160.01	2140.98	122215.56	57.08	136.221	56.86	407.348	0.052
Stromboli CA	ST-13-17	st17_ol14	89.14	1493.46	1531.72	1466.31	82226.07	56.08	138.667	55.86	332.542	0.042
Stromboli CA	ST-13-17	st17_ol15	86.19	1446.49	1449.67	1837.34	102940.03	56.03	138.792	55.81	414.086	0.053
Stromboli CA	ST-13-17	st17_ol16	90.51	1590.36	1666.71	1349.34	71730.16	53.16	146.278	52.95	311.549	0.040
Stromboli CA	ST-13-17	st17_ol17	77.24	779.58	245.43	2987.61	164365.51	55.02	141.342	54.80	128.939	0.016
Stromboli CA	ST-13-17	st17_ol18	69.93	1122.15	1090.66	3827.27	210398.49	54.97	141.451	54.76	836.070	0.106
Stromboli CA	ST-13-17	st17_ol19	88.06	1433.02	1494.75	1555.38	89815.86	57.75	134.661	57.52	361.144	0.046
Stromboli CA	ST-13-17	st17_ol20	87.43	1414.78	1407.96	1637.49	94189.79	57.52	135.187	57.30	360.907	0.046
Stromboli CA	ST-13-17	st17_ol21	88.51	1433.17	1547.62	1560.50	85800.16	54.98	141.428	54.77	358.027	0.046
Stromboli KS	ST-13-04	st04_ol1	72.50	1920.02	789.49	3860.45	193541.84	50.13	155.104	49.94	533.710	0.068
Stromboli KS	ST-13-04	st04_ol2	75.88	2021.00	727.68	3378.36	172751.14	51.13	152.070	50.94	412.382	0.052
Stromboli KS	ST-13-04	st04_ol3	69.52	2006.38	410.79	4469.72	212597.02	47.56	163.487	47.38	321.076	0.041
Stromboli KS	ST-13-04	st04_ol4	69.80	2076.11	452.27	4353.21	212784.42	48.88	159.085	48.69	348.734	0.044
Stromboli KS	ST-13-04	st04_ol5	69.66	2174.86	408.45	4462.02	212071.79	47.53	163.609	47.34	317.050	0.040
Stromboli KS	ST-13-04	st04_ol6	68.15	1900.90	341.94	4757.08	220499.52	46.35	167.761	46.17	284.786	0.036
Stromboli KS	ST-13-04	st04_ol7	69.99	2204.36	404.55	4401.45	209710.78	47.65	163.205	47.46	309.253	0.039
Stromboli KS	ST-13-04	st04_ol8	69.69	2078.53	392.81	4457.38	212839.85	47.75	162.849	47.57	304.495	0.039
Stromboli KS	ST-13-04	st04_ol9	69.90	2172.24	396.73	4437.44	210376.53	47.41	164.019	47.23	304.532	0.039

Stromboli KS	ST-13-04	st04_ol10	69.76	2237.59	389.69	4443.55	210882.90	47.46	163.851	47.27	301.066	0.038
Stromboli KS	ST-13-04	st04_ol11	67.87	1871.92	323.18	4903.37	223452.12	45.57	170.636	45.39	272.718	0.035
Stromboli KS	ST-13-04	st04_ol12	70.08	2220.33	392.82	4382.98	209297.30	47.75	162.841	47.57	298.939	0.038
Stromboli KS	ST-13-04	st04_ol13	70.44	2369.11	411.61	4317.05	207187.51	47.99	162.025	47.81	307.868	0.039
Stromboli KS	ST-13-04	st04_ol14	69.98	2174.09	437.43	4432.00	211521.74	47.73	162.931	47.54	334.440	0.043
Stromboli KS	ST-13-04	st04_ol15	68.49	2080.99	351.36	4603.65	219328.00	47.64	163.218	47.46	288.150	0.037
Stromboli KS	ST-13-04	st04_ol16	68.57	2121.53	363.88	4595.97	218026.71	47.44	163.918	47.25	297.306	0.038
Stromboli KS	ST-13-04	st04_ol17	70.06	2188.21	380.32	4386.73	209033.61	47.65	163.186	47.47	289.690	0.037

Olivine points around spinel (ppm)

Island	Sample	Olivine	Fo	Ca	Ni	Mn	Fe	Fe/Mn	Mn/FeO	FeO/MnO	Ni*FeO/MgO	NiO*FeO/MgO
Alicudi	AL-13-02	Al2-ol16-sp1-1	84.13	1027.16	2275.35	1937.51	118102.13	60.96	127.569	60.72	764.898	0.097
Alicudi	AL-13-02	Al2-ol16-sp1-2	83.52	1084.35	2051.68	2036.67	122432.56	60.11	129.355	59.88	721.666	0.092
Alicudi	AL-13-02	Al2-ol16-sp1-3	85.78	863.47	2651.72	1716.16	107267.50	62.50	124.408	62.26	783.818	0.100
Alicudi	AL-13-02	Al2-ol16-sp1-4	87.01	791.99	2841.15	1529.30	98229.56	64.23	121.063	63.98	755.948	0.096
Alicudi	AL-13-02	Al2-ol16-sp1-5	85.25	908.51	2542.27	1777.72	110781.77	62.32	124.783	62.08	784.182	0.100
Alicudi	AL-13-02	Al2-ol17-sp1-1	83.57	1378.84	1645.69	2086.27	123544.77	59.22	131.313	58.99	576.877	0.073
Alicudi	AL-13-02	Al2-ol17-sp1-2	83.30	1377.41	1599.16	2123.68	125483.39	59.09	131.602	58.86	571.440	0.073
Alicudi	AL-13-02	Al2-ol17-sp1-3	83.02	1384.56	1575.58	2157.17	127299.04	59.01	131.770	58.78	574.550	0.073
Alicudi	AL-13-02	Al2-ol17-sp1-4	83.01	1385.28	1587.63	2148.47	126666.20	58.96	131.894	58.73	579.207	0.074
Alicudi	AL-13-02	Al2-ol17-sp1-5	83.30	1368.83	1633.73	2095.24	124089.41	59.22	131.298	59.00	583.744	0.074
Alicudi	AL-13-02	Al2-ol18-sp1-1	83.52	1427.45	1599.06	1908.43	119523.35	62.63	124.160	62.39	562.374	0.072
Alicudi	AL-13-02	Al2-ol18-sp1-2	85.31	1401.00	1771.11	1700.55	109143.75	64.18	121.157	63.93	543.533	0.069
Alicudi	AL-13-02	Al2-ol18-sp1-3	85.78	1398.86	1831.51	1637.98	105625.56	64.49	120.586	64.24	541.201	0.069
Alicudi	AL-13-02	Al2-ol18-sp1-4	84.82	1390.99	1759.61	1725.38	111660.24	64.72	120.156	64.47	561.370	0.071
Alicudi	AL-13-02	Al2-ol18-sp1-5	83.07	1411.01	1587.07	1967.41	124314.28	63.19	123.064	62.94	576.653	0.073
Alicudi	AL-13-02	Al2-ol18-sp2-1	91.40	1305.22	2086.47	1162.11	65603.60	56.45	137.746	56.23	349.933	0.045
Alicudi	AL-13-02	Al2-ol18-sp2-2	90.84	1340.24	2128.70	1189.39	69919.49	58.79	132.277	58.56	382.717	0.049
Alicudi	AL-13-02	Al2-ol18-sp2-3	90.18	1360.26	2107.53	1252.58	75019.97	59.89	129.834	59.66	408.959	0.052
Alicudi	AL-13-02	Al2-ol18-sp2-4	90.41	1325.95	2115.69	1255.64	73220.58	58.31	133.350	58.09	399.892	0.051
Alicudi	AL-13-02	Al2-ol18-sp2-5	91.33	1299.50	2092.13	1166.57	66427.82	56.94	136.558	56.72	354.191	0.045

Alicudi	AL-13-02	Al2-ol19-sp1-1	83.06	1429.59	2009.11	1966.82	122382.43	62.22	124.970	61.98	730.554	0.093
Alicudi	AL-13-02	Al2-ol19-sp1-2	83.13	1416.73	1968.09	2016.70	123899.41	61.44	126.570	61.20	711.858	0.091
Alicudi	AL-13-02	Al2-ol19-sp1-3	83.38	1418.16	2077.74	1968.19	122403.15	62.19	125.036	61.95	738.333	0.094
Alicudi	AL-13-02	Al2-ol19-sp1-4	83.08	1438.88	2074.00	1998.54	123792.42	61.94	125.539	61.70	752.733	0.096
Alicudi	AL-13-02	Al2-ol19-sp1-5	83.08	1447.46	2051.22	2011.71	124218.83	61.75	125.932	61.51	744.715	0.095
Alicudi	AL-13-02	Al2-ol20-sp1-1	87.30	1739.81	1824.56	1567.45	95260.64	60.77	127.950	60.54	473.041	0.060
Alicudi	AL-13-02	Al2-ol20-sp1-2	87.44	1645.46	1835.87	1534.59	95705.95	62.37	124.684	62.12	470.130	0.060
Alicudi	AL-13-02	Al2-ol20-sp1-3	88.38	1824.87	1935.25	1446.31	88457.52	61.16	127.141	60.92	453.605	0.058
Alicudi	AL-13-02	Al2-ol20-sp1-4	87.64	1850.61	1886.26	1515.71	92341.78	60.92	127.637	60.69	474.287	0.060
Alicudi	AL-13-02	Al2-ol20-sp1-5	88.36	1883.49	1928.52	1460.22	88395.78	60.54	128.453	60.30	452.922	0.058
Alicudi	AL-13-03	Al3-ol21-sp1-1	89.92	1872.05	1655.69	1393.03	76350.21	54.81	141.876	54.60	330.800	0.042
Alicudi	AL-13-03	Al3-ol21-sp1-2	90.00	1866.33	1653.49	1386.72	75747.17	54.62	142.358	54.41	327.426	0.042
Alicudi	AL-13-03	Al3-ol21-sp1-3	89.82	1926.38	1644.94	1411.62	76961.97	54.52	142.627	54.31	332.299	0.042
Alicudi	AL-13-03	Al3-ol21-sp1-4	89.51	1918.51	1628.44	1426.38	79322.26	55.61	139.829	55.40	340.291	0.043
Alicudi	AL-13-03	Al3-ol21-sp1-5	89.84	1919.94	1650.06	1393.54	77046.24	55.29	140.645	55.07	332.788	0.042
Filicudi	FL-13-03B	fl03b-ol30-sp1-1	80.95	1339.53	495.98	2317.26	138147.74	59.62	130.434	59.39	208.011	0.026
Filicudi	FL-13-03B	fl03b-ol30-sp1-2	81.02	1363.83	507.86	2305.71	137639.19	59.69	130.263	59.46	212.071	0.027
Filicudi	FL-13-03B	fl03b-ol30-sp1-3	81.16	1374.55	514.97	2308.16	137582.43	59.61	130.455	59.38	213.124	0.027
Filicudi	FL-13-03B	fl03b-ol30-sp1-4	81.09	1368.83	509.39	2307.50	137527.22	59.60	130.470	59.37	211.668	0.027
Filicudi	FL-13-03B	fl03b-ol30-sp1-5	81.03	1361.69	502.22	2312.28	137900.47	59.64	130.387	59.41	209.637	0.027
Filicudi	FL-13-03B	fl03b-ol30-sp2-1	80.95	1383.85	491.03	2311.18	138428.46	59.90	129.828	59.66	205.994	0.026
Filicudi	FL-13-03B	fl03b-ol30-sp2-2	80.99	1354.54	491.77	2333.07	138740.28	59.47	130.763	59.24	205.774	0.026
Filicudi	FL-13-03B	fl03b-ol30-sp2-3	81.11	1355.25	493.31	2321.52	138454.12	59.64	130.384	59.41	204.758	0.026
Filicudi	FL-13-03B	fl03b-ol30-sp2-4	80.95	1389.56	496.42	2315.41	138098.76	59.64	130.376	59.41	208.288	0.027
Filicudi	FL-13-03B	fl03b-ol30-sp2-5	81.01	1363.83	507.47	2299.96	137695.96	59.87	129.885	59.64	211.979	0.027
Filicudi	FL-13-03B	fl03b-ol30-sp3-1	81.03	1383.13	501.07	2307.86	138709.18	60.10	129.379	59.87	209.138	0.027
Filicudi	FL-13-03B	fl03b-ol30-sp3-2	81.16	1371.69	504.98	2308.75	138070.76	59.80	130.027	59.57	208.981	0.027
Filicudi	FL-13-03B	fl03b-ol30-sp3-3	81.26	1388.85	493.83	2308.09	137943.23	59.77	130.110	59.53	202.985	0.026
Filicudi	FL-13-03B	fl03b-ol30-sp3-4	81.15	1402.43	497.74	2309.76	137442.46	59.51	130.679	59.27	206.148	0.026
Filicudi	FL-13-03B	fl03b-ol30-sp3-5	81.01	1383.13	501.65	2319.99	137726.28	59.37	130.987	59.14	209.605	0.027
Filicudi	FL-13-03B	fl03b-ol31-sp1-1	86.56	1579.70	808.96	1750.47	101853.03	58.19	133.641	57.96	223.812	0.028

Filicudi	FL-13-03B	fl03b-ol31-sp1-2	86.40	1588.99	796.20	1780.92	101679.63	57.09	136.197	56.87	223.318	0.028
Filicudi	FL-13-03B	fl03b-ol31-sp1-3	86.43	1587.56	804.04	1781.01	101440.90	56.96	136.525	56.74	225.009	0.029
Filicudi	FL-13-03B	fl03b-ol31-sp1-4	86.37	1592.57	803.95	1770.20	101216.95	57.18	135.996	56.96	226.184	0.029
Filicudi	FL-13-03B	fl03b-ol31-sp1-5	86.16	1611.87	821.29	1767.17	101488.34	57.43	135.401	57.21	235.052	0.030
Filicudi	FL-13-03B	fl03b-ol32-sp1-1	85.43	1548.25	606.59	1901.16	109066.10	57.37	135.547	57.15	184.341	0.023
Filicudi	FL-13-03B	fl03b-ol32-sp1-2	85.41	1525.38	622.36	1922.28	109561.43	57.00	136.432	56.77	189.429	0.024
Filicudi	FL-13-03B	fl03b-ol32-sp1-3	85.28	1564.69	620.71	1941.84	109092.53	56.18	138.413	55.96	190.907	0.024
Filicudi	FL-13-03B	fl03b-ol32-sp1-4	85.08	1522.52	611.94	1955.17	109940.90	56.23	138.288	56.01	191.304	0.024
Filicudi	FL-13-03B	fl03b-ol32-sp1-5	85.21	1510.36	584.96	1928.79	109326.59	56.68	137.189	56.46	180.966	0.023
Filicudi	FL-13-03B	fl03b-ol32-sp2-1	85.25	1538.96	618.14	1932.78	109445.57	56.63	137.323	56.41	190.642	0.024
Filicudi	FL-13-03B	fl03b-ol32-sp2-2	85.28	1571.84	647.35	1918.86	109000.00	56.80	136.891	56.58	199.120	0.025
Filicudi	FL-13-03B	fl03b-ol32-sp2-3	85.25	1604.72	642.54	1926.74	108938.57	56.54	137.531	56.32	198.154	0.025
Filicudi	FL-13-03B	fl03b-ol32-sp2-4	85.22	1570.41	636.93	1943.19	109545.10	56.37	137.937	56.16	196.903	0.025
Filicudi	FL-13-03B	fl03b-ol32-sp2-5	85.11	1563.97	613.13	1955.75	109706.07	56.09	138.625	55.88	191.121	0.024
Salina	SL-13-05	sl5-ol3-sp1-1	86.16	1413.87	1596.48	1740.86	101633.75	58.38	133.194	58.16	456.978	0.058
Salina	SL-13-05	sl5-ol3-sp1-2	87.49	1416.73	1614.67	1577.97	93366.25	59.17	131.422	58.94	411.398	0.052
Salina	SL-13-05	sl5-ol3-sp1-3	87.27	1413.87	1582.34	1576.18	94878.69	60.20	129.180	59.96	411.439	0.052
Salina	SL-13-05	sl5-ol3-sp1-4	85.61	1380.99	1547.64	1777.64	105358.48	59.27	131.200	59.04	463.673	0.059
Salina	SL-13-05	sl5-ol4-sp1-1	78.18	1355.25	1003.62	2816.94	157961.12	56.08	138.671	55.86	499.273	0.064
Salina	SL-13-05	sl5-ol4-sp1-2	83.74	1310.22	1389.78	1981.11	120239.50	60.69	128.121	60.46	481.015	0.061
Salina	SL-13-05	sl5-ol4-sp1-3	84.73	1315.23	1505.90	1903.47	113608.86	59.69	130.285	59.45	483.913	0.062
Salina	SL-13-05	sl5-ol4-sp1-4	81.00	1376.70	1246.92	2426.66	139286.94	57.40	135.475	57.18	521.381	0.066
Salina	SL-13-05	sl5-ol5-sp1-1	81.34	1329.52	1186.93	2321.64	136417.57	58.76	132.338	58.53	485.188	0.062
Salina	SL-13-05	sl5-ol5-sp1-2	81.74	1305.93	1288.83	2266.64	133753.50	59.01	131.776	58.78	513.089	0.065
Salina	SL-13-05	sl5-ol5-sp1-3	81.49	1328.09	1227.26	2321.77	135470.45	58.35	133.270	58.12	496.797	0.063
Salina	SL-13-05	sl5-ol5-sp1-4	81.28	1343.82	1168.85	2347.21	136814.93	58.29	133.406	58.06	479.788	0.061
Salina	SL-13-05	sl5-ol6-sp1-1	80.23	1303.79	1281.03	2502.24	145139.19	58.00	134.061	57.78	562.786	0.072
Salina	SL-13-05	sl5-ol6-sp1-2	81.40	1307.36	1358.46	2309.85	136802.49	59.23	131.295	59.00	553.426	0.070
Salina	SL-13-05	sl5-ol6-sp1-3	83.09	1306.65	1433.52	2073.81	125225.51	60.38	128.776	60.15	520.145	0.066
Salina	SL-13-05	sl5-ol6-sp1-4	82.13	1310.94	1393.28	2214.77	132311.04	59.74	130.164	59.51	540.462	0.069
Salina	SL-13-05	sl5-ol7-sp1-1	77.93	1303.07	1254.30	2733.35	155694.40	56.96	136.515	56.74	633.010	0.081

Salina	SL-13-05	sl5-ol7-sp1-2	77.97	1319.51	1248.80	2726.72	155193.62	56.92	136.624	56.70	628.769	0.080
Salina	SL-13-05	sl5-ol7-sp1-3	77.83	1342.39	1166.68	2810.58	157672.63	56.10	138.611	55.88	592.249	0.075
Salina	SL-13-05	sl5-ol7-sp1-4	78.19	1312.37	1199.09	2752.47	156108.86	56.72	137.105	56.50	596.031	0.076
Salina	SL-13-05	sl5-ol8-sp1-1	75.17	1685.49	869.72	2943.92	172575.43	58.62	132.650	58.39	512.043	0.065
Salina	SL-13-05	sl5-ol8-sp1-2	75.03	1583.27	851.57	2944.29	173398.13	58.89	132.037	58.67	505.080	0.064
Salina	SL-13-05	sl5-ol8-sp1-3	75.27	1636.88	872.92	2934.51	172496.11	58.78	132.287	58.55	511.337	0.065
Salina	SL-13-05	sl5-ol8-sp1-4	76.00	1624.73	835.81	2895.90	170181.18	58.77	132.322	58.54	470.376	0.060
Salina	SL-13-05	sl5-ol8-sp2-1	75.65	1531.09	799.50	2903.78	171339.04	59.01	131.785	58.78	458.641	0.058
Salina	SL-13-05	sl5-ol8-sp2-2	75.61	1550.39	804.27	2930.09	171209.18	58.43	133.080	58.21	462.459	0.059
Salina	SL-13-05	sl5-ol8-sp2-3	75.18	1642.60	832.73	2959.52	173645.41	58.67	132.531	58.45	490.089	0.062
Salina	SL-13-05	sl5-ol9-sp1-1	77.37	1295.93	1257.85	2644.09	157104.20	59.42	130.872	59.19	655.771	0.083
Salina	SL-13-05	sl5-ol9-sp1-2	78.03	1270.19	1258.68	2599.46	155555.99	59.84	129.944	59.61	631.743	0.080
Salina	SL-13-05	sl5-ol9-sp1-3	78.56	1269.48	1266.61	2583.68	154335.93	59.73	130.176	59.50	616.303	0.078
Salina	SL-13-05	sl5-ol9-sp1-4	78.51	1280.20	1274.55	2581.16	153870.92	59.61	130.442	59.38	622.009	0.079
Salina	SL-13-05	sl5-ol10-sp1-1	80.59	1246.60	1129.98	2404.03	140014.00	58.24	133.514	58.02	485.147	0.062
Salina	SL-13-05	sl5-ol10-sp1-2	81.46	1225.88	1156.88	2300.19	135450.23	58.89	132.051	58.66	469.185	0.060
Salina	SL-13-05	sl5-ol10-sp1-3	81.68	1278.06	1171.13	2251.71	133671.07	59.36	130.989	59.13	468.297	0.060
Salina	SL-13-05	sl5-ol10-sp1-4	81.32	1288.06	1134.02	2315.45	136043.55	58.75	132.348	58.53	464.376	0.059
Salina	SL-13-05	sl5-ol11-sp1-1	74.34	1250.89	692.28	3233.30	178367.03	55.17	140.958	54.95	425.967	0.054
Salina	SL-13-05	sl5-ol11-sp1-2	75.31	1213.01	701.79	3121.64	173531.88	55.59	139.882	55.37	410.108	0.052
Salina	SL-13-05	sl5-ol11-sp1-3	74.77	1231.59	711.29	3189.21	176531.88	55.35	140.481	55.14	427.856	0.054
Salina	SL-13-05	sl5-ol11-sp1-4	73.41	1280.91	693.92	3284.04	182406.69	55.54	140.000	55.33	447.936	0.057
Salina	SL-13-05	sl5-ol12-sp1-1	72.56	1380.99	1029.84	3295.49	185310.26	56.23	138.287	56.01	694.206	0.088
Salina	SL-13-05	sl5-ol12-sp1-2	72.80	1340.24	979.29	3333.43	186208.40	55.86	139.204	55.64	652.139	0.083
Salina	SL-13-05	sl5-ol12-sp1-3	73.23	1376.70	1007.77	3210.12	182190.51	56.76	137.011	56.54	656.554	0.084
Salina	SL-13-05	sl5-ol12-sp1-4	73.80	1366.69	1082.89	3136.68	179557.54	57.24	135.839	57.02	685.137	0.087
Salina	SL-13-05	sl5-ol12-sp2-1	68.93	1481.06	867.91	3715.92	203327.37	54.72	142.112	54.51	697.427	0.089
Salina	SL-13-05	sl5-ol12-sp2-4	72.10	1360.97	823.71	3595.22	193325.04	53.77	144.609	53.56	568.202	0.072
Salina	SL-13-05	sl5-ol13-sp1-1	80.19	1357.40	1348.65	2423.12	142793.93	58.93	131.954	58.70	593.860	0.076
Salina	SL-13-05	sl5-ol13-sp1-2	79.33	1349.54	1342.36	2504.70	147704.51	58.97	131.862	58.74	623.260	0.079
Salina	SL-13-05	sl5-ol13-sp1-3	79.23	1352.39	1332.12	2547.34	149024.11	58.50	132.920	58.28	622.381	0.079
Salina	SL-13-05	sl5-ol13-sp1-4	79.64	1366.69	1320.30	2502.79	146081.65	58.37	133.226	58.14	601.722	0.077

Salina	SL-13-05	sl5-ol14-sp1-1	75.07	1684.77	777.97	2943.20	174390.36	59.25	131.237	59.02	460.496	0.059
Salina	SL-13-05	sl5-ol14-sp1-2	74.59	1682.63	778.78	2964.00	174954.90	59.03	131.738	58.80	472.777	0.060
Salina	SL-13-05	sl5-ol14-sp1-3	75.57	1657.61	820.71	2884.41	171027.22	59.29	131.145	59.06	472.811	0.060
Salina	SL-13-05	sl5-ol14-sp1-4	75.14	1690.49	856.31	2900.55	173557.54	59.84	129.956	59.60	504.924	0.064
Salina	SL-13-05	sl5-ol14-sp2-1	74.27	1683.35	779.63	2939.25	175358.48	59.66	130.337	59.43	481.353	0.061
Salina	SL-13-05	sl5-ol14-sp2-2	74.42	1726.23	791.52	2960.06	175166.41	59.18	131.404	58.95	484.919	0.062
Salina	SL-13-05	sl5-ol14-sp2-3	74.59	1681.20	797.86	2964.51	175181.18	59.09	131.591	58.86	484.384	0.062
Salina	SL-13-05	sl5-ol14-sp2-4	74.23	1691.21	785.23	2986.09	176740.28	59.19	131.379	58.96	485.830	0.062
Salina	SL-13-05	sl5-ol15-sp1-1	75.65	1303.79	1352.47	3093.49	173474.34	56.08	138.667	55.86	776.073	0.099
Salina	SL-13-05	sl5-ol15-sp1-2	73.61	1358.11	1180.08	3306.33	182954.90	55.33	140.528	55.12	754.272	0.096
Salina	SL-13-05	sl5-ol15-sp1-3	74.02	1345.25	1203.05	3255.56	180582.43	55.47	140.187	55.25	752.668	0.096
Salina	SL-13-05	sl5-ol15-sp1-4	75.42	1313.80	1392.13	3080.40	173307.15	56.26	138.213	56.04	808.761	0.103
Salina	SL-13-08	sl8-ol22-sp1-1	76.66	1593.28	718.12	2950.34	168523.13	57.12	136.136	56.90	389.702	0.050
Salina	SL-13-08	sl8-ol22-sp1-2	76.32	1604.72	734.68	2958.00	169320.01	57.24	135.846	57.02	406.355	0.052
Salina	SL-13-08	sl8-ol22-sp1-3	76.28	1596.85	768.71	2961.75	169544.11	57.24	135.839	57.02	426.014	0.054
Salina	SL-13-08	sl8-ol22-sp1-4	76.49	1508.22	707.45	2981.88	170004.37	57.01	136.392	56.79	387.473	0.049
Salina	SL-13-08	sl8-ol22-sp1-5	76.21	1591.85	757.35	2997.33	169944.81	56.70	137.147	56.48	421.369	0.054
Salina	SL-13-08	sl8-ol22-sp2-1	75.95	1632.59	709.60	3043.98	171414.38	56.31	138.087	56.09	400.408	0.051
Salina	SL-13-08	sl8-ol22-sp2-2	75.79	1654.75	708.69	3036.81	172080.46	56.66	137.229	56.45	403.521	0.051
Salina	SL-13-08	sl8-ol22-sp2-3	75.58	1612.58	676.84	3025.74	172100.44	56.88	136.713	56.66	389.793	0.050
Salina	SL-13-08	sl8-ol22-sp2-4	75.64	1582.56	673.56	3034.17	172722.92	56.93	136.599	56.71	386.578	0.049
Salina	SL-13-08	sl8-ol22-sp2-5	75.88	1574.70	684.55	3008.29	171924.50	57.15	136.063	56.93	387.876	0.049
Salina	SL-13-08	sl8-ol23-sp1-1	80.48	1000.71	1304.64	2480.27	141199.55	56.93	136.592	56.71	564.047	0.072
Salina	SL-13-08	sl8-ol23-sp1-2	80.54	679.06	1315.53	2463.78	140788.61	57.14	136.080	56.92	566.667	0.072
Salina	SL-13-08	sl8-ol23-sp1-3	80.65	884.20	1330.38	2388.81	139429.79	58.37	133.225	58.14	569.011	0.072
Salina	SL-13-08	sl8-ol23-sp1-4	80.85	1208.01	1320.65	2363.74	138974.37	58.79	132.259	58.57	557.612	0.071
Salina	SL-13-08	sl8-ol23-sp1-5	80.62	1347.39	1295.08	2407.28	140237.78	58.26	133.482	58.03	555.012	0.071
Salina	SL-13-08	sl8-ol23-sp2-1	80.56	1187.99	1278.23	2468.75	141218.27	57.20	135.939	56.98	549.677	0.070
Salina	SL-13-08	sl8-ol23-sp2-2	80.60	1375.98	1277.23	2447.58	140525.87	57.41	135.438	57.19	548.112	0.070
Salina	SL-13-08	sl8-ol23-sp2-3	80.27	1445.32	1254.05	2495.00	143185.60	57.39	135.497	57.17	549.551	0.070
Salina	SL-13-08	sl8-ol23-sp2-4	80.17	634.02	1233.25	2591.53	145623.26	56.19	138.383	55.97	543.789	0.069
Salina	SL-13-08	sl8-ol23-sp2-5	80.37	862.76	1271.86	2486.96	141799.24	57.02	136.381	56.80	553.842	0.071

Salina	SL-13-08	sl8-ol24-sp1-1	83.87	1286.63	1199.60	1991.19	119116.79	59.82	129.986	59.59	411.125	0.052
Salina	SL-13-08	sl8-ol24-sp1-2	83.87	1294.50	1185.94	2016.81	119308.74	59.16	131.447	58.93	406.495	0.052
Salina	SL-13-08	sl8-ol24-sp1-3	83.85	1282.34	1177.04	2018.26	119549.82	59.23	131.277	59.00	404.235	0.051
Salina	SL-13-08	sl8-ol24-sp1-4	83.82	1283.77	1191.10	2001.80	119580.40	59.74	130.173	59.51	409.880	0.052
Salina	SL-13-08	sl8-ol24-sp1-5	83.76	1295.93	1191.70	1994.69	119188.39	59.75	130.137	59.52	411.923	0.052
Salina	SL-13-08	sl8-ol25-sp1-1	84.25	1377.41	1753.24	2026.54	115831.93	57.16	136.046	56.94	584.326	0.074
Salina	SL-13-08	sl8-ol25-sp1-2	83.87	1333.10	1742.67	2073.96	118253.06	57.02	136.379	56.80	597.244	0.076
Salina	SL-13-08	sl8-ol25-sp1-3	84.35	1335.95	1783.52	2010.75	114834.06	57.11	136.159	56.89	589.885	0.075
Salina	SL-13-08	sl8-ol25-sp1-4	84.79	1371.69	1824.35	1936.65	112052.75	57.86	134.396	57.64	583.227	0.074
Salina	SL-13-08	sl8-ol25-sp1-5	84.93	1350.96	1826.43	1920.97	111505.37	58.05	133.963	57.82	577.787	0.074
Stromboli CA	ST-13-09	st9_ol1-sp1-1	90.67	1264.47	2185.48	1265.71	71493.78	56.48	137.666	56.27	401.072	0.051
Stromboli CA	ST-13-09	st9_ol1-sp1-2	90.58	1264.47	2183.95	1270.23	72000.00	56.68	137.186	56.46	404.986	0.052
Stromboli CA	ST-13-09	st9_ol1-sp1-3	90.48	1272.34	2315.82	1270.84	71905.91	56.58	137.431	56.36	434.492	0.055
Stromboli CA	ST-13-09	st9_ol1-sp1-4	90.77	1251.61	2271.67	1248.72	70765.94	56.67	137.215	56.45	411.833	0.052
Stromboli CA	ST-13-09	st9_ol1-sp2-1	75.72	1554.68	994.64	3022.17	166863.92	55.21	140.836	55.00	568.627	0.072
Stromboli CA	ST-13-09	st9_ol1-sp2-2	79.98	1378.13	1326.22	2501.94	140851.48	56.30	138.126	56.08	591.791	0.075
Stromboli CA	ST-13-09	st9_ol1-sp2-3	86.43	1248.75	2066.75	1777.56	99965.79	56.24	138.272	56.02	578.511	0.074
Stromboli CA	ST-13-09	st9_ol1-sp2-4	86.27	1254.47	1967.33	1751.48	101153.97	57.75	134.643	57.53	558.110	0.071
Stromboli CA	ST-13-09	st9_ol1-sp3-1	90.46	1383.13	2377.11	1271.56	71433.90	56.18	138.418	55.96	447.091	0.057
Stromboli CA	ST-13-09	st9_ol1-sp3-2	88.76	1548.96	2603.76	1382.48	78995.33	57.14	136.087	56.92	587.982	0.075
Stromboli CA	ST-13-09	st9_ol1-sp3-3	88.09	1377.41	2563.55	1429.22	85220.84	59.63	130.411	59.40	618.012	0.079
Stromboli CA	ST-13-09	st9_ol1-sp3-4	90.34	1358.83	2406.50	1275.72	72456.45	56.80	136.910	56.58	458.901	0.058
Stromboli CA	ST-13-09	st9_ol2-sp1-1	85.87	868.48	1262.16	1713.03	106618.97	62.24	124.936	62.00	370.260	0.047
Stromboli CA	ST-13-09	st9_ol2-sp1-2	82.66	1343.82	1372.70	2140.40	125087.09	58.44	133.058	58.21	513.233	0.065
Stromboli CA	ST-13-09	st9_ol2-sp1-3	85.83	1430.31	1514.03	1660.08	104055.99	62.68	124.057	62.44	445.704	0.057
Stromboli CA	ST-13-17	st17-ol26-sp1-1	85.76	1326.66	1523.17	1887.68	104305.06	55.26	140.729	55.04	450.694	0.057
Stromboli CA	ST-13-17	st17-ol26-sp1-2	84.99	1241.60	1454.83	1993.80	110251.87	55.30	140.623	55.08	458.026	0.058
Stromboli CA	ST-13-17	st17-ol26-sp1-3	84.08	1157.26	1374.71	2089.85	117167.14	56.06	138.698	55.85	463.880	0.059
Stromboli CA	ST-13-17	st17-ol26-sp1-4	86.10	1346.68	1554.60	1841.21	102104.34	55.46	140.223	55.24	447.187	0.057
Stromboli CA	ST-13-17	st17-ol26-sp1-5	85.40	1284.49	1477.61	1936.48	107510.01	55.52	140.063	55.30	450.182	0.057
Stromboli CA	ST-13-17	st17-ol27-sp1-1	84.99	1340.96	2135.90	1903.95	110107.10	57.83	134.462	57.61	672.371	0.086

Stromboli CA	ST-13-17	st17-ol27-sp1-2	87.31	1429.59	2157.11	1628.97	94208.75	57.83	134.456	57.61	558.980	0.071
Stromboli CA	ST-13-17	st17-ol27-sp1-3	88.77	1504.65	2102.12	1476.37	83632.97	56.65	137.271	56.43	473.963	0.060
Stromboli CA	ST-13-17	st17-ol27-sp1-4	88.10	1503.93	2109.98	1549.19	88193.23	56.93	136.593	56.71	507.784	0.065
Stromboli CA	ST-13-17	st17-ol27-sp1-5	86.41	1375.98	2142.97	1733.54	99836.91	57.59	135.021	57.37	600.541	0.076
Stromboli CA	ST-13-17	st17-ol28-sp1-1	82.92	1267.33	1823.25	2149.50	123286.05	57.36	135.576	57.13	669.384	0.085
Stromboli CA	ST-13-17	st17-ol28-sp1-2	83.78	1357.40	1863.82	2051.53	117594.09	57.32	135.660	57.10	643.258	0.082
Stromboli CA	ST-13-17	st17-ol28-sp1-3	84.79	1426.02	1831.94	1954.53	111814.93	57.21	135.926	56.99	585.669	0.075
Stromboli CA	ST-13-17	st17-ol28-sp1-4	83.86	1331.67	1742.87	2069.60	119094.87	57.54	135.130	57.32	597.713	0.076
Stromboli CA	ST-13-17	st17-ol28-sp1-5	82.16	1237.31	1809.50	2201.78	128041.99	58.15	133.715	57.93	700.167	0.089
Stromboli CA	ST-13-17	st17-ol29-sp1-1	90.17	1850.61	1571.91	1356.56	73997.67	54.55	142.554	54.34	305.342	0.039
Stromboli CA	ST-13-17	st17-ol29-sp1-2	90.41	1744.82	1652.84	1322.44	72125.19	54.54	142.577	54.33	312.444	0.040
Stromboli CA	ST-13-17	st17-ol29-sp1-3	90.45	1738.38	1672.61	1329.50	72154.74	54.27	143.279	54.06	314.756	0.040
Stromboli CA	ST-13-17	st17-ol29-sp1-4	90.27	1726.95	1647.10	1340.44	73536.55	54.86	141.744	54.65	316.294	0.040
Stromboli CA	ST-13-17	st17-ol29-sp1-5	90.08	1826.30	1596.19	1350.61	74811.04	55.39	140.386	55.18	313.188	0.040
Stromboli CA	ST-13-17	st17-ol29-sp2-1	90.44	1596.14	1658.84	1314.15	71521.77	54.42	142.878	54.21	312.666	0.040
Stromboli CA	ST-13-17	st17-ol29-sp2-2	90.49	1592.57	1654.78	1313.44	71313.37	54.30	143.218	54.08	310.128	0.039
Stromboli CA	ST-13-17	st17-ol29-sp2-3	90.54	1643.32	1646.75	1312.73	71087.87	54.15	143.595	53.94	306.825	0.039
Stromboli CA	ST-13-17	st17-ol29-sp2-4	90.47	1596.14	1660.15	1315.90	71643.08	54.44	142.826	54.23	311.670	0.040
Stromboli CA	ST-13-17	st17-ol29-sp2-5	90.47	1591.14	1664.83	1310.53	71594.09	54.63	142.340	54.42	312.587	0.040
Stromboli CA	ST-13-17	st17-ol29-sp3-1	89.67	1573.98	1643.30	1379.77	76705.29	55.59	139.875	55.38	337.274	0.043
Stromboli CA	ST-13-17	st17-ol29-sp3-2	89.39	1567.55	1632.90	1396.17	78983.67	56.57	137.454	56.35	345.565	0.044
Stromboli CA	ST-13-17	st17-ol29-sp3-3	89.48	1581.13	1625.66	1405.56	78426.91	55.80	139.362	55.58	340.717	0.043
Stromboli CA	ST-13-17	st17-ol29-sp3-4	89.70	1576.84	1635.89	1375.31	76742.61	55.80	139.355	55.58	334.912	0.043
Stromboli CA	ST-13-17	st17-ol29-sp3-5	89.78	1573.27	1643.74	1372.27	76326.59	55.62	139.805	55.41	333.402	0.042
Stromboli CA	ST-13-17	st17-ol29-sp3-6	89.71	1573.27	1649.12	1363.85	76635.30	56.19	138.388	55.97	337.295	0.043

Olivine transect core-rim (ppm)

Island	Sample	Olivine	Fo	Ca	Ni	Mn	Fe	Fe/Mn	Mn/FeO	FeO/MnO	Ni*FeO/MgO	NiO*FeO/MgO
Alicudi	AL-13-02	Al2_ol1-6 core	92.21	703.03	3234.73	867.64	59755.35	68.87	112.907	68.60	486.975	0.062
Alicudi	AL-13-02	Al2_ol1-5	90.94	722.90	3191.73	1051.23	69265.82	65.89	118.016	65.63	566.607	0.072
Alicudi	AL-13-02	Al2_ol1-4	89.27	753.45	3137.78	1274.76	81813.40	64.18	121.161	63.93	672.371	0.086
Alicudi	AL-13-02	Al2_ol1-3	86.65	902.91	2870.26	1637.33	101734.90	62.13	125.148	61.89	788.218	0.100
Alicudi	AL-13-02	Al2_ol38-1 rim	86.66	1329.15	1896.49	1668.09	98302.81	58.93	131.951	58.70	520.437	0.066
Alicudi	AL-13-02	Al2_ol38-2	87.98	1322.61	1959.88	1522.13	90511.90	59.46	130.769	59.23	477.294	0.061
Alicudi	AL-13-02	Al2_ol38-3	90.51	1340.97	2032.66	1230.36	72264.92	58.73	132.393	58.51	379.834	0.048
Alicudi	AL-13-02	Al2_ol38-4	91.89	1146.75	1971.65	1107.48	62308.76	56.26	138.212	56.04	310.096	0.039
Alicudi	AL-13-02	Al2_ol38-5 core	91.53	1224.83	2003.74	1114.31	65105.93	58.43	133.090	58.20	330.441	0.042
Alicudi	AL-13-02	Al2_ol43-5 core	92.07	1094.62	1900.87	1114.71	61257.70	54.95	141.501	54.74	291.708	0.037
Alicudi	AL-13-02	Al2_ol43-4	92.10	1204.25	1949.38	1103.10	61098.51	55.39	140.393	55.17	298.218	0.038
Alicudi	AL-13-02	Al2_ol43-3	91.65	1323.11	2039.36	1146.84	64392.41	56.15	138.493	55.93	331.079	0.042
Alicudi	AL-13-02	Al2_ol43-2	90.74	1360.74	2083.18	1232.08	71367.17	57.92	134.245	57.70	379.005	0.048
Alicudi	AL-13-02	Al2_ol43-1 rim	90.31	1374.85	2087.11	1282.71	74888.91	58.38	133.190	58.16	399.267	0.051
Alicudi	AL-13-02	Al2-ol16-sp1-1 bis (rim)	83.15	1035.05	2224.13	2087.14	126067.17	60.40	128.739	60.17	803.334	0.102
Alicudi	AL-13-02	Al2-ol16-sp1-2 bis	87.87	740.97	2990.83	1389.54	92227.17	66.37	117.158	66.12	735.999	0.094
Alicudi	AL-13-02	Al2-ol16-sp1-3 bis	90.38	758.69	3087.86	1039.20	73501.02	70.73	109.942	70.45	586.005	0.075
Alicudi	AL-13-02	Al2-ol16-sp1-4 bis (core)	90.72	998.44	3072.24	961.56	70010.85	72.81	106.800	72.53	559.859	0.071
Alicudi	AL-13-02	Al2-ol16-sp1-5 bis	89.46	752.85	2954.13	1114.32	80246.72	72.01	107.979	71.74	620.243	0.079
Alicudi	AL-13-02	Al2-ol18-sp1-1 bis (rim)	91.97	1039.51	1866.69	1130.37	61916.76	54.78	141.961	54.56	290.438	0.037
Alicudi	AL-13-02	Al2-ol18-sp1-2 bis	91.96	1018.78	1873.74	1114.16	61603.94	55.29	140.637	55.08	291.939	0.037
Alicudi	AL-13-02	Al2-ol18-sp1-3 bis	92.02	1065.63	1898.79	1101.03	61345.69	55.72	139.564	55.50	293.694	0.037
Alicudi	AL-13-02	Al2-ol18-sp1-4 bis	91.95	1179.33	1986.43	1107.86	61733.12	55.72	139.549	55.51	309.969	0.039
Alicudi	AL-13-02	Al2-ol18-sp1-5 bis (core)	92.00	1177.79	1980.97	1101.65	61587.16	55.90	139.095	55.69	306.918	0.039

Chapter 4.
Conclusion

4.1 Summary

The Aeolian Arc exhibits strong along-arc geochemical variations. Based on the systematics of B, Be, Li, and As contents in the Aeolian lavas, this study infers that fluids from the subducting altered oceanic lithosphere influence the whole arc. We confirmed the presence of a slab melt component at the edges of the Aeolian Arc, especially evident in the potassic lavas in Stromboli, that display some of the highest Be contents reported in arc global lavas.

Our new isotopic data (Sr-, Nd-, Pb-, and Hf-isotopes) agree with past studies pointing out a possible mixing of intraplate and depleted mantle source composition. Our results overlap perfectly the literature data showing the increasing metasomatism toward east and the effect of Ionian sediment on Stromboli rocks isotopic composition in agreement with the Be budgets.

My research proposes that the melt component is represented by a partial melt of sediments transported by the subducting Ionian slab. Hot asthenosphere inflow around the edges of the subducting Ionian Plate and/or parallel to the trench could potentially explain the presence of this component. This process explains why the Aeolian Arc shares clear geochemical similarities to hot subduction zones like the Cascades and the Mexican Volcanic Belt, rather than the expected cold conditions from numerical models.

Peccerillo (2001) also proposed a common mantle source for Stromboli, Vesuvius and the Phlegrean Fields based on compositional analogies. The high precision olivine data described in this study confirm some similarities between Stromboli and Vesuvius source corresponding to a

peridotite source. Only few olivines from Alicudi might look alike olivines from a pyroxenite source, but their lower Ni content exclude this possibility.

Future studies should focus on the Palinuro and Lamentini seamounts because of their location between Vesuvius and Stromboli. This makes them key to clarifying the possible connection between Vesuvius and the other volcanoes of the Campanian volcanic province and the Aeolian Arc eastern sector.

4.2 Future work

Data presented in this report are subject of several papers, submitted and in preparation. In particular, one paper is in review at G-cubed with the title "Sediment melt signatures at the edges of the Aeolian Arc: Implications for hot vs. cold subduction zone numerical models". One manuscript related to the magma sources defined by the high precision olivine chemistry is in preparation and will be submitted to an international scientific journal with recognized impact factor. A third paper will possibly focus on the modeling of the Italian volcanism (starting from the Aeolian Island region) and will include the new Ionian sediment compositions (with B and Be) and the new isotope data (Sr, Nd, Hf and Pb). For a better understanding of the subducting components, we also plan to expand this PhD research with the collection of B isotopes in olivine-hosted melt inclusion in order to make a comparison between mineral and bulk data.

REFERENCES

Avanzinelli R, Elliott T, Tommasini S, Conticelli S (2008) Constraints on the genesis of potassium-rich Italian volcanic rocks from U/Th disequilibrium. Journal of Petrology 49(2):195-223 doi:10.1093/petrology/egm076

Avanzinelli R, Prytulak J, Skora S, Heumann A, Koetsier G, Elliott T (2012) Combined 238U–230Th and 235U–231Pa constraints on the transport of slab-derived material beneath the Mariana Islands. Geochimica et Cosmochimica Acta 92:308-328 doi:10.1016/j.gca.2012.06.020

Baccheschi P, Margheriti L, Steckler MS (2008) SKS splitting in Southern Italy: Anisotropy variations in a fragmented subduction zone. Tectonophysics 462(1-4):49-67 doi:10.1016/j.tecto.2007.10.014

Baccheschi P, Margheriti L, Steckler MS, Boschi E (2011) Anisotropy patterns in the subducting lithosphere and in the mantle wedge: A case study—The southern Italy subduction system. Journal of Geophysical Research 116(B8) doi:10.1029/2010jb007961

Barberi F, Gandino A, Gioncada A, La Torre P, Sbrana A, Zenucchini C (1994) The deep structure of the Eolian arc (Filicudi-Panarea-Vulcano sector) in light of gravity, magnetic and volcanological data. Journal of Volcanology and Geothermal Research 61(3–4):189-206 doi:http://dx.doi.org/10.1016/0377-0273(94)90003-5

Barberi F, Innocenti F, Ferrara G, Keller J, Villari L (1974) Evolution of Eolian arc volcanism (southern Tyrrhenian Sea). . Earth and Planetary Science Letters 21(3):269-276

Barca D, Trua T (2012) Magma emplacement at anomalous spreading ridge: Constraints due to plagioclase crystals from basalts of Marsili seamount (Southern Tyrrhenian back-arc). Journal of Volcanology and Geothermal Research 241-242:61-77 doi:10.1016/j.jvolgeores.2012.06.021

Barker AK, Holm PM, Troll VR (2014) The role of eclogite in the mantle heterogeneity at Cape Verde. Contributions to Mineralogy and Petrology 168(3):1-15 doi:10.1007/s00410-014-1052-0

Barry TL, Pearce JA, Leat PT, Millar IL, le Roex AP (2006) Hf isotope evidence for selective mobility of high-field-strength elements in a subduction setting: South Sandwich Islands. Earth and Planetary Science Letters 252(3-4):223-244 doi:10.1016/j.epsl.2006.09.034

Batanova VG, Sobolev AV, Kuzmin DV (2015) Trace element analysis of olivine: High precision analytical method for JEOL JXA-8230 electron probe microanalyser. Chemical Geology 419:149-157 doi:10.1016/j.chemgeo.2015.10.042

Bebout GE (2007) Metamorphic chemical geodynamics of subduction zones. Earth and Planetary Science Letters 260(3-4):373-393 doi:10.1016/j.epsl.2007.05.050

Bebout GE, Ryan JG, Leeman WP, Bebout AE (1999) Fractionation of trace elements by subduction-zone metamorphism—effect of convergent-margin thermal evolution. Earth and Planetary Science Letters 171(1):63-81

Beccaluva L, Bonatti E, Dupuy C, Ferrara G, Innocenti F, Lucchini F, Macera P, Petrini R, Rossi PL, Serri G, Seyler M, Siena F (1990) Geochemistry and mineralogy of volcanic rocks from ODP sites 650, 651, 655 and 654 in the Tyrrhenian Sea. Proc ODP, Scientific Results 107:49-74

Beccaluva L, Gabbianelli G, Lucchini F, Rossi PL, Savelli C (1985) Petrology and K/Ar ages of volcanics dredged from the Eolian seamounts: implications for geodynamic evolution of the southern Tyrrhenian basin. Earth and Planetary Science Letters 74(2):187-208

Beccaluva L, Rossi PL, Serri G (1982) Neogene to Recent volcanism of the southern Tyrrhenian-Sicilian area: Implications for the geodynamic evolution of the Calabrian arc. Earth Evol Sci 3:222-238

Benton LD, Ryan JG, Tera F (2001) Boron isotope systematics of slab fluids as inferred from a serpentine seamount, Mariana forearc. Earth and Planetary Science Letters 187(3–4):273-282 doi:http://dx.doi.org/10.1016/S0012-821X(01)00286-2

Billi A, Barberi G, Faccenna C, Neri G, Pepe F, Sulli A (2006) Tectonics and seismicity of the Tindari Fault System, southern Italy: Crustal deformations at the transition between ongoing contractional and extensional domains located above the edge of a subducting slab. Tectonics 25(2):n/a-n/a doi:10.1029/2004tc001763

Billi A, Faccenna C, Bellier O, Minelli L, Neri G, Piromallo C, Presti D, Scrocca D, Serpelloni E (2011) Recent tectonic reorganization of the Nubia-Eurasia convergent boundary heading for the closure of the western Mediterranean. Bulletin de la Societe Geologique de France 182(4):279-303 doi:10.2113/gssgfbull.182.4.279

Bonelli R, Frezzotti ML, Zanon V, Peccerillo A (2004) Evolution of the volcanic plumbing systemof Alicudi (Aeolian Islands - Italy): evidence from fluid and melt inclusionsin quartz xenoliths.

Bortoluzzi G, Ligi M, Romagnoli C, Cocchi L, Casalbore D, Sgroi T, Cuffaro M, Tontini FC, D'Oriano F, Ferrante V, Remia A, Riminucci F (2010) Interactions between volcanism and tectonics in the western Aeolian sector, southern Tyrrhenian Sea. Geophysical Journal International 183(1):64-78 doi:10.1111/j.1365-246X.2010.04729.x

Brenan JM, Ryerson FJ, Shaw HF (1998) The role of aqueous fluids in the slab-to-mantle transfer of boron, beryllium, and lithium during subduction: experiments and models. Geochimica et Cosmochimica Acta 62(19):3337-3347

Brenan JM, Shaw HF, Ryerson FJ (1995) Experimental evidence for the origin of lead enrichment in convergent-margin magmas. Nature 378:54–56

Buttles J, Olson P (1998) A laboratory model of subduction zone anisotropy. Earth and Planetary Science Letters 164(1):245-262

Calanchi N, Peccerillo A, Tranne CA, Lucchini F, Rossi PL, Kempton P, Barbieri M, Wu TW (2002) Petrology and geochemistry of volcanic rocks from the island of Panarea: Implications for mantle evolution beneath the Aeolian island arc (southern Tyrrhenian Sea). Journal of Volcanology and Geothermal Research 115(3):367-395

Calanchi N, Romagnoli C, Rossi PL (1995) Morphostructural features and some petrochemical data from the submerged area around Alicudi and Filicudi volcanic islands (Aeolian Arc, southern Tyrrhenian Sea). Marine Geology 123(3–4):215-238 doi:http://dx.doi.org/10.1016/0025-3227(95)00002-G

Calanchi N, Tranne C, Lucchini F, Rossi P (1999a) Geological map of the Island of Panarea and Basiluzzo, Aeolian island, 1: 10000 scale. GNV, Siena

Calanchi N, Tranne CA, Lucchini F, Rossi PL, Villa IM (1999b) Explanatory notes to the geological map (1: 10,000) of Panarea and Basiluzzo islands (Aeolian arc. Italy). Acta Vulcanologica 11(2):223-244 %@ 1121-9114

Capaldi G, Civetta L, Gillot P (1985) Geochronology of Plio-Pleistocene volcanic rocks from southern Italy. Rend Soc Ital Mineral Petrol 40:25-44

Carminati E, Lustrino M, Cuffaro M, Doglioni C (2010) Tectonics, magmatism and geodynamics of Italy: What we know and what we imagine. Journal of the Virtual Explorer 36 doi:10.3809/jvirtex.2010.00226

Carminati E, Lustrino M, Doglioni C (2012) Geodynamic evolution of the central and western Mediterranean: Tectonics vs. igneous petrology constraints. Tectonophysics 579:173-192 doi:10.1016/j.tecto.2012.01.026

Chauvel C, Blichert-Toft J (2001) A hafnium isotope and trace element perspective on melting of the depleted mantle. Earth and Planetary Science Letters 190(3–4):137-151 doi:http://dx.doi.org/10.1016/S0012-821X(01)00379-X

Chauvel C, Bureau S, Poggi C (2011) Comprehensive Chemical and Isotopic Analyses of Basalt and Sediment Reference Materials. Geostandards and Geoanalytical Research 35(1):125-143 doi:10.1111/j.1751-908X.2010.00086.x

Chen Z, Schellart WP, Duarte JC (2015) Overriding plate deformation and variability of fore-arc deformation during subduction: Insight from geodynamic models and application to the Calabria subduction zone. Geochemistry, Geophysics, Geosystems:n/a-n/a doi:10.1002/2015gc005958

Chiarabba C, De Gori P, Speranza F (2008) The southern Tyrrhenian subduction zone: Deep geometry, magmatism and Plio-Pleistocene evolution. Earth and Planetary Science Letters 268(3-4):408-423 doi:10.1016/j.epsl.2008.01.036

Class C, Miller DM, Goldstein SL, Langmuir CH (2000) Distinguishing melt and fluid subduction components in Umnak Volcanics, Aleutian Arc. Geochemistry, Geophysics, Geosystems 1(6):n/a-n/a doi:10.1029/1999gc000010

Corazzato C, Francalanci L, Menna M, Petrone CM, Renzulli A, Tibaldi A, Vezzoli L (2008) What controls sheet intrusion in volcanoes? Structure and petrology of the Stromboli sheet complex, Italy. Journal of Volcanology and Geothermal Research 173(1-2):26-54 doi:10.1016/j.jvolgeores.2008.01.006

Crisci GM, Rosa R, Esperança S, Mazzuoli R, Sonnino M (1991) Temporal evolution of a three component system: the island of Lipari (Aeolian Arc, southern Italy). Bulletin of Volcanology 53(3):207-221 doi:10.1007/bf00301231

Dallai L, Cioni R, Boschi C, D'Oriano C (2011) Carbonate-derived CO2 purging magma at depth: Influence on the eruptive activity of Somma-Vesuvius, Italy. Earth and Planetary Science Letters 310(1-2):84-95 doi:10.1016/j.epsl.2011.07.013

Davì M, De Rosa R, Donato P, Vetere F, Barca D, Cavallo A (2009) Magmatic Evolution and plumbing system of ring-fault volcanism: the Vulcanello Peninsula (Aeolian Islands, Italy). European Journal of Mineralogy 21(5):1009-1028 doi:10.1127/0935-1221/2009/0021-1955

Davì M, De Rosa R, Holtz F (2010) Mafic enclaves in the rhyolitic products of Lipari historical eruptions; relationships with the coeval Vulcano magmas (Aeolian Islands, Italy). Bulletin of Volcanology 72(8):991-1008 doi:10.1007/s00445-010-0376-5

Davis FA, Humayun M, Hirschmann MM, Cooper RS (2013) Experimentally determined mineral/melt partitioning of first-row transition elements (FRTE) during partial melting of peridotite at 3GPa. Geochimica et Cosmochimica Acta 104:232-260 doi:10.1016/j.gca.2012.11.009

De Astis G, Dellino P, La Volpe L, Lucchi F, Tranne C (2006a) Geological map of the island of Vulcano (Aeolian Islands). University of Bari, University of Bologna, and INGV

De Astis G, Dellino P, La Volpe L, Lucchi F, Tranne C (2013a) Geological map of the island of Vulcano, scale 1: 10,000 (Aeolian archipelago). The Aeolian Islands volcanoes Geological Society, London, Memoirs 37 doi:10.1144/m37

De Astis G, Kempton PD, Peccerillo A, Wu TW (2006b) Trace element and isotopic variations from Mt. Vulture to Campanian volcanoes: constraints for slab detachment and mantle inflow beneath southern Italy. Contributions to Mineralogy and Petrology 151(3):331-351 doi:10.1007/s00410-006-0062-y

De Astis G, La Volpe L, Peccerillo A, Civetta L (1997) Volcanological and petrological evolution of Vulcano Island (Aeolian Arc, southern Tyrrhenian Sea). Journal of Geophysical Research: Solid Earth (1978–2012) 102(B4):8021–8050

De Astis G, Lucchi F, Dellino P, La Volpe L, Tranne CA, Frezzotti ML, Peccerillo A (2013b) Geology, volcanic history and petrology of Vulcano (central Aeolian archipelago). Geological Society, London, Memoirs 37(1):281-349 doi:10.1144/m37

De Astis G, Peccerillo A, Kempton PD, La Volpe L, Wu TW (2000) Transition from calc-alkaline to potassium-rich magmatism in subduction environments: geochemical and Sr, Nd, Pb isotopic constraints from the island of Vulcano (Aeolian arc). Contributions to Mineralogy and Petrology 139(6):684-703

De Astis G, Ventura G, Vilardo G (2003) Geodynamic significance of the Aeolian volcanism (Southern Tyrrhenian Sea, Italy) in light of structural, seismological, and geochemical data. Tectonics 22(4):n/a-n/a doi:10.1029/2003tc001506

De Hoog JCM, Gall L, Cornell DH (2010) Trace-element geochemistry of mantle olivine and application to mantle petrogenesis and geothermobarometry. Chemical Geology 270(1-4):196-215 doi:10.1016/j.chemgeo.2009.11.017

De Rosa R, Guillou H, Mazzuoli R, Ventura G (2003) New unspiked K–Ar ages of volcanic rocks of the central and western sector of the Aeolian Islands: reconstruction of the volcanic stages. Journal of Volcanology and Geothermal Research 120(3):161-178

Di Roberto A, Rosi M, Bertagnini A, Marani MP, Gamberi F, Del Principe A (2008) Deep water gravity core from the Marsili Basin (Tyrrhenian Sea) records Pleistocenic–Holocenic explosive events and instability of the Aeolian Archipelago, (Italy). Journal of Volcanology and Geothermal Research 177(1):133-144 doi:10.1016/j.jvolgeores.2008.01.009

Doglioni C, Merlini S, Cantarella G (1999) Foredeep geometries at the front of the Apennines in the Ionian Sea (central Mediterranean). Earth and Planetary Science Letters 168(3–4):243-254 doi:http://dx.doi.org/10.1016/S0012-821X(99)00059-X

Doherty AL, Cannatelli C, Raia F, Belkin HE, Albanese S, Lima A, De Vivo B (2015) Geochemistry of selected lavas of the Panarea volcanic group, Aeolian Arc, Italy. Mineralogy and Petrology 109(5):597-610 doi:10.1007/s00710-015-0385-3

Eiler JM, Carr MJ, Reagan M, Stolper E (2005) Oxygen isotope constraints on the sources of Central American arc lavas. Geochemistry, Geophysics, Geosystems 6(7):n/a-n/a doi:10.1029/2004gc000804

Ellam RM (1986) The transition of calc-alkaline to potassic volcanism in the Aeolian Islands, southern Italy. Open University

Ellam RM, Harmon RS (1990) Oxygen isotope constraints on the crustal contribution to the subduction-related magmatism of the Aeolian Islands, southern Italy. Journal of Volcanology and Geothermal Research 44(1):05-122

Ellam RM, Hawkesworth CJ, Menzies MA, Rogers NW (1989) The volcanism of southern Italy: Role of subduction and the relationship between potassic and sodic alkaline magmatism. Journal of Geophysical Research 94(B4):4589 doi:10.1029/JB094iB04p04589

Ellam RM, Menzies MA, Hawkesworth CJ, Leeman WP, Rosi M, Serri G (1988) The transition from calc-alkaline to potassic orogenic magmatism in the Aeolian Islands, Southern Italy. Bulletin of Volcanology 50(6):386-398

Elliott T (2003) Tracers of the slab. Inside the Subduction Factory 138:23-45 doi:10.1029/138gm03

Elliott T, Plank T, Zindler A, White W, Bourdon B (1997) Element transport from slab to volcanic front at the Mariana arc. Journal of Geophysical Research 102(B7):14991 doi:10.1029/97jb00788

Faccenna C, Molin P, Orecchio B, Olivetti V, Bellier O, Funiciello F, Minelli L, Piromallo C, Billi A (2011) Topography of the Calabria subduction zone (southern Italy): Clues for the origin of Mt. Etna. Tectonics 30(1):n/a-n/a doi:10.1029/2010tc002694

Falsaperla S, Lanzafame G, Longo V, Spampinato S (1999) Regional stress field in the area of Stromboli (Italy): insights into structural data and crustal tectonic earthquakes. Journal of Volcanology and Geothermal Research 88(3):147-166

Feig ST, Koepke J, Snow JE (2006) Effect of water on tholeiitic basalt phase equilibria: an experimental study under oxidizing conditions. Contributions to Mineralogy and Petrology 152(5):611-638 doi:10.1007/s00410-006-0123-2

Ferrari L (2004) Slab detachment control on mafic volcanic pulse and mantle heterogeneity in central Mexico. Geology 32(1):77 doi:10.1130/g19887.1

Ferrari L, Orozco-Esquivel T, Manea V, Manea M (2012) The dynamic history of the Trans-Mexican Volcanic Belt and the Mexico subduction zone. Tectonophysics 522-523:122-149 doi:10.1016/j.tecto.2011.09.018

Foley SF, Prelevic D, Rehfeldt T, Jacob DE (2013) Minor and trace elements in olivines as probes into early igneous and mantle melting processes. Earth and Planetary Science Letters 363:181-191 doi:http://dx.doi.org/10.1016/j.epsl.2012.11.025

Forni F, Ellis BS, Bachmann O, Lucchi F, Tranne CA, Agostini S, Dallai L (2015) Erupted cumulate fragments in rhyolites from Lipari (Aeolian Islands). Contributions to Mineralogy and Petrology 170(5-6) doi:10.1007/s00410-015-1201-0

Forni F, Lucchi F, Peccerillo A, Tranne CA, Rossi PL, Frezzotti ML (2013) Stratigraphy and geological evolution of the Lipari volcanic complex (central Aeolian archipelago). Geological Society, London, Memoirs 37(1):213-279 doi:10.1144/m37.10

Francalanci L, Avanzinelli R, Nardini I, Tiepolo M, Davidson JP, Vannucci R (2012) Crystal recycling in the steady-state system of the active Stromboli volcano: a 2.5-ka story inferred from in situ Sr-isotope and trace element data. Contributions to Mineralogy and Petrology 163(1):109-131 doi:10.1007/s00410-011-0661-0

Francalanci L, Avanzinelli R, Tommasini S, Heuman A (2007) A west-east geochemical and isotopic traverse along the volcanism of the Aeolian Island arc, southern Tyrrhenian Sea, Italy: Inferences on mantle source processes. Geological Society of America Special Papers 418:235-263 doi:10.1130/2007.2418(12)

Francalanci L, Bertagnini A, Métrich N, Renzulli A, Vannucci R, Landi P, Del Moro S, Menna M, Petrone CM, Nardini I (2008) Mineralogical, geochemical, and isotopic characteristics of the ejecta from the 5 April 2003 paroxysm at Stromboli, Italy: Inferences on the preeruptive magma dynamics. The Stromboli Volcano: An Integrated Study of the 2002-2003 Eruption:331-345

Francalanci L, Lucchi F, Keller J, De Astis G, Tranne CA (2013) Eruptive, volcano-tectonic and magmatic history of the Stromboli volcano (north-eastern Aeolian archipelago). Geological Society, London, Memoirs 37(1):397-471 doi:10.1144/m37.13

Francalanci L, Manetti P, Peccerillo A (1989) Volcanological and magmatological evolution of Stromboli volcano (Aeolian Islands): the roles of fractional crystallization, magma mixing, crustal contamination and source heterogeneity. Bulletin of Volcanology 51(5):355-378

Francalanci L, Santo AP (1993) Magmatological evolution of Filicudi volcanoes, Aeolian Islands, Italy: constraints from mineralogical, geochemical and isotopic data. Acta Vulcanologica 3:203-227

Francalanci L, Taylor SR, McCulloch MT, Woodhead JD (1993) Geochemical and isotopic variations in the calc-alkaline rocks of Aeolian arc, southern Tyrrhenian Sea, Italy: constraints on magma genesis. Contributions to Mineralogy and Petrology 113(3):300-313

Francalanci L, Tommasini S, Conticelli S (2004) The volcanic activity of Stromboli in the 1906–1998 AD period: mineralogical, geochemical and isotope data relevant to the understanding of the plumbing system. Journal of Volcanology and Geothermal Research 131(1-2):179-211 doi:10.1016/s0377-0273(03)00362-7

Francalanci L, Tommasini S, Conticelli S, Davies GR (1999) Sr isotope evidence for short magma residence time for the 20th century activity at Stromboli volcano, Italy. Earth and Planetary Science Letters 167(1):61-69

Frezzotti ML (2004) Silica-rich Melts in Quartz Xenoliths from Vulcano Island and their Bearing on Processes of Crustal Anatexis and Crust-Magma Interaction beneath the Aeolian Arc, Southern Italy. Journal of Petrology 45(1):3-26 doi:10.1093/petrology/egg080

Frezzotti ML, Peccerillo A, Bonelli R (2003) Magma ascent rates and depths of crustal magma reservoirs beneath the Aeolian volcanic Arc (Italy): Inferences from fluid and melt inclusions in xenoliths. In: Benedetto De V, Robert JB (eds) Developments in Volcanology, vol Volume 5. Elsevier, pp 185-205

Gabbianelli G, Gillot PY, Lanzafame G, Romagnoli C, Rossi PL (1990) Tectonic and volcanic evolution of Panarea (Aeolian Islands, Italy). Marine Geology 92(3–4):313-326 doi:http://dx.doi.org/10.1016/0025-3227(90)90011-8

Gabbianelli G, Romagnoli C, Rossi P, Calanchi N (1993) Marine geology of the Panarea-Stromboli area (Aeolian Archipelago, Southeastern Tyrrhenian sea). Acta Vulcanol 3:11-20

Gabbianelli G, Romagnoli C, Rossi P, Calanchi N, Lucchini F (1991) Submarine morphology and tectonics of Vulcano (Aeolian Islands, Southeastern Tyrrhenian Sea). Acta Vulcanol 1:135-141

Gale A, Dalton CA, Langmuir CH, Su Y, Schilling J-G (2013) The mean composition of ocean ridge basalts. Geochemistry, Geophysics, Geosystems 14(3):489-518 doi:10.1029/2012gc004334

Gamberi F, Marani M, Landuzzi V, Magagnoli A, Penitenti D, Rosi M, Bertagnini A, Di Roberto A (2006) Sedimentologic and volcanologic investigation of the deep tyrrhenian sea: preliminary result of cruise VST02. Annals of geophysic 49(2/3):767–781

Gamberi F, Marani M, Savelli C (1997) Tectonic, volcanic and hydrothermal features of a submarine portion of the Aeolian arc (Tyrrhenian Sea). Marine Geology 140(1):167-181

Gazel E, Carr MJ, Hoernle K, Feigenson MD, Szymanski D, Hauff F, van den Bogaard P (2009) Galapagos-OIB signature in southern Central America: Mantle refertilization by arc-hot spot interaction. Geochemistry, Geophysics, Geosystems 10(2):n/a-n/a doi:10.1029/2008gc002246

Gazel E, Hayes JL, Hoernle K, Kelemen P, Everson E, Holbrook WS, Hauff F, van den Bogaard P, Vance EA, Chu S, Calvert AJ, Carr MJ, Yogodzinski GM (2015) Continental crust generated in oceanic arcs. Nature Geoscience 8(4):321-327 doi:10.1038/ngeo2392

Gazel E, Hoernle K, Carr MJ, Herzberg C, Saginor I, den Bogaard Pv, Hauff F, Feigenson M, Swisher C (2011) Plume–subduction interaction in southern Central America: Mantle upwelling and slab melting. Lithos 121(1-4):117-134 doi:10.1016/j.lithos.2010.10.008

Gertisser R, Keller J (2000) From basalt to dacite: origin and evolution of the calc-alkaline series of Salina, Aeolian Arc, Italy. Contributions to Mineralogy and Petrology 139(5):607-626

Gillot P (1987) Histoire volcanique des Iles Eoliennes: arc insulaire ou complexe orogénique anulaire. Doc Trav IGAL 11:35-42

Gillot P, Keller J (1993) Radiochronological dating of Stromboli. Acta Vulcanol 3:69-77

Gillot P, Villari L (1980) K/Ar geochronological data on the Aeolian arc volcanism: a preliminary report. IIV Catania (CNR) Open File Report 3(80):145

Gioncada A, Clocchiatti R, Sbrana A, Bottazzi P, Massare D, Ottolini L (1998) A study of melt inclusions at Vulcano (Aeolian Islands, Italy): insights on the primitive magmas and on the volcanic feeding system. Bulletin of Volcanology 60(4):286-306 doi:10.1007/s004450050233

Gioncada A, Mazzuoli R, Bisson M, Pareschi MT (2003) Petrology of volcanic products younger than 42 ka on the Lipari–Vulcano complex (Aeolian Islands, Italy): an example of volcanism controlled by tectonics. Journal of Volcanology and Geothermal Research 122(3-4):191-220 doi:10.1016/s0377-0273(02)00502-4

Grove TL, Till CB, Krawczynski MJ (2012) The Role of H2O in Subduction Zone Magmatism. Annual Review of Earth and Planetary Sciences 40(1):413-439 doi:10.1146/annurev-earth-042711-105310

Gutscher M-A, Dominguez S, de Lepinay BM, Pinheiro L, Gallais F, Babonneau N, Cattaneo A, Le Faou Y, Barreca G, Micallef A, Rovere M (2016) Tectonic expression of an active slab tear from high-resolution seismic and bathymetric data offshore Sicily (Ionian Sea). Tectonics 35(1):39-54 doi:10.1002/2015tc003898

Gvirtzman Z, Nur A (1999) The formation of Mount Etna as the consequence of slab rollback. Nature 401(6755):782-785

Gvirtzman Z, Nur A (2001) Residual topography, lithospheric structure, and sunken slabs in the central Mediterranean. Earth and Planetary Science Letters 187(1):117-130

Hacker BR, Kelemen PB, Behn MD (2011) Differentiation of the continental crust by relamination. Earth and Planetary Science Letters 307(3-4):501-516 doi:10.1016/j.epsl.2011.05.024

Hattori KH, Arai S, Clarke DB (2002) Selenium, Tellurium, Arsenic and Antimony contents of primary mantle sulfides. The Canadian Mineralogist 40(2):637-650 doi:10.2113/gscanmin.40.2.637

Hattori KH, Guillot S (2007) Geochemical character of serpentinites associated with high- to ultrahigh-pressure metamorphic rocks in the Alps, Cuba, and the Himalayas: Recycling of elements in subduction zones. Geochemistry, Geophysics, Geosystems 8(9):n/a-n/a doi:10.1029/2007gc001594

Hawkesworth C, Turner S, Peate D, McDermott F, Van Calsteren P (1997) Elemental U and Th variations in island arc rocks: implications for U-series isotopes. Chemical Geology 139(1):207-221

Hermann J (2002) Allanite: thorium and light rare earth element carrier in subducted crust. Chemical Geology 192(3–4):289-306 doi:http://dx.doi.org/10.1016/S0009-2541(02)00222-X

Hermann J, Rubatto D (2009) Accessory phase control on the trace element signature of sediment melts in subduction zones. Chemical Geology 265(3-4):512-526 doi:10.1016/j.chemgeo.2009.05.018

Hermann J, Spandler C, Hack A, Korsakov AV (2006) Aqueous fluids and hydrous melts in high-pressure and ultra-high pressure rocks: Implications for element transfer in subduction zones. Lithos 92(3–4):399-417 doi:http://dx.doi.org/10.1016/j.lithos.2006.03.055

Herzberg C (2006) Petrology and thermal structure of the Hawaiian plume from Mauna Kea volcano. Nature 444(7119):605-609 doi:10.1038/nature05254

Herzberg C (2011) Identification of Source Lithology in the Hawaiian and Canary Islands: Implications for Origins. Journal of Petrology 52(1):113-146 doi:10.1093/petrology/egq075

Herzberg C, Asimow PD, Ionov DA, Vidito C, Jackson MG, Geist D (2013) Nickel and helium evidence for melt above the core-mantle boundary. Nature 493(7432):393-397 doi:10.1038/nature11771

Hofmann AW (1997) Mantle geochemistry: the message from oceanic volcanism. Nature 385(6613):219-229

Honnorez J, Keller J (1968) Xenolithe in vulkanischen Gesteinen der Äolischen Inseln (Sizilien). Geologische Rundschau 57(3):719-736

Hornig-Kjarsgaard I, Keller J, Koberski U, Stadlbauer E, Francalanci L, Lenhart R (1993) Geology, stratigraphy and volcanological evolution of the island of Stromboli, Aeolian arc, Italy. Acta Vulcanol 3:21-68

Ishikawa T, Nakamura E (1994) Origin of the slab component in arc lavas from across-arc variation of B and Pb isotopes. Nature 370(6486):205-208

Ishikawa T, Tera F (1997) Source, composition and distribution of the fluid in the Kurile mantle wedge: Constraints from across-arc variations of B/Nb and B isotopes. Earth and Planetary Science Letters 152(1–4):123-138 doi:http://dx.doi.org/10.1016/S0012-821X(97)00144-1

Ishikawa T, Tera F (1999) Two isotopically distinct fluid components involved in the Mariana Arc: Evidence from Nb/B ratios and B, Sr, Nd, and Pb isotope systematics. Geology 27(1):83-86

Jarosewich E, Nelen JA, Norberg JA (1980) Reference Samples for Electron Microprobe Analysis*. Geostandards Newsletter 4(1):43-47 doi:10.1111/j.1751-908X.1980.tb00273.x

Jochum KP, Wilson SA, Abouchami W, Amini M, Chmeleff J, Eisenhauer A, Hegner E, Iaccheri LM, Kieffer B, Krause J, McDonough WF, Mertz-Kraus R, Raczek I, Rudnick RL, Scholz D, Steinhoefel G, Stoll B, Stracke A, Tonarini S, Weis D, Weis U, Woodhead JD (2011) GSD-1G and MPI-DING Reference Glasses for In Situ and Bulk Isotopic Determination. Geostandards and Geoanalytical Research 35(2):193-226 doi:10.1111/j.1751-908X.2010.00114.x

Johnson MC, Plank T (1999) Dehydration and melting experiments constrain the fate of subducted sediments. Geochemistry, Geophysics, Geosystems 1(12):n/a-n/a doi:10.1029/1999gc000014

Jolis EM, Freda C, Troll VR, Deegan FM, Blythe LS, McLeod CL, Davidson JP (2013) Experimental simulation of magma–carbonate interaction beneath Mt. Vesuvius, Italy. Contributions to Mineralogy and Petrology 166(5):1335-1353 doi:10.1007/s00410-013-0931-0

Kastens KA, Mascle J (1990) The geological evolution of the Tyrrhenian Sea: an introduction to the scientific results of ODP Leg 107. Proceedings of the Ocean Drilling Program, Scientific Results 107:3-26

Kawamoto T, Kanzaki M, Mibe K, Matsukage KN, Ono S (2012) Separation of supercritical slab-fluids to form aqueous fluid and melt components in subduction zone magmatism. Proceedings of the National Academy of Sciences 109(46):18695-18700 doi:10.1073/pnas.1207687109

Kelemen PB, Yogodzinski GM, Scholl DW (2003) Along-strike variation in the Aleutian island arc: Genesis of high Mg# andesite and implications for continental crust. Inside the Subduction Factory, Geophys Monogr Ser 138:223-276

Keller J (1974) Petrology of some volcanic rock series of the Aeolian Arc, southern Tyrrhenian Sea: Calc-alkaline and shoshonitic associations. Contributions to Mineralogy and Petrology 46(1):29-47

Keller J (1980a) The island of Salina. Rend Soc It Miner Petrol 36:489-524

Keller J (1980b) The island of Vulcano. Rend Soc Ital Mineral Petrol 36(1):369-414

Keller J, Hornig-Kjarsgaard I, Koberski U, Stadlbauer E, Lenhart R (1993) Geological map of the island of Stromboli—scale 1: 10,000. Acta Vulcanologica 3

Kelley KA, Plank T, Ludden J, Staudigel H (2003) Composition of altered oceanic crust at ODP Sites 801 and 1149. Geochemistry, Geophysics, Geosystems 4(6):n/a-n/a doi:10.1029/2002gc000435

Kessel R, Schmidt MW, Ulmer P, Pettke T (2005) Trace element signature of subduction-zone fluids, melts and supercritical liquids at 120-180 km depth. Nature 437(7059):724-727 doi:10.1038/nature03971

Kimura JI, Stern RJ (2008) Neogene volcanism of the Japan island arc: The Kh relationship revisited. Circum‐Pacific Tectonics, Geologic Evolution, and Ore Deposits, Ariz Geol Soc Dig 22:187-202

Klimm K, Blundy JD, Green TH (2008) Trace element partitioning and accessory phase saturation during H2O-saturated melting of basalt with implications for subduction zone chemical fluxes. Journal of Petrology 49(3):523-553 doi:10.1093/petrology/egn001

Krienitz MS, Garbe-Schonberg CD, Romer RL, Meixner A, Haase KM, Stroncik NA (2012) Lithium isotope variations in Ocean Island Basalts—Implications for the development of mantle heterogeneity. Journal of Petrology 53(11):2333-2347 doi:10.1093/petrology/egs052

Kundu B, Gahalaut VK (2011) Slab detachment of subducted Indo-Australian plate beneath Sunda arc, Indonesia. Journal of earth system science 120(2):193-204

Landi P, Corsaro RA, Francalanci L, Civetta L, Miraglia L, Pompilio M, Tesoro R (2009) Magma dynamics during the 2007 Stromboli eruption (Aeolian Islands, Italy): Mineralogical, geochemical and isotopic data. Journal of Volcanology and Geothermal Research 182(3-4):255-268 doi:10.1016/j.jvolgeores.2008.11.010

Landi P, Francalanci L, Pompilio M, Rosi M, Corsaro RA, Petrone CM, Nardini I, Miraglia L (2006) The December 2002–July 2003 effusive event at Stromboli volcano, Italy: Insights into the shallow plumbing system by petrochemical studies. Journal of Volcanology and Geothermal Research 155(3-4):263-284 doi:10.1016/j.jvolgeores.2006.03.032

Le Roux V, Dasgupta R, Lee CTA (2011) Mineralogical heterogeneities in the Earth's mantle: Constraints from Mn, Co, Ni and Zn partitioning during partial melting. Earth and Planetary Science Letters 307(3-4):395-408 doi:10.1016/j.epsl.2011.05.014

Leeman WP (1996) Boron and other fluid-mobile elements in volcanic arc lavas: Implications for subduction processes. 96:269-276 doi:10.1029/GM096p0269

Leeman WP, Sisson VB (1996) Geochemistry of boron and its implications for crustal and mantle processes. Boron: Mineralogy, Petrology and Geochemistry in the Earth's Crust:645-707

Leocat E, Gillot P-Y, Peccerillo A (2009) Temporal evolution of the Western and Central volcanism of the Aeolian Island Arc (Italy, southern Tyrhhenian Sea). In: EGU General Assembly Conference Abstracts, vol 11. p 13106

London D, Evensen JM (2002) Beryllium in silicic magmas and the origin of beryl-bearing pegmatites. Reviews in Mineralogy and Geochemistry 50(1):445-486 doi:10.2138/rmg.2002.50.11

Lucchi F, Gertisser R, Keller J, Forni F, De Astis G, Tranne CA (2013a) Eruptive history and magmatic evolution of the island of Salina (central Aeolian archipelago). Geological Society, London, Memoirs 37(1):155-211 doi:10.1144/m37.6

Lucchi F, Keller J, De Astis G, Francalanci L, Tranne C (2013b) Geological map of Stromboli, scale 1: 10000 (Aeolian archipelago). The Aeolian Islands volcanoes Geological Society, London, Memoirs 37 doi:10.1144/m37.6

Lucchi F, Peccerillo A, Keller J, Tranne CA, Rossi PL (2013c) The Aeolian Islands Volcanoes. In, vol. Geological Society of London,

Lucchi F, Peccerillo A, Tranne CA, Rossi PL, Frezzotti ML, Donati C (2013d) Volcanism, calderas and magmas of the Alicudi composite volcano (western Aeolian archipelago). Geological Society, London, Memoirs 37(1):83-111 doi:10.1144/m37.7

Lucchi F, Santo AP, Tranne CA, Peccerillo A, Keller J (2013e) Volcanism, magmatism, volcano-tectonics and sea-level fluctuations in the geological history of Filicudi (western Aeolian archipelago). Geological Society, London, Memoirs 37(1):113-153 doi:10.1144/m37.8

Lucchi F, Tranne C, Calanchi N, Rossi P (2004) Geological cartography in volcanic areas: the case of Lipari (Aeolian Islands). Mapping Geology in Italy Agenzia per la Protezione dell'Ambiente e per i servizi Tecnici, Dipartimento difesa del suolo, Servizio Geologico d'Italia:138-146

Lucchi F, Tranne C, Forni F, Rossi P (2013f) Geological map of the island of Lipari, scale 1: 10 000 (Aeolian archipelago). The Aeolian Islands Volcanoes Geological Society, London, Memoirs 37 doi:10.1144/m37

Lucchi F, Tranne C, Keller J, Gertisser R, Forni F, De Astis G (2013g) Geological map of the island of Salina, scale 1: 10000 (Aeolian archipelago). The Aeolian Islands Volcanoes Geological Society, London, Memoirs 37 doi:10.1144/m37

Lucchi F, Tranne C, Keller J, Rossi P (2013h) Geological map of the Panarea volcanic group, scale 1: 10,000 (Aeolian archipelago). The Aeolian Islands volcanoes Geological Society, London, Memoirs 37 doi:10.1144/m37

Lucchi F, Tranne C, Peccerillo A, Rossi P (2013i) Geological map of the island of Alicudi, scale 1: 10000 (Aeolian archipelago). The Aeolian Islands Volcanoes Geological Society, London, Memoirs 37 doi:10.1144/m37

Lucchi F, Tranne C, Rossi P (2013j) Geological map of the island of Filicudi, scale 1: 10000 (Aeolian archipelago). The Aeolian Islands Volcanoes Geological Society, London, Memoirs 37 doi:10.1144/m37

Lucchi F, Tranne CA, Peccerillo A, Keller J, Rossi PL (2013k) Geological history of the Panarea volcanic group (eastern Aeolian archipelago). Geological Society, London, Memoirs 37(1):351-395 doi:10.1144/m37.12

Lucchi F, Tranne CA, Rossi PL (2010) Stratigraphic approach to geological mapping of the late Quaternary volcanic island of Lipari (Aeolian archipelago, southern Italy). Geological Society of America Special Papers 464:1-32 doi:10.1130/2010.2464(01)

Lustrino M, Duggen S, Rosenberg CL (2011) The Central-Western Mediterranean: Anomalous igneous activity in an anomalous collisional tectonic setting. Earth-Science Reviews 104(1-3):1-40 doi:10.1016/j.earscirev.2010.08.002

Mallik A, Dasgupta R (2012) Reaction between MORB-eclogite derived melts and fertile peridotite and generation of ocean island basalts. Earth and Planetary Science Letters 329-330:97-108 doi:10.1016/j.epsl.2012.02.007

Mallik A, Dasgupta R (2013) Reactiveinfiltration of MORB-Eclogite-Derived carbonated silicate melt into fertile peridotite at 3 GPa and genesis of alkalic magmas. Journal of Petrology 54(11):2267-2300 doi:10.1093/petrology/egt047

Mallik A, Dasgupta R (2014) Effect of variable CO2on eclogite-derived andesite and lherzolite reaction at 3 GPa-Implications for mantle source characteristics of alkalic ocean island basalts. Geochemistry, Geophysics, Geosystems 15(4):1533-1557 doi:10.1002/2014gc005251

Mallik A, Nelson J, Dasgupta R (2015) Partial melting of fertile peridotite fluxed by hydrous rhyolitic melt at 2–3 GPa: implications for mantle wedge hybridization by sediment melt and generation of ultrapotassic magmas in convergent margins. Contributions to Mineralogy and Petrology 169(5) doi:10.1007/s00410-015-1139-2

Manetti P, Pasquarè G, Tibaldi A, Tsegaye A (1995a) Carta geologica delle isole di Alicudi e Filicudi (Isole Eolie). CNR, Gruppo Nazionale per la Vulcanologia

Manetti P, Pasquarè G, Tibaldi A, Tsegaye A (1995b) Geology, structure and evolution of the island of Alicudi, Aeolian Volcanic Arc, Italy. Acta Vulcanologica 7(1):7-12

Manetti P, Pasquare G, Tsegaye A (1995c) A new geovolcanological map of Filicudi Island (Aeolian Arc, Italy). Acta Vulcanologica 7(1):1-5

Manetti P, Pasquaré G, Tsegaye A (1988) Geology of the island of Filicudi (Aeolian Arc). Bollettino del GNV (National Group of Volcanology) 4:368-382

Mann U, Schmidt MW (2015) Melting of pelitic sediments at subarc depths: 1. Flux vs. fluid-absent melting and a parameterization of melt productivity. Chemical Geology 404:150-167 doi:10.1016/j.chemgeo.2015.02.032

Manning C (2004) The chemistry of subduction-zone fluids. Earth and Planetary Science Letters 223(1-2):1-16 doi:10.1016/j.epsl.2004.04.030

Marani MP, Trua T (2002) Thermal constriction and slab tearing at the origin of a superinflated spreading ridge: Marsili volcano (Tyrrhenian Sea). Journal of Geophysical Research 107(B9) doi:10.1029/2001jb000285

Marschall HR, Korsakov AV, Luvizotto GL, Nasdala L, Ludwig T (2009) On the occurrence and boron isotopic composition of tourmaline in (ultra)high-pressure metamorphic rocks. Journal of the Geological Society 166(4):811-823 doi:10.1144/0016-76492008-042

Marschall HR, Schumacher JC (2012) Arc magmas sourced from mélange diapirs in subduction zones. Nature Geoscience 5(12):862-867 doi:10.1038/ngeo1634

Martin LAJ, Hermann J, Gauthiez-Putallaz L, Whitney DL, Vitale Brovarone A, Fornash KF, Evans NJ (2014) Lawsonite geochemistry and stability - implication for trace element and water cycles in subduction zones. Journal of Metamorphic Geology 32(5):455-478 doi:10.1111/jmg.12093

Martindale M, Skora S, Pickles J, Elliott T, Blundy J, Avanzinelli R (2013) High pressure phase relations of subducted volcaniclastic sediments from the west pacific and their implications for the geochemistry of Mariana arc magmas. Chemical Geology 342:94-109 doi:10.1016/j.chemgeo.2013.01.015

Matzen AK, Baker MB, Beckett JR, Stolper EM (2013) The Temperature and Pressure Dependence of Nickel Partitioning between Olivine and Silicate Melt. Journal of Petrology 54(12):2521-2545 doi:10.1093/petrology/egt055

Mazza SE, Gazel E, Johnson EA, Kunk MJ, McAleer R, Spotila JA, Bizimis M, Coleman DS (2014) Volcanoes of the passive margin: The youngest magmatic event in eastern North America. Geology 42(6):483-486 doi:10.1130/g35407.1

Mazzuoli R, Tortorici L, Ventura G (1995) Oblique rifting in Salina, Lipari and Vulcano islands (Aeolian islands, southern Italy). Terra Nova 7(4):444-452 doi:10.1111/j.1365-3121.1995.tb00540.x

Metrich N, Bertagnini A, Di Muro A (2009) Conditions of Magma Storage, Degassing and Ascent at Stromboli: New Insights into the Volcano Plumbing System with Inferences on the Eruptive Dynamics. Journal of Petrology 51(3):603-626 doi:10.1093/petrology/egp083

Morris JD, Leeman WP, Tera F (1990) The subducted component in island arc lavas: constraints from Be isotopes and B-Be systematics. Nature 344(6261):31-36

Mullen EK, Weis D (2015) Evidence for trench-parallel mantle flow in the northern Cascade Arc from basalt geochemistry. Earth and Planetary Science Letters 414:100-107 doi:10.1016/j.epsl.2015.01.010

Nazzareni S, Molin G, Peccerillo A, Zanazzi P (2001) Volcanological implications of crystal-chemical variations in clinopyroxenes from the Aeolian Arc, Southern Tyrrhenian Sea (Italy). Bulletin of Volcanology 63(1):73-82 doi:10.1007/s004450100125

Neri G (2002) Seismotomography of the crust in the transition zone between the southern Tyrrhenian and Sicilian tectonic domains. Geophysical Research Letters 29(23) doi:10.1029/2002gl015562

Neri G, Marotta AM, Orecchio B, Presti D, Totaro C, Barzaghi R, Borghi A (2012) How lithospheric subduction changes along the Calabrian Arc in southern Italy: geophysical evidences. International Journal of Earth Sciences 101(7):1949-1969 doi:10.1007/s00531-012-0762-7

Noll PD, Newsom HE, Leeman WP, Ryan JG (1996) The role of hydrothermal fluids in the production of subduction zone magmas: evidence from siderophile and chalcophile trace elements and boron. Geochimica et Cosmochimica Acta, 60(4):587-611

Orecchio B, Presti D, Totaro C, D'Amico S, Neri G (2015) Investigating slab edge kinematics through seismological data: The northern boundary of the Ionian subduction system (south Italy). Journal of Geodynamics 88:23-35 doi:10.1016/j.jog.2015.04.003

Panza G, Peccerillo A, Aoudia A, Farina B (2007) Geophysical and petrological modelling of the structure and composition of the crust and upper mantle in complex geodynamic settings: The Tyrrhenian Sea and surroundings. Earth-Science Reviews 80(1-2):1-46 doi:10.1016/j.earscirev.2006.08.004

Panza GF, Aoudia A, Pontevivo A, Chimera G, Raykova R (2003) The lithosphere-asthenosphere: Italy and surroundings. Episodes 26(169–174)

Panza GF, Pontevivo A, Saraò A, Aoudia A, Peccerillo A (2004) Structure of the lithosphere–asthenosphere and volcanism in the Tyrrhenian Sea and surroundings. Memorie Descrittive Carta Geologica d'Italia 64:29-56

Peccerillo A (2001) Geochemical similarities between the Vesuvius, Phlegraean Fields and Stromboli Volcanoes: petrogenetic, geodynamic and volcanological implications. Mineralogy and Petrology 73(1-3):93-105

Peccerillo A (2005) Plio-quaternary volcanism in Italy. Springer-Verlag Berlin Heidelberg

Peccerillo A, Dallai L, Frezzotti ML, Kempton PD (2004) Sr–Nd–Pb–O isotopic evidence for decreasing crustal contamination with ongoing magma evolution at Alicudi volcano (Aeolian arc, Italy): implications for style of magma-crust interaction and for mantle source compositions. Lithos 78(1-2):217-233 doi:10.1016/j.lithos.2004.04.040

Peccerillo A, De Astis G, Faraone D, Forni F, Frezzotti ML (2013) Compositional variations of magmas in the Aeolian arc: implications for petrogenesis and geodynamics. Geological Society, London, Memoirs 37(1):491-510 doi:10.1144/m37.15

Peccerillo A, Frezzotti ML (2015) Magmatism, mantle evolution and geodynamics at the converging plate margins of Italy. Journal of the Geological Society 172(4):407-427 doi:10.1144/jgs2014-085

Peccerillo A, Frezzotti ML, De Astis G, Ventura G (2006) Modeling the magma plumbing system of Vulcano (Aeolian Islands, Italy) by integrated fluid-inclusion geobarometry, petrology, and geophysics. Geology 34(1):17-20 doi:10.1130/g22117.1

Peccerillo A, Kempton PD, Harmon RS, Wu TW, Santo AP, Boyce AJ, Tripodo A (1993) Petrological and geochemical characteristics of the Alicudi volcano, Aeolian Islands, Italy: Implications for magma genesis and evolution. Acta Vulcanologica 3:235 - 249

Peccerillo A, Taylor SR (1976) Geochemistry of Eocene calc-alkaline volcanic rocks from the Kastamonu area, northern Turkey. Contributions to mineralogy and petrology 58(1):63-81

Peccerillo A, Wu TW (1992) Evolution of calc-alkaline magmas in continental arc volcanoes: evidence from Alicudi, Aeolian arc (southern Tyrrhenian Sea, Italy). Journal of Petrology 33(6):1295-1315

Pertermann M, Hirschmann MM (2002) Trace-element partitioning between vacancy-rich eclogitic clinopyroxene and silicate melt. American Mineralogist 87(10):1365-1376 doi:10.2138/am-2002-1012

Petrone CM, Braschi E, Francalanci L (2009) Understanding the collapse–eruption link at Stromboli, Italy: a microanalytical study on the products of the recent Secche di Lazzaro phreatomagmatic activity. Journal of Volcanology and Geothermal Research 188(4):315-332

Pirard C, Hermann J (2014) Experimentally determined stability of alkali amphibole in metasomatised dunite at sub-arc pressures. Contributions to Mineralogy and Petrology 169(1) doi:10.1007/s00410-014-1095-2

Piromallo C, Morelli A (2003) Pwave tomography of the mantle under the Alpine-Mediterranean area. Journal of Geophysical Research 108(B2) doi:10.1029/2002jb001757

Plank T (2014) The chemical composition of subducting sediments. Treatise of Geochemistry, 2nd ed:607-629 doi:10.1016/b978-0-08-095975-7.00319-3

Plank T, Kelley KA, Zimmer MM, Hauri EH, Wallace PJ (2013) Why do mafic arc magmas contain ~4wt% water on average? Earth and Planetary Science Letters 364:168-179 doi:10.1016/j.epsl.2012.11.044

Plank T, Langmuir CH (1993) Tracing trace elements from sediment input to volcanic output at subduction zones. Nature 362(6422):739-743

Plank T, Langmuir CH (1998) The chemical composition of subducting sediment and its consequences for the crust and mantle. Chemical Geology 145(3):325-394

Pontevivo A, Panza GF (2006) The Lithosphere-Asthenosphere System in the Calabrian Arc and Surrounding Seas – Southern Italy. Pure and Applied Geophysics 163(8):1617-1659 doi:10.1007/s00024-006-0093-3

Prelević D, Jacob DE, Foley SF (2013) Recycling plus: A new recipe for the formation of Alpine–Himalayan orogenic mantle lithosphere. Earth and Planetary Science Letters 362:187-197 doi:10.1016/j.epsl.2012.11.035

Putirka K, Ryerson FJ, Perfit M, Ridley WI (2011) Mineralogy and Composition of the Oceanic Mantle. Journal of Petrology 52(2):279-313 doi:10.1093/petrology/egq080

Redi D (2014) Pyroxene and olivine chemistry as an indicator of melt evolution. A contribution to the understanding of Somma-Vesuvius eruptive behaviour. PhD Thesis, Dipartimento di Scienze della Terra, dell'Ambiente e delle Risorse, Università di Napoli Federico II

Renzulli A, Serri G, Santi P, Mattioli M, Holm PM (2001) Origin of high-silica liquids at Stromboli volcano (Aeolian Islands, Italy) inferred from crustal xenoliths. Bulletin of Volcanology 62(6-7):400-419 doi:10.1007/s004450000108

Richards S, Lister G, Kennett B (2007) A slab in depth: Three-dimensional geometry and evolution of the Indo-Australian plate. Geochemistry, Geophysics, Geosystems 8(12):n/a-n/a doi:10.1029/2007gc001657

Romagnoli C (2013) Characteristics and morphological evolution of the Aeolian volcanoes from the study of submarine portions. Geological Society, London, Memoirs 37(1):13-26 doi:10.1144/m37.3

Romagnoli C, Calanchi N, Gabbianelli G, Lanzafame G, Rossi P (1989) Contributi delle ricerche di geologia marina alla caratterizzazione morfostrutturale ed evolutiva dei complessi vulcanici di Salina, Lipari e Vulcano (Isole Eolie). Boll GNV 5:971-975

Romagnoli C, Casalbore D, Bortoluzzi G, Bosman A, Chiocci FL, D'Oriano F, Gamberi F, Ligi M, Marani M (2013) Bathy-morphological setting of the Aeolian Islands. Geological Society, London, Memoirs 37(1):27-36 doi:10.1144/m37.4

Romagnoli C, Kokelaar P, Rossi P, Sodi A (1993) The submarine extension of Sciara del Fuoco feature (Stromboli isl.): morphologic characterization. Acta Vulcanol 3:91-98

Rosenbaum G, Gasparon M, Lucente FP, Peccerillo A, Miller MS (2008) Kinematics of slab tear faults during subduction segmentation and implications for Italian magmatism. Tectonics 27(2):n/a-n/a doi:10.1029/2007tc002143

Rosi M (1980a) Geological map of the island of Stromboli (Aeolian Islands). Rendiconti della Società Italiana di Mineralogia e Petrologia 36

Rosi M (1980b) The island of Stromboli. Rend Soc Ital Mineral Petrol 36(1):345-368

Rottura A, Del Moro A, Pinarelli L, Petrini R, Peccerillo A, Caggianelli A, Bargossi M, Piccarreta G (1991) Relationships between intermediate and acidic rocks in orogenic granitoid suites: petrological, geochemical and isotopic (Sr, Nd, Pb) data from Capo Vaticano (southern Calabria, Italy). Chemical Geology 92(1):153-176

Rudnick RL (1995) Making continental crust. Nature 378(6557):571-577

Ruprecht P, Plank T (2013) Feeding andesitic eruptions with a high-speed connection from the mantle. Nature 500(7460):68-72 doi:10.1038/nature12342

Ryan J, Morris J, Bebout G, Leeman B (1996a) Describing chemical fluxes in subduction zones: insights from "Depth-Profiling" studies of arc and forearc rocks. In: Subduction Top to Bottom, vol. American Geophysical Union, pp 263-268

Ryan JG (2002) Trace-element systematics of Beryllium in terrestrial materials. Reviews in Mineralogy and Geochemistry 50(1):121-145 doi:10.2138/rmg.2002.50.3

Ryan JG, Chauvel C (2014) The subduction-zone filter and the impact of recycled materials on the evolution of the mantle. Treatise of Geochemistry, 2nd ed:479-508 doi:10.1016/b978-0-08-095975-7.00211-4

Ryan JG, Langmuir CH (1988) Beryllium systematics in young volcanic rocks: Implications for 10Be*. Geochimica et Cosmochimica Acta 52(1):237-244 doi:http://dx.doi.org/10.1016/0016-7037(88)90073-7

Ryan JG, Langmuir CH (1993) The systematics of boron abundances in young volcanic rocks. Geochimica et Cosmochimica Acta 57(7):1489-1498

Ryan JG, Leeman WP, Morris JD, Langmuir CH (1996b) The boron systematics of intraplate lavas: Implications for crust and mantle evolution. Geochimica et Cosmochimica Acta 60(3):415-422 doi:http://dx.doi.org/10.1016/0016-7037(95)00402-5

Saginor I, Gazel E, Condie C, Carr MJ (2013) Evolution of geochemical variations along the Central American volcanic front. Geochemistry, Geophysics, Geosystems 14(10):4504-4522 doi:10.1002/ggge.20259

Santo A, Chen Y, Clark A, Farrar E, Tsegaye A (1995) 40Ar/39Ar ages of the Filicudi island volcanics: implications for the volcanological history of the Aeolian Arc, Italy. Acta vulcanol 7(1):13-18

Santo AP (2000) Volcanological and geochemical evolution of Filicudi (Aeolian Islands, south Tyrrhenian Sea, Italy). Journal of Volcanology and Geothermal Research 96:79–101

Santo AP, Jacobsen SB, Baker J (2004) Evolution and genesis of calc-alkaline magmas at Filicudi Volcano, Aeolian Arc (Southern Tyrrhenian Sea, Italy). Lithos 72(1-2):73-96 doi:10.1016/j.lithos.2003.08.005

Savov IP, Ryan JG, D'Antonio M, Fryer P (2007) Shallow slab fluid release across and along the Mariana arc-basin system: Insights from geochemistry of serpentinized peridotites from the Mariana fore arc. Journal of Geophysical Research 112(B9) doi:10.1029/2006jb004749

Savov IP, Ryan JG, D'Antonio M, Kelley K, Mattie P (2005) Geochemistry of serpentinized peridotites from the Mariana Forearc Conical Seamount, ODP Leg 125: Implications for the elemental recycling at subduction zones. Geochemistry, Geophysics, Geosystems 6(4):n/a-n/a doi:10.1029/2004gc000777

Scambelluri M, Tonarini S (2012) Boron isotope evidence for shallow fluid transfer across subduction zones by serpentinized mantle. Geology 40(10):907-910 doi:10.1130/g33233.1

Schellart WP (2008) Kinematics and flow patterns in deep mantle and upper mantle subduction models: Influence of the mantle depth and slab to mantle viscosity ratio. Geochemistry, Geophysics, Geosystems 9(3):n/a-n/a doi:10.1029/2007gc001656

Schiano P, Clocchiatti R, Ottolini L, Sbrana A (2004) The relationship between potassic, calc-alkaline and Na-alkaline magmatism in South Italy volcanoes: A melt inclusion approach. Earth and Planetary Science Letters 220(1-2):121-137 doi:10.1016/s0012-821x(04)00048-2

Schmidt MW, Poli S (1998) Experimentally based water budgets for dehydrating slabs and consequences for magma generation. Earth and Planetary Science Letters 163(1):361-379

Skora S, Blundy J (2010) High-pressure hydrous phase relations of radiolarian clay and implications for the involvement of subducted sediment in arc magmatism. Journal of Petrology 51(11):2211-2243 doi:10.1093/petrology/egq054

Skora S, Blundy JD, Brooker RA, Green ECR, de Hoog JCM, Connolly JAD (2015) Hydrous phase relations and trace element partitioning behaviour in calcareous sediments at subduction-zone conditions. Journal of Petrology 56(5):953-980 doi:10.1093/petrology/egv024

Søager N, Portnyagin M, Hoernle K, Holm PM, Hauff F, Garbe-Schönberg D (2015) Olivine Major and Trace Element Compositions in Southern Payenia Basalts, Argentina: Evidence for Pyroxenite–Peridotite Melt Mixing in a Back-arc Setting. Journal of Petrology 56(8):1495-1518 doi:10.1093/petrology/egv043

Sobolev AV, Hofmann AW, Kuzmin DV, Yaxley GM, Arndt NT, Chung SL, Danyushevsky LV, Elliott T, Frey FA, Garcia MO, Gurenko AA, Kamenetsky VS, Kerr AC, Krivolutskaya NA, Matvienkov VV, Nikogosian IK, Rocholl A, Sigurdsson IA, Sushchevskaya NM, Teklay M (2007) The amount of recycled crust in sources of mantle-derived melts. Science 316(5823):412-417 doi:10.1126/science. 1138113

Sobolev AV, Hofmann AW, Sobolev SV, Nikogosian IK (2005) An olivine-free mantle source of Hawaiian shield basalts. Nature 434(7033):590-597
doi:http://www.nature.com/nature/journal/v434/n7033/suppinfo/nature03411_S1.html

Spandler C, Pirard C (2013) Element recycling from subducting slabs to arc crust: A review. Lithos 170-171:208-223 doi:10.1016/j.lithos.2013.02.016

Stegman DR, Freeman J, Schellart WP, Moresi L, May D (2006) Influence of trench width on subduction hinge retreat rates in 3-D models of slab rollback. Geochemistry Geophysics Geosystems 7(3) doi:10.1029/2005gc001056

Straub SM, LaGatta AB, Martin-Del Pozzo AL, Langmuir CH (2008) Evidence from high-Ni olivines for a hybridized peridotite/pyroxenite source for orogenic andesites from the central Mexican Volcanic Belt. Geochemistry, Geophysics, Geosystems 9(3):n/a-n/a doi:10.1029/2007gc001583

Straub SM, Layne GD (2002) The systematics of boron isotopes in Izu arc front volcanic rocks. Earth and Planetary Science Letters 198(1):25-39

Syracuse EM, van Keken PE, Abers GA (2010) The global range of subduction zone thermal models. Physics of the Earth and Planetary Interiors 183(1-2):73-90 doi:10.1016/j.pepi.2010.02.004

Tibaldi A, Pasquarè G (2010) Geological map of the island of Stromboli, Italy, 1:10 000 scale. Geological Society of America, Boulder, Special Papers 464

Tollstrup D, Gill J, Kent A, Prinkey D, Williams R, Tamura Y, Ishizuka O (2010) Across-arc geochemical trends in the Izu-Bonin arc: Contributions from the subducting slab, revisited. Geochemistry, Geophysics, Geosystems 11(1):n/a-n/a doi:10.1029/2009gc002847

Tommasini S, Heumann A, Avanzinelli R, Francalanci L (2007) The fate of high-angle dipping slabs in the subduction factory: an integrated trace element and radiogenic isotope (U, Th, Sr, Nd, Pb) study of Stromboli Volcano, Aeolian Arc, Italy. Journal of Petrology 48(12):2407-2430 doi:10.1093/petrology/egm066

Tonarini S, Agostini S, Doglioni C, Innocenti F, Manetti P (2007) Evidence for serpentinite fluid in convergent margin systems: The example of El Salvador (Central America) arc lavas. Geochemistry, Geophysics, Geosystems 8(9):n/a-n/a doi:10.1029/2006gc001508

Tonarini S, Leeman WP, Ferrara G (2001) Boron isotopic variations in lavas of the Aeolian volcanic arc, South Italy. Journal of Volcanology and Geothermal Research 110(1):155-170

Tonarini S, Leeman WP, Leat PT (2011) Subduction erosion of forearc mantle wedge implicated in the genesis of the South Sandwich Island (SSI) arc: Evidence from boron isotope systematics. Earth and Planetary Science Letters 301(1-2):275-284 doi:10.1016/j.epsl.2010.11.008

Tranne C, Lucchi F, Calanchi N, Rossi P, Campanella T, Sardella A (2002a) Geological map of the island of Filicudi (Aeolian Islands). LAC Firenze

Tranne CA, Lucchi F, Calanchi N, Lanzafame, G., Rossi PL (2002b) Geological map of the island of Lipari (Aeolian Islands), (scale 1:12 500). University of Bologna and INGV,

Trela J, Vidito C, Gazel E, Herzberg C, Class C, Whalen W, Jicha B, Bizimis M, Alvarado GE (2015) Recycled crust in the Galápagos Plume source at 70 Ma: Implications for plume evolution. Earth and Planetary Science Letters 425:268-277 doi:10.1016/j.epsl.2015.05.036

Trua T, Clocchiatti R, Schiano P, Ottolini L, Marani M (2010) The heterogeneous nature of the Southern Tyrrhenian mantle: Evidence from olivine-hosted melt inclusions from back-arc magmas of the Marsili seamount. Lithos 118(1-2):1-16 doi:10.1016/j.lithos.2010.03.008

Trua T, Marani M, Barca D (2014) Lower crustal differentiation processes beneath a back-arc spreading ridge (Marsili seamount, Southern Tyrrhenian Sea). Lithos 190-191:349-362 doi:10.1016/j.lithos.2013.12.014

Trua T, Marani M, Gamberi F (2011) Magmatic evidence for African mantle propagation into the southern Tyrrhenian backarc region. Geological Society of America Special Papers 478:307-331 doi:10.1130/2011.2478(16

Trua T, Serri G, Marani M (2007) Geochemical features and geodynamic significance of the southern Tyrrhenian backarc basin. Geological Society of America Special Papers 418:221-233 doi:10.1130/2007.2418(11

Trua T, Serri G, Marani MP (2003) Lateral flow of African mantle below the nearby Tyrrhenian plate: geochemical evidence. Terra Nova 15(6):433-440 doi:10.1046/j.1365-3121.2003.00509.x

Trua T, Serri G, Rossi PL (2004) Coexistence of IAB-type and OIB-type magmas in the southern Tyrrhenian back-arc basin: evidence from recent seafloor sampling and geodynamics implications. Memorie Descrittive Carta Geologica d'Italia 44:83–96

Tumanian M, Frezzotti ML, Peccerillo A, Brandmayr E, Panza GF (2012) Thermal structure of the shallow upper mantle beneath Italy and neighbouring areas: Correlation with magmatic activity and geodynamic significance. Earth-Science Reviews 114(3-4):369-385 doi:10.1016/j.earscirev.2012.07.002

Turner S, Bourdon B, Gill J (2003) Insights into magma genesis at convergent margins from U-series isotopes. Reviews in mineralogy and geochemistry 52(1):255-315

Turner S, Handler M, Bindeman I, Suzuki K (2009) New insights into the origin of O–Hf–Os isotope signatures in arc lavas from Tonga–Kermadec. Chemical Geology 266(3-4):187-193 doi:10.1016/j.chemgeo.2009.05.027

van Keken PE, Hacker BR, Syracuse EM, Abers GA (2011) Subduction factory: 4. Depth-dependent flux of H2O from subducting slabs worldwide. Journal of Geophysical Research 116(B1) doi:10.1029/2010jb007922

Vannucci R, Kobayashi K, Nakamura E, Tiepolo M, Schiavi F, Bertagnini A, Metrich N (2006) Recent Stromboli (Italy): Insights into magma sources and processes from melt inclusions. Geochimica et Cosmochimica Acta 70(18, Supplement):A667 doi:http://dx.doi.org/10.1016/j.gca.2006.06.1246

Ventura G (2013) Kinematics of the Aeolian volcanism (Southern Tyrrhenian Sea) from geophysical and geological data. Geological Society, London, Memoirs 37(1):3-11 doi:10.1144/m37.2

Ventura G, Milano G, Passaro S, Sprovieri M (2013) The Marsili Ridge (Southern Tyrrhenian Sea, Italy): An island-arc volcanic complex emplaced on a 'relict' back-arc basin. Earth-Science Reviews 116:85-94 doi:10.1016/j.earscirev.2012.11.005

Ventura G, Vilardo G, Milano G, Pino NA (1999) Relationships among crustal structure, volcanism and strike–slip tectonics in the Lipari–Vulcano volcanic complex (Aeolian Islands, Southern Tyrrhenian Sea, Italy). Physics of the Earth and Planetary Interiors 116(1):31-52

Villari L (1980a) The island of Alicudi. Rendiconti della Società Italiana di Mineralogia e Petrologia 36:441-466

Villari L (1980b) The island of Filicudi. Rendiconti della Società Italiana di Mineralogia e Petrologia 36:467-488

Voltaggio M, Branca M, Tedesco D, Tuccimei P, Di Pietro L (2004) 226Ra-excess during the 1631-1944 activity period of Vesuvius (Italy). Geochimica et Cosmochimica Acta 68(1):167-181 doi:10.1016/s0016-7037(03)00236-9

Weldeab S, Emeis K-C, Hemleben C, Siebel W (2002) Provenance of lithogenic surface sediments and pathways of riverine suspended matter in the Eastern Mediterranean Sea: evidence from 143Nd/144Nd and 87Sr/86Sr ratios. Chemical Geology 186(1–2):139-149 doi:http://dx.doi.org/10.1016/S0009-2541(01)00415-6

White WM, Albarède F, Télouk P (2000) High-precision analysis of Pb isotope ratios by multi-collector ICP-MS. Chemical Geology 167(3–4):257-270 doi:http://dx.doi.org/10.1016/S0009-2541(99)00182-5

White WM, Klein EM (2014) Composition of the Oceanic Crust.457-496 doi:10.1016/b978-0-08-095975-7.00315-6

Whittaker JM, Müller RD, Sdrolias M, Heine C (2007) Sunda-Java trench kinematics, slab window formation and overriding plate deformation since the Cretaceous. Earth and Planetary Science Letters 255(3-4):445-457 doi:10.1016/j.epsl.2006.12.031

Zanon V (2003) Magmatic feeding system and crustal magma accumulation beneath Vulcano Island (Italy): Evidence from CO2fluid inclusions in quartz xenoliths. Journal of Geophysical Research 108(B6) doi:10.1029/2002jb002140

Zanon V, Nikogosian I (2004) Evidence of crustal melting events below the island of Salina (Aeolian arc, southern Italy). Geological Magazine 141(4):525-540 doi:10.1017/s0016756804009124

Zimmer MM, Plank T, Hauri EH, Yogodzinski GM, Stelling P, Larsen J, Singer B, Jicha B, Mandeville C, Nye CJ (2010) The role of water in generating the calc-alkaline trend: new volatile data for Aleutian magmas and a new tholeiitic index. Journal of Petrology 51(12):2411-2444 doi:10.1093/petrology/egq062

Zindler A, Hart S (1986) Chemical geodynamics. Annual review of earth and planetary sciences 14:493-571

A)

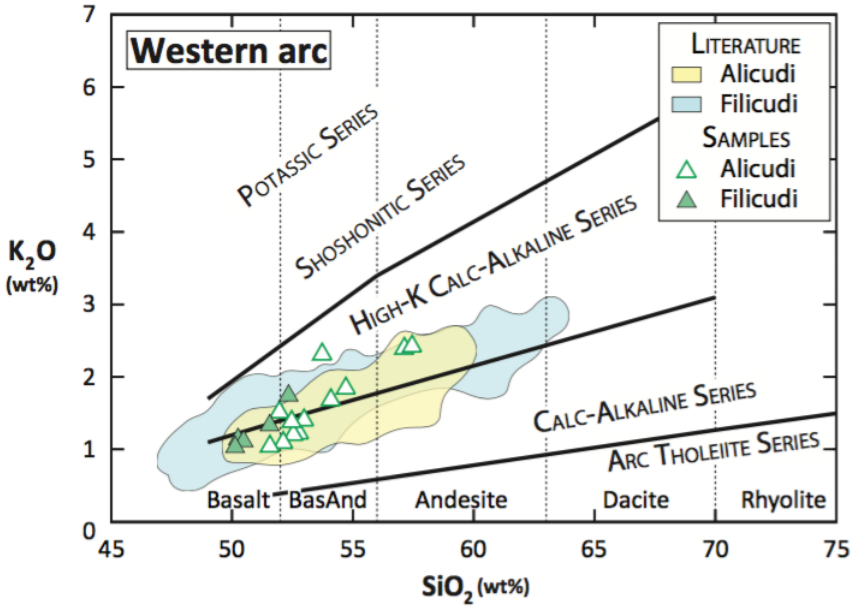
Western arc
Literature
Alicudi
Filicudi
Samples
Alicudi
Filicudi
Potassic Series
Shoshonitic Series
High-K Calc-Alkaline Series
Calc-Alkaline Series
Arc Tholeiite Series
Basalt
BasAnd
Andesite
Dacite
Rhyolite
K2O (wt%)
SiO2 (wt%)

B)

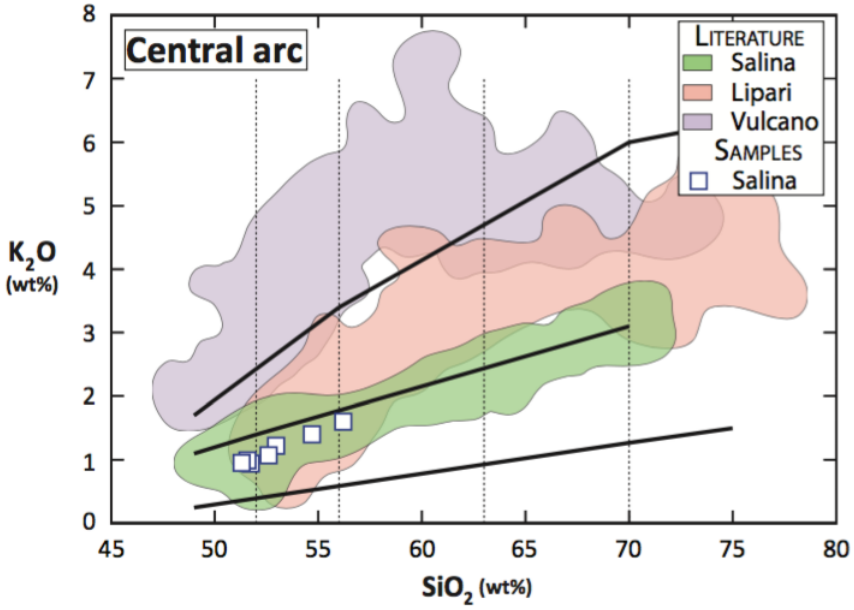
Central arc
Literature
Salina
Lipari
Vulcano
Samples
Salina
K2O (wt%)
SiO2 (wt%)

C)

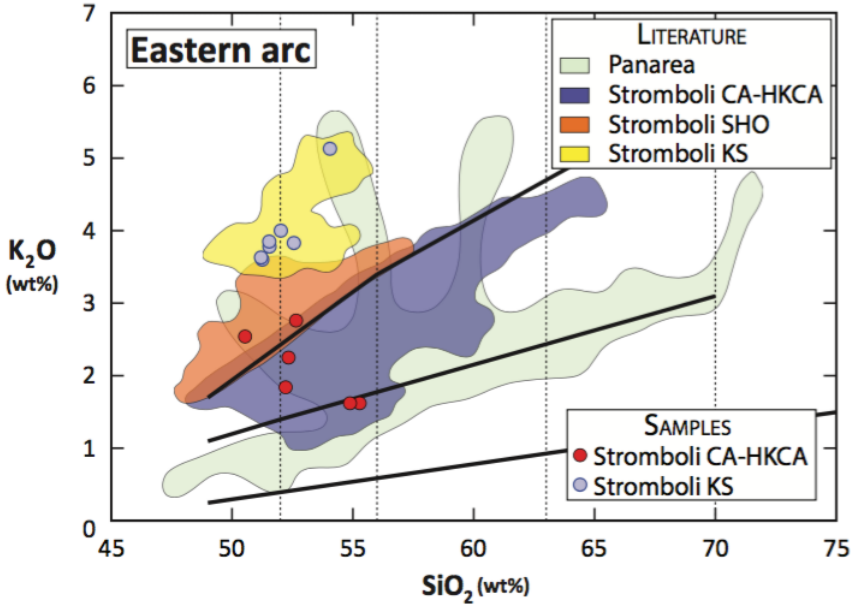
Eastern arc
Literature
Panarea
Stromboli CA-HKCA
Stromboli SHO
Stromboli KS
Samples
Stromboli CA-HKCA
Stromboli KS
K2O (wt%)
SiO2 (wt%)

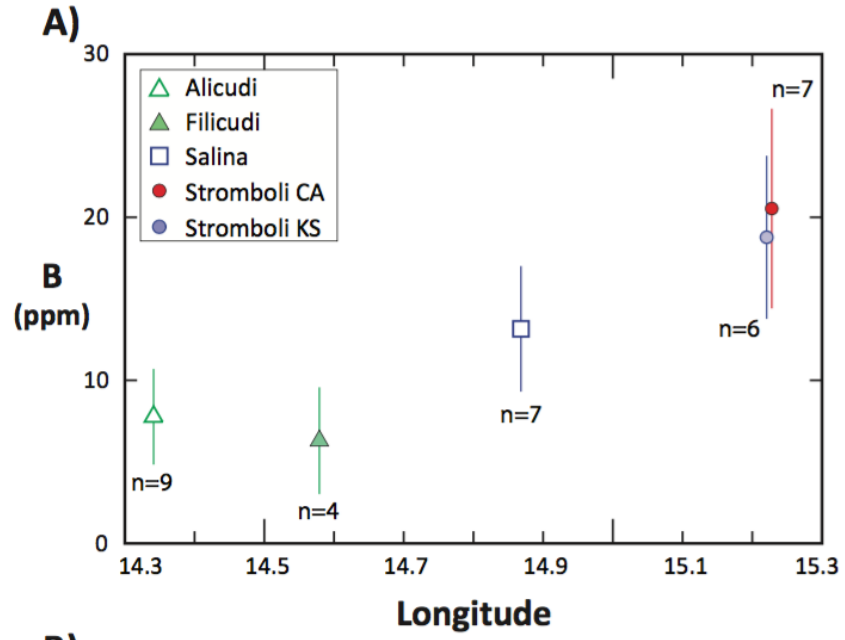
A)
Alicudi
Filicudi
Salina
Stromboli CA
Stromboli KS
B
(ppm)
n=9
n=4
n=7
n=6
n=7
30
20
10
0
14.3
14.5
14.7
14.9
15.1
15.3
Longitude

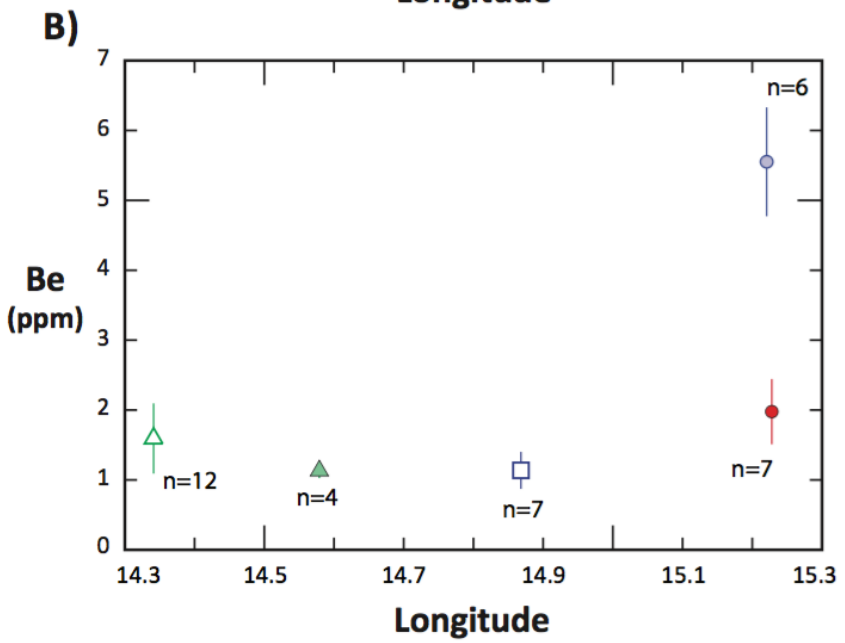
B)
Be
(ppm)
n=12
n=4
n=7
n=7
n=6
7
6
5
4
3
2
1
0
14.3
14.5
14.7
14.9
15.1
15.3
Longitude

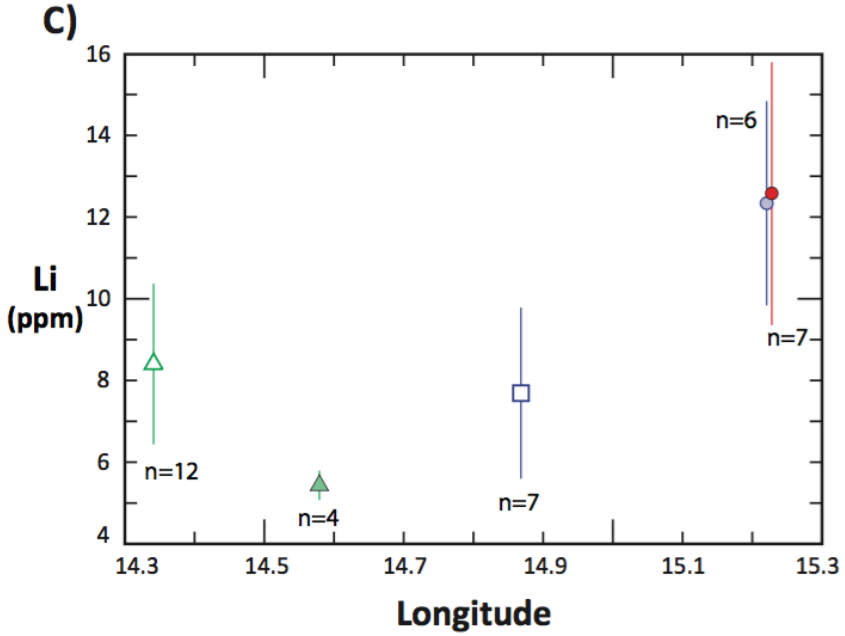
C)
Li
(ppm)
n=12
n=4
n=7
n=6
n=7
16
14
12
10
8
6
4
14.3
14.5
14.7
14.9
15.1
15.3
Longitude

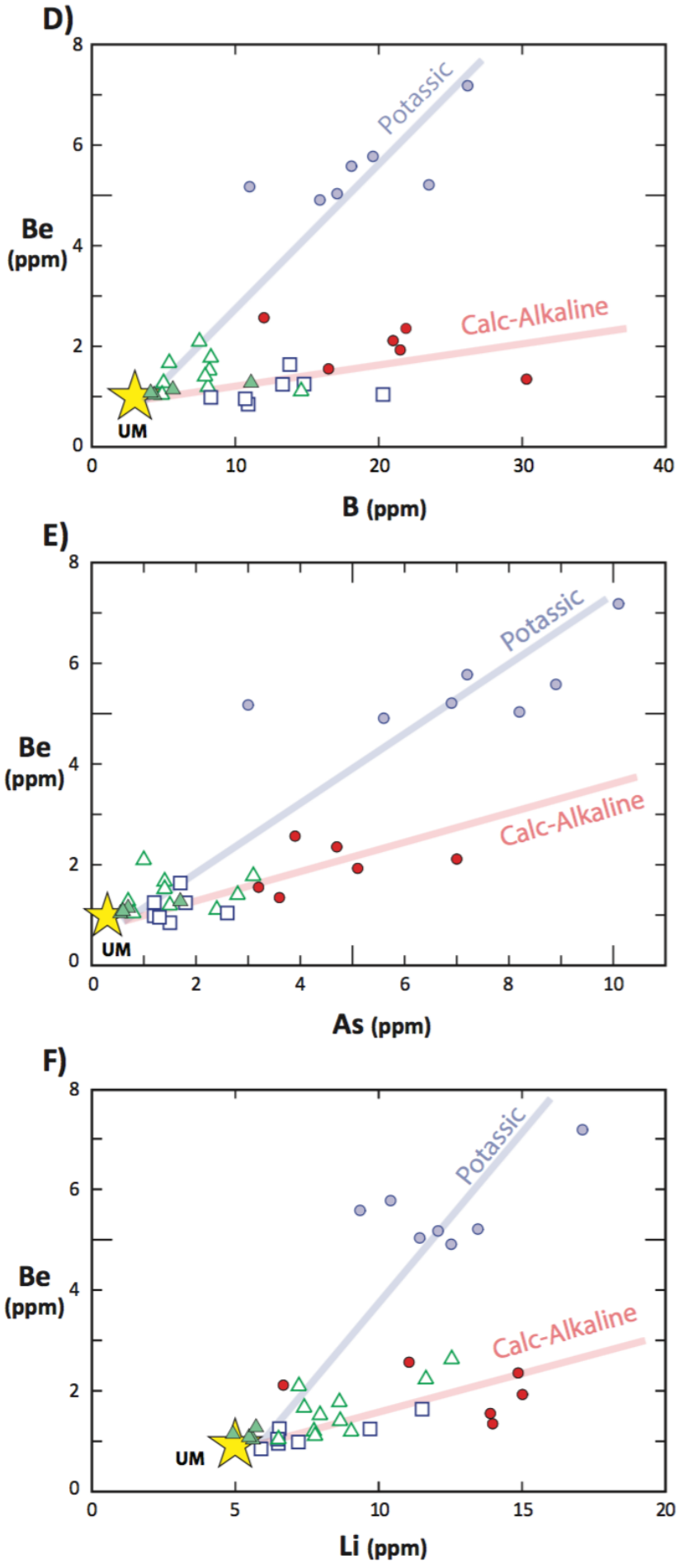
D)
Be (ppm)
B (ppm)
Potassic
Calc-Alkaline
UM
E)
Be (ppm)
As (ppm)
Potassic
Calc-Alkaline
UM
F)
Be (ppm)
Li (ppm)
Potassic
Calc-Alkaline
UM

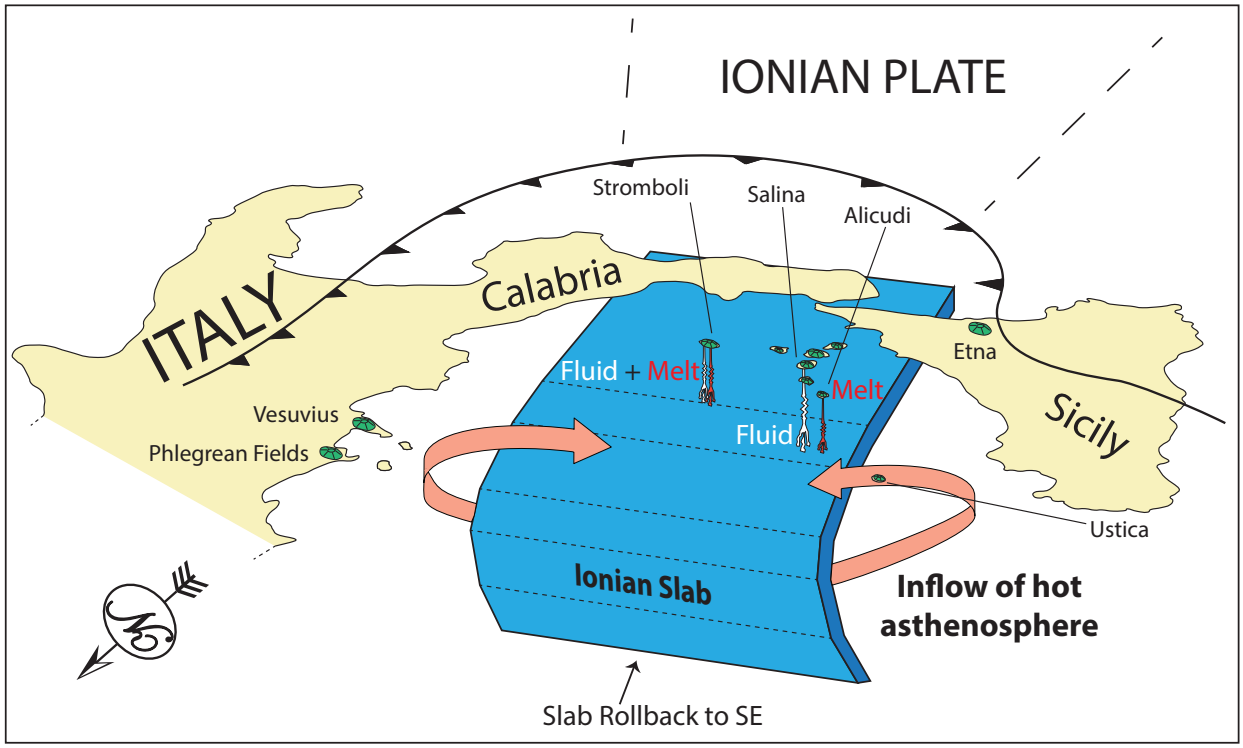

Figure 2.6 Schematic model representing the Ionian slab subduction system below the Aeolian Arc modified from Trua et al. (2007). Orange arrows indicate the asthenospheric mantle inflow over the edges of the Ionian Plate rollbacking towards the SE. The predominant melt components are represented in red under Stromboli and Alicudi. The predominant fluid component is represented in white under Stromboli and Salina.

Seismic studies and numerical models in the southern Tyrrhenian area (Chiarabba et al., 2008; Baccheschi et al., 2008; 2011; Faccenna et al., 2011; Neri et al., 2012) suggest the presence of African-related asthenospheric flow around the edges of the narrow Ionian Plate due to a slab tear caused by the rollback motion of the Ionian slab (Gvirtzman and Nur, 1999; Gutscher et al., 2016), which heavily affected the mantle wedge of the Aeolian Arc (e.g., Faccenna et al., 2011). Also, recent work by Chen et al. (2015) based on dynamic laboratory models of progressive subduction in three-dimensional space, highlights the possibility of a toroidal asthenosphere return flow induced by the slab rollback of the Ionian Plate. Our new data confirm a sediment melt component at the edges of the arc, possibly connected to hot asthenosphere flow at the edges of the slab that may be responsible for the melt signature (Fig. 2.6). Alternatively, buoyant diapirs of slab material can potentially detach from the subducting slab and enter a regime of elevated